Vol. 60 MARCH, 1956 No. 3

THE JOURNAL OF PHYSICAL CHEMISTRY

(Registered in U. S. Patent Office)

THE JOURNAL OF PHYSICAL CHEMISTRY

(Registered in U. S. Patent Office)

Published monthly by the American Chemical Society at 20th and Northampton Sts., Easton, Pa.

Entered as second-class matter at the Post Office at Easton, Pennsylvania.

The *Journal of Physical Chemistry* is devoted to the publication of selected symposia in the broad field of physical chemistry and to other contributed papers.

Manuscripts originating in the British Isles, Europe and Africa should be sent to F. C. Tompkins, The Faraday Society, 6 Gray's Inn Square, London W. C. 1, England.

Manuscripts originating elsewhere should be sent to W. Albert Noyes, Jr., Department of Chemistry, University of Rochester, Rochester 20, N. Y.

Correspondence regarding accepted copy, proofs and reprints should be directed to Assistant Editor, Allen D. Bliss, Department of Chemistry, Simmons College, 300 The Fenway, Boston 15, Mass.

Business Office: Alden H. Emery, Executive Secretary, American Chemical Society, 1155 Sixteenth St., N. W., Washington 6, D. C.

Advertising Office: Reinhold Publishing Corporation, 430 Park Avenue, New York 22, N. Y.

Articles must be submitted in duplicate, typed and double spaced. They should have at the beginning a brief Abstract, in no case exceeding 300 words. Original drawings should accompany the manuscript. Lettering at the sides of graphs (black on white or blue) may be pencilled in and will be typeset. Figures and tables should be held to a minimum consistent with adequate presentation of information. Photographs will not be printed on glossy paper except by special arrangement. All footnotes and references to the literature should be numbered consecutively and placed in the manuscript at the proper places. Initials of authors referred to in citations should be given. Nomenclature should conform to that used in *Chemical Abstracts*, mathematical characters marked for italic, Greek letters carefully made or annotated, and subscripts and superscripts clearly shown. Articles should be written as briefly as possible consistent with clarity and should avoid historical background unnecessary for specialists.

Symposium papers should be sent in all cases to Secretaries of Divisions sponsoring the symposium, who will be responsible for their transmittal to the Editor. The Secretary of the Division by agreement with the Editor will specify a time after which symposium papers cannot be accepted. The Editor reserves the right to refuse to publish symposium articles, for valid scientific reasons. Each symposium paper may not exceed four printed pages (about sixteen double spaced typewritten pages) in length except by prior arrangement with the Editor.

Remittances and orders for subscriptions and for single copies, notices of changes of address and new professional connections, and claims for missing numbers should be sent to the American Chemical Society, 1155 Sixteenth St., N. W., Washington 6, D. C. Changes of address for the *Journal of Physical Chemistry* must be received on or before the 30th of the preceding month.

Claims for missing numbers will not be allowed (1) if received more than sixty days from date of issue (because of delivery hazards, no claims can be honored from subscribers in Central Europe, Asia, or Pacific Islands other than Hawaii), (2) if loss was due to failure of notice of change of address to be received before the date specified in the preceding paragraph, or (3) if the reason for the claim is "missing from files."

Subscription Rates (1956): members of American Chemical Society, $8.00 for 1 year; to non-members, $16.00 for 1 year. Postage free to countries in the Pan American Union; Canada, $0.40; all other countries, $1.20. $12.50 per volume, foreign postage $1.20, Canadian postage $0.40; special rates for A.C.S. members supplied on request. Single copies, current volume, $1.35; foreign postage, $0.15; Canadian postage $0.05. Back issue rates (starting with Vol. 56): $15.00 per volume, foreign postage $1.20, Canadian, $0.40; $1.50 per issue, foreign postage $0.15, Canadian postage $0.05.

The American Chemical Society and the Editors of the *Journal of Physical Chemistry* assume no responsibility for the statements and opinions advanced by contributors to This Journal.

The American Chemical Society also publishes *Journal of the American Chemical Society, Chemical Abstracts, Industrial and Engineering Chemistry, Chemical and Engineering News, Analytical Chemistry, Journal of Agricultural and Food Chemistry* and *Journal of Organic Chemistry*. Rates on request.

(Continued from first page of cover)

THE JOURNAL OF
PHYSICAL CHEMISTRY

VOLUME 60 MARCH 20, 1956 NUMBER 3

FACTORS RESPONSIBLE FOR THE STABILITY OF DETERGENT MICELLES

BY IRVING REICH[1]

University of Southern California, Los Angeles, Calif.

Received August 7, 1953

The theory of Debye, which ascribes micelle formation to the opposition between hydrocarbon-chain attraction and ionic repulsion, leads to grossly incorrect calculations of micelle size distribution. Theories which depend on ionic repulsion are also unable to account for the formation of micelles by non-ionic detergents. A general theory for the formation of micelles by non-ionic detergents is outlined, based on the Hartley picture of micelle structure. For ordinary solutes, the energy of the system decreases indefinitely as the degree of aggregation increases. For detergents, the energy of the system no longer decreases after aggregates reach a certain size. Consequently further aggregation does not occur, since that would involve an entropy decrease. A general equation for micelle size distribution is developed, and the modifications required for ionic detergents are discussed.

Introduction

In 1949 Debye[2,3] outlined a general theory of micelle formation. This theory was intended to explain why micelles do not grow indefinitely and separate out as an ordinary phase. In Debye's theory, limitation of micelle size is attributed to electrostatic repulsion between the head groups of the detergent ions which make up the micelle.

In the first part of the present paper, it is shown that this theory is incorrect due to two rather fundamental errors. In the rest of this paper a theory is outlined explaining the formation of micelles in terms of an entropy effect.

Debye's Theory of Micelle Formation

Debye assumed the micelles to be disk-shaped McBain platelets. He assumed that as the micelle grows, each entering detergent ion releases the same amount of hydrocarbon-chain adhesional energy, so that this energy is proportional to the size of the micelle. Then the total work of assembling the micelle is

$$W = N^{3/2}w_e - Nw_m \qquad (1)$$

where N is the number of detergent ions in the micelle, w_m is the work of hydrocarbon-chain adhesion per ion, and w_e is a constant which relates to work done against electrostatic repulsion of the ionic head groups. Plotting W against N gives a curve with a minimum. Debye considered the value of N at which the minimum occurs to specify the stable micelle size since "work is required to increase or decrease the equilibrium number N_0."

In deriving equation 1, the effect of gegenions in screening the electrostatic repulsion between head groups is neglected. Hobbs[4] attempted to refine the theory by taking into account the effect of the gegenion atmosphere, but mathematical difficulties prevented the development of general equations.

The above theory appears to be incorrect in three ways:

(1) The stable micelle size (or size distribution) must be that which results in minimum free energy for the system. This is quite different from the criterion of minimum free energy per micelle.

(2) Growth of micelles will involve a decrease in the number of independent particles in the system, and hence will involve a decrease in total entropy. This must be taken into account.

(3) Energy of hydrocarbon chain adhesion per ion must increase as the micelle grows. If it remained constant, as Debye assumes, growth beyond dimer size would not occur.

(1) Lever Brothers Research Center, Edgewater, New Jersey.
(2) P. Debye, THIS JOURNAL, **53**, 1 (1949).
(3) P. Debye, *Ann. N. Y. Acad. Sci.*, **51**, 573 (1949).
(4) M. E. Hobbs, THIS JOURNAL, **55**, 675 (1951).

Suppose C molecules of detergent are present in the system and they aggregate to form C/N micelles of N molecules each. Then, accepting equation 1, the total energy of micelle formation will be $(C/N)\ (N^{3/2}w_e - Nw_m)$ or $C(N^{1/2}w_e - w_m)$. It is this rather than $N^{3/2}w_e - Nw_m$ which must be minimized to determine the stable micelle size. However if $C(N^{1/2}w_e - w_m)$ is plotted against N, it is found to increase steadily with increasing N without passing through a minimum. Consequently there would be no preferred micelle size. Instead aggregates of all sizes would be present—dimers in highest concentration and larger aggregates in steadily decreasing concentrations. This is a picture which differs radically from generally accepted ideas about micelle size distributions.

More correctly we should plot free energy rather than total energy against N, which means that a temperature–entropy term should be subtracted from the total energy. The more disperse the system, the greater will be the entropy. Hence entropy will favor the smaller as against the larger aggregates without changing the trend of the curve.

In order to account for the existence of a preferred micelle size, account must be taken of the variation of w_m with N. Debye's assumption that w_m is constant appeared to lead to a preferred micelle size only because of the incorrect minimization of energy per micelle instead of energy of the system.

Micelles of Non-ionic Detergents.—Non-ionic detergents, such as polyoxyethylene derivatives of fatty acids or fatty alcohols, are known to form micelles in much the same way as ionic detergents.[5,6] These molecules do not have ionic groups capable of exerting long-range electrostatic forces. Consequently a general theory of micelle formation cannot involve ionic-group repulsion as an essential element.

Unquestionably the repulsion between head groups plays an important role in determining the critical concentrations and sizes of ionic micelles. Unfortunately a general quantitative treatment of the problem does not appear possible at present owing to the difficulty of specifying the effect of the gegenion atmosphere. There is much to be said in favor of focussing our attention on the simpler case of non-ionic micelles in attempting to set up any general theory of micelle formation. The remainder of this paper will consist of an outline of a theory of non-ionic micelle formation, followed by a brief discussion of the modifications required in proceeding to ionic micelles.

Thermodynamic Equations Governing Aggregation.—In any solution, solute aggregates of all sizes have finite probabilities of existence. The solute consists of an equilibrium mixture of all aggregate sizes. At equilibrium, there will be a definite aggregate-size distribution which may be shown by plotting aggregate concentration $[A_N]$ against aggregate size N. The equilibrium size distribution will be that which gives lowest free energy for the system. Of course some aggregate sizes may be present in undetectably small concentrations or even in concentrations so small that a system of ordinary size will only rarely form a single aggregate.

The monomer is in equilibrium with aggregates of each size, so that the concentration of monomer determines the concentration of aggregates of each size. This is to say that the concentration of monomer determines the complete size-distribution curve. In dealing with micelle formation, it is convenient to consider how the size-distribution curve changes as the monomer concentration is increased to the critical concentration.

In Fig. 1, four types of size distribution are shown. Curve 1 represents an ordinary solution. Monomer is present at appreciable concentration. Dimers and higher aggregates are present at undetectably low concentrations. Curve 2 represents a hypothetical system which would occur if the energy of aggregation specified in equation 1 were correct. Aggregates of all sizes exist in steadily decreasing concentration. Curve 3 represents ordinary phase separation. As in curve 1, monomer is present in substantial concentration, while dimers and higher aggregates are present only in very low concentrations. But here the concentration curve rises for aggregates of very large size. Finally curve 4 represents micelle formation. The left-hand portion of the curve resembles the corresponding parts of curves 1 and 3. However at some value of N, generally in the range 50–200, the concentration rises and then falls again, so that a considerable concentration of small aggregates is present. When the concentration of an ordinary solute is increased, a critical concentration is eventually reached at which the situation changes from that of curve 1 to that of curve 3. When the concentration of a detergent is increased, the change at the critical concentration is from the situation of curve 1 to that of curve 4.

In a solution, aggregates of each size are formed reversibly from monomer

$$NA = A_N \qquad (2)$$

so that the standard free energy of formation is

$$\Delta F^\circ = -kT \ln K \qquad (3)$$

or

$$\Delta E^\circ - T\Delta S^\circ = -kT \ln \frac{[A_N]}{[A]^N} \qquad (4)$$

which may be rearranged to give

$$\ln [A_N] = \frac{T\Delta S^\circ - \Delta E^\circ}{kT} + N \ln [A] \qquad (5)$$

Equation 5 is a perfectly general thermodynamic size distribution equation. It gives aggregate concentration $[A_N]$ as a function of N. This size distribution function may be calculated at a series of different monomer concentrations [A], to determine what happens when [A] reaches its critical concentration. However ΔS° and ΔE° vary with the aggregate size N. They must be evaluated as functions of N before the equation can be employed.

It will be assumed that the monomer and aggregates form ideal solutions. In that case, activities are equal to concentrations, and these will be expressed in mole fractions. This has the advantage

(5) J. W. McBain and E. Gonick, *J. Am. Chem. Soc.*, **69**, 334 (1947).
(6) L. M. Kushner and W. D. Hubbard, THIS JOURNAL, **58**, 1163 1954).

of defining the standard states as pure liquid monomer and pure liquid aggregates. ΔS° is the entropy change involved when N moles of pure liquid monomer forms one mole of pure liquid N-mer. It does not include any entropy of dilution.

The important assumption will now be made that s, the standard entropy change per molecule, is the same regardless of the size of the aggregate formed. This is undoubtedly true for large aggregates. If it is true for smaller aggregates also, then

$$\Delta S^\circ = Ns \tag{6}$$

and, from equation 5

$$\ln [A_N] = \frac{NsT - \Delta E^\circ}{kT} + N \ln [A] \tag{7}$$

The remaining step is to evaluate ΔE^0.

One possibility is to employ equation 1, setting ΔE^0 equal to $N^{3/2}w_e - Nw_m$, so that

$$\ln [A_N] = N\left(\frac{sT + w_m}{kT} + \ln [A]\right) - N^{3/2}\left(\frac{w_e}{kT}\right) \tag{8}$$

Since w_e is positive, the second term is negative. The first term also is negative, except in physically meaningless cases where $[A_N]$ is greater than 1. Hence $\ln [A_N]$ always decreases with increasing N. At very low monomer concentration [A], the size distribution, is that shown in curve 1 of Fig. 1. At higher monomer concentration, it is that shown in curve 2 of Fig. 1. This is the conclusion reached earlier by qualitative reasoning. The same types of size distribution obtain if the electrostatic repulsion work is eliminated by setting the second term equal to zero. Clearly the aggregation energy specified in equation 1 is not correct.

As the first step toward setting up a more valid specification of aggregation energy, it will be helpful to consider an ordinary solute rather than a detergent. Suppose we have an aliphatic hydrocarbon dissolved in water. Each molecule will show some tendency to fold up on itself because of the tendency of segments of the chain to escape from the water and contact each other. To permit calculation, it will be assumed that each molecule or aggregate is a tightly-packed sphere which does not include any water. When molecules join to form an aggregate, the total surface is reduced.

If ϵ is the total surface energy of a single molecule sphere, then the maximum energy change when N molecules aggregate would be $-N\epsilon$. This would hold only for very large aggregates; for small aggregates the energy change would be less, since appreciable hydrocarbon surface would remain exposed to contact with water. It is readily calculated that when N spheres unite to make a larger sphere, the fraction of the original surface which is eliminated is $1 - 1/N^{1/3}$. Hence the energy of aggregation is

$$\Delta E^\circ = -N\epsilon(1 - 1/N^{1/3}) \tag{9}$$

On substituting this into equation 7, we obtain

$$\ln [A_N] = \frac{NsT + N\epsilon(1 - 1/N^{1/3})}{kT} + N \ln [A] \tag{10}$$

This equation predicts phase separation at a critical concentration defined by

$$\ln [A] = \frac{-\epsilon - sT}{kT} \tag{11}$$

for if we set $\ln [A]$ equal to $(-\epsilon - sT)/kT + \Delta$ in equation 10, we get

$$\ln [A_N] = -N^{2/3}(\epsilon/kT) + N\Delta \tag{12}$$

If Δ is zero or negative, $\ln [A_N]$ falls rapidly with N, so that the aggregate size distribution is as shown in curve 1 of Fig. 1. If Δ becomes infinitesimally greater than zero, the aggregate size distribution follows the same course for low values of N, but for very large values of N, concentrations become appreciable, and in fact infinite aggregates will form. This is the size distribution shown in curve 3 of Fig. 1. Thus the concentration defined in equation 11 is a critical concentration at which a new phase separates.

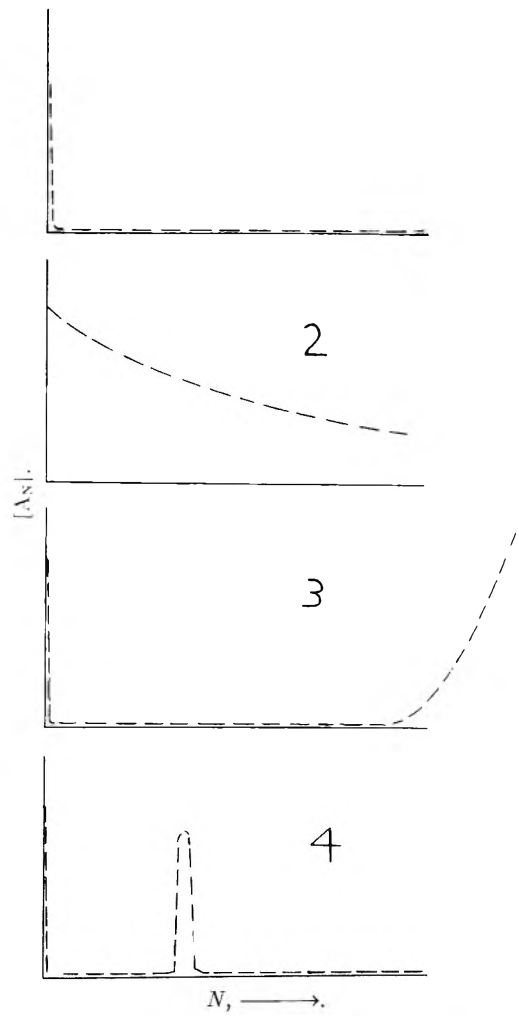

Fig. 1.—Types of aggregate size distribution: 1, ordinary solute; 2, hypothetical system obeying equation 1; 3, phase separation; 4, micelle formation.

The case of non-ionic detergent molecules may now be considered. The hydrocarbon portion of the molecule is assumed to be curled up into a tightly-packed sphere. This, while not likely to be an exact picture, is probably reasonably close to the fact.[7] Of the total surface of the molecule, A, a portion S is covered by the polar group, while the remainder, $A - S$, consists of hydrocarbon surface. When molecules unite to form an aggregate, the

(7) A. E. Alexander and P. Johnson, "Colloid Science," Vol. II, Clarendon Press, Oxford, 1949, p. 671.

hydrocarbon chains are assumed to blend together to form a larger sphere, with the polar groups occupying the surface. This is essentially the Harley picture of micelle structure.

Here again let ϵ be the total energy of the hydrocarbon–water interface of a single molecule. The energy of aggregation will be $-\epsilon$ multiplied by the fraction of the original hydrocarbon surface area which is eliminated by aggregation. Since the original hydrocarbon surface is $NA - NS$ and the hydrocarbon surface of the aggregate is $N^{2/3}A - NS$, the fraction eliminated on aggregation is $A/(1 - 1/N^{1/3})(A - S)$. If, for example, the polar group covers one fourth of the surface of the curled-up molecule, so that $A/(A - S)$ is 4/3, the fraction of the surface eliminated will increase with N to the value 1 at $N = 64$. An aggregate of 64 of these molecules will be in effect a tiny oil droplet with its surface completely covered by polar groups. All of the hydrocarbon will then be withdrawn from contact with water and will be in contact with other hydrocarbon.

In this case the stable micelle size should be 64 molecules. Aggregates should grow to this size for the same reason that they grew in the previous case—in order to eliminate as much as possible of their hydrocarbon surface from contact with the water and thus to minimize the energy of the system. However for the case of the dissolved hydrocarbon, the fraction of the hydrocarbon surface which was eliminated became 1 only for infinite aggregates, so that aggregates grew indefinitely. Here it becomes 1 for aggregates of very small size. There is no energetic reason for these to grow larger. Accordingly their further growth would not be expected, since that would involve a decrease in total number and a corresponding decrease in the entropy of the system. Aggregates of the size at which the surface becomes completely covered with polar groups will be called "complete micelles." On thermodynamic grounds it is certain that some aggregates larger and smaller than complete micelles will be present. It is necessary to show that their concentrations drop away rapidly as N becomes larger or smaller than the complete micelle value.

If an aggregate grew larger than the complete micelle size and still remained spherical, the surface would not accommodate all of the polar groups. Some polar groups would have to be buried in the interior. This is unlikely energetically. Such large aggregates would presumably be flattened sufficiently to create enough extra surface to accommodate all the polar groups. Thus as N increases beyond the complete micelle size, the aggregates become larger and flatter. The fraction of the hydrocarbon surface eliminated remains 1.

Accordingly for values of N less than that of the complete micelle, equation 7 becomes

$$\ln [A_N] = \frac{NsT + N\epsilon\left(\frac{A}{A-S}\right)(1 - 1/N^{1/3})}{kT} + N \ln [A] \quad (13)$$

while for values of N greater than that of the complete micelle equation 7 becomes

$$\ln [A_N] = \frac{NsT + N\epsilon}{kT} + N \ln [A] \quad (14)$$

The value of N for the complete micelle is given by

$$\left(\frac{A}{A-S}\right)(1 - 1/N^{1/3}) = 1 \quad (15)$$

Rough calculations of aggregate size distribution can now be made, based on approximate values of A/S, ϵ and s. Taking a polyoxyethylene ether of dodecyl alcohol as the non-ionic detergent, it will be assumed arbitrarily that the polar group covers one-fourth of the curled up hydrocarbon portion of the molecule. Then $A = 4S$ and, from equation 15, the size of the complete micelle is given by $N = 64$.

In calculations of this type it has sometimes been assumed that the standard entropy change s is approximated by the entropy of fusion of the appropriate hydrocarbon. The entropy of fusion of dodecane is 16.8 cal./deg. However this approximation does not seem satisfactory if the Hartley micelle structure is postulated, since the micelle interior is assumed to be liquid rather than crystalline solid. It seems more reasonable to view the standard entropy change as the entropy change of condensing dodecane vapor into liquid. However the vapor must be assumed to have first been compressed to the density of the liquid, so that no volume change occurs during the condensation. The quantity desired can be calculated as

Satd. dodecane vapor	—A→	Compressed vapor (density 0.751)	—B→	Liquid (density 0.751)

During step A, one mole of dodecane vapor at 25° is compressed from its saturation pressure (0.115 mm.) to a pressure sufficient to increase its density to 0.751 g./cc. The vapor is assumed to behave as a perfect gas. The entropy change is $R \ln P_1/P_2$, which in this case is -26.68 cal./mole deg.

During step B the compressed vapor condenses to a liquid occupying the same volume. The change in configuration and organization of the dodecane molecules involves the entropy change s' which we wish to calculate.

The over-all entropy change for steps A + B is simply the ordinary entropy of condensation $-\Delta H_{vap}/T$. Here this is -49.16 cal./mole deg. Subtracting from this the value for step A, -26.68, we have -22.5 cal./mole deg. or $-11.35\ k$ as the value for s'. This is the standard entropy change for the hydrocarbon portions of the molecules. However there will also be some entropy decrease due to the restriction of the movement of the polyoxyethylene chains. The micelle may be looked upon as a tiny hydrocarbon oil droplet with waving polyoxyethylene tentacles emerging from its surface. The portions of the polyoxyethylene chains within a few atoms' distance of the oil-drop surface will be greatly restricted as to position and freedom of motion. This restriction involves an entropy decrease which is estimated as of the order of two-thirds s', or about $-8k$. Thus the total standard entropy of micelle formation is of the order of $-20k$, and this value will be used in the calculations.

The interfacial energy ϵ may be calculated by multiplying the surface area of a molecule-sphere by the macroscopically-determined interfacial energy of the hydrocarbon. The total interfacial energy

of dodecane against water is 65.3 ergs/cm.^{2}. This leads to a value of $40kT$ for the interfacial energy of a curled-up molecule of dodecane. Since we are assuming that one-fourth of the hydrocarbon surface is permanently screened off by the polyoxyethylene group, the value for ϵ of the detergent becomes $30kT$.

Specifying $A = 4S$, $s = -20k$, and $\epsilon = 30kT$, equations 13 and 14 become

$$N \leq 64: \quad \ln [A_N] = N(20 + \ln [A]) - 40N^{2/3} \quad (15)$$

$$N \geq 64: \quad \ln [A_N] = N(10 + \ln [A]) \quad (16)$$

These equations may be used to calculate the entire aggregate size distribution curve at any concentration of monomer. Thus at monomer concentration [A] = 2.01×10^{-5} (curve 3 of Fig. 2), ln A_N falls away rapidly with increasing N. Although it rises again to a maximum at $N = 64$, the concentration of these aggregates never exceeds the undetectably small value of e^{-52}. Hence the solution is essentially an ordinary solution of monomer. However as the concentration of monomer is increased, the maximum rises, so that at monomer concentration [A] = 3.67×10^{-5}, large numbers of micelles of sizes in the neighborhood of $N = 64$ are present.

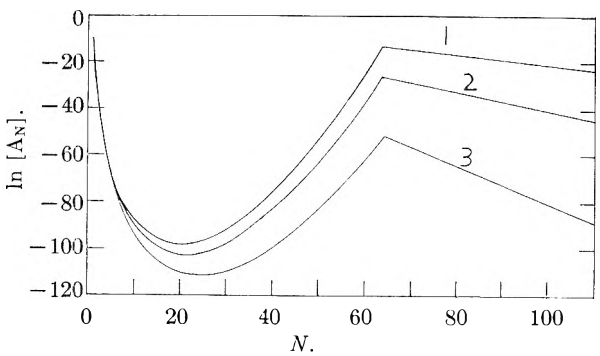

Fig. 2.—Semilogarithmic plot of calculated aggregate size distributions for non-ionic detergent at different monomer concentrations: 1, [A] = 3.67×10^{-5}; 2, [A] = 3.00×10^{-5}; 3, [A] = 2.01×10^{-6}.

The sharpness which micelles appear and the narrowness of their size distribution is seen more clearly in Fig. 3, where aggregate concentrations are plotted as actual weight per cent. concentrations instead of as logarithms of mole fractions. The detergent is assumed to have a molecular weight of 500. The monomer concentrations chosen here are much closer together than those in Fig. 2. It is clear that there is a sharp critical micelle concentration at a detergent concentration of about 0.097%. At a detergent concentration slightly less, 0.0947%, very few micelles are present. On the other hand to increase the monomer concentration to 0.0997% requires the presence of over 0.5% of detergent, most of which goes to form micelles. Approximately 90% of the micelles are in the size region 64 to 74.

A complete micelle in the sense defined above may not be attainable. If the polar group screens off a small enough portion of the molecule, the aggregate may grow to twice the chain length of the molecule before its surface is completely covered with polar groups. The aggregate cannot grow larger as a sphere without polar groups being pulled into the interior. Hence any further growth would involve flattening of the aggregate. Such growth would not decrease the fraction of the hydrocarbon surface eliminated and hence would not be favored. In this case, therefore, the stable micelle would be a sphere whose diameter is twice the length of the detergent molecule.

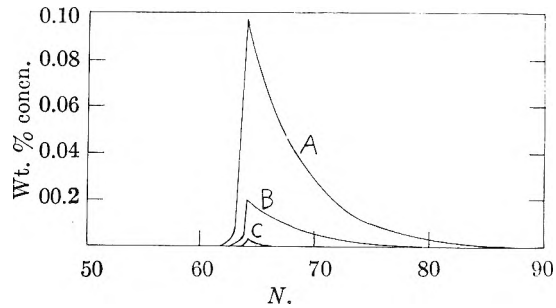

Fig. 3.—Direct plot of calculated aggregate size distributions for non-ionic detergent at different monomer concentrations: A, [A] = 0.0997%; B, [A] = 0.097%; C, [A] = 0.0947%.

According to the foregoing treatment, the size of micelles depends on the geometric ratio S/A. On the other hand the critical micelle concentration depends on the relative magnitudes of the standard entropy s and standard energy ϵ. Precise calculations of critical concentrations and sizes depend on evaluation of these quantities.

It would be expected that, for detergents with short polyoxyethylene chains, the critical micelle concentration would increase with polyoxyethylene chain length, due to the increasing entropy change when the motion of these chains is restricted. However for detergents with long polyoxyethylene chains, critical concentration should no longer vary with chain length, since the outer portions of the polyoxyethylene chains would not suffer much restriction in their movement. Critical concentration should always decrease with increasing hydrocarbon chain length since this would increase ϵ. Micelle size should increase with increasing hydrocarbon chain length, since this would result in larger A. However it should not be appreciably influenced by the polyoxyethylene chain length beyond the first few units.

Dr. Marjorie J. Vold of this University has pointed out to the writer that it may be necessary to consider the energy of dehydration of the polyoxyethylene groups. As the micelle grows, these groups will be forced closer together. If dehydration of ether oxygen occurs, the energy associated with this must be subtracted from ϵ.

The McBain Micelle

The above calculations have been based on Hartley's picture of the micelle. An alternative picture is that of McBain. The micelle is assumed to grow in two dimensions as a platelet, with the hydrocarbon chains aligned parallel to each other and the polar groups covering the flat faces. No matter how large such an aggregate may become, the hydrocarbon–water interface will never be eliminated completely, since the detergent molecules at the edge will have their hydrocarbon chains ex-

posed to water. The usual assumption will be made that the platelet aggregates are disk-shaped.

The original separate molecules, as before, are assumed to be curled up into spheres. The process of forming a McBain aggregate may be analyzed into two steps. First the molecules uncurl, assuming cylindrical shape. This involves an increase in hydrocarbon surface with a corresponding energy change $N\epsilon_1$. Then the molecules form the disk aggregate. In this process the flat ends of the hydrocarbon chains are completely covered. This involves an energy change $-N\epsilon_2$. The sides of the hydrocarbon cylinders are covered except for the exposed portions of the cylinders at the edge of the aggregate. If ϵ_3 is the total interfacial energy of the cylinder side, then the energy change which occurs when the aggregate is formed is $-N\epsilon_3(1 - 1/N^{1/2})$. Thus the standard energy of forming an aggregate is

$$\Delta E^\circ = N\epsilon_1 - N\epsilon_2 - N\epsilon_3(1 - 1/N^{1/2}) \quad (17)$$

When this is substituted into equation 7, the aggregate size distribution obtained is that for phase separation rather than for micelle formation. The critical concentration is given by

$$\ln [A] = \frac{\epsilon_1 - \epsilon_2 - \epsilon_3 - sT}{kT} \quad (18)$$

The situation here is like that defined by equations 10–12. At monomer concentrations less than the critical concentration, very few aggregates are present. When the monomer concentration is raised to the critical value, the aggregates grow to infinite size.

It follows that, according to the theory here proposed, micelles of non-ionic detergents must have the structure proposed by Hartley rather than that proposed by McBain.

Preston[8] pointed out that soaps and other colloidal electrolytes exhibit transition temperatures. Above the transition temperature micelles form at a certain critical concentration. Below the transition temperature, when the critical concentration is attained, a solid phase separates out. This may be explained if the transition temperature is considered a microscopic melting point. Below the transition temperature the hydrocarbon chains in an aggregate are aligned parallel to each other forming a crystalline plate. Accordingly aggregates grow to infinite size. Above the transition temperature the hydrocarbon chains form a liquid sphere, so that the aggregate is of the Hartley type and is limited in size.

This treatment apparently ignores the effect of electrostatic repulsion energy which must be a factor for the ionic detergents which Preston considered. However Halsey[9] has shown that when an aggregate reaches large enough size, each entering detergent ion will be repelled only by the portions of the aggregate near its entry point. The more distant parts of the aggregate would be screened off by a cloud of gegenions. The work of electrical repulsion per entering ion would then become constant rather than increasing and would no longer limit the growth of the aggregate. Hence the transition from liquid to crystalline state for the hydrocarbon chains would permit infinite growth of the aggregate and the electrical work would be merely a constant factor to be subtracted from the hydrocarbon adhesion work.

Micelle Formation by Ionic Detergents.—The formation of micelles by ionic detergents may be accounted for in the same way as their formation by non-ionic detergents. However the additional factor of electrostatic repulsion between ionic head groups must be introduced. As a first approximation, we may adopt Debye's function, adding the term $-w_eN^{3/2}/kT$ to the right-hand sides of equations 13 and 14. This does not change the general form of the size distribution curve. However it causes smaller aggregates to be favored as against larger ones and results in a decreased average micelle size and an increased critical micelle concentration. If w_e is of sufficient magnitude, the stable micelle size may be considerably smaller than the "complete micelle" defined earlier. Before the aggregate had reached completion, the electrical work term would grow larger than the hydrocarbon-adhesion energy, preventing further growth, even though the aggregate still had exposed hydrocarbon.

If we assume the aggregates to be crystalline platelets, we must add $-w_eN^{3/2}/kT$ to equation 17. Substituting this into equation 7 leads to a modified equation which predicts micelle formation. Thus it appears that electrical repulsion may be capable of stabilizing a McBain-type micelle. However the electrical work term employed here does not take into account the screening of repulsion by the gegenions. This effect will become increasingly important as the aggregate grows. Indeed, as Halsey[9] has shown, for a sufficiently large aggregate the $N^{1/2}$ factor becomes simply N, so that the aggregate is not stabilized against further growth. Without exact calculation of the potential due to gegenions, it is not possible to determine whether electrical repulsion is in fact capable of stabilizing McBain micelles.

Appendix

Since this paper was first submitted for publication, Ooshika[10] has published a theory of micelle formation. Ooshika here points out the incorrectness of Debye's treatment in assuming constant energy of hydrocarbon chain adhesion and in minimizing the free energy of the micelle rather than of the entire system.

Ooshika's treatment does not account for the formation of micelles by non-ionic detergents. The micelle size which he calculates is given by $N = w_s/w_e$. For non-ionic detergents, where w_e is zero, the aggregates would become infinite.

Acknowledgment.—The author wishes to express his thanks to Dr. Marjorie J. Vold and to Dr. Karol J. Mysels of the University of Southern California for their helpful suggestions. This study was part of a program at the University of Southern California supported by the Lever Brothers Company.

(8) W. C. Preston, THIS JOURNAL, **52**, 84 (1948).

(9) G. D. Halsey, Jr., *ibid.*, **57**, 87 (1953).

(10) Y. Ooshika, *J. Colloid Sci.*, **9**, 254 (1954).

STUDIES ON ION EXCHANGE RESINS. XV. SELECTIVITY COEFFICIENTS OF METHACRYLIC ACID RESINS TOWARD ALKALI METAL CATIONS

BY HARRY P. GREGOR, MARY JANE HAMILTON,[1] RAMESH J. OZA[2] AND FABIAN BERNSTEIN[3]

Contribution from the Department of Chemistry of the Polytechnic Institute of Brooklyn, New York

Received May 26, 1955

The selective uptake of lithium, sodium and potassium by a series of methacrylic acid cation-exchange resins of various divinylbenzene contents was measured; the general order of preference was lithium > sodium > potassium. This preference became more marked as the degree of cross-linking increased, or as the degree of neutralization of any given resin increased. This resin behavior was compared with the association evidenced by the alkali metal acetates. Values of relative alkali metal resinate activity coefficients were compared with analogous acetate values, giving fairly good agreement. Also, integration of the Gibbs–Duhem equation for a two-component system led to a simple expression which correlated the selectivity coefficients with the DVB content of the resin and the composition of the resin phase.

A previous paper in this series[4] described the uptake by carboxylic acid cation-exchange resins of various bases from solutions of different concentrations and ionic strengths, where the *p*H of the solution phase, the absorptive capacity and the swelling of the resins were measured. This behavior was correlated with the general properties of polymeric electrolytes. This contribution describes the selective uptake of one cationic species over another by these resin systems with lithium, sodium and potassium, where the resin acid is neutralized to different degrees and coefficients measured at different temperatures.

Experimental

Procedures.—The same methacrylic acid–divinylbenzene copolymers were used in this study as in the previous one[4]; for details of the preparation and conditioning procedures the reader is referred to this earlier paper.

The practical (molal) selectivity coefficient K_d for the cation-exchange process where cation (2) is displaced from the resin phase by cation (1) originally present in the solution phase is defined as

$$K_b = K_2^1 = \left(\frac{M_1}{M_2}\right)\left(\frac{m_2}{m_1}\right)$$

where an upper case letter (M) denotes the molality of an ion in the resin phase, calculated from the water content. A lower case letter (m) is the molality of the corresponding ion in the solution phase. The relationship between K_d and the true thermodynamic equilibrium constant for the exchange processes has been described.[5]

Selectivity coefficients were determined using three similar techniques. The selective uptake of two cations from solutions of their hydroxides (potassium–lithium, Fig. 1) was measured by weighing air-dried hydrogen form resin (of known moisture content) into inert plastic bottles, adding a standard solution containing the two cations as their hydroxides, and shaking to equilibrium. A 3–4 fold excess of base over resin acid (in terms of equivalents) was used. The volume of base was sufficiently large so that errors due to water sorbed by the resin were negligible. After equilibrium, the solution phase was filtered off and analyzed for total base and also for the reference cation (potassium) by means of the flame photometer (Perkin–Elmer, Model 52 A). The distribution coefficient could then be calculated. Since only one of the competing cations in but one of the phases (solution) was determined directly, the other terms being calculated by difference, this procedure gave the least precise results and was for this reason restricted to systems where K_d was near unity and where X_K, the mole fraction of exchange cations (excluding hydrogen) in the resin phase was about 0.5. Where more accurate K_d determinations were required the total base and the potassium content of the resin were also determined. Here the exchange cations were eluted from centrifuged resin with an excess of standard hydrochloric acid. The accuracy of K_d as determined in this manner was considerably improved because two of the four concentration terms were determined directly.

Potassium–sodium exchange (Fig. 2) was measured at different *p*H levels by passing a large excess of a phosphate buffer solution containing mixtures of sodium and potassium at an ionic strength of about 0.2 through a 0.1-g. bed of resin until equilibrium was reached. The resin was rinsed quickly with a small amount of water and the cations eluted with an excess of standard acid and determined flame-photometrically.

Selectivity coefficients for resin systems at different degrees of neutralization α, defined as moles of base added per mole of resin acid (Fig. 3) were determined by shaking the hydrogen form resin with different amounts of equimolar mixtures of potassium chloride and the hydroxide of either lithium or sodium. After equilibration, the potassium content of both the resin and solution phases was determined.

All data reported are equilibrium values. Systems were shaken in every case for twice the period of time required to obtain equilibrium. Where the K_d values were very large or very small, equilibrium was approached from both directions. All experiments were carried out at room temperatures (24–26°) unless otherwise stated. The systems were kept carbonate-free. The use of inert plastic bottles eliminated errors due to sodium contamination from glass.

The accuracy of the K_d values was set by that of the flame photometric determination of potassium which was accurate to $\pm 1\%$. K_d values in the range of 0.2 to 5 were accurate to within $\pm 3\%$. When the mole fraction of potassium in the resin was low, K_d values maintained this latter accuracy, but when X_K was high (> 0.9) the K_d values were probably accurate to but $\pm 10\%$.

When two bases were used, the solution concentration was kept in the range 0.03–0.04 M; when base–chloride solutions were employed to give systems of different degrees of neutralization the concentration range was 0.01–0.05 M. In these concentration ranges the total capacity of the resins was fairly constant, although where necessary corrections were made for changes in capacity.[4] For potassium–sodium exchange the solution ionic strength was 0.2.

Results

Selectivity coefficients for the exchange of potassium with lithium (from 0.03–0.04 M solutions of their hydroxides) with different resins are shown in Fig. 1. The selective uptake of potassium meas-

(1) A portion of this work is abstracted from the thesis of Mary Jane Hamilton, submitted in partial fulfillment of the requirements for the degree of Master of Science in Chemistry, Polytechnic Institute of Brooklyn, June, 1950.

(2) A portion of this work is abstracted from the thesis of Ramesh J. Oza, submitted in partial fulfillment of the requirements for the degree of Master of Science in Chemistry, Polytechnic Institute of Brooklyn, June, 1952.

(3) A portion of this work is abstracted from the Dissertation of Fabian Bernstein, submitted in partial fulfillment of the requirements for the degree of Doctor of Philosophy in Chemistry, Polytechnic Institute of Brooklyn, February, 1952.

(4) H. P. Gregor, M. J. Hamilton, J. Becher and F. Bernstein, THIS JOURNAL, **59**, 874 (1955).

(5) H. P. Gregor and J. I. Bregman, *J. Colloid Sci.*, **6**, 323 (1951).

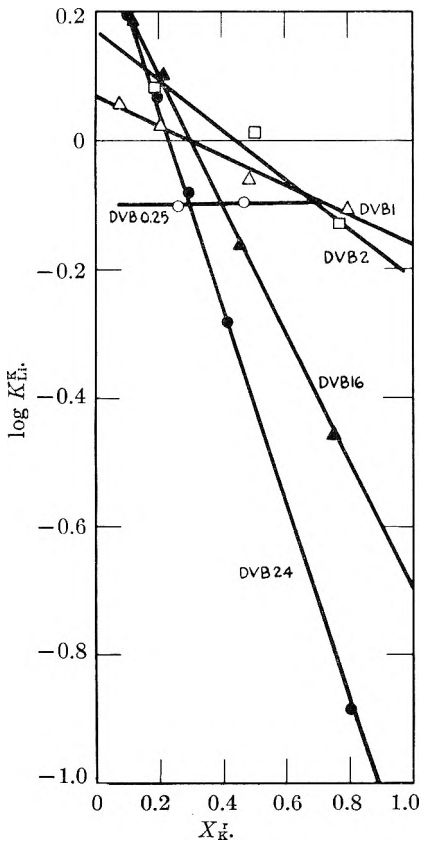

Fig. 1.—Selectivity coefficients for potassium-lithium exchange from base solutions as a function of the fraction of resin exchange sites occupied by potassium. Resins are: ○, DVB 0.25; △, DVB 1; □, DVB 2; ▲, DVB 16; ●, DVB 24.

ured against sodium from buffer solution at *p*H 7 is given in Fig. 2. Determinations were also performed at *p*H 6 and 8; at all three *p*H levels the data were substantially the same, usually within experimental error. The total capacity of the resins in the mixed potassium–sodium state was the same at the different mole fractions (X^{r}_{K}) studied, in agreement with the earlier observations that the capacity at the same degree of neutralization and ionic strength was the same to alkali metal cations.[4] At *p*H levels of 6, 7 and 8 the corresponding capacities in millimoles/g. were: DVB 0.5–6.7, 9.7, 11.5; DVB 2–4.5, 7.2, 9.2; DVB 16–1.4, 2.6, 4.6.

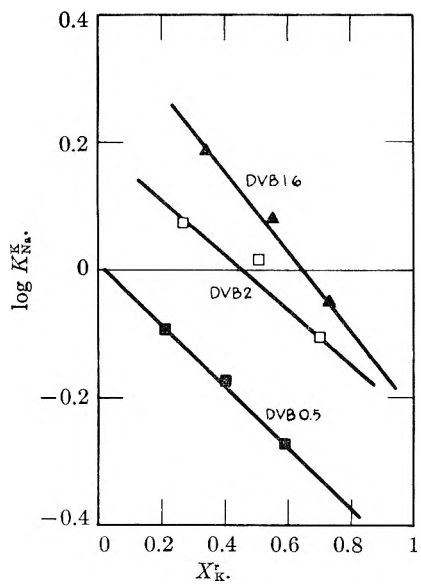

Fig. 2.—Selectivity coefficients for potassium–sodium exchange in buffered solutions at *p*H 7. Resins are: ■, DVB 0.5; □, DVB 2; ▲, DVB 16.

The selective uptake of potassium over sodium and lithium at different degrees of neutralization α of resin DVB 6 is shown in Fig. 3. Here the total concentration of the solution phase was 0.01–0.05 *M*. Values of *p*H at different degrees of neutralization were as follows: α = 0.2, *p*H 6.5; 0.4, 7.0; 0.65, 7.4; 0.85, 8.7.

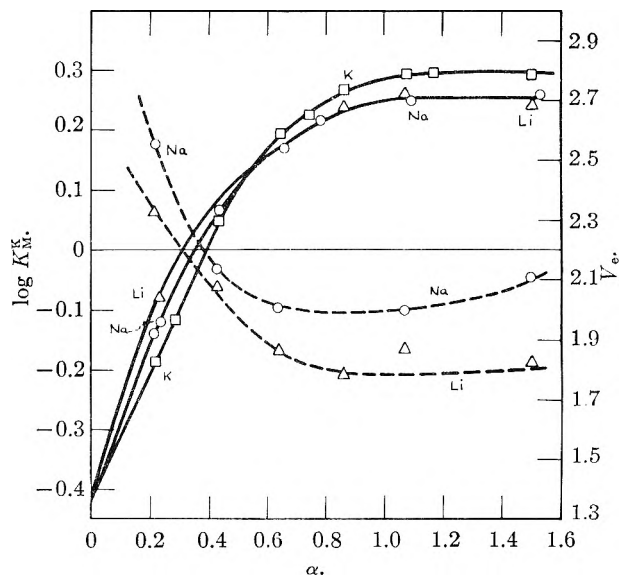

Fig. 3.—Variation of specific external volume of resin DVB 6 in alkali metal states with degree of neutralization α (right-hand ordinate), and K_d as a function of α for potassium–lithium and potassium–sodium exchange. Cations are: lithium (△), sodium (○), potassium (□); exchange, shown dotted.

The selective uptake of potassium over lithium from 0.03–0.04 *M* solutions of their hydroxides with resins DVB 0.25, 1, 2, 16 and 24 was measured at 4° in addition to the measurements at 25°. In every case no significant variation in K_d was observed, nor was any consistent trend seen to occur. Since ΔH is therefore nearly zero, one can conclude that appreciable changes in enthalpy such as those which correspond to changes in hydration of the lithium ion are not taking place, or that such changes as do occur compensate for one another as regards enthalpy contributions.

Discussion

Figure 1 shows that fully neutralized methacrylic acid resins show a low order of preference for potassium over lithium when the resin phase is rich in lithium ($X^{r}_{K} \cong 0.1$). With potassium-rich resins this preference is reversed and the resin prefers lithium over potassium to a marked degree. Further, these effects are relatively weak for resins of low degrees of cross-linking, increasing in magnitude as the cross-linking increases.

With potassium–sodium exchange (Fig. 2) the resins also show a decrease in potassium selectivity

as the mole fraction of potassium in the resin phase increases. The order of preference is low, being 2:1 or 1:2 in the range examined. Here the low cross-linked resins show the strongest preferences, that for sodium.

Figure 3 shows K^{K}_{Na} and K^{K}_{Li} for resin DVB 6 at different degrees of neutralization. At $\alpha = 0.2$ the resin prefers potassium but at $\alpha \geq 0.4$ this preference is reversed, in the order of Li > Na > K. Figure 3 also shows the swelled volumes V_e of these resins.[4] Selectivity is favored for those ions giving smaller resin volumes; this behavior is consistent with that generally observed with cation and anion-exchange systems.[5,6]

The thermodynamic equilibrium constant for potassium-lithium exchange is

$$RT \ln K_a = RT \ln \left[\left(\frac{M_K}{M_{Li}}\right)\left(\frac{\Gamma_K}{\Gamma_{Li}}\right)\left(\frac{m_{Li}}{m_K}\right)\left(\frac{A_w}{a_w}\right)^g \right] = \pi(\bar{V}_{Li} - \bar{V}_K - g\bar{V}_w)$$

where Γ_K is the single cationic activity coefficient and A_w the activity of water in the resin phase, and where g moles of water are transferred from the solution to the resin phase per mole of each cation being exchanged. As a first approximation, the solvent term and the pressure–volume term can be set equal to zero. In dilute solution phases ratios of solute molalities are nearly equal to ratios of activities; the expression above therefore considers only solution molalities. It then becomes

$$K_a = \frac{M_K \Gamma_K m_{Li}}{M_{Li} \Gamma_{Li} m_K} = K_d \frac{\Gamma_K}{\Gamma_{Li}} = 1 \text{ and } K_d = \Gamma_{Li}/\Gamma_K$$

Multiplying and dividing by the activity coefficient of the resinate (R) which is being treated here as a 1-1 electrolyte leads to the expression

$$K_d = \frac{\Gamma_{Li}\Gamma_R}{\Gamma_K \Gamma_R} = \left(\frac{\Gamma_{LiR}}{\Gamma_{KR}}\right)^2$$

where Γ_{KR} is the mean activity coefficient of the potassium resinate, etc.

K_d can then be calculated if mean activity coefficients of the resinate are known. These values are not available, but nevertheless a comparison can be made on the basis first of the assumption that the molality of a cationic species in the resin phase will vary linearly with its mole fraction. Thus if the molalities at $X^{r}_{K} = 0$ and $X^{r}_{K} = 1$ are known, the molality at any value of X^{r}_{K} can be determined. Further, it is assumed that there is little, if any, interaction between the lithium and potassium resinates. At a given molality, then, the mean activity coefficient of the alkali resinate is independent of the concentration of other resinates present. Further, it is assumed that the ratio of the mean activity coefficients of the lithium and potassium resinates may be approximated by the corresponding ratio of the mean activity coefficients of the lithium and potassium acetates.

The order of the activity coefficients of the alkali salts of the halogen acids is reversed in the alkali hydroxides and acetates. The general order for chlorides, bromides and iodides is Li > Na > K. For the acetates and hydroxides it is K > Na > Li. Harned and Owen[7] discuss this problem and suggest that the reversal is due to solvent interaction with the ions ("local hydrolysis") which results in association between anion and cation through the solvent dipole.

The data of Fig. 1 for K^{K}_{Li} can thus be explained qualitatively in terms of the assumptions made above. In Fig. 4, the mean activity coefficients of the alkali metal acetates are plotted against their molalities.[7] It can be seen that in general the values for potassium are higher, but that if the resin is largely in the lithium state, *i.e.*, the molality of lithium is large compared to potassium, $\gamma_{LiAc} > \gamma_{KAc}$ and by analogy Γ_{LiR} would be greater than Γ_{KR}. This effect would be enhanced as the total molality increases, that is, as the degree of cross-linking increases. Thus for small values of X^{r}_{K} there would be a preference for potassium, but for intermediate and large values of X^{r}_{K} there would be a cross-over and the resin would prefer lithium.

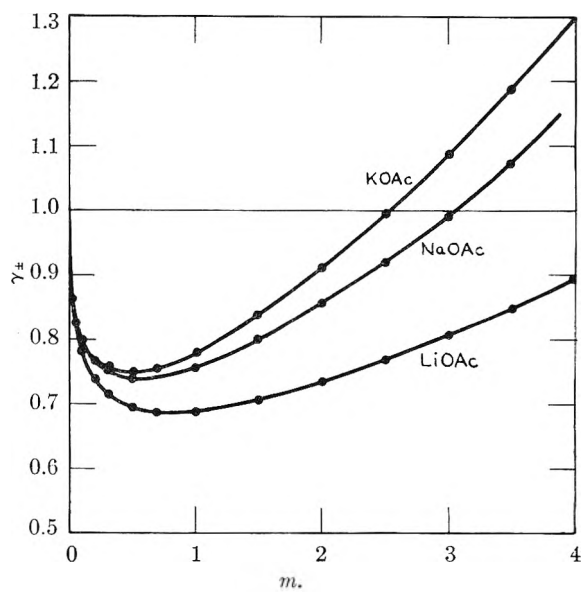

Fig. 4.—Mean molal activity coefficients of alkali acetates in aqueous solution.

In view of the assumptions made above, Table I was constructed and the K_d values for the various DVB resins compared with $(\gamma_{LiAc}/\gamma_{KAc})$.[2]

For resin DVB 1, there is essentially no agreement; K_d decreases slightly with X^{r}_{K} while $(\gamma_{LiAc}/\gamma_{KAc})^2$ increases slightly.

The data for resin DVB 2 show reasonably good agreement except that the calculated values are somewhat low; there is excellent agreement with resin DVB 16. There is also fairly good agreement with the DVB 24 data, and here the calculated values are somewhat high. With resins DVB 16 and 24 where high osmotic pressures are present, the pressure–volume term is appreciable and would make for an increased preference for lithium.

Obviously, calculations of this type are useful only for qualitative comparisons. They do show a relationship between the mean activity coefficients

(6) H. P. Gregor, J. Belle and R. A. Marcus, *J. Am. Chem. Soc.*, **77**, 2317 (1955).

(7) H. S. Harned and B. B. Owen, "The Physical Chemistry of Electrolytic Solutions," Reinhold Publ. Corp., New York, N. Y., 1950.

TABLE I

EXPERIMENTAL AND CALCULATED SELECTIVITY COEFFICIENTS FOR POTASSIUM–LITHIUM EXCHANGE

m^r_K	m^r_{Li}	X^r_K	K_d	$\frac{\gamma^2_{LiOAc}}{\gamma^2_{KOAc}}$
		DVB 1		
0.11	1.32	0.08	1.14	0.78
.29	1.11	.21	1.05	.84
.64	0.70	.48	0.87	.84
1.01	.26	.80	.79	.86
		DVB 2		
0.52	2.24	0.19	1.21	1.00
1.39	1.37	.50	1.03	0.73
2.11	0.64	.77	0.74	.56
		DVB 16		
0.55	4.33	0.11	1.54	1.53
1.03	3.72	.22	1.26	1.23
2.04	2.46	.45	0.69	0.70
3.15	1.05	.75	.35	.38
		DVB 24		
0.53	4.82	0.10	1.57	1.69
1.03	4.25	.20	1.16	1.38
1.53	3.67	.29	0.83	1.04
2.14	2.96	.42	.52	0.74
3.90	0.95	.80	.13	.29

of the alkali metal salts of polymers and their monomeric analogs. In the case of the carboxyl resins these comparisons are particularly useful because association between the exchange cation and the fixed anion appears to be the principal causative effect. The same general considerations also apply to anion-exchange processes.[6,8,9]

With sulfonic acid resins where hydration of the cation appears to be the dominant factor, comparisons of the type given above are used but have a different physical basis. The hydration of one cation obviously affects that of the other cationic species and therefore their hydrated sizes and effective molalities. It is for this reason that applications of Harned's Rule by Glueckauf[10] give good agreement. Harned's Rule has as its physical basis (in large measure) differences in hydration; an excellent discussion of the hydration theory has been given by Robinson and Stokes.[11]

While in theory one could determine osmotic coefficients for the solvent in linear and weakly cross-linked resins and use these values to calculate mean resinate activities, several theoretical difficulties supervene because of differences in the entropies of linear and cross-linked resins, as has been discussed by Gregor, *et al.*[12–15]

The assumption that simple ion-pair formation between the fixed carboxylate groups and the exchange cations is responsible here is not valid because this would lead to the prediction that K_d does not vary appreciably with X^r_K.[6] Binding of the alkali metal ions to the polymer is due in large part to the charge on the polymeric chain,[4,16] and therefore a simple ion-pair formation association constant cannot be applied.

The variation in K_d with the degree of neutralization α (Fig. 3) is consistent with the concepts just discussed. At low degrees of charge the concentration of the resinate is low (the hydrogen form resin is appreciably swelled[4]) and the charge upon the chain is also low. Therefore, specific binding does not occur to a significant degree and pressure-volume effects would determine K_d. As α increases so does specific binding. K_d becomes fairly constant at $\alpha > 1$, as expected.

It is noted from Fig. 1 that log K_d is nearly a linear function of X^r_K. A plot of log (M_K/M_{Li}) *vs.* log (m_K/m_{Li}) also gives reasonably straight lines, as expected. These plots suggest an application of the Gibbs–Duhem–Margules expressions. When the Gibbs–Duhem expression for a binary system is expanded in powers of the product of the mole fractions X_1X_2, the higher members of the series discarded and the expression integrated,[17] a simple relationship between the activity (a) of each component and its mole fraction in terms of a common constant β is obtained. The expression

$$X_1 \frac{d \ln a_1}{dX_1} = \alpha + \beta X_1(1 - X_1)$$

upon integration becomes

$$\ln a_1 = \alpha \ln X_1 + \beta X_1 - \beta X_1^2/2 + \text{constant}$$

At $X_1 = 1$, $a_1 = a_1^0$, and evaluating the constant of integration one obtains

$$\ln a_1 = \alpha \ln X_1 + \ln a_1^\circ - \frac{\beta}{2}(X_1^2 - 2X_1 + 1)$$

For an ideal system β must be zero and the expression becomes $a_1 = X_1^\alpha a_1^0$. Therefore, $\alpha = 1$. Then

$$a_1 = X_1 a_1^\circ \exp\left[-\frac{\beta}{2}(1 - X_1)^2\right]$$

If the resin phase is now treated as a binary system composed of potassium and lithium resinates with the pure resinates taken as the reference states ($\Gamma^0 = 1$), their activities become

$$\frac{A_K}{A_{Li}} = \frac{A_K^\circ}{A_{Li}^\circ}\frac{X_K}{X_{Li}} \exp\left[-\frac{\beta}{2}(1 - 2X_K)\right]$$

Since $A_K = X_K\Gamma_K$

$$\log \frac{\Gamma_K}{\Gamma_{Li}} = -\log B + k(1 - 2X_K) = -\log K^K_{Li}$$

where the constant $B = A^0_{Li}/A^0_K$. This latter expression is similar in form to Harned's Rule. Then the relationship between K^K_{Li} and X_K is

$$\log K^K_{Li} = \log K_d = \log B + p(1 - 2X_K)$$

If log K^K_{Li} is plotted against $(1 - 2X_K)$ excellent

(8) H. P. Gregor, *J. Am. Chem. Soc.*, **73**, 3537 (1951).
(9) H. P. Gregor, J. Belle and R. A. Marcus, *ibid.*, **76**, 1984 (1954).
(10) E. Glueckauf, *Proc. Roy. Soc.* (*London*), **A214**, 207 (1952).
(11) R. A. Robinson and R. H. Stokes, *Ann. N. Y. Acad. Sci.*, **51**, 573 (1949).
(12) H. P. Gregor, *J. Am. Chem. Soc.*, **73**, 642 (1951).
(13) H. P. Gregor, B. R. Sundheim, K. M. Held and M. H. Waxman, *J. Colloid Sci.*, **7**, 511 (1952).
(14) H. P. Gregor, M. H. Waxman and B. R. Sundheim, THIS JOURNAL, **57**, 969 (1953).
(15) H. P. Gregor and M. Frederick, *Ann. N. Y. Acad. Sci.*, **57**, 87 (1953).
(16) J. R. VanWazer and D. A. Campanella, *J. Am. Chem. Soc.*, **72**, 655 (1950).
(17) A. W. Porter, *Trans. Faraday Soc.*, **16**, 336 (1920).

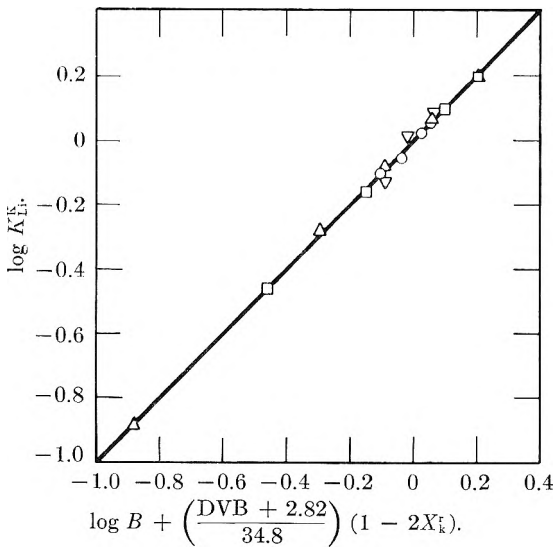

Fig. 5.—Plot of expression $\log K_{Li}^{K} = \log B + [(\text{DVB} + 2.82)/34.8](1 - 2X_K^r)$ showing fit of experimental points for potassium–lithium exchange. The resins are: ○, DVB 1; ▽, DVB 2; □, DVB 16; △, DVB 24.

straight line relationships are obtained, similar to Fig. 1. Values of B and p can be calculated from this plot, and it is found that the p's are linear function of the percentage cross-linking. Therefore the relationship DVB = $ap + b$ was postulated and values of a and b determined from a plot of DVB *vs.* p are: $a = 34.8$; $b = -2.82$. The final expression relating K_{Li}^{K} and X_K^r is

$$\log K_{Li}^{K} = \log B + \left(\frac{\text{DVB} + 2.82}{34.8}\right)(1 - 2X_K^r)$$

Figure 5 shows a plot of this function with all experimental points.

This simple expression therefore allows one to express the selectivity coefficient as a function of the mole fraction in terms of a parameter B which is itself a function of the DVB content. The values of B are: DVB 1, 0.91; DVB 2, 0.96; DVB 16, 0.63; DVB 24, 0.39. This latter expression is useful as a means of expressing a group of related data; there is no basis at this time for assigning physical parameters to the various contents.

This investigation was supported in part by the Office of Naval Research, and in part by a research grant RG-2934 from the Division of Research Grants of the National Institutes of Health, Public Health Service.

KINETICS OF LUMINESCENCE QUENCHING IN LIQUID SCINTILLATORS

BY B. LIONEL FUNT AND EDWARD NEPARKO[1]

Contribution from the Department of Chemistry, University of Manitoba, Winnipeg, Manitoba, Canada

Received July 18, 1955

The kinetics of luminescence quenching in liquid scintillator solutions containing dissolved oxygen have been studied. A mechanism is postulated which is in good agreement with the experimental data for the eight systems reported. The experimental rate constants have been compared with rates of collision obtained from simple kinetic theory. Such a comparison indicates an extremely efficient collisional mechanism with almost every collision effectively deactivating the solute molecule.

It is now well established that traces of dissolved oxygen decrease the luminescence of liquid scintillator solutions.[2] The mechanism of the process, however, has not been clearly demonstrated, and the magnitude of the quenching effects recently has been questioned.[2b]

Studies of fluorescence quenching under ultraviolet excitation also show that oxygen acts as an efficient quenching agent.[3,4] Bowen[4] has suggested that studies of the kinetics of such systems were of considerable theoretical interest since the quenching process can be considered typical of fast reaction in which most collisions are effective.

A detailed study of the kinetics of oxygen quenching in liquid scintillator solutions, therefore, appeared warranted in order to test and establish the validity of some of the previous experimental data and to investigate the theoretical basis of the quenching process.

By analogy to the Stern–Volmer equation and its modifications used by Bowen, the following mechanism was postulated

$$\begin{aligned}
&S + h\nu \longrightarrow S^* && k_T && (1)\\
&S^* \longrightarrow S && k_D && (2)\\
&S^* + M \longrightarrow S + M^* && k_E && (3)\\
&M^* \longrightarrow M + h\nu' && k_f && (4)\\
&M^* + Q \longrightarrow M + Q && k_q && (5)
\end{aligned}$$

Hence

$$F_0/F - 1 = \frac{F_0 - F}{F} = F_{rel} = \frac{k_q}{k_f} Q = KQ \quad (6)$$

where S represents solvent molecule; M, solute; Q, quencher; K, the quenching constant; F_0, the luminescent output in the absence of quencher, and F, the luminescent output in the presence of quencher. The transfer steps from solvent to solute have been added in accordance with the present theories of the energy transfer process in liquid scintillator solutions.[5-11] They do not, however,

(1) Holder of National Research Council of Canada Scholarship.

(2) (a) R. W. Pringle, L. D. Black, B. L. Funt and S. Sobering, *Phys. Rev.*, **92**, 1582 (1953); (b) D. G. Ott, F. N. Hayes, J. E. Hammel and J. F. Kephart, *Nucleonics*, **13**, 62 (1955).

(3) E. J. Bowen and W. S. Metcalfe, *Proc. Roy. Soc. (London)*, **206A**, 437 (1951).

(4) E. J. Bowen, *Trans. Faraday Soc.*, **50**, 97 (1954).

(5) H. Kallmann and M. Furst, *Phys. Rev.*, **79**, 857 (1950).

(6) H. Kallmann and M. Furst, *ibid.*, **81**, 853 (1951).

(7) H. Kallmann and M. Furst, *ibid.*, **85**, 816 (1952).

(8) M. Furst and H. Kallmann, *ibid.*, **94**, 503 (1954).

(9) R. K. Swank, *Ann. Rev. Nucl. Sci.*, **4**, 111 (1954).

(10) R. K. Swank and W. L. Buck, *Phys. Rev.*, **91**, 927 (1953).

(11) E. J. Bowen and R. Livingston, *J. Am. Chem. Soc.*, **76**, 6300 (1954).

change the form of the resultant equation[6] from that obtained by the Stern–Volmer mechanism.[12] It should be noted that k_f is the reciprocal of the mean life of the luminescent molecule, and its value may be measured directly by appropriate fast circuitry.

Experimental

Apparatus.—The liquid scintillator solution was placed in a flat bottomed cylindrical cell, of 25 mm. o.d., 100 mm. length provided with a stopcock. This cell was degassed by alternate freezing and thawing on a vacuum line. A minimum of four freezing and thawing cycles was found sufficient for the removal of dissolved gases. The evacuated cell was then allowed to return to room temperature and increments of oxygen were introduced by a low pressure gas buret system.

The pulse height of the resultant solution was then determined relative to an anthracene crystal of the same weight. For this purpose, the cell was mounted on an EMI No. 1361 V × 5055 photo tube and was excited by a Cs^{137} source. The pulses were fed to an Atomic Instrument No. 204C amplifier, and thence to a Dynatron N/101 pulse analyzer, and finally to an Atomic Instrument 162-A glow transfer counter. The variation of luminescent output with oxygen concentration was thus determined.

Chemicals.—Scintillation grade chemicals obtained from the Arapahoe Chemical Company were used without further purification. These were *p*-bis-(2,5-phenyloxazolyl-benzene) (POPOP),[13] phenylbiphenylyloxadiazole-1,3,4 (PBD), 2,5-diphenyloxazole (PPO), *p*-diphenylbenzene (*p*-terphenyl), 2-(naphthyl)-5-phenyloxazole (NPO). Eastman Kodak Co. reagent grade xylene, *p*-xylene and toluene were employed.

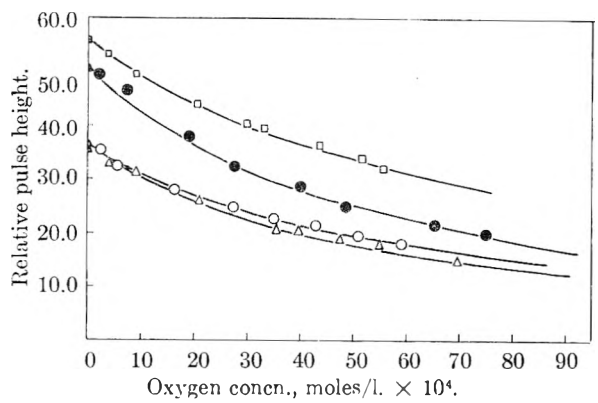

Fig. 1.—Variation of luminescent output with oxygen concentration. Solid curve calculated from equation 6. Experimental points as follows: □, xylene 4 g./l. PBD; ●, *p*-xylene 4 g./l. terphenyl, 0.1 g./l. POPOP; ○, xylene 6 g./l. terphenyl; △, *p*-xylene 4 g./l. terphenyl.

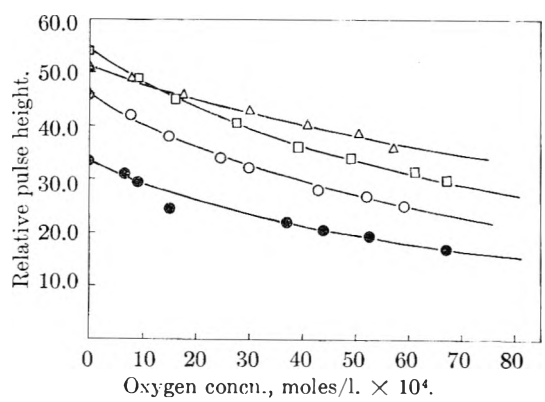

Fig. 2.—Variation of luminescent output with oxygen concentration. Solid curve calculated from equation 6. Experimental points as follows: △, toluene 8 g./l. PBD; ●, toluene 5 g./l. terphenyl; □, toluene 4 g./l. PBD; ○, toluene 5 g./l. terphenyl, 0.1 g./l. PPO.

(12) O. Stern and M. Volmer, *Phys. Z.*, **20**, 183 (1919).

(13) F. N. Hayes, C. R. Rogers and D. G. Ott, *J. Am. Chem. Soc.*, **77**, 1850 (1955).

Results

The variation of luminescent output as a function of oxygen concentration is shown in Figs. 1 and 2. The pulse height data were determined relative to an anthracene crystal of the same weight and are expressed as percentages on the anthracene scale. The geometry of the liquid scintillator cells did not provide a very effective means of light collection. Although powdered MgO reflectors were used, the absolute pulse height efficiencies were slightly lower than those obtained with wider and shorter cells of the same volume. Since the same geometry was used throughout this work, the relative pulse heights are comparable and the advantages of the longer cylindrical cells in the vacuum procedure compensated for their poorer light collection properties.

Figures 1 and 2 show the magnitude of the oxygen quenching effect in a number of commonly employed liquid scintillator solutions. It should be noted that the *curves are the theoretical curves obtained from equation 6.* whereas the points represent experimentally determined values. The variation of the points about the curve is within experimental error, and represents extremely good agreement with the postulated mechanism for the quenching reaction. The value of F_0 for equation 6 was determined from the relative pulse height efficiency of the evacuated solution. The nitrogen bubbling procedure previously described,[2a] yields exactly the same value for this point.

Plots of the relative luminescent efficiency $(F_0 - F)/F$ *versus* oxygen concentration are shown in Fig. 3. Excellent agreement is obtained with a linear relationship in quencher concentration as predicted by equation 6.

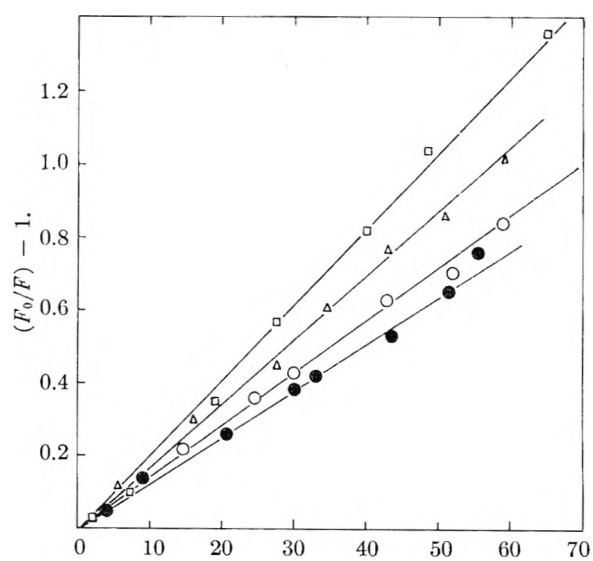

Fig. 3.—Linear plots of relative light output as a function of oxygen concentration: □, *p*-xylene 4 g./l. terphenyl; 0.1 g./l. POPOP; △, xylene 6 g./l. terphenyl; ○, toluene 5 g./l. terphenyl; 0.1 g./l. PPO; ●, xylene 4 g./l. PBD.

The slopes of eight lines, four of which are shown in Fig. 3, have been used to determine values of the

TABLE I

RATE CONSTANTS FOR LUMINESCENCE QUENCHING

1 Solutions	2 Quenching constant, $K = k_q/k$	3 $k_q = K/\tau$	4 Molar concn. for 10% quenching	5 Collisions per 2×10^{-9} sec.
p-Xylene 4 g./l. terphenyl 0.1 g./l. POPOP	210	1.05×10^{11}	5×10^{-4}	0.2
p-Xylene 4 g./l. terphenyl	213	1.07×10^{11}	5×10^{-4}	.2
Xylene 4 g./l. PBD	132	6.6×10^{10}	9×10^{-4}	.4
Xylene 6 g./l. terphenyl	175	8.8×10^{10}	6×10^{-4}	.1
Toluene 8 g./l. PBD	68	3.4×10^{10}	1.5×10^{-3}	.6
Toluene 4 g./l. PBD	125	6.3×10^{10}	8×10^{-4}	.4
Toluene 5 g./l. terphenyl	141	7.1×10^{10}	7×10^{-4}	.2
Toluene 5 g./l. terphenyl 0.1 g./l. PPO	143	7.2×10^{10}	8.5×10^{-4}	.2

quenching constants K shown in Table I, and for the calculation of the theoretical curves for Figs. 1 and 2.

If one assumes an average value of 2×10^{-9} seconds[9] for the liquid scintillator solutions, it is possible to calculate k_q from the relationship $k_q = K/\tau$ for the systems reported here. The values of k_q are tabulated in Table I.

Self quenching effects have not been considered in this work, and the values of k_q vary with the concentration of the primary solute. Studies of self quenching for several of the primary solutes, have, however, been reported.[5-7]

The magnitude of air quenching can be estimated from the F_{rel} values corresponding to O_2 solubility in the solvent at its partial pressure. In xylene, the solubility is approximately 1.4×10^{-3} M at 18°. It can be seen from Figs. 1 and 2 that the relative decreases in luminescent output at this concentration are not constant for the various solutions investigated.

The solubility figures given by Ott, *et al.*,[2b] are lower due to the lower partial pressure of O_2 at Los Alamos.

An insight to the molecular mechanisms involved can be obtained from a calculation of the effectiveness of collisions between solute and quencher molecules. For such a comparison, one may arbitrarily select a molar concentration for 10% quenching[14] ($F/F_0 = 0.9$) and calculate from simple kinetic theory the number of collisions between solute and quencher molecules that will occur within the lifetime of the excited solute molecule. For these calculations collisional cross sections of 2, 5, 6 and 8 Å. were assumed for oxygen, terphenyl, PPO and PBD, respectively. A comparison of encounter frequency and collision frequency in fluorescent solutions has been presented by Bowen.[4,14] For the purposes of the present analyses the gas collision frequency was deemed sufficient to indicate the magnitude of the quenching process. The relevant quantities are given in columns 4 and 5 of Table I. The data show that for 10% quenching between 0.1 and 0.6 collision occurs between a given solute molecule and oxygen molecule in 2×10^{-9} second. For 50% quenching, the values are ten times as great, and between 1 and 6 collisions occur between an activated molecule and the quencher molecule within its lifetime.

If one considers the encounter theory of repeated collisions between adjacent molecules in a liquid the limiting value of k_q in quenching[4] is $k_q = 8RT/3000\eta$.

For xylene this yields a value of 1×10^{10} which agrees reasonably with the experimental results listed in Table I.

These data show that the quenching process is characterized by an extremely efficient collisional mechanism, in which almost every bimolecular collision is effective in robbing the activated solute molecule of its excess energy. Kinetic studies of fluorescent solutions have yielded the same conclusion and, in fact, it would appear that such work may be the means of shedding further light on the general problem of bimolecular collisions in the liquid state.[4]

The authors are indebted to the National Research Council of Canada for a grant in aid of this work and for scholarship aid to E.N.

(14) E. J. Bowen and F. Wokes, "Fluorescence of Solutions," Longmans, Green, New York, N. Y., 1953.

FLOW PROPERTIES OF ALUMINUM DILAURATE-TOLUENE GELS

BY NEILL WEBER AND WALTER H. BAUER

Department of Chemistry, Walker Laboratory, Rensselaer Polytechnic Institute, Troy, N. Y.

Received August 2, 1955

Flow properties of aluminum dilaurate in toluene gels at 25° have been studied in a pressure capillary viscometer over a range of mean rate of shear from 10^{-3} to 10^{+6} cm.$^{-1}$. Flow curves, mean rate of shear *versus* wall shearing stress, obtained for gels of 1, 2, 3, 5% weight per cent. soap in toluene, showed three types of flow. A region of Newtonian flow with high viscosity was found at shear rates below 10^{-2} sec.$^{-1}$. When a critical shear stress range was exceeded, the shear rate rapidly increased with small increase in shear stress. At shear rates above 100 sec.$^{-1}$, a third regime of flow was found, in which a plot of log shear rate *versus* log shear stress approached a constant slope, always greater than unity, and the flow curve was a very marked function of the length to radius ratio of the capillary used. The shear modulus of elasticity and the viscosity were measured for 2, 3 and 5% weight per cent. soap in toluene gels at shear rates below 10^{-2} sec.$^{-1}$.

Systems of aluminum soaps dispersed in hydrocarbon solvents exhibit a wide variety of rheological properties, ranging from those characteristic of inelastic fluids in dilute dispersions to those typical of plastic solids in gels of high soap concentration. Studying the flow properties of aluminum soap dissolved in gasoline, Carver and Van Wazer[1] showed the presence of a structure affecting flow which was partially destroyed under shear and restored after rest. They interpreted their results to show a yield value for extension, but there was no Bingham yield value. Goldberg and Sandvik,[2] measuring elastic constants for aluminum soap gels in Varsol, found that the dynamic viscosity and the elastic shear modulus were functions of the rate of shear. Complete recovery of the original elastic properties was found after a period of rest. Dilute solutions of aluminum soaps in benzene were found by Alexander and Gray[3] to show streaming birefringence under low rates of shear. The viscosity, double refraction, and extinction angle were measured at various rates of shear. Garner, Nissan and Wood,[4] studying gels of aluminum stearate in petrol, found that the apparent viscosity at different rates of shear was at first constant. Above a value of one for the rate of shear, the viscosity began to decrease, reaching another approximately constant value at very high rates of shear in a capillary viscometer. Unusually large inlet end effects were found when the flow of the gels in pipes was studied. It is thus apparent that various regions of flow are exhibited by hydrocarbon gels of aluminum soaps, according to the range of rate of shear, the applied shearing stress, and the concentration of the soap used. In any attempt to correlate the structure of the aluminum soap polymers and the nature of the parent fatty acid with the flow properties of soap–hydrocarbon gels, it is thus necessary to study the flow properties in instruments in which rates of shear may be varied over very wide ranges. For the purposes of this investigation, therefore, a capillary viscometer was constructed, so that a very wide range of flow rate might be studied in a single capillary if desired. In order to provide a basis for comparison, a study of the flow properties of aluminum hydroxydilaurate gels in toluene was undertaken. Although this investigation was conducted at 25°, toluene was chosen so that measurements subsequently could be made at lower temperatures.

(1) E. K. Carver and J. R. Van Wazer, THIS JOURNAL, **51**, 751 (1947).

(2) H. Goldberg and O. Sandvik, *Anal. Chem.*, **19**, 123 (1947).

(3) V. R. Gray and A. E. Alexander, THIS JOURNAL, **53**, 9 (1949).

(4) F. H. Garner, A. H. Nissan and G. F. Wood, *Phil. Trans. Roy. Soc.*, **243**, 37 (1950).

Experimental

Materials.—Aluminum hydroxydilaurate was prepared as previously described.[5] Aluminum analysis showed that the ratio of moles of fatty acid per mole of aluminum was 1.98 to 1.99 in successive lots of 100 g. prepared. Infrared absorption measurements showed no free fatty acid. Toluene, Eimer and Amend reagent grade, was shaken successively with sulfuric acid, mercury and sodium The toluene was then distilled through a column packed with glass helices, and a fraction was used which boiled at 110.7° and 765 mm.

Gel Preparation.—In the preparation of aluminum dilaurate–toluene gels, weighed portions of soap, dried over phosphorus pentoxide, were added to measured weights of toluene in jars which were then sealed. The suspension of soap and toluene was shaken manually until gelation had proceeded to a stage at which elastic properties had developed and the settling rate of particles was slow. The gels were then transferred to anodized aluminum storage tubes, fitted with vapor tight caps. The operations described were carried out in a box with an atmosphere dried by phosphorus pentoxide. It was found to be very important to avoid the absorption of water by the soap during gel preparation. The storage tubes containing the gel samples were placed in a rotating mount and aged for 24 hours at 55°, in order to ensure uniformity and to complete the dispersion of the soap. Before flow measurements were made, gels were stored for 48 hours at the operating temperature. Gels prepared in this manner were reproducible and showed no change in flow properties in a 3-month period, in the range of 1 to 8% soap by weight.

Flow Measurement—Capillaries.—In the measurement of flow rates, fourteen capillaries were used, having lengths varying from 2.9 to 37.8 cm., and diameters varying from 0.0203 to 0.0643 cm.

Capillary Viscometer.—A capillary viscometer was constructed with a removable base containing a standard-taper opening for receiving a capillary tube. A metal head of the same taper was cast on each of the viscometer capillary tubes, which were thus interchangeably mounted flush with the surface of the base plate. Viscometer body cylinders, 1.5″ in diameter and 10″ long, with closely fitted, but freely sliding pistons were constructed of stainless steel. The cylinders, provided with gas tight caps, were loaded with gel and stored at the test temperature. When flow measurement was to be made, a piston was inserted in the loaded viscometer cylinder, which was then fitted with a base plate carrying a capillary tube. Air entrapped was allowed to escape through a valve in the piston which rested on the gel. The viscometer tube was mounted vertically and connected through a port to a large reservoir of compressed nitrogen which provided constant driving pressures. The volume rate of flow of the gel through the capillary was calculated from the rate of descent of the piston and its cross-sectional area. For measurement of the movement of the piston, a rod, having finely turned grooves at regular intervals, was fastened to the piston, projecting vertically upward, travelling in a thick-walled glass tube mounted in the head cover

(5) W. W. Harple, S. E. Wiberley and W. H. Bauer, *Anal. Chem.*, **24**, 635 (1952).

plate. As the piston moved when the viscometer was operated, the grooves in the rod affected the intensity of a light beam directed through the guide tube to a photo cell. A Dumont 304-A oscillograph with a Fairchild F26A recorder camera was used to monitor the output of the photo tube.

The driving pressure was measured either by a Bourdon gage at the nitrogen input port or by a capacitance gage in contact with the gel below the piston. The direct current output from a link coupled oscillator and power supply of the capacitor gage was fed into an oscilloscope, and the resulting pressure trace was visibly observed or photographed. The gage, previously described,[6] was converted for use in the range of 0 to 15 lb./sq. in. by reduction of the diaphragm thickness. The pressure applied was usually measured by the Bourdon gage, because it was found that there was no significant pressure loss over the piston under any operating condition. The whole viscometer was housed in an Aminco constant temperature air cabinet, in which the temperature was regulated to 25 ± 0.1°.

Flow rates for which the mean rates of shear were less than 100 sec.$^{-1}$ were measured in a separate apparatus, similar to that described by Bingham and Robertson.[7] Movement of the gel meniscus in a capillary tube partially filled with gel from a reservoir was observed with a cathetometer, or the efflux from the tube was weighed to determine very small flow rates.

Calibration of Viscometer Tubes.—Pyrex capillary tubes showing minimum deviations of the bore from that of a circular cylinder were selected. Uniformity of the bore was checked by measurements of the length of a mercury drop moved along the length of the capillary tube. The assembled viscometer was calibrated with a National Bureau of Standards oil L-13, 0.8213 poise viscosity at 25°, using capillaries whose length to radius ratio varied from 1021 to 208.

From the flow rates, the driving pressures corrected for kinetic energy, and the measured dimensions of the capillary tubes used, shear stresses were calculated for values of wall rate of shear from 1×10^3 to 3×10^4 sec.$^{-1}$. When the shear stresses were plotted *versus* the rates of shear obtained, all points fell on a straight line through the origin. The viscosity for the NBS L-13 oil obtained from the slope of this plot was 0.823 at 25.0°. At constant driving pressure, a uniform flow rate of gel was rapidly established and maintained as the driving piston moved down the viscometer body cylinder.

Experimental Results

The results of flow measurements on 1, 2, 3 and 5% by weight aluminum dilaurate gels in toluene are shown in Fig. 1. From the mean driving pressure, P, corrected for kinetic energy losses, and the flow rate, Q, the maximum shearing stress at the wall, τ, and the mean rate of shear, D, were calculated. For flow of gel in a capillary of length L and radius R, the following relations were used

$$\tau = \frac{RP}{2L} \quad \text{and} \quad D = \frac{4Q}{\pi R^3}$$

In the region in which the rate of shear, D, exceeded approximately 100 sec.$^{-1}$ flow rates were determined in a series of capillaries of various length to radius ratios. At low rates of shear, the flow curve was found to be independent of the capillary length to radius ratio.

Flow data were also obtained with a series of capillaries for gels of 1, 2, 4, 5 and 8% aluminum dilaurate in toluene, in the region of shear rate through which marked dependence of the flow on the length to radius ratio of the capillary was found. The results are plotted in Fig. 2. Flow was observed after a sufficient lapse of time for all gels, even under the lowest shear stresses applied.

(6) F. Bellinger, *et al.*, *Ind. Eng. Chem.*, **38**, 164 (1946).

(7) E. C. Bingham and J. W. Robertson, *Kolloid Z.*, **47**, 1 (1929).

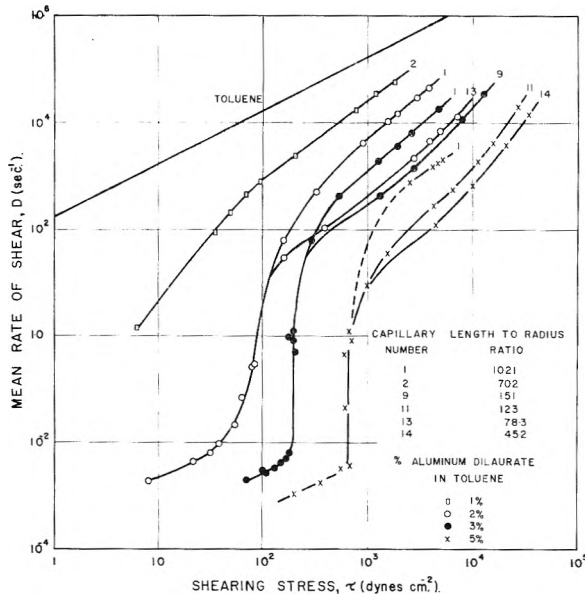

Fig. 1.—Capillary flow curves for aluminum dilaurate in toluene gels at 25°.

In order to obtain data from which a modulus of elasticity could be calculated, measurements of initial axial extension of gel in a capillary under suddenly applied stresses were made. Results for gels of 2% by weight aluminum dilaurate in toluene are shown in Fig. 3 in which axial extension is plotted as a function of time. Flow of the gel occurred after an initial extension at the various constant shearing stresses, τ, indicated, followed by a rapid initial elastic return in those cases when the stress was suddenly released.

Discussion

Three distinct regimes of flow are shown by the aluminum soap–toluene gels. Below the mean rate of shear of 10^{-2} sec.$^{-1}$, the 2% soap gel, for instance, flows as a Newtonian liquid of very high viscosity, 4.8×10^3 poise, under shearing stresses up to 40 dynes cm.$^{-2}$. In the range of shearing stress of from 40 to 100 dynes cm.$^{-2}$, the rate of shear rapidly increases, as if a yield value had been exceeded. When the shear rate is greater than 100 sec.$^{-1}$, a third type of flow is shown, in which the flow curve, log D *versus* log τ, approaches a constant slope, always greater than unity, behavior typical of systems exhibiting shear rate thinning. The unusual dependence of the flow curve on capillary length to radius ratio shown in this region results from abnormally high inlet losses, similar to those reported by Garner, Nissan and Wood[4,8] for flow of aluminum soap–hydrocarbon gels in capillaries and pipes. Such losses may be ascribed to capillary entrance work arising from the partial disruption of a network formed by the association of the rigid linear soap polymer units postulated by Ludke.[9]

The fraction of the total flow work performed which is expended at the capillary entrance diminishes as the L/R ratio increases, since the apparent shearing stress, Fig. 4, required to maintain a fixed

(8) G. F. Wood, A. H. Nissan and F. H. Garner, *J. Inst. Petroleum*, **33**, 71 (1947).

(9) W. O. Ludke, S. E. Wiberley, J. Goldenson and W. H. Bauer, THIS JOURNAL, **59**, 222 (1955).

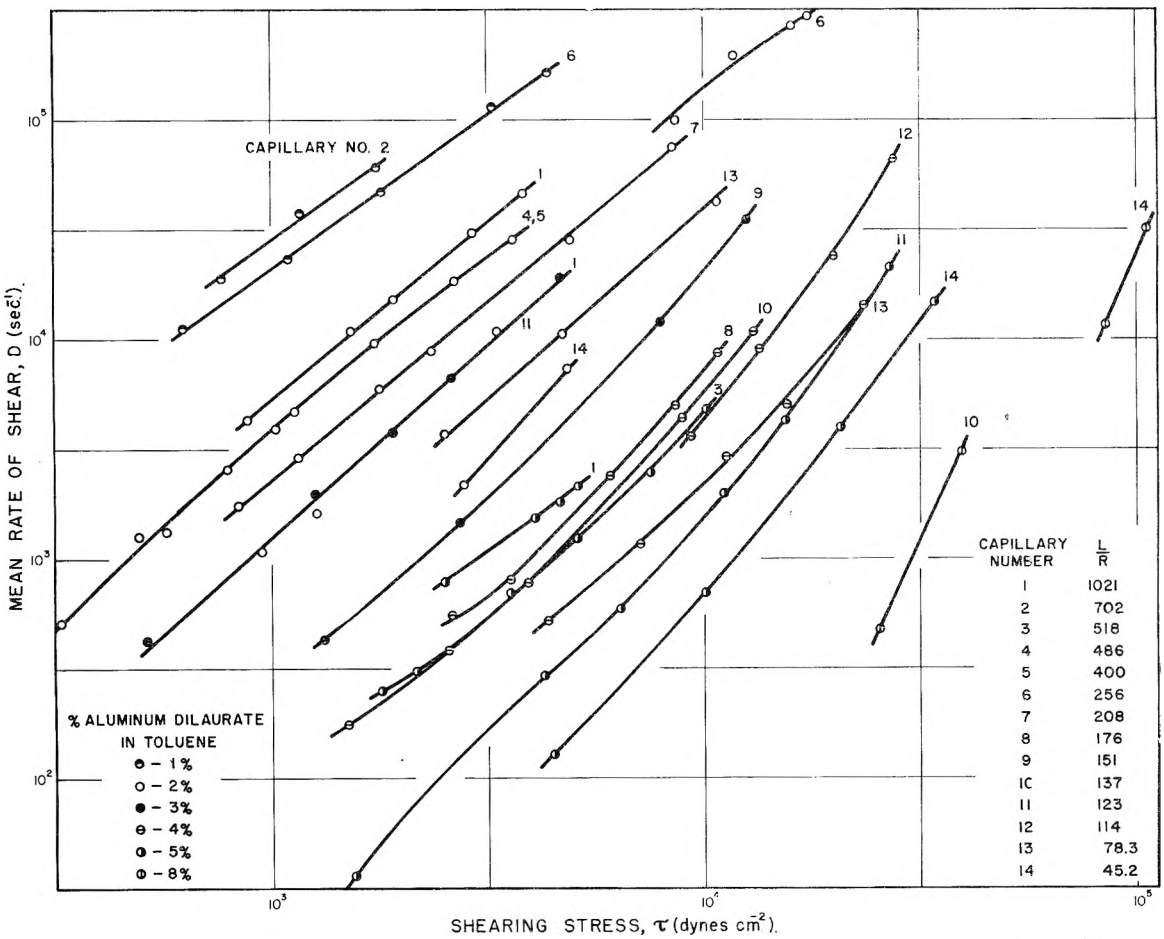

Fig. 2.—Effects of capillary length to radius rate L/R and soap concentration on flow curves of aluminum dilaurate in toluene at 25°.

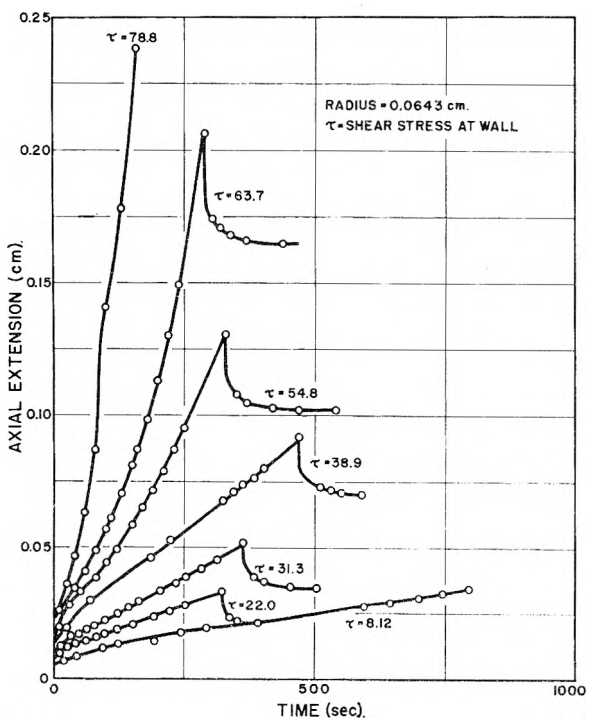

Fig. 3.—Axial extension of 2% by weight aluminum dilaurate in toluene at various rapidly applied constant wall shear stresses, at 25°. Shearing stress was suddenly removed after a time interval for τ = 63.7, 54.8, 38.9, 31.3 and 22.0 cm.$^{-1}$.

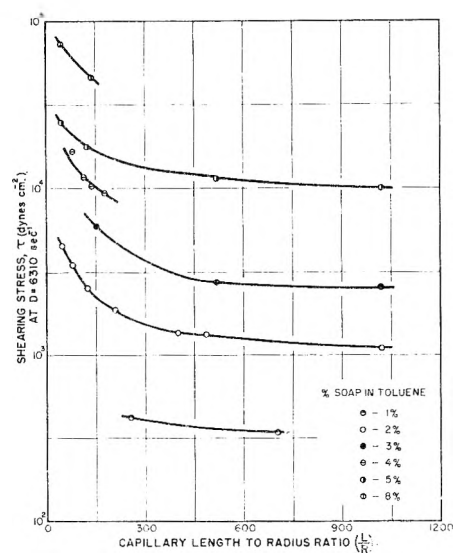

Fig. 4.—Shear stress at constant mean rate of shear, D = 6310 sec.$^{-1}$ *versus* capillary length to radius ratio, for aluminum dilaurate in toluene gels at 25°.

rate of shear approaches a constant value as L/R increases. This is in agreement with the results of Carver and Van Wazer,[1] who found that the shearing stress measured at constant rate of shear fell off similarly as strain increased, finally approaching a constant value.

As shown in Fig. 3, when various small constant

pressures were rapidly applied to a reservoir of gel connected to a volume of gel in a partially filled capillary, a rapid initial elastic axial extension took place followed by slow flow of the gel along the tube. When the applied stress was suddenly relieved, a rapid initial axial return was observed, not ascribable to surface tension effects. The initial axial extension for each suddenly applied stress was obtained by extrapolation of the curve of axial extension *versus* time to zero time. Thus initial axial extensions, L_A, were obtained, from which an instantaneous elastic modulus, G, was calculated[7] from the relation

$$G = \tau R/2L_A$$

where τ is the shear stress at the wall, and R is the capillary radius. For those gels which showed a constant ratio of τ/D at shear rates below 100 sec.$^{-1}$, in the region of Newtonian flow, viscosities were calculated. Results of the determination of elastic moduli and viscosities are given in Table I.

TABLE I

ELASTIC AND VISCOUS PROPERTIES OF ALUMINUM DILAURATE-TOLUENE GELS

Wt. % soap in gel	Shear modulus of elasticity, dynes cm.$^{-2}$	Viscosity, poise $\times 10^{-3}$
2	95	4.8
3	380	39
5	1300	184

Pronounced elastic properties and high low rate of shear viscosity appear abruptly in the gels as the concentration of soap is increased when a concentration of 1% by weight of aluminum dilaurate in toluene is reached. Evidently at this critical concentration, the soap polymer particles are sufficiently large and close that interaction leading to a three dimensional structure becomes important.

The viscosity of 4800 poise shown by the 2% aluminum dilaurate in toluene gel at shear rates below 100 sec.$^{-1}$ is in marked contrast with the apparent viscosity of 0.083 given by the ratio of τ/D when a mean rate of shear of 4.6×10^4 sec.$^{-1}$ is reached. When it is considered that for the 2% aluminum dilaurate gel in toluene the measured ratio of τ/D varies by an order of magnitude of 10^5, and that three distinct ranges of flow are found in a single capillary as the rate of shear changes from 10^{-3} to 10^5 cm.$^{-1}$, it is clear that for correlation of soap structure with flow properties of derived gels,[10] instruments allowing very wide range of shearing stresses are required. A capillary viscometer such as the one described in this report, in which a single capillary tube may be used to cover the whole range of measurement if desired, offers many advantages when comparisons of flow properties of various materials is desired.

Acknowledgment.—Acknowledgment is made to the Koehler Instrument Company, Jamaica, N. Y., for advice and assistance in the construction of the viscometer used in this study. This work was conducted under contract between the Chemical Corps, U. S. Army, and Rensselaer Polytechnic Institute.

(10) L. Finkelstein, THIS JOURNAL, **52**, 1460 (1947).

CRYSTAL STRUCTURE OF γ-AlOOH AND γ-ScOOH

BY W. O. MILLIGAN AND J. L. MCATEE

Department of Chemistry, The Rice Institute, Houston, Texas

Received August 4, 1955

The unit structure, space group symmetry and detailed atomic arrangement of γ-AlOOH (bohmite) and γ-ScOOH have been determined. The unit structure is orthorhombic end-centered on (100) and the most probable space group is D_{2h}^{17}-Amam.

Bohmite, γ-AlOOH, has been found to exist in nature[1,2] and may be prepared in the laboratory in a variety of ways.[3-6] From the close similarity of the powder X-radiograms of bohmite and the mineral lepidocrocite, γ-FeOOH, it has been concluded that the structures are analogous.[7,8] The existence of the closely related compound γ-ScOOH has clearly been established by X-ray diffraction and dehydration isobaric studies,[9-11] but quantitative X-ray studies have not been made.

There are two crystalline modifications of the monohydrate of aluminum oxide with the formula AlOOH. The modification corresponding to diaspore, α-AlOOH, has been found to be isomorphous with goethite, α-FeOOH, of known structure.[12] The second modification corresponding to bohmite, γ-AlOOH, is isomorphous with lepidocrocite, γ-FeOOH. The structure of lepidocrocite has been determined by Ewing employing oscillation and rotation photographs of a naturally occurring single crystal.[13] Reichertz and Yost[14] employing powder methods, determined parameters for the various ions in the crystal structure of bohmite that lead to a hydrogen bond distance of 2.47 ± 0.07 Å., which is considerably less than similar distances previously reported[15] with the exception of a value of

(1) J. Bohm, *Z. anorg. Chem.*, **149**, 203 (1925).
(2) J. De Lapparent, *Bull. soc. franc. Mineral*, **53**, 255 (1930).
(3) J. Bohm and H. Niclassen, *Z. anorg. Chem.*, **132**, 1 (1924).
(4) J. D. Edwards and M. Tosterud, THIS JOURNAL, **37**, 483 (1933).
(5) H. Lehl, *ibid.*, **40**, 47 (1936).
(6) H. B. Weiser and W. O. Milligan, *Advances in Colloid Sci.*, **1**, 227 (1942).
(7) S. Goldstaub, *Bull. soc. franc. Mineral*, **59**, 148 (1936).
(8) R. Hocart and J. De Lapparent, *Comp. rend.*, **189**, 995 (1929).
(9) R. Fricke and A. Seitz, *Z. anorg. Chem.*, **255**, 13 (1947).
(10) W. O. Milligan, THIS JOURNAL, **55**, 497 (1951).
(11) W. O. Milligan and H. B. Weiser, *ibid.*, **42**, 669 (1938).
(12) F. J. Ewing, *J. Chem. Phys.*, **3**, 203 (1935).
(13) F. J. Ewing, *ibid.*, **3**, 420 (1935).
(14) P. P. Reichertz and W. J. Yost, *ibid.*, **14**, 495 (1946).
(15) L. Pauling, "The Nature of the Chemical Bond," Cornell University Press, Ithaca, N. Y., 1948.

2.42 Å. for the OHO distance in nickel dimethylglyoxime.[16]

Milligan and Weiser,[11] from dehydration isobars of scandium trihydroxide and X-ray diffraction studies, reported the existence of scandium oxide monohydrate, γ-ScOOH, which they believed to be isomorphous with bohmite. The crystallite size obtained, however, was of such dimensions that the X-radiograms consisted of broad and diffuse bands which could not be employed in a quantitative determination of the structure. The existence of scandium oxide monohydrate was later confirmed by Fricke and Seitz.[9]

In the present investigation the unit structure, space group symmetry and detailed atomic arrangement of γ-AlOOH and γ-ScOOH have been determined. Since numerous attempts to grow single crystals of both of these monohydrates failed, it was necessary to confine the work done here to powder techniques.

Experimental

A. Preparation of γ-AlOOH.—Several samples of bohmite were employed in the determination of its structure. Two samples of well-crystallized material were obtained from the Aluminum Company of America, while two others were prepared in this Laboratory.

The two samples of bohmite prepared here were precipitated from $N/10$ solutions of aluminum chloride and sulfate with a slight excess of dilute ammonium hydroxide. Both samples were washed in a centrifuge with distilled water until the supernatant liquid was free of the anion. The samples were then placed in a platinum capsule in a special steel bomb capable of operation at temperatures as high as 600° and pressures as high as 30,000 lb./sq. inch. The sample prepared from aluminum chloride was heated in the bomb for 7 days at 350° and 5,000 lb./sq. inch, while the product precipitated from aluminum sulfate was heated at 400° and 6,000 lb./sq. inch for five days. After removal from the bomb, the crystalline powders were washed five times with distilled water in a centrifuge, then allowed to dry at room temperature.

All of the samples of bohmite prepared here and those obtained from the Aluminum Company of America gave identical X-ray diffraction patterns whose spacings agreed with published patterns.

B. Preparation of γ-ScOOH.—The method of preparation of γ-ScOOH was that employed by Milligan and Weiser.[11] Three separate samples of γ-ScOOH were prepared here, differing in the method of the initial precipitation and the time of heating in the bomb. These were prepared as follows.

1. To a solution of 0.1 M scandium chloride at room temperature, freshly distilled ammonium hydroxide was added in slight excess. The precipitate was immediately washed in a centrifuge with distilled water until free of chloride ion.

2. Freshly distilled ammonium hydroxide was added to a boiling solution of 0.1 M scandium chloride, the precipitate immediately being washed in a centrifuge with boiling distilled water and finally with cold water. Washing was continued until the wash water no longer gave a positive test for chloride ion when tested with silver nitrate.

3. To a boiling solution of 0.1 M scandium chloride, freshly distilled ammonium hydroxide was added in slight excess, the precipitate was then allowed to digest for 30 minutes before being washed as described in (2) above.

The washed samples were put separately in a platinum bucket which was then placed in the high temperature bomb. Samples one and two were heated for six days at 350° and 6,000 lb./sq. inch, while sample three was heated for seven days at 350° and 5,500 lb./sq. inch. After heating, the products were washed with distilled water, and then allowed to dry in air at room temperature.

The three samples of γ-ScOOH, prepared as described above, gave identical X-ray diffraction patterns, which, except for a slight displacement of the interplanar spacings, closely resembled that of γ-AlOOH.

C. X-Ray Diffraction Examination.—Two types of X-ray apparatus were employed. A high angle Norelco recording X-ray spectrometer using filtered Cu Kα radiation and a General Electric apparatus using Cu Kα and Cr Kα radiation monochromated by means of a sodium chloride crystal monochromator.

The observed intensities were obtained from the X-ray spectrometer tracings by computing the area beneath the peaks using Simpson's rule. The X-ray photographs obtained from the General Electric apparatus were run on a modified Kipp and Zonen microphotometer.

Structure Determination

A. Unit Cell.—The experimental results from the X-ray diffraction examination of γ-AlOOH and γ-ScOOH lead to an orthorhombic unit cell with values of the axes as shown in Table I.

TABLE I

VALUES OF THE LATTICE CONSTANTS, Å.

	γ-AlOOH	γ-ScOOH
a_0	3.69	4.01
b_0	12.24	13.01
c_0	2.86	3.24

The determination of the lattice constants by any of the precision methods such as those of Bradley and Jay[17] or Cohen[18] require the use of lines with a Bragg angle greater than approximately 60°. The lines obtained in this investigation which obey this condition were all too broad to justify the use of either of the above-mentioned methods to determine the unit cell dimensions. For this reason, the lattice constants reported here were calculated by methods of successive approximation to obtain the best agreement between the experimental and calculated spacings. The lattice values determined here for bohmite were found to agree with those reported by Reichertz and Yost.[14] A comparison of the computed and experimental interplanar spacings for γ-AlOOH and γ-ScOOH are shown in Tables III and IV, respectively.

The assignment of four formulas of AlOOH and ScOOH per unit cell gives calculated densities of 3.09 and 3.07 g./cm.^{3}, respectively, which are to be compared to the measured values of 2.99 and 3.02 g./cm.^{3} obtained by use of a pycnometer.

B. Space Group Symmetry and Prediction of the Atomic Structure.—The general extinctions observed for aluminum and scandium oxide monohydrate are the same as those observed by Ewing for lepidocrocite[13] which leads to D_{2h}^{17}-Amam, C_{2v}^{12}-A2am, or C_{2v}^{16}-C2cm; with D_{2h}^{17} as the most probable space group. All atoms are in positions 4(c); Ou $^1/_4$, Ou$'$ $^1/_4$, etc.

By application of Pauling's rules for the coördination theory of ionic crystals, the predicted atomic arrangement in γ-FeOOH, γ-AlOOH and γ-ScOOH may be obtained. This structure consists of aluminum or scandium-centered octahedra joined by the sharing of edges in such a way that the oxygens O_I, near the middle of the layer are common to four octahedra and corresponds to O^{--}, while the oxygens O_{II} on the outer ridges of the layers are common to two octahedra and corresponds to

(16) L. E. Godycki, R. E. Rundle, R. C. Voter and C. V. Banks, *J. Chem. Phys.*, **19**, 1205 (1951).

(17) A. J. Bradley and A. H. Jay, *Proc. Phys. Soc.*, **44**, 563 (1932).

(18) W. M. Cohen, *Rev. Sci. Inst.*, **6**, 68 (1935).

$(OH)^-$. The successive layers are held together by hydrogen bonds. The values for the atomic parameters are shown in Table II.

TABLE II

ATOMIC PARAMETERS

	γ-AlOOH		γ-ScOOH	
	Expt.	Calcd.	Expt.	Calcd.
u	−0.315	−0.322	−0.334	−0.318
u_I	+ .287	+ .291	+ .266	+ .282
u_{II}	+ .083	+ .080	+ .066	+ .071

C. Intensity Computations.—Relative intensities were calculated to determine the structure of γ-AlOOH and γ-ScOOH employing the usual equations.[19]

Computations were also made to determine the effect of absorption of the X-rays in the powder samples.[20] However, since the absorption coefficient and the sample radius (0.024 cm.) are small for both γ-AlOOH and γ-ScOOH, the effect of absorption was found to be negligible in all cases.

Debye–Waller temperature corrections were determined by the method of least squares.

The calculated intensities were determined by varying the predicted values of the atomic parameters over small ranges consistent with the structure described above. The parameters which gave the best agreement of the observed with the calculated intensities, are shown in Table II. Comparisons of the calculated and observed relative intensities using the above parameters are presented in Table III for γ-AlOOH and in Table IV for γ-ScOOH.

It is difficult to determine the error involved in the parameters given in Table II; however, changes of ±0.002 in the aluminum or scandium parameter, and changes of ±0.005 for the oxygen parameters cause the calculated intensities to be in general disagreement with the observed intensities.

Discussion of the Results

The structures of aluminum and scandium oxide monohydrate as obtained here are in good agreement with the predicted atomic arrangement. The interatomic distances have been computed and are presented in Table V.

TABLE III

COMPARISON OF CALCULATED AND OBSERVED INTENSITIES FOR γAlOOH

	Interplanar spacings		X-Ray spectrometer CuKα		Crystal monochromator Cu Kα		Cr Kα	
hkl	$d_{calcd.}$	$d_{obsd.}$	Calcd.	Obsd.	Calcd.	Obsd.	Calcd.	Obsd.
020	6.119	6.108	10.00	10.00	10.00	10.00	10.00	10.0
120	3.160	3.160	5.89	6.06	6.05	6.10	5.77	5.7
040	3.061	3.066	.09	wk.	.09		0.08	
011	2.799		.00		.00		0.00	
140	2.356		.03		.02		0.02	
031	2.342	2.340	4.94	5.29	5.56	5.55	5.20	5.2
111	2.222		.01		.01		0.01	
060	2.040		.09	wk.	.10		0.10	
131	1.982	1.966	.37	0.55	.45	0.58	0.42	0.4
051	1.859	1.851	3.25	3.53	4.00	5.66	4.00	4.0
200	1.845	1.841	2.20	3.08	2.76		2.59	2.7
160	1.785		.00		.00		0.00	
220	1.767	1.761	.57	0.66	.73	0.70	0.71	1.1
151	1.661	1.663	.80	1.28	1.07	1.46	1.07	1.9
240	1.580		.02		.04		0.03	
211	1.538	1.530	.02	0.67	.04	0.59	0.03	0.9
080	1.530		.52		.74		0.82	
071	1.491		.00		.00		0.00	
231	1.483	1.455	1.50	1.41	2.14	1.89	2.62	3.0
002	1.429	1.425	.72	0.89	1.07	1.22	1.49	2.1
180	1.413		.09		.14		0.21	
022	1.392	1.394	.20	0.29	.31	0.41	0.48	0.7
171	1.383	1.384	79	0.80	1.20	1.03	1.89	1.9
260	1.368	1.364	07	wk.	.11	0.15	0.18	wk.
251	1.310	1.310	1.27	1.47	1.98	2.49	4.08	4.4
122	1.302	1.301	.47	0.70	.73	0.90	1.54	1.9
042	1.295		.01		.02		0.04	
091	1.228		.05		.08		0.20	
0100	1.224	1.221	.04	0.12	.07	0.28	0.24	[b]
142	1.222		.03		.04		0.14	
320	1.206	1.201	.19	0.17	.31	0.26	1.22	[b]
280	1.177	1.171	.30	0.33	.52	0.56	3.05	[b]
062	1.170		.04		.07		0.48	
191	1.165		.00		.00		0.00	
1100	1.161	1.160	.40	0.33	.69	0.50	5.86	
271	1.160		.00		.00		0.00	
340	1.141		.01					
202	1.130	1.127	.47	0.59[a]				
311	1.125		.01					
162	1.116		.00					
222	1.111	1.108	.15	0.19[a]				
331	1.089	1.080	.02	0.03[a]				
242	1.060		.01					
360	1.053		.00					
082	1.044	1.043	.19	0.21[a]				
0111	1.037		.07					
351	1.026	1.028	.19	0.14[a]				
291	1.022		.04					
2100	1.020	1.021	.04	0.09[a]				
0120	1.020		.02					
182	1.005	0.998	.05	0.03[a]				
1111	0.995		.03					
262	.989	.986	.05	0.06[a]				
1120	.983		.04					
380	.958		.02					
013	.949	.945	.00	0.20[a]				
371	.948		.18					
0102	.930	.925	.03	0.20[a]				
033	.927		.06					
400	.922	.920	.12	0.22[a]				
322	.922		.13					
113	.919		.02	0.07[a]				
420	912		.05					
282	.909	.909	.26	0.29[a]				
2111	.904		.05					
1102	.901	.905	.36	0.31[a]				
133	.900		.01					
0131	.894	.897	.05	0.11[a]				
2120	.892		.03					
342	.892	.885	.01	0.23[a]				
053	.888		.15					
440	.884		.00					
411	.875		.00					
391	.869	.870	.00	0.27[a]				
1131	.868		.23					
3100	.867	.866	.18	0.25[a]				
153	.863	.863	.14	0.19[a]				
431	.858		.01					
362	.848		.00					
213	.844		.01					
460	.841	.838	.02	wk.				
073	.836		.00					
2102	.830		.07					
0122	.830	.830	.03	0.31[a]				
233	.829		.08					
451	.826	.826	.35	0.33[a]				
173	.816	.819	.20	0.13[a]				
1122	.810	.807	.08	0.06[a]				
2131	.805	.804	.14	0.14[a]				
253	.800	.800	.16	0.34[a]				
382	.796		.06					
3111	.793	.798	.03	0.15[a]				
480	.790		.21					
3120	.786		.06					
471	.784		.00					

[a] Obs. intensities for $K\alpha_1$ only. [b] Lines too broad to determine the intensities.

(19) "Internationale Tabellen zur Bestimmung von Kristallstrukturen," Gebruder Borntraeger, Berlin, 1935.

(20) A. J. Bradley, *Proc. Phys. Soc.*, **47**, 879 (1935).

TABLE IV

COMPARISON OF CALCULATED AND OBSERVED INTENSITIES FOR γ-ScOOH

hkl	Interplanar spacings $d_{calcd.}$	$d_{obsd.}$	Relative intensities: X-Ray spectrometer Cu Kα Calcd.	Obsd.	Crystal monochromator Cu Kα Calcd.	Obsd.
020	6.506	6.510	10.00	10.00	10.00	10.00
120	3.412	3.414	5.14	5.57	5.69	5.70
040	3.253		0.02		0.02	
011	3.146		0.06		0.06	
031	2.596	2.595	4.34	5.02	5.27	4.99
140	2.525	2.525	0.24	0.26	0.30	wk.
111	2.474	2.473	0.56	0.84	0.70	1.14
131	2.179	2.185	0.20	0.34	0.27	0.39
160	2.168	2.170	0.09	0.12	0.13	
051	2.028	2.026	2.02	2.88	2.97	1.73
200	2.004	2.009	1.48	2.44	2.19	3.42
220	1.914	1.916	0.48	0.52	0.75	0.93
160	1.906	1.907	0.12	0.14	0.18	
151	1.809	1.805	1.29	1.96	2.10	1.50
240	1.706		0.00		0.00	
211	1.690		.03		0.05	
071	1.686		.01		0.01	
080	1.626	1.620	.32	0.90	0.61	1.71
002	1.620		.54		1.12	
231	1.586	1.588	.50	1.56	1.03	2.28
022	1.572		.19		0.38	
180	1.506	1.494	.06	1.10	0.12	1.55
171	1.495		.57		1.22	
260	1.471	1.471	.05	0.10	0.11	
122	1.463	1.462	.36	0.64	0.82	1.34
042	1.450		.00		0.00	
251	1.425	1.427	.70	0.81	1.64	1.14
142	1.363	1.364	.08	0.06	0.14	
091	1.324		.00		.01	
320	1.308	1.311	.10	0.17	.27	0.98
0100	1.301		.01		.04	
062	1.298		.03		.08	
202	1.267	1.262	.29	0.72	.81	1.87
280	1.262		.17		.37	
271	1.256	1.250	.00	0.12	.01	
191	1.254		.05		.14	
1100	1.237	1.236	.21	0.68	.62	1.30
222	1.237		.11		.26	
340	1.235		.02		.07	
162	1.234		.03		.08	
311	1.225	1.226	.05	0.12		
331	1.187		.02			
242	1.174		.00			
082	1.147	1.145	.10	0.11[a]		
360	1.137		.01			
351	1.115	1.116	.10	0.10[a]		
0111	1.110		.03			
182	1.103	1.102	.02	0.08[a]		
291	1.102		.01			
2100	1.091	1.087	.01	0.07[a]		
262	1.089		.03			
0120	1.084		.00			
013	1.076		.00			
1111	1.070		.00			
033	1.048	1.045	.07	0.07[a]		
1120	1.046		.04			
113	1.039		.03			
380	1.032	1.030	.01	0.11[a]		
371	1.028		.09			
322	1.018	1.019	.06	0.10[a]		
0102	1.014		.01			
133	1.008	1.004	.01	0.3[a]		
400	1.002		.19			
053	0.997	0.994	.06	0.2[a]		
282	0.996		.11			

[a] Obsd. intensities for $K\alpha_1$ only.

TABLE V

INTERATOMIC DISTANCES IN γ-AlOOH AND γ-ScOOH, Å.

Atom	Neighbors in same octahedron	AlOOH	ScOOH	Neighbors in next layer	AlOOH	ScOOH
Al,Sc	2 O_{II}	1.87	2.17			
	2 O_I	1.99	2.08			
	2 O_I	1.88	2.06			
O_I	2 O_I	2.86	3.24	2 O_{II}	3.82	4.10
	4 O_{II}	2.82	3.21			
	4 O_I	2.54	2.71			
	1 O_{II}	2.58	2.74			
O_{II}	2 O_{II}	2.86	3.24	2 O_I	3.82	4.10
	4 O_I	2.82	3.21	4 O_{II}	3.05	3.17
	1 O_I	2.58	2.74	2 O_{II}	2.70	2.72

NOTE: Al–Al neighbors: 2.86 and 2.92 Å; Sc–Sc neighbors: 3.24 and 3.12 Å.

There is considerable distortion of the octahedral units in the layers from the shape of a regular octahedron as evidenced by the interatomic distances. This distortion has the effect of flattening out the portion of the octahedra which are in the interior of the double layer, and a corresponding stretching of the edges away from the layer. The Al–O distances of 1.87, 1.99 and 1.88 Å. can be compared with the similar distances of 1.99 and 1.85 Å. found in corundum,[21] both bohmite and corundum exhibiting the effect of Al–Al repulsion. The Sc–O distances of 2.17, 2.08 and 2.06 Å. are found to be quite similar to the corresponding distance of 2.10 Å. in scandium oxide.[22] The lengths 2.54 and 2.58 Å. for the shared O–O edge in bohmite are in good correspondence with the value 2.50 Å. found in corundum, while the corresponding lengths in γ-ScOOH of 2.71 and 2.74 Å. are in agreement with the interpolated value of 2.61 Å. found in scandium oxide.

In the discussion of the "ideal" structures of γ-AlOOH and γ-ScOOH, it was mentioned that the $(OH)^-$ anions are on the outer surfaces of the layers. It is now possible to show that these anions give rise to hydrogen bonds holding the layers of octahedra together. As in lepidocrocite and diaspore, the hydrogen bonds are postulated to explain certain O–O distances. The hydrogen bonds, or OHO groups, which hold the layers together are taken to be the shortest unshared O–O distances in the structure. These distances of 2.70 and 2.72 Å. for γ-AlOOH and γ-ScOOH, respectively, must be regarded as a hydrogen bond since the repulsive forces between the oxygens would otherwise be effective in raising the distance above 2.72 Å. The values of 2.70 and 2.72 Å. are likewise in good agreement with the hydrogen bridge distance found in other compounds: *e.g.*, 2.70 Å. in γ-FeOOH, 2.71

(21) L. Pauling, *J. Am. Chem. Soc.*, **47**, 781 (1925).
(22) L. Pauling and M. D. Shappell, *Z. Krist.*, **75**, 128 (1930).

Å. in α-AlOOH and α-FeOOH, and in many organic compounds.[15] The stoichiometric composition of the crystals is explained by the association of one hydrogen with each 2.70 or 2.72 Å. distance.

The structure determined here for γ-AlOOH easily explains its tabular habit. Since the OHO bonds are relatively weak, there is excellent cleavage on (010) corresponding to the breaking of these weak OHO bonds, hence its existence as orthorhombic plates.[2,23] This property would also account for the increased breadth and relative intensity of the (020) reflection found for some samples of γ-AlOOH.

From X-ray and electron diffraction examinations, Milligan and Weiser[23] recently reported that transparent films of γ-AlOOH exhibit orientation. The formation of these thin films and the orientation effects noted are easily accounted for by the layer structure found for γ-AlOOH. No microscopic crystals of γ-ScOOH have been observed, but electron micrograph studies have shown that it also exists as orthorhombic plates.

Summary

1. The unit structure, space group symmetry, and detailed atomic arrangement of γ-AlOOH, bohmite, and the isomorphous compound γ-ScOOH have been determined. Both were found to be isomorphous with lepidocrocite, γ-FeOOH.

2. The unit of structure of γ-AlOOH and γ-ScOOH is orthorhombic end-centered on (100) and has the axes $a_0 = 3.69$, $b_0 = 12.24$ and $c_0 = 2.86$ for γ-AlOOH; and $a_0 = 4.01$, $b_0 = 13.01$, and $c_0 = 3.24$ for γ-ScOOH.

3. The most probable space group is D_{2h}^{17}-Amam, with all atoms in 4(c). The parameters were determined to be: $u_{Al} = -0.322$, $u_O = 0.291$ and $u_{OH} = 0.080$ in γ-AlOOH, while the values $u_{Sc} = -0.318$, $u_O = 0.282$ and $u_{OH} = 0.071$ are the parameters in γ-ScOOH.

4. The elements of the structure are aluminum or scandium-centered oxygen octahedra. The octahedra are joined together by sharing edges to form a "double" layer, and the successive layers held together by hydrogen bonds.

5. The hydrogen bonds are postulated to account for short, unshared O–O distances of 2.70 and 2.72 Å. in γ-AlOOH and γ-ScOOH, respectively. These values are in good agreement with those found for many other compounds containing hydrogen bonds.

(23) W. O. Milligan and H. B. Weiser, THIS JOURNAL, **55**, 490 (1951).

THE EFFECT OF THE SUBSTRATE ON THE CRYSTALLIZATION OF METALLIC FILMS

BY FLORENCE I. METZ AND ROBERT A. LAD

Lewis Flight Propulsion Laboratory, National Advisory Committee for Aeronautics, Cleveland, Ohio

Received August 4, 1955

The effect of surface heterogeneity and sample preparation on the crystallization behavior of metallic films were studied. The experiments indicate that the metal film technique may be a useful tool for the study of surface heterogeneities which cannot be examined by more direct means. Thin films of gold, silver and zinc deposited by vacuum evaporation on alkali halide single crystal surfaces were found to be composed of crystallites of two size ranges. The smaller crystallites formed on all the surfaces studied, while crystallites larger by several orders of magnitude were found to form in addition on known defects and on water polished and heated surfaces. The formation on heated surfaces of the sites which nucleated the large crystallites was found to be a second-order rate process with an activation energy of 122 kcal. for NaCl and 85 kcal. for KBr. The formation of the sites is also accelerated by X-ray bombardment or the application of tensile stress. The possible relation of the nucleation sites to mosaic boundaries and surface cracks is discussed.

Introduction

Interest in the nature of the surface of alkali halide single crystals prompted this study of the structure of evaporated metal films. It has been shown[1] that surface cracks act as nucleation sites for the crystallization of silver and gold deposited on quartz and hard glass substrates. It was found that metal atoms sputtered onto the substrate at relatively low temperatures were mobile after striking the surface and that crystallites formed in rows along surface cracks in the substrate.

The large discrepancy between the actual strength of rock salt (750 lb./in.²) and that computed theoretically (390,000 lb./in.²) has been attributed to the presence of "Griffith cracks."[2–5] These cracks are presumed to act as centers of stress concentration and thus lead to fracture at low nominal stresses. Although the work of Joffe[3–5] indicated that such cracks might be present, no direct evidence for their presence has been put forth. The applicability of the technique of Andrade and Martindale to this problem was investigated by this study of the effect of known heterogeneities and various surface treatments on the structure of films of gold, silver and zinc. Evaporation rather than sputtering was used because it avoided the complications due to chemical reactions between the metal and alkali halide which arise during sputtering.[1] The surfaces studied were subjected to pretreatments such as polishing, heating, X-irradiation and the application of stress. In addition, surfaces containing cleavage steps, scratches and large cracks were used.

(1) E. N. daC. Andrade and J. G. Martindale, *Phil. Trans.*, **A235**, 69 (1935).

(2) A. A. Griffith, *Phil. Trans. Roy. Soc.*, **A221**, 163 (1920); *Proc. Intern. Congr. Appl. Mech. (Delft)*, 55 (1924).

(3) A. Joffe, M. W. Kirpitschewa and M. A. Lewitsky, *Z. Physik.*, **22**, 286 (1924).

(4) A. Joffe and M. A. Lewitsky, *ibid.*, **31**, 576 (1925).

(5) A. Joffe, *Internat. Conf. Phys. London*, **2**, 77 (1934).

Experimental

Metal Film Preparation.—Films of gold, silver and zinc were deposited on the substrates by vacuum evaporation

at a distance of 6 cm. to a computed thickness of 25 atom layers. Microscopic examination under oblique illumination at an angle of 15° with the horizontal showed the films to be composed of crystallites, which were so small as to be barely discernible at a magnification of 140×. This array of crystallites occurred in all of the films studied. Some of the films also contained crystallites of a size several orders of magnitude larger. They were found to be distributed over the surface in three general ways—singly, in clusters and in rows. These groupings were in addition to the expected deposits along obvious cleavage steps, and the conditions of substrate preparation under which they occurred will be discussed below.

For a given surface preparation, gold, silver and zinc yielded the same results. The metal crystallites increased in size in the aforementioned order, but the relative difference in size from the larger crystallites to the background remained the same. Silver was used for most of the experiments. An increase in film thickness caused the background crystallite size to increase more rapidly than that of the larger ones until, for films thicker than 100 atom layers, no difference in crystallite size was observable. Heating the specimens after the silver deposition had the same effect as increasing the total amount of silver: namely, an increase in background size and consequent decrease in detectability of the originally larger crystallites. An increase in the time of evaporation from 15 seconds to 15 minutes resulted in an increase in crystallite size which made no significant change in resolution. The pressure at which evaporation took place had no effect provided it was below 10^{-3} mm.

Films on Water Polished Surfaces.—Specimens were cleaved to approximately 4 × 8 × 20 mm. from random pieces of single crystal NaCl and KBr obtained from the Harshaw Chemical Company. The specimens were annealed at high temperature (200° below the melting point) for 24 hours and furnace cooled over a period of 36 hours. The surface layers of the specimen were then dissolved away with water. Immediate rinsing with ethanol followed by acetone left one face with a surface free of all imperfections which could be detected microscopically with either transmitted or oblique light. The metallic film which was deposited immediately after the surface was prepared was composed of a uniform layer of small crystallites. The larger crystallites mentioned above occurred only rarely and never in groups.

Films on Scratched and Cracked Surfaces.—The occurrence of large crystallites along scratches was investigated. Fine scratches were made with a counterbalanced sapphire needle ground to a chisel edge as well as with the diamond indenter from a Tukon hardness tester. Rows of large crystallites were found to deposit along both edges of the scratch.

A narrow flaw was produced by extending a cleavage part way through the crystal normal to the surface under study. Silver deposited as large crystallites along edges of the cleavage crack and also in a row beyond the point where separation was visible. The irregularity of the crack made it impossible to estimate the minimum width which would attract a double row of crystallites.

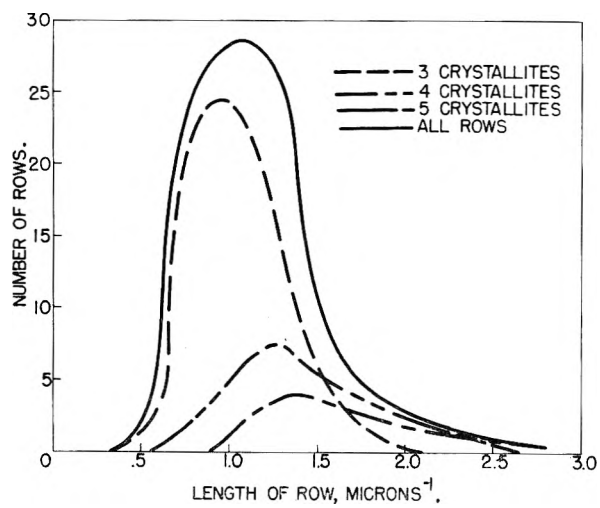

Fig. 1.—Length distribution of crystallite rows on water polished NaCl heated at 110° before silver deposition.

Nucleation at a cleavage crack for silver migrating on the surface was also demonstrated. An aluminum foil shield containing a circular hole 3.5 mm. in diameter was placed over a cracked surface so that the shortest distance between the hole and the crack was 1 mm. After a 15-second evaporation, silver crystallites were found along the edges of the crack in numbers equal to those found when similar surfaces were not shielded. It appeared that all of the silver which migrated under the shield came to rest along the crack since no background was visible except in the unshielded portion of the surface.

Films on Heat Treated Surfaces.—Specimens which had been heated after water polishing also contained nucleation sites for the large crystallites. The crystallites were found to occur in three ways—singly, in clusters and in rows. Since similar behavior was noted for water polished specimens which had been stored at room temperature for several months, the nucleation sites appeared to result from a rate process. A quantitative study of the occurrence of the crystallite rows was undertaken because they were amenable to measurement and it was desirable to obtain some knowledge concerning the presumably linear defects beneath them.

The distribution of lengths for the rows was studied for those rows satisfying two criteria: (1) the centers of the crystallites formed a straight line (as determined with a straight edge on a photographic negative at 140×), and (2) the spacing between the crystallites was no more than their diameter. The distribution of lengths for such rows occurring on water polished and heated crystals is shown in Fig. 1. Although the cut off at shorter lengths is due to the necessary choice of 3 crystallites as a minimum, the absence of lengths greater than *ca.* 2×10^{-4} cm. is felt to be of significance. The length distribution was not dependent on the heating time or temperature. This led to the conclusion that the nucleation sites did not grow once formed. Initial annealing at lower temperatures and for shorter times gave rise to a less uniform distribution of crystallites over the surface and to lines of somewhat longer length.

The rate of formation of the linear nucleation sites was studied on cleaved, water polished specimens. After the surface preparation, the specimens were maintained at the desired temperature in an air thermostat held constant to within ±0.1°. The silver film was deposited immediately after the heat treatment. Photomicrographs were taken of several areas on each specimen. Each photograph represented an area of 0.38 mm.^{2} and contained up to 400 crystallite rows meeting the criteria outlined above. The number of rows for each determination was the average over 2 to 5 photographs.

The rate of formation of nucleation sites varies rapidly with temperature. At room temperature the process requires months, while at temperatures above 130° it is practically complete in less than one hour. The data fit a second order rate equation of the form

$$\frac{n}{n_\infty} = \frac{kt}{1 + kt}$$

where n and n_∞ are the number of rows per unit area at time t and infinite time, and k is the rate constant. At 115°, the largest deviation of the data from the rate curve is 6% (Fig. 2). The rapid change in rate with temperature restricted measurements to the temperature range 105–135°. The activation energy over this range was 115 kcal. for NaCl (Fig. 3). Data at these temperatures yielded a value of 85 kcal. for KBr. A summary of the data is contained in Table I.

While the maximum number of rows, n, remained substantially constant for the temperature range 110–190° (Fig. 4), the occurrence of crystallite rows disappeared rather abruptly above 200°. Experiments indicated that nucleation sites already present disappear at higher temperatures. Two crystals were heated at 135° for a period long enough to ensure that the process had gone essentially to completion (1 hr.). At this time, one crystal was withdrawn and coated, while the other was raised to 210° for one hour and then coated. The first crystal yielded a typical pattern while the second had lost all the tendency to form large crystallites. Its surface was like that of a water polished, unheated specimen.

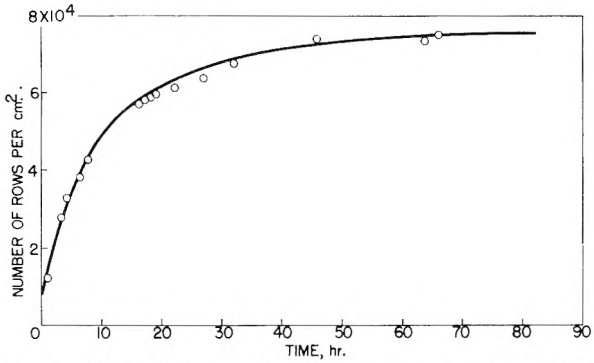

Fig. 2.—The effect of pretreatment time at 115° on the occurrence of crystallite rows on NaCl.

The possible effect of water vapor on the rate phenomenon was studied. No difference was found for specimens heated in air and *in vacuo*. In addition, specimens were heated in water vapor at 25 mm. pressure. They were found to contain numerous solution pits after they were coated. However, the unattacked portions of the surfaces still contained crystallite rows in the expected numbers. It was concluded that water vapor did not play a role in the formation of nucleation sites.

TABLE I

SUMMARY OF RATE DATA

	Temp., °C.	k, hr.$^{-1}$	N_∞, cm.$^{-2}$ × 10^{-4}
NaCl	105.6	5.42×10^{-3}	16.3
	111.8	1.62×10^{-2}	10.2
	115.0	1.41×10^{-1}	8.4
	120.8	2.65	8.8
	124.5	4.89	8.0
	126.2	7.68	8.8
KBr	119.2	7.29×10^{-3}	7.0
	127.0	1.22×10^{-1}	8.5
	135.0	5.95×10^{-1}	6.3

Films on Irradiated Surfaces.—The rate of formation of nucleation sites at room temperature is increased by X-ray irradiation. An X-ray tube having a tungsten target and a beryllium window was used at 50 kv. and 30 ma. Exposures of the specimens at various distances from the tube window yielded the same rate for X-ray intensities from 18,000 to 72,000 R./hr. The rate obtained was comparable to that obtained by heating at 115° without irradiation.

Films on Stressed Surfaces.—Application of a tensile stress of 0.3 kg./mm.^{2} parallel to the face under study also increased the rate of formation of nucleation sites to the 115° value. This stress is approximately 0.1% of the ultimate strength of dry specimens not water treated.

Angular Distribution of Crystallite Rows.—If the defects in the substrate were linear, they might be expected to bear a relation to the crystal structure of the alkali halide. Preliminary results of the measurement of the angular distribution have been reported[6] for the angle between the crystallite row and the (100) direction. The crystallite rows tend to form at preferred angles which are the same for all specimens. Attempts to correlate these preferred angles with crystal structure were not particularly successful because the crystal specimens were composed of zones disoriented by a few degrees. Thus combination of data from many crystals in order to utilize a statistical number tended to obscure the features of the distribution curves.

Discussion

The experiments outlined above indicate that the metal film technique may be a useful tool for the study of surface heterogeneities which cannot be examined by more direct means. Surfaces with known flaws always contained large crystallites while highly uniform surfaces did not. It would seem therefore that the presence of large crystallites is good evidence for the existence of surface irregularities.

(6) R. A. Lad, *J. Appl. Phys.*, **23**, 800 (1952).

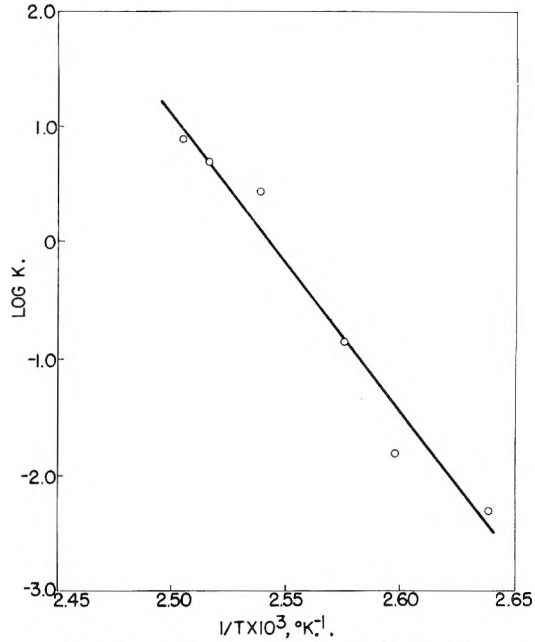

Fig. 3.—Activation energy plot for NaCl.

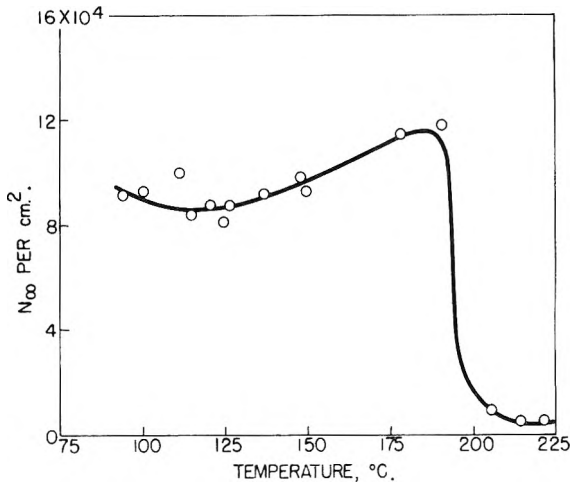

Fig. 4.—Variation of n_∞ with temperature.

The nature of the imperfections which served as nucleation points for the single crystallites, clusters and linear arrays cannot be deduced from these experiments. However, the results obtained from the quantitative study of the linear arrays are of interest in the light of other work. The linear arrays occurred in numbers comparable to the concentrations of both dislocations and vacancies believed[7] to be present in this type of crystal. It is also of interest to note that the number of arrays (10^5 per cm.^{2}) and their average length (1.5×10^{-4} cm.) are consistent with accepted sizes for mosaics in melt grown rock salt crystals.[8] One might postulate that the surface treatments led to the formation of dislocation or vacancy arrays which could act as nucleation sites.

(7) F. Seitz, *Phys. Rev.*, **79**, 890 (1950); **79**, 1002 (1950).

(8) P. P. Ewald and M. Renninger, *Intern. Conf. Phys. London*, **2**, 57 (1934).

Another hypothesis that adequately describes the results is that of crack formation in the water polished surfaces by an activated process. When an interior crystal plane is converted into a surface plane by dissolution of the planes above it, a non-equilibrium system results. Because the equilibrium spacing is of the order of 6% smaller in the surface plane than in the interior,[9] the surface so formed will be under tension. The tendency will thus be toward contraction and the dissipation of the strain energy by the formation of new surface in cracks. The possibility of crack formation of this type was first suggested by Lennard-Jones.[9]

(9) J. E. Lennard-Jones and B. M. Dent, *Proc. Roy. Soc. (London)*, **121**, 247 (1928).

The tendency for the linear defects to align themselves at preferred angles may be interpreted as due to the formation of cracks along planes of low free energy. An electron diffraction study of both heat treated and X-irradiated NaCl[10] has also given evidence that these treatments result in crystallographic changes in the surface layers. Further work is needed to relate these observations to the results of this investigation.

Acknowledgments.—The authors would like to thank Dr. S. L. Simon for many helpful discussions during the course of this work and Dr. L. A. Girifalco for suggestions concerning the preparation of this paper.

(10) H. Leider, private communication.

HOMOGENEOUS CATALYTIC ACTIVATION OF MOLECULAR HYDROGEN IN AQUEOUS SOLUTION BY SILVER SALTS

BY A. H. WEBSTER AND J. HALPERN

Metal Chemistry Laboratory, Department of Mining and Metallurgy, University of British Columbia, Vancouver, Canada

Received July 18, 1955

In aqueous solution, salts of silver were found to activate molecular hydrogen homogeneously as evidenced by their catalytic effect on the reduction of $Cr_2O_7^=$ and Ce^{++++} by H_2. The kinetics are represented by: $-d[H_2]/dt = k[Ag^+]^2[H_2]$, where $k = 4.0 \times 10^8 \exp[-15{,}800/RT]$ liter^2 mole^{-2} sec.$^{-1}$, in perchlorate solution. A mechanism is proposed involving a termolecular rate-determining step, in which an H_2 molecule reacts simultaneously with two Ag^+ ions thereby becoming activated. The results are compared with those obtained earlier for the activation of H_2 by Cu^{++} and Hg^{++} salts. It is concluded that the activation process may involve the simultaneous transfer of two electrons from the H_2 molecule to the catalyst.

Introduction

Recent work in this Laboratory has revealed a number of systems in which molecular hydrogen, in aqueous solution, is apparently activated homogeneously by interaction with a dissolved metal ion or metal-containing complex. In particular, such activity has been demonstrated for certain cupric[1] and mercuric[2] salts, as evidenced by the fact that these salts are reduced homogeneously by H_2 and, in some cases, can act as catalysts for the homogeneous hydrogenation of other dissolved compounds such as dichromate and ceric salts.

The present paper describes an extension of these studies to certain salts of the univalent metal ion, Ag^+. Some indications that silver salts may activate hydrogen have been provided by earlier observations on the formation of metallic silver by hydrogen treatment of aqueous solutions of silver salts[3] and on the absorption of hydrogen by silver permanganate solutions.[4] However no detailed investigations of such systems appeared to have been made, particularly under conditions where complications arising from possible heterogeneous reactions were absent. Hence the essential nature of the homogeneous interaction between H_2 and Ag^+ remained to be elucidated. Recently the homogeneous activation of hydrogen in pyridine solution by silver acetate has been reported.[5]

In the present study, a procedure similar to that used earlier to study the activity of cupric salts,[1d] was adopted, *i.e.*, the ability of Ag^+ to activate hydrogen homogeneously was determined by measuring its catalytic effect on the reaction between H_2 and $Cr_2O_7^=$ under conditions where no metallic silver was formed. Most of the measurements were made in perchlorate solution in which Ag^+ is believed to be essentially uncomplexed.

Experimental

C.P. grade chemicals were used throughout. $K_2Cr_2O_7$, NaOH, $HClO_4$, HNO_3 and $AgNO_3$ were obtained from Nichols Chemical Co. $AgClO_4$, $NaClO_4$ and $Ce(ClO_4)_4$ were G. F. Smith Co. products. H_2 and N_2 gases were supplied by Canadian Liquid Air Co.

The experimental solutions were prepared by mixing aliquots of standardized stock solutions of the various reagents in desired proportions and diluting with distilled water. Mixtures containing $AgClO_4$ were first boiled and filtered through sintered glass to remove any AgCl which might result from the presence of traces of chloride impurities in the perchlorate reagents.

The final solutions were analyzed for $Cr_2O_7^=$ with a Beckman DU spectrophotometer using the 3500 Å. peak. Corrections were applied for the slight variation of optical density with acid concentration and for the small absorption of the reaction product, Cr^{+++}. The concentration of Ag^+ was determined by titration with KCNS using a ferric indicator. Where Ce^{++++} was used (in place of $Cr_2O_7^=$) its concentration was measured volumetrically by adding an excess of standardized $FeSO_4$ solution and back-titrating with $Ce(HSO_4)_4$.

(1) (a) J. Halpern and R. G. Dakers, *J. Chem. Phys.*, **22**, 1272 (1954); (b) R. G. Dakers and J. Halpern, *Can. J. Chem.*, **32**, 969 (1954); (c) E. Peters and J. Halpern, *ibid.*, **33**, 356 (1955); (d) E. Peters and J. Halpern, THIS JOURNAL, **59**, 793 (1955).

(2) (a) J. Halpern, G. J. Korinek and E. Peters, *Research (London)*, **7**, S61 (1954); (b) G. J. Korinek and J. Halpern, THIS JOURNAL, **60**, 285 (1956).

(3) M. N. Beketoff, *Compt. rend.*, **48**, 442 (1859).

(4) (a) F. Hein and W. Daniel, *Z. anorg. Chem.*, **181**, 78 (1929); (b) F. Hein, W. Daniel and H. Schwedler, *ibid.*, **233**, 161 (1937).

(5) L. Wright, S. Weller and G. A. Mills, THIS JOURNAL, **59**, 1060 (1955).

The glass reaction apparatus was completely immersed in a water-bath whose temperature was controlled to ±0.03°. The H_2 gas was first passed through an aqueous $NaNO_3$ solution (of approximately the same ionic strength as the reacting solution) to saturate it with water vapor, and then dispersed, through a sintered glass plate, into a flask containing the reacting solution (250 ml.). To follow the reaction, samples of the solution were withdrawn periodically during the experiment, quenched by cooling in an ice-bath, and the concentration of unreacted $Cr_2O_7^=$ (or Ce^{++++}) determined as described earlier. Prior to introducing the H_2, the apparatus was placed in the water-bath and allowed to remain for about 30 minutes while attaining thermal equilibrium. The solution was sampled and analyzed during this period to ascertain that it was completely stable in the absence of hydrogen. Zero reaction time, recorded at the instant that the flow of H_2 was commenced, may be subject to an uncertainty of up to a few minutes because of the time required for the solutions to become saturated with H_2.

The atmospheric pressure was recorded during the experiment and the H_2 partial pressure was calculated by subtracting the solution vapor pressure (estimated from available data for comparable $NaClO_3$ solutions). Different H_2 partial pressures were achieved, in a series of experiments designed to determine the effect of this variation, by using H_2-N_2 gas mixtures of various proportions. These mixtures were analyzed for H_2 by combustion over CuO.

Results

In the presence of $AgClO_4$, $Cr_2O_7^=$ [6] was found to react with H_2, over a wide range of conditions, according to the following stoichiometric relation

$$Cr_2O_7^= + 3H_2 + 8H^+ \longrightarrow 2Cr^{+++} + 7H_2O \quad (1)$$

In no case could any change in the Ag^+ concentration be detected, nor was there any indication of formation of metallic silver until after the reduction of $Cr_2O_7^=$ had gone to completion.

A series of typical rate plots, representing the disappearance of $Cr_2O_7^=$ according to the above reaction, are shown in Fig. 1. The rate is seen to be essentially of zero order with respect to the changing concentration of $Cr_2O_7^=$ during the reaction and unaffected by variations in the initial concentration. Addition of $Cr(ClO_4)_3$ in amounts comparable to those formed during the reaction were also found to be without effect on the rate. A small induction period was noted at the commencement of most of the reactions, before the final zero-order rate was attained. This may be an apparent effect resulting from the uncertainty in the zero reaction time, mentioned earlier, or it may be due to the presence in the solution of a trace amount of an impurity which reduces preferentially to $Cr_2O_7^=$. For example, it is estimated that less than 10^{-5} *M* ClO_3^- could account for the observed effect.

It may be concluded that $Cr_2O_7^=$ does not participate directly in the rate-determining step of the reaction although, as shown earlier,[1c,1d] its reduction serves as a convenient measure of the rate of activation of H_2 in the solution. Therefore, it was considered more appropriate to express the results in terms of the equivalent rate of reaction of H_2 per liter of solution, $-d[H_2]/dt$, based on the stoichiometric equivalence of the reaction, *i.e.*

$$\frac{-d[H_2]}{dt} = -3\,\frac{d[Cr_2O_7^=]}{dt} \quad (2)$$

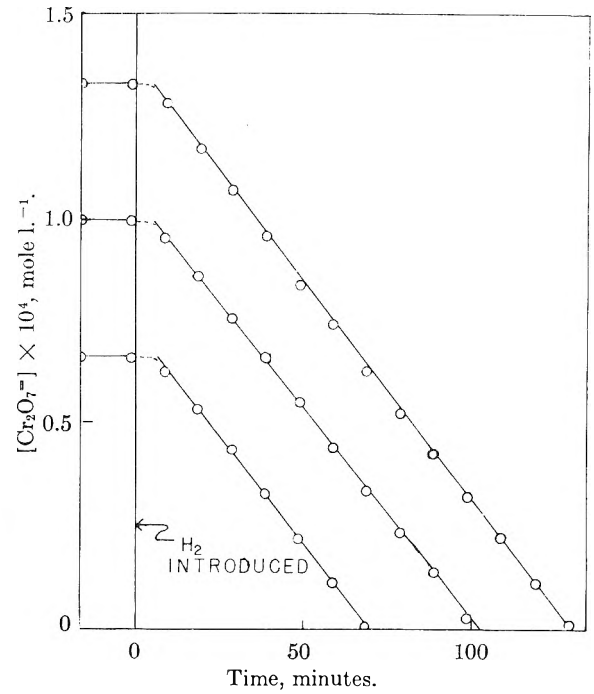

Fig. 1.—Typical rate plots for the reduction of $Cr_2O_7^=$ by H_2; 0.1 *M* $AgClO_4$; 0.5 *M* $HClO_4$; 50°; 0.83 atm. H_2.

Values of $-d[H_2]/dt$ were calculated from the measured zero-order rate of disappearance of $Cr_2O_7^=$ and were generally reproducible to within ±5%.

Evidence for the absence of any interaction, such as complex formation, between Ag^+ and $Cr_2O_7^=$ in solution, is provided by the observation that the absorption spectrum of $Cr_2O_7^=$ is unaffected by addition of Ag^+.

The suggestion that $Cr_2O_7^=$ does not take part in the rate-determining step, receives support from the result of an experiment (see Table I) in which Ce^{++++} was substituted for $Cr_2O_7^=$ as the reaction label. Within the experimental error involved in the comparison, the rate of reaction of H_2, calculated from the zero-order rate of reduction of Ce^{++++}, was the same as that determined using $Cr_2O_7^=$.

Evidence for the homogeneous character of the reaction is provided by the results of another experiment (see Table I) in which the reaction vessel was packed with 2.2 g. of Pyrex glass wool. The rate was the same as in an unpacked vessel.

Figure 2 shows the rate of reaction to be directly proportional to the partial pressure of hydrogen. Since the solubility of hydrogen in water obeys Henry's law in the region under consideration,[7] it may also be concluded that the rate is proportional to the solution concentration of hydrogen, $[H_2]$. Variation of the H_2 flow rate in the system, between 0.09 and 0.35 l./min., did not affect the rate, indi-

(6) For convenience, and in accordance with common usage, the formula $Cr_2O_7^=$ is employed in this paper to denote all the Cr(VI) in the solution. It is probable, however, that at the high acidities used, other forms of Cr(VI), especially $HCrO_4^-$ and H_2CrO_4, are present and may, in fact, predominate. Since Cr(VI) is used in this system only as a label to measure the amount of H_2 reacted, its exact form is not of importance. This shifting equilibrium does not affect the validity of the spectrophotometric analysis since the optical density of Cr(VI) was calibrated experimentally for each acidity.

(7) H. A. Pray, C. E. Schweickert and B. H. Minnich, *Ind. Eng. Chem.*, **44**, 1146 (1952).

TABLE I

RATE OF REACTION OF H_2 IN SOLUTIONS OF DIFFERENT COMPOSITIONS

Temp., °C.	Reactant *M*	$HClO_4$, *M*	$NaClO_4$, *M*	$k \times 10^3$, $l.^2$ mole^{-2} sec.$^{-1}$
49.6	1.67×10^{-4} $K_2Cr_2O_7$	0.10	0.90	7.93
49.6	1.67×10^{-4} $K_2Cr_2O_7$	.20	.80	7.82
49.6	1.67×10^{-4} $K_2Cr_2O_7$	.50	.50	8.07
49.6	1.67×10^{-4} $K_2Cr_2O_7$	.75	.25	8.05
49.6	1.67×10^{-4} $K_2Cr_2O_7$	1.00	.00	8.68
49.6	1.67×10^{-4} $K_2Cr_2O_7$	1.00	.00	8.36
49.6	1.67×10^{-4} $K_2Cr_2O_7$	1.29	.00	8.38
49.6	1.67×10^{-4} $K_2Cr_2O_7$	0.50	.00	8.22
49.6	1.67×10^{-4} $K_2Cr_2O_7$	.50	.50	7.97
49.6	1.67×10^{-4} $K_2Cr_2O_7$	.50	1.00	7.77
49.6	1.67×10^{-4} $K_2Cr_2O_7$	.50	1.50	7.35
49.6	1.67×10^{-4} $K_2Cr_2O_7$	.50	2.00	6.67
49.6	1.67×10^{-4} $K_2Cr_2O_7$	.50	0.00	8.25
49.6	1.67×10^{-4} $K_2Cr_2O_7$	.50	.00	8.05[a]
50.0	0.67×10^{-4} $K_2Cr_2O_7$	.50	.00	8.07
50.0	1.00×10^{-4} $K_2Cr_2O_7$	.50	.00	8.20
50.0	1.33×10^{-4} $K_2Cr_2O_7$	.50	.00	8.07
50.0	1.20×10^{-4} $Ce(ClO_4)_4$	.50	.00	7.82
30.0	1.67×10^{-4} $K_2Cr_2O_7$	.50	.00	1.69
40.0	1.67×10^{-4} $K_2Cr_2O_7$	.50	.00	3.78
50.0	1.67×10^{-4} $K_2Cr_2O_7$	.50	.00	8.23
60.0	1.67×10^{-4} $K_2Cr_2O_7$	.50	.00	17.6
70.0	1.67×10^{-4} $K_2Cr_2O_7$	.50	.00	35.9

[a] Reaction vessel packed with 2.2 g. of Pyrex glass wool.

cating that the latter is not limited, under the experimental conditions used, by absorption of the gas. Other aspects of the kinetics also bear this out.

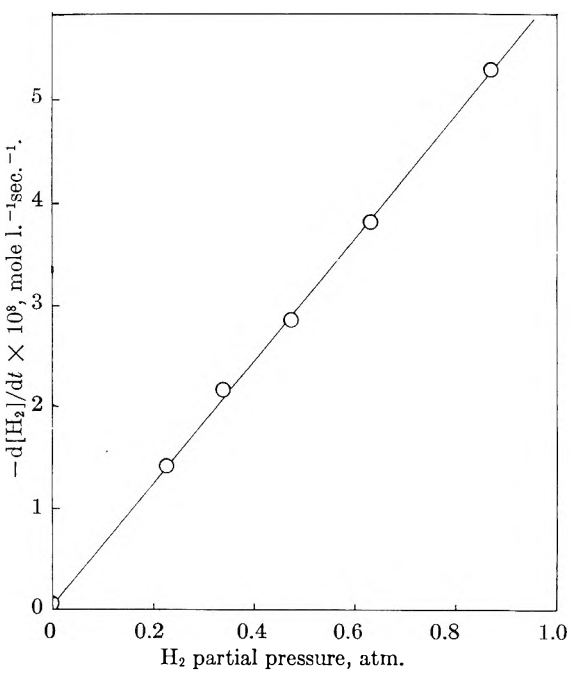

Fig. 2.—Dependence of the rate on H_2 partial pressure; 0.1 *M* $AgClO_4$; 0.5 *M* $HClO_4$; 49.6°.

The catalytic influence of Ag^+ on the reaction is clearly demonstrated in Fig. 3 which shows rate plots for the reduction of $Cr_2O_7^=$ by H_2 in solutions containing various amounts of $AgClO_4$. No reaction could be detected in the absence of Ag^+, while progressively higher rates were obtained as the Ag^+ concentration was increased up to 0.108 *M*. The nature of the dependence is quantitatively depicted in Fig. 4, where the reaction rates, determined at 40, 50 and 70°, are plotted as functions of the concentration and square of the concentration of Ag^+. At each temperature it is observed that the results conform closely to a second-

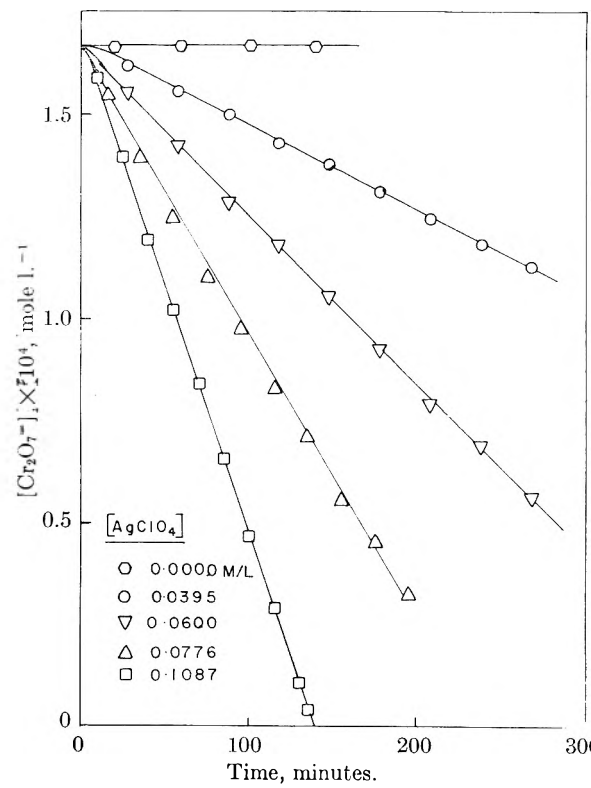

Fig. 3.—Rate plots for the reduction of $Cr_2O_7^=$ by H_2 at 50° in solutions containing different amounts of $AgClO_4$; 0.5 *M* $HClO_4$; 0.83 atm. H_2.

order dependence, the rate being essentially proportional to $[Ag^+]^2$. Detailed inspection reveals only a slight deviation from this relation in the direction of lower order, reflected in the fact that the linear plots of rate against $[Ag^+]^2$ do not quite extrapolate to the origin, although the uncatalyzed rate is found experimentally to be negligible; the possible significance of this will be discussed later.

Similar results, also shown in Fig. 4, were obtained when nitrate was substituted for perchlorate. The slope of the plot of rate *vs.* $[AgNO_3]^2$ (for solutions containing 0.5 *M* HNO_3) is about 10% lower than that for comparable perchlorate solutions, possibly the result of some complexing between Ag^+ and NO_3^- or the influence of a small salt effect on the reaction or on the solubility of H_2.

The results listed in Table I show that essentially no effect on the rate was observed when the $HClO_4$ concentration was varied between 0.1 and 1.0 *M* (the total ionic strength being held constant at 1.1 by simultaneous variation of the $NaClO_4$ concentration). Also a negligible effect was observed when the $NaClO_4$ concentration was varied between zero and 1.0 *M* in the presence of constant concentrations of 0.1 *M* $AgClO_4$ and 0.5 *M* $HClO_4$. At higher $NaClO_4$ concentrations (1.5–2 *M*) a slight decrease in the rate was noted. Unfortunately no measurements of salt effect could be made in solutions of much lower total ionic strength (*i.e.* <0.1) because of the need to maintain critical minimum concentrations of both $AgClO_4$ and $HClO_4$ in the solution in order to obtain measurable reaction rates and to prevent the precipitation of the slightly soluble silver dichromate.

Rates were measured at five temperatures ranging from 30 to 70°, and are listed in Table I. The results conform to a good Arrhenius plot from whose slope an apparent activation energy of 15.8 ± 0.5 kcal./mole was calculated.

Discussion

The kinetic results may be summarized in the relations

$$-\mathrm{d}\,[H_2]/dt = k[Ag^+]^2[H_2] \quad (3)$$

$$= k[Ag^+]^2\alpha P_{H_2} \quad (4)$$

where α is Henry's constant, denoting the solubility of H_2 and P_{H_2} is the measured H_2 partial pressure.

The experimental data yield the following expression for the rate constant

$$k = 4 \times 10^8 \exp.\left[\frac{-15{,}800}{RT}\right] \mathrm{l.^2\ mole^{-2}\ sec.^{-1}} \quad (5)$$

Values of k were calculated from equation 4, using Wiebe and Gaddy's values[8] of solubility of H_2 in water.

These kinetics suggest that the rate-determining step of the reaction, in which the hydrogen apparently is activated, is a termolecular process involving the interaction of one H_2 molecule with two Ag^+ ions. The product of this combination then reacts rapidly with $Cr_2O_7^=$ to reduce the latter and yield the observed reaction products. This sequence of steps may be represented as

$$H_2 + 2Ag^+ \xrightarrow[\text{slow}]{k} (Ag_2 \ldots H_2)^{++} \quad (6)$$

(8) R. Wiebe and V. L. Gaddy, *J. Am. Chem. Soc.*, **56**, 76 (1934).

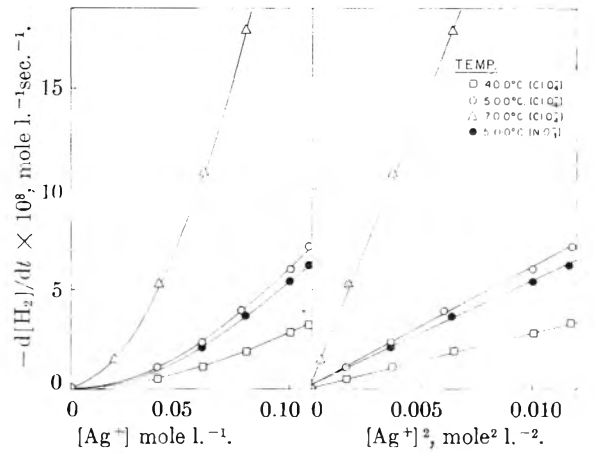

Fig. 4.—Dependence of the rate on the concentration of Ag^+ in perchlorate and nitrate solutions.

followed by

$$(Ag_2 \ldots H_2)^{++} + {}^1/_3Cr_2O_7^= + {}^8/_3H^+ \xrightarrow[\text{fast}]{} {}^2/_3Cr^{+++} + {}^7/_3H_2O + 2Ag^+ \quad (7)$$

The stoichiometry and kinetics of the over-all process correspond to those observed.

The detailed nature of the product of the rate-determining step is not resolved. It is possible that a stable intermediate complex (such as that depicted in equation 6) is formed, which carries the hydrogen in active form, and which proceeds to react with $Cr_2O_7^=$ before it can rearrange to form more stable products. Alternatively it is possible that Ag^+ itself is reduced homogeneously, to free Ag atoms or Ag_2 molecules, in the rate-determining step, *i.e.*

$$H_2 + 2Ag^+ \longrightarrow 2Ag^0 + 2H^+ \quad (8)$$

or

$$H_2 + 2Ag^+ \longrightarrow Ag_2 + 2H^+ \quad (9)$$

followed by rapid reaction of the dissolved Ag or Ag_2 with $Cr_2O_7^=$, so that no metallic silver is formed until after all the $Cr_2O_7^=$ is reduced. Neglecting stabilization of the uncharged Ag or Ag_2 by solvation, the endothermicities of reactions (8) and (9) are estimated, from thermochemical data[9] and the recently determined dissociation energy of Ag_2,[10] to be 87.6 and 46.2 kcal./mole, respectively, both considerably in excess of the observed activation energy. It is unlikely that the difference could be accounted for by simple solvation of the Ag or Ag_2 and consequently the earlier suggestion, involving the formation of an intermediate complex $(Ag_2 \ldots H_2)^{++}$ (or $2(Ag \ldots H)^+$) in which additional stabilization energy is derived through some form of electron sharing between the Ag and H atoms, is favored. Providing the intermediate reacts rapidly with $Cr_2O_7^=$, these various alternatives cannot be distinguished kinetically.

The observed frequency factor of the reaction, 4×10^8 l.^{2} mole^{-2} sec.$^{-1}$, corresponds to an entropy of activation $\Delta S_c^{\pm}$, at 50°, of −22 e.u. Unfortunately few data are available for other termolecular reactions on which to base a comparison of these values,

(9) W. M. Latimer, "The Oxidation States of the Elements and Their Potentials in Aqueous Solution," Prentice-Hall, Inc., New York, N. Y., 1952.

(10) B. Kleman and S. Lindkvist, *Arkiv Fys.*, **9**, 385 (1955).

but approximate calculations,[11] based on collision theory, lead to an expected value of 10^9–10^{10} l.^{2} mole^{-2} sec.$^{-1}$ for the frequency factor of a simple gas-phase termolecular reaction. While this is of the same order as the observed value and thus provides some indication of the plausibility of the proposed mechanism, the agreement should be interpreted with caution in view of the uncertainties involved in the calculation and comparison.

A possible alternative to a termolecular rate-determining step, consistent with the observed third-order kinetics, would be a bimolecular step in which an intermediate binary complex, Ag_2^{++} or AgH_2^+ (in equilibrium with its components), reacts with an H_2 molecule or Ag^+ ion, respectively, to give, in common with the earlier mechanism, a ternary activated complex containing two Ag^+ ions and one H_2 molecule. Two such possible schemes are

Scheme A:

$$2Ag^+ \underset{k_2}{\overset{k_1}{\rightleftharpoons}} (Ag_2)^{++} \quad \text{(fast)} \qquad (10a)$$

$$(Ag_2)^{++} + H_2 \xrightarrow[k_3]{} (Ag_2..H_2)^{++} \quad \text{(slow)} \qquad (10b)$$

Scheme B:

$$Ag^+ + H_2 \underset{k_2}{\overset{k_1}{\rightleftharpoons}} (Ag..H_2)^+ \quad \text{(fast)} \qquad (11a)$$

$$(Ag..H_2)^+ + Ag^+ \xrightarrow[k_3]{} (Ag_2..H_2)^{++} \quad \text{(slow)} \qquad (11b)$$

In either of the above cases, unless the steady-state concentration of the intermediate binary complex is fairly high, these alternatives are not readily distinguishable kinetically from a single termolecular step and are not intrinsically more probable.[12] In the absence of any other evidence for the formation of such intermediates, there would appear to be no reason to favor these mechanisms over the simple termolecular mechanism proposed earlier.

The essential independence of the rate, within fairly wide limits, of the H^+ and ClO_4^- concentrations provides some support for the conclusion that the observed catalytic activity is associated with simple Ag^+ ions, rather than with OH^- or ClO_4^- complexes, whose concentrations in these solutions are probably very small. Apart from this, the apparent absence of a salt effect on varying the $NaClO_4$ concentration from zero to 1.0 M (in the presence of 0.1 M $AgClO_4$ and 0.5 M $HClO_4$) is inconclusive and throws little light on the reaction mechanism, since these measurements refer to a concentration region in which the activity coefficients of most electrolytes remain nearly constant with varying ionic strength.[13] In more dilute solutions, an increase in rate with increasing ionic strength would be predicted on the basis of the Debye–Hückel theory, since the proposed mechanism involves the combination of two ions of like charge in the rate-determining step. Unfortunately it was not possible, for the experimental reasons mentioned earlier, to make any measurements in the region ($\mu < 0.05$) where these considerations might be expected to apply.

A commonly noted tendency[13] for the activity coefficients of many electrolytes, particularly salts of polyvalent cations (which the activated complex would approximate), to increase at very high ionic strength, may account for the observed slight decrease in rate when the $NaClO_4$ concentration was increased above 1 M. A salting out of H_2 under these conditions might also contribute to a decreased rate.

In some respects the present results resemble those obtained earlier for the activation of H_2 in aqueous solution by Cu^{++} and Hg^{++} salts.[1,2] An important difference is that with the latter ions, the reactions are of first order with respect to the catalyst, only one Cu^{++} or Hg^{++} ion apparently being required to activate each H_2 molecule. It has been suggested[14] that the catalytic activity of these ions is associated with their electron-accepting properties and that the activation process involves a transfer or partial transfer of electrons from H_2 to the catalyst. The present results are not inconsistent with this view but suggest the modification that the most favored path of activation of H_2 is apparently by simultaneous transfer of both its electrons. This would explain the fact that two Ag^+ ions are required simultaneously to activate an H_2 molecule in aqueous solution while only one Cu^{++} or Hg^{++} ion, each with a fairly high affinity for two electrons, suffices.

It is of interest that similar kinetics, *i.e.*, of second order in the catalyst concentration, were obtained for the activation of H_2 in quinoline solution by another univalent metal salt, CuOAc.[15] This was originally taken as indicating that H_2 was activated by interaction with the dimeric molecule $Cu_2(OAc)_2$ but recently Calvin and Wilmarth,[16] on the basis of a careful re-examination of this system, have proposed a termolecular rate-determining step in which H_2 is activated by simultaneous interaction with two CuOAc molecules. The striking parallel between this system and the present one, is readily evident.

Although the kinetic results leave little doubt that the most favorable path of activation of H_2 in aqueous solutions of Ag^+ salts is by interaction with two Ag^+ ions, the small deviation from the exact proportionality between the rate and $[Ag^+]^2$ in the direction of a lower order of dependence, mentioned earlier, suggests that an alternative catalytic path, involving only one Ag^+ ion, may also be possible although less favorable. The relative contribution of the reaction proceeding by such a path should become more pronounced at lower Ag^+ concentrations, but unfortunately the technique used in the present study precluded any measurements in the region below 0.02 M Ag^+ because of the slow rates involved. It is hoped to extend the investigation to this region in the future by using a modified technique. This question is of particular interest in view of recent work[5] on the

(11) A. A. Frost and R. G. Pearson, "Kinetics and Mechanism," John Wiley and Sons Inc., New York, N. Y., 1953, p. 72.

(12) Ref. 11, p. 181.

(13) B. E. Conway, "Electrochemical Data," Elsevier Publishing Co., New York, N. Y., 1952, pp. 75–83.

(14) J. Halpern and E. Peters, *J. Chem. Phys.*, **23**, 605 (1955).

(15) (a) M. Calvin, *Trans. Faraday Soc.*, **34**, 1181 (1938); *J. Am. Chem. Soc.*, **61**, 2230 (1939); (b) S. Weller and G. A. Mills, *ibid.*, **75**, 769 (1953); (c) W. K. Wilmarth and M. K. Barsh, *ibid.*, **75**, 2237 (1953).

(16) M. Calvin and W. K. Wilmarth, *J. Am. Chem. Soc.*, **78**, in press (1956).

activation of H_2 by AgOAc and CuOAc in pyridine solution where (in contrast to the quinoline system) first-order rates in the catalyst concentration were observed.

Acknowledgment.—Support of this work through a grant and a Fellowship award to one of the authors (A.H.W.) from Canadian Industries, Ltd., is gratefully acknowledged.

KINETICS OF THE REACTION OF MOLECULAR HYDROGEN WITH MERCURIC AND MERCUROUS PERCHLORATES IN AQUEOUS SOLUTION

By G. J. Korinek and J. Halpern

Metal Chemistry Laboratory, Department of Mining and Metallurgy, University of British Columbia, Vancouver, Canada

Received August 18, 1955

The kinetics of the reduction of Hg^{++} and Hg_2^{++} by molecular hydrogen in aqueous perchlorate solution have been examined. The results are shown to be consistent with a mechanism in which H_2 is activated initially by homogeneous interaction with either Hg^{++} or Hg_2^{++}, in the rate-determining step. The final products are determined by thermodynamic considerations. The total rate of reaction of H_2 is given by $(k_1[Hg^{++}] + k_2[Hg_2^{++}])[H_2]$, where $k_1 = 4.2 \times 10^{10} \exp[-18{,}100/RT]$ and $k_2 = 1.2 \times 10^{11} \exp[-20{,}400/RT]$ liter mole^{-1} sec.$^{-1}$, respectively. Possible mechanisms of the activation process are discussed.

Introduction

A preliminary study of the reduction of mercuric acetate by molecular hydrogen in aqueous solution, was described in an earlier paper.[1] The bimolecular kinetics suggest that H_2 is activated homogeneously by interaction with $Hg(OAc)_2$, or other mercuric acetate complexes, in the rate-determining step. However, detailed interpretation of the kinetics was difficult because of uncertainties relating to the extent of complexing between Hg^{++} and OAc^- and to the possible influence, on the reaction, of the mercurous acetate product. Hence it seemed desirable to undertake a similar study using perchlorate solutions, in which cations such as Hg^{++} and Hg_2^{++} are believed to be essentially uncomplexed. During the course of this investigation it proved necessary also to resolve the kinetics of the reaction of Hg_2^{++} with H_2.

The work which is described in this paper forms part of a series of recent investigations, conducted in this Laboratory, on the homogeneous catalytic activation of molecular hydrogen in aqueous solution by metal ions. Related studies on cupric[2] and silver[3] salts have been described earlier but, apart from the preliminary investigation on $Hg(OAc)_2$, no previous kinetic work on the present system appears to have been reported.

Experimental

All chemicals employed were of Reagent grade. $Hg(ClO_4)_2$ and $NaClO_4$ were obtained from G. F. Smith Chemical Company. Other reagents were Baker and Adamson products. The solutions used in the kinetic experiments were prepared by diluting standardized stock solutions with distilled water. H_2 and N_2 gases were obtained from Canadian Liquid Air Company.

The solutions were analyzed for Hg_2^{++} by potentiometric titration with $KMnO_4$. The total Hg concentration was determined by titration with KCNS using a ferric indicator, following oxidation with $KMnO_4$. The concentration of Hg^{++}, estimated from the difference between these two values, always agreed well with that determined directly by the cyanide method.[4]

The kinetic experiments were made in a cylindrical autoclave similar to that described earlier.[2b] It was constructed entirely of 316 stainless steel which proved inert to all the solutions used and without effect on the reaction. The inside dimensions of the vessel were about 6 in. diameter by 9 in. height. A stirrer shaft, thermometer well, thermoregulator well and sampling tube, extending below the surface of the solution, were connected through the lid. The solution was stirred with an impeller of 3 in. diameter which was generally rotated at 970 r.p.m. The partial pressure of H_2 was controlled by a standard gas regulator. The autoclave was heated externally with a gas burner, connected through a solenoid valve which was actuated by an electronic relay. Using a mercury thermoregulator the temperature of the solution could be controlled to within $\pm 0.1°$.

Four liters of solution, of desired composition, was placed in the autoclave which was then sealed, flushed with nitrogen and heated to the reaction temperature. The solution was allowed to remain at temperature under nitrogen, usually for about 30 minutes, during which it was sampled and analyzed to ascertain its stability in the absence of hydrogen. The nitrogen was then discharged and hydrogen was introduced and maintained throughout the experiment at a constant partial pressure. Zero reaction time, recorded at the instant of introduction of the hydrogen, may be subject to an uncertainty of up to a few minutes because of the time required for the solutions to become saturated. During the course of the reaction, the solution was sampled periodically and analyzed as described earlier.

Results and Discussion

The results of a typical rate experiment are depicted in Fig. 1. No change in solution composition occurred in the absence of hydrogen. The reaction in the presence of hydrogen can best be described in terms of two clearly defined stages. Stage A corresponds to the reduction of Hg^{++} to Hg_2^{++} according to the stoichiometric equation

$$2Hg^{++} + H_2 \longrightarrow Hg_2^{++} + 2H^+ \qquad (1)$$

It is characterized by a progressive decrease in the mercuric ion concentration, $[Hg^{++}]$, and an equivalent increase in the mercurous ion concentration, $[Hg_2^{++}]$, the total concentration of dissolved Hg remaining constant. This stage persists until about 99% of the Hg^{++} has been reduced to Hg_2^{++}.

During the following stage, B, the remaining Hg^{++}, and the Hg_2^{++} formed in the first stage, are

(1) J. Halpern, G. J. Korinek and E. Peters, *Research (London)*, **7**, S 61 (1954).

(2) (a) J. Halpern and R. G. Dakers, *J. Chem. Phys.*, **22**, 1272 (1954); (b) R. G. Dakers and J. Halpern, *Can. J. Chem.*, **32**, 969 (1954); (c) E. Peters and J. Halpern, *ibid.*, **33**, 356 (1955); (d) E. Peters and J. Halpern, THIS JOURNAL, **59**, 793 (1955).

(3) A. H. Webster and J. Halpern, *ibid.*, **60**, 280 (1956).

(4) I. M. Kolthoff and V. A. Stenger, "Volumetric Analysis," Vol. 2, Interscience Publishers, Inc., New York, N. Y., 1947, p. 197.

both reduced to metallic Hg, the net reactions being

$$Hg^{++} + H_2 \longrightarrow Hg + 2H^+ \qquad (2)$$

and

$$Hg_2^{++} + H_2 \longrightarrow 2Hg + 2H^+ \qquad (3)$$

Thus the concentrations of both Hg^{++} and Hg_2^{++} decrease progressively.

The transition between the two stages may be unambiguously defined by the time, t_M, at which $[Hg_2^{++}]$, determined analytically, is a maximum. Visually, t_M, whose significance will be discussed later, was characterized by the first appearance of metallic mercury.

Figure 1 shows that a plot of log $[Hg_2^{++}]$ against time, during stage B of the reaction, is linear, corresponding to apparent first-order kinetics. On the other hand the plot of log $[Hg^{++}]$ against time, during stage A, diverges from its initial linearity, the "first-order rate constant" increasing progressively as the reaction proceeds. It will be shown subsequently that this is due to the catalytic influence of the Hg_2^{++} which is being formed.

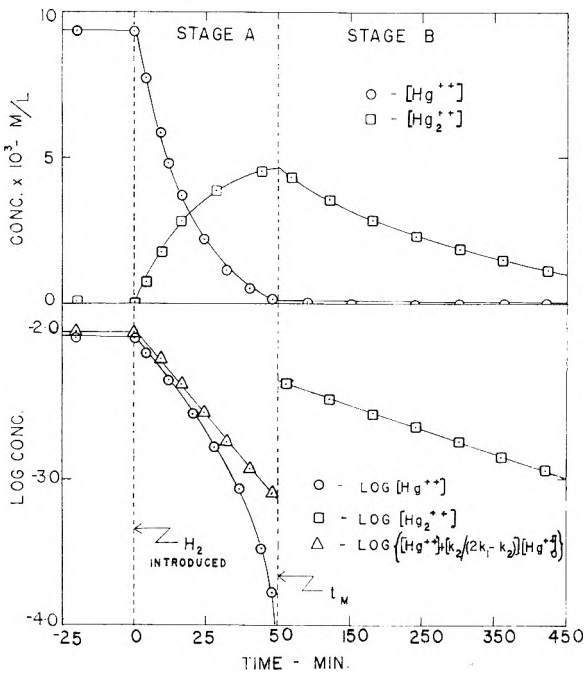

Fig. 1.—Typical rate plots for the reduction of $Hg(ClO_4)_2$ by H_2 in 0.05 *M* $HClO_4$ solution; 74.8°, 4.0 atm. H_2. (Note compression of time scale for stage B.)

The significance of the two reaction stages is readily understandable in terms of the relative reduction potentials of Hg^{++} and Hg_2^{++} ($E^0_{Hg^{++} \rightarrow Hg_2^{++}} = 0.910$ v.; $E^0_{Hg_2^{++} \rightarrow Hg} = 0.796$ v.), which suggest, in agreement with the observations just described, that the reduction of Hg^{++} to Hg_2^{++} should proceed nearly to completion before the reduction of Hg_2^{++} to Hg commences.[5] The conditions determining the relative tendencies of these two reactions to proceed, at any point, are expressed by the following equilibrium, which appears to be readily reversible

$$Hg + Hg^{++} \rightleftharpoons Hg_2^{++} \qquad (4)$$

(5) W. M. Latimer, "The Oxidation States of the Elements and Their Potentials in Aqueous Solution," Second Edition, Prentice-Hall, Inc., New York, N. Y., 1952, pp. 175–179.

whence

$$[Hg_2^{++}]/[Hg^{++}] = K \qquad (5)$$

Thus it seems likely that t_M, marking the onset of stage B and the first appearance of metallic Hg, corresponds to the point at which the ratio $[Hg_2^{++}]/[Hg^{++}]$, which increases progressively during stage A, first attains the value K. The ratio must remain constant at this value, throughout stage B, during which the solution is in contact with metallic Hg.

It will be shown that these results, as well as other features of the kinetics, are entirely consistent with a mechanism in which H_2 is activated initially by homogeneous interaction with either dissolved Hg^{++} or Hg_2^{++}, *i.e.*

$$H_2 + Hg^{++} \xrightarrow{k_1} X \qquad (6)$$

$$H_2 + Hg_2^{++} \xrightarrow{k_2} Y \qquad (7)$$

These two independent bimolecular processes are rate-controlling and give rise to active intermediates, X and Y, which undergo further rapid reactions to give the observed products. The total rate of reaction of hydrogen, $-d[H_2]/dt$, at any time during either stage A or B, is thus given by

$$-\frac{d[H_2]}{dt} = k_1[Hg^{++}][H_2] + k_2[Hg_2^{++}][H_2] \qquad (8)$$

The final products are determined by the thermodynamic considerations discussed earlier and are different for the two stages of the reaction.

Stage A.—The reaction occurring during this stage is represented by equation 1. Application of equation 8 gives

$$-\frac{d[H_2]}{dt} = -\frac{1}{2}\frac{d[Hg^{++}]}{dt} = k_1[Hg^{++}][H_2] + k_2[Hg_2^{++}][H_2] = k_1[Hg^{++}][H_2] + \frac{k_2}{2}([Hg^{++}]_0 - [Hg^{++}])[H_2] \qquad (9)$$

since

$$[Hg^{++}]_0 = [Hg^{++}] + 2[Hg_2^{++}] \qquad (10)$$

where $[H_2]$ is the concentration of H_2 in the solution, $[Hg^{++}]_0$ is the initial Hg^{++} concentration. On integration and rearrangement, equation 9 becomes

$$\log\left(\frac{[2k_1/(2k_1 - k_2)][Hg^{++}]_0}{[Hg^{++}] + [k_2/(2k_1 - k_2)][Hg^{++}]_0}\right) = \frac{(2k_1 - k_2)[H_2]}{2.303}t \qquad (11)$$

Since $[H_2]$ was held constant throughout each experiment, this corresponds to a linear relation between log $\{[Hg^{++}] + [k_2/(2k_1 - k_2)][Hg^{++}]_0\}$ and time. Typical plots of this function are shown in Figs. 1 and 2. In no case could any deviation from linearity be detected.

As suggested earlier, t_M corresponds to the time at which the ratio $[Hg_2^{++}]/[Hg^{++}]$ first attains the value K. It is given by the following expression, obtained by combining equations 5, 10 and 11.

$$t_M = \frac{2.303}{[H_2](2k_1 - k_2)}\log\left(\frac{k_1(1 + 2K)}{k_1 + Kk_2}\right) \qquad (12)$$

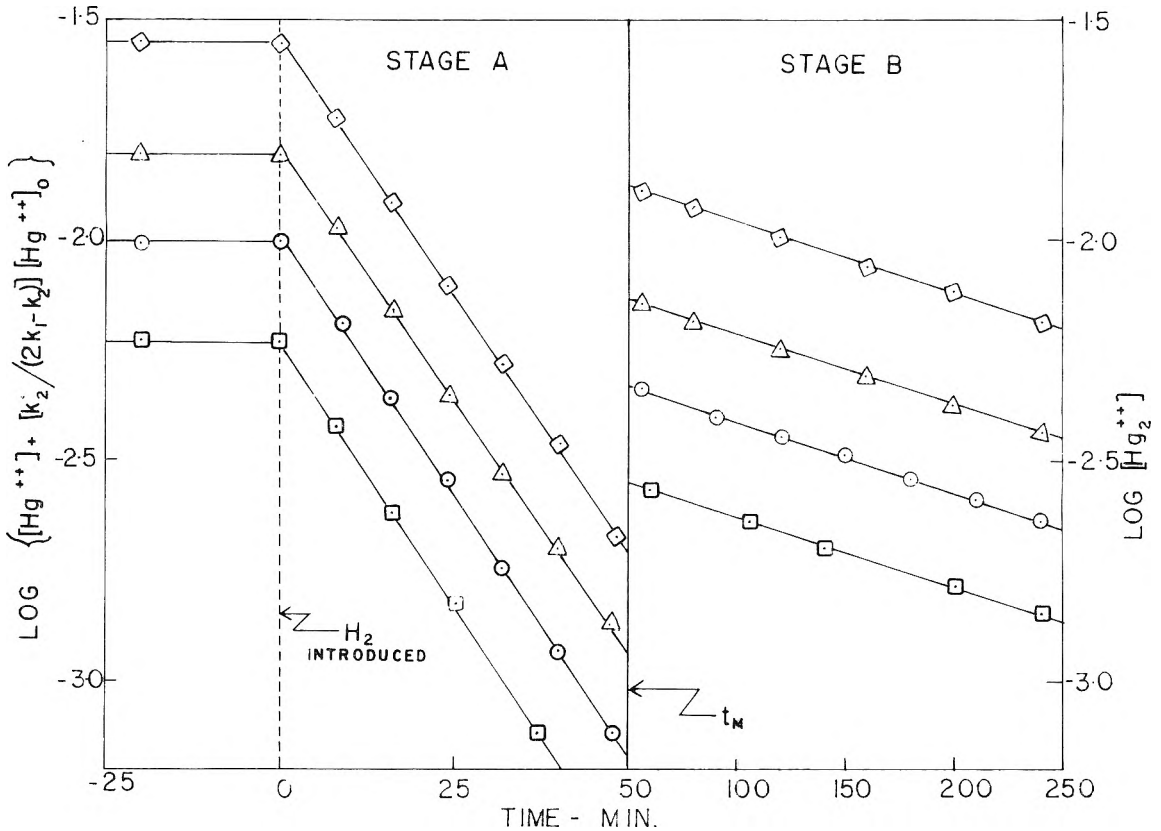

Fig. 2.—Log plots showing effect of varying initial $Hg(ClO_4)_2$ concentration on the rate at 74.8°, 4.0 atm. H_2. (Note compression of time scale for stage B.)

Stage B.—The reactions occurring during this stage are represented by equations 2 and 3. Application of equation 8 gives

$$-\frac{d[H_2]}{dt} = -\left(\frac{d[Hg^{++}]}{dt} + \frac{d[Hg_2^{++}]}{dt}\right) = k_1[Hg^{++}][H_2] + k_2[Hg_2^{++}][H_2] \quad (13)$$

Combining this with equation 5, which defines the ratio $[Hg_2^{++}]/[Hg^{++}]$ throughout this stage, the following expression is obtained

$$-\left(1 + \frac{1}{K}\right)\frac{d[Hg_2^{++}]}{dt} = \left(\frac{k_1}{K} + k_2\right)[Hg_2^{++}][H_2] \quad (14)$$

On integration this becomes

$$\log\left(\frac{[Hg_2^{++}]_0}{[Hg_2^{++}]}\right) = \frac{(k_1 + k_2K)[H_2]}{2.303(1 + K)}t \quad (15)$$

This is in agreement with the first-order disappearance of Hg_2^{++}, which was always observed during stage B of the reaction, as shown by the linear plots of log $[Hg_2^{++}]$ against time in Figs. 1 and 2.

The following procedure was employed in evaluating the rate constants k_1 and k_2 from the kinetic data.

1. A preliminary value of k_1 was estimated from the initial slope of a plot of log $[Hg^{++}]$ *vs.* t for stage A. Since initially $[Hg_2^{++}] << [Hg^{++}]$, equation 9 reduces to: $-d[Hg^{++}]/dt = 2k_1[H_2][Hg^{++}]$, which becomes on integration, log $([Hg^{++}]_0/[Hg^{++}]) = (2k_1[H_2]/2.303)t$. The fact that $k_1 > k_2$, favors this procedure.

2. This preliminary value of k_1 was used to calculate k_2 from the slope of the stage B plot of log $[Hg_2^{++}]$ *vs.* t, which corresponds, according to equation 15, to $-(k_1 + k_2K)[H_2]/2.303\ (1 + K)$. Values of K used in this calculation are listed in Table I. Since $k_2K > k_1$ and $K >> 1$, values of k_2 determined in this way are not very sensitive to errors in either k_1 or K.

3. Using this value of k_2, the function log $\{[Hg^{++}] + [k_2/(2k_1 - k_2)][Hg^{++}]_0\}$ was calculated and plotted against time for stage A, giving a straight line whose slope corresponds, according to equation 11, to $-(2k_1 - k_2)[H_2]/2.303$. The final value of k_1 was calculated from this slope. If it differed significantly from the preliminary value, the whole procedure (*i.e.*, steps 2 and 3) was repeated to self-consistency.

The values of $[H_2]$ used in these calculations were estimated from the measured H_2 partial pressure, P_{H_2}, assuming Henry's law, *i.e.*

$$[H_2] = \alpha P_{H_2} \quad (16)$$

Values of α used, are listed in Table I. Evidence that the solutions remained saturated with H_2

TABLE I

VALUES OF K AND α USED IN CALCULATION OF k_1 AND k_2

Temp., °C.	K[a]	α,[b] mole $l.^{-1}$ $atm.^{-1}$
64.4	69.7	7.2×10^{-4}
74.8	67.1	7.3×10^{-4}
84.9	65.0	7.5×10^{-4}
95.5	62.8	7.8×10^{-4}
99.5	62.1	8.0×10^{-4}

[a] Estimated by a linear extrapolation of log K *vs.* $1/T$ based on data for the range 0 to 40°, of Schwarzenbach and Anderegg, ref. 9. [b] From data for the solubility of H_2 in water, of R. Wiebe and V. L. Gaddy, *J. Am. Chem. Soc.*, 56, 76 (1934).

throughout the reaction, and hence that this relation applies, was provided by the observation that varying the stirring velocity was without effect on the rate. Other aspects of the kinetics also support this conclusion.

Values of k_1 determined by the above procedure usually agreed to within $\pm 5\%$ in duplicate experiments and values of k_2 to within $\pm 3\%$. Data given in Table II show that, in agreement with the kinetic relations just derived, these rate constants were found to be substantially independent of the Hg^{++} concentration and the H_2 partial pressure.

TABLE II

RATES OF REACTION OF Hg^{++} AND Hg_2^{++} WITH H_2 UNDER VARIOUS CONDITIONS

$[Hg(ClO_4)_2]_0$, M	$[HClO_4]$, M	$[NaClO_4]$, M	Temp., °C.	P_{H_2}, atm.	k_1, l. mole^{-1} sec.$^{-1}$	k_2, l. mole^{-1} sec.$^{-1}$
0.0055	0.05	0.0	74.8	4.0	0.168	0.0187
.0094	.05	.0	74.8	4.0	.161	.0188
.0148	.05	.0	74.8	4.0	.161	.0187
.0262	.05	.0	74.8	4.0	.161	.0188
.0094	.025	.0	74.8	4.0	.161	.0180
.0094	.05	.0	74.8	4.0	.161	.0188
.0094	.075	.0	74.8	4.0	.162	.0188
.0094	.10	.0	74.8	4.0	.164	.0187
.0094	.05	.0	74.8	4.0	.166	.0185
.0094	.05	.2	74.8	4.0	.163	.0193
.0094	.05	.4	74.8	4.0	.169	.0188
.0094	.05	.6	74.8	4.0	.169	.0192
.0094	.05	.8	74.8	4.0	.179	.0196
.0094	.05	1.0	74.8	4.0	.183	.0183
.0094	.05	.0	64.4	4.0	.077	.0077
.0094	.05	.0	84.9	4.0	.361	.0451
.0094	.05	.0	95.5	4.0	.697	.101
.0094	.05	.0	99.5	4.0	.952	.129
.0094	.05	.0	74.8	1.0	.166	.0198
.0094	.05	.0	74.8	2.0	.162	.0190
.0094	.05	.0	74.8	3.0	.163	.0188
.0094	.05	.0	74.8	5.0	.170	.0200
.0094[a]	.05	.0	74.8	4.0	.162	.0192
.0094[b]	.05	.0	74.8	4.0	...	.0180

[a] 40 g. of stainless steel powder added. [b] 80 g. of metallic mercury added.

Values of t_M, calculated from the measured k_1 and k_2 values by means of equation 12, agreed consistently with the observed values of t_M.

Direct evidence for the homogeneous character of the reaction is furnished by the results of an experiment (see Table II) in which 40 g. of stainless steel powder, of the same composition as the autoclave, was added to the solution; no effect on the reaction rates could be detected.

In another experiment (see Table II) 80 g. of metallic Hg was added to the solution initially. It reacted immediately with Hg^{++} according to equation 4, forming Hg_2^{++}, until the equilibrium defined by equation 5 was established. The subsequent reaction with H_2 was identical with that normally observed for stage B.

Results are listed in Table II which show that varying the $HClO_4$ concentration between 0.025 and 0.10 M, and the $NaClO_4$ concentration between zero and 0.6 M, had substantially no effect on the reaction rates. Addition of larger amounts of $NaClO_4$, up to 1.0 M, appeared to increase k_1 slightly (about 10%) but was without effect on k_2. These results are consistent with the postulated bimolecular rate-determining steps, represented by equation 6 and 7, in which one of the reactants, *i.e.*, H_2, is uncharged. They also provide support for the conclusion that the reactions are those of simple Hg^{++} and Hg_2^{++} ions, rather than of OH^- or ClO_4^- complexes.

Rates were measured at five temperatures ranging from 64.4 to 99.5°. Good Arrhenius plots, shown in Fig. 3, were obtained when log k_1 and log k_2 were plotted against $1/T$. The apparent activation energies, E_1 and E_2, calculated from the slopes of these plots, are 18,100 ± 600 and 20,400 ± 600 cal./mole, respectively. From these values, the following expressions for the rate constants are obtained

$$k_1 = 4.2 \times 10^{10} \exp\left[-\frac{18{,}100}{RT}\right] \text{ l. mole}^{-1} \text{ sec.}^{-1} \quad (17)$$

and

$$k_2 = 1.2 \times 10^{11} \exp\left[-\frac{20{,}400}{RT}\right] \text{ l. mole}^{-1} \text{ sec.}^{-1} \quad (18)$$

These frequency factors, and the corresponding entropies of activation, $\Delta S^{\pm}_{c_1} = -12.2 \pm 2$ e.u., and $\Delta S^{\pm}_{c_2} = 10.2 \pm 2$ e.u. (each at 74.8°), are normal[6] for simpler bimolecular reactions such as those represented by equations 6 and 7.

Conclusions

It has been demonstrated that the kinetic results are entirely consistent with a proposed mechanism in which H_2 becomes activated initially through homogeneous bimolecular interaction with either Hg^{++} or Hg_2^{++} and is thus rendered capable of entering into reactions, the detailed course of which is determined by the known thermodynamics of the system. However, the kinetic data alone do not permit the detailed configurations of the intermediate species which are formed in the rate-determining steps, to be resolved.

In this connection, it is of interest that Topham and White[7] recently demonstrated that Hg^{++} and Hg_2^{++} are also reduced homogeneously in aqueous solution by HCOOH and concluded that the rate-determining process is the transfer of an electron from the formate ion to Hg^{++} or Hg_2^{++}. In view of the kinetic similarity of the two systems, it is suggested that an analogous mechanism (*i.e.*, involving electron-transfer from H_2 to Hg^{++} or Hg_2^{++}) may also be applicable in the present case. Such a mechanism had been proposed earlier[8] to explain the activation of H_2 by other metal ions.

Recent work[3] on the activation of H_2 by Ag^+, where the kinetics were found to be of second order in the Ag^+ concentration, suggests that in this case the most favorable path may involve the simultaneous transfer of 2 electrons from the H_2. While there is no kinetic evidence on which to base an extension of this conclusion to the present system, it would appear reasonable in the light of the high 2-electron affinities of both Hg^{++} and Hg_2^{++} in

(6) G. K. Rollefson, THIS JOURNAL, **56**, 976 (1952).
(7) A. R. Topham and A. G. White, *J. Chem. Soc.*, 105 (1952).
(8) J. Halpern and E. Peters, *J. Chem. Phys.*, **23**, 605 (1955).

aqueous solution. Thus available thermodynamic data[5,9] indicate that the following reactions

$$Hg^{++}(aq) + H_2 \longrightarrow Hg^0 + 2H^+(aq) \quad (19)$$

and

$$Hg_2^{++}(aq) + H_2 \longrightarrow 2Hg^0 + 2H^+(aq) \quad (20)$$

involving the formation of free Hg atoms, are exothermic by about 27 and 12 kcal./mole, respectively (neglecting solvation of the uncharged H_2 molecules and Hg atoms).

It thus appears possible that reactions (19) and (20) represent the rate-determining processes in the present system and that the reducing intermediates which are formed (designated as X and Y in equations 6 and 7), are essentially free Hg atoms. Alternatively, it is possible that the electron-transfer process in the rate-determining step is not complete and that hydrogen-carrying intermediates such as $(Hg\,..\,H_2)^{++}$ and $(Hg_2\,..\,H_2)^{++}$ are formed, which are stabilized by electron sharing and which react directly with Hg^{++}, Hg_2^{++} or with metallic Hg to form the observed reaction products. Provided that the secondary reactions are all fast, these various possibilities cannot be distinguished kinetically.

It is of interest that the values of k_1 reported here for perchlorate solutions are about ten times higher than those found earlier for the corresponding reaction of mercuric salts with H_2 in acetate solutions, where the mercuric ion is presumably present largely in the form of acetate complexes.[10] On the other hand it has been shown[2c,d] that addition of acetate increases the rate of reaction of Cu^{++} with H_2 up to 120 times. The reason for the opposite influences of acetate in the two systems is not clear at this point.

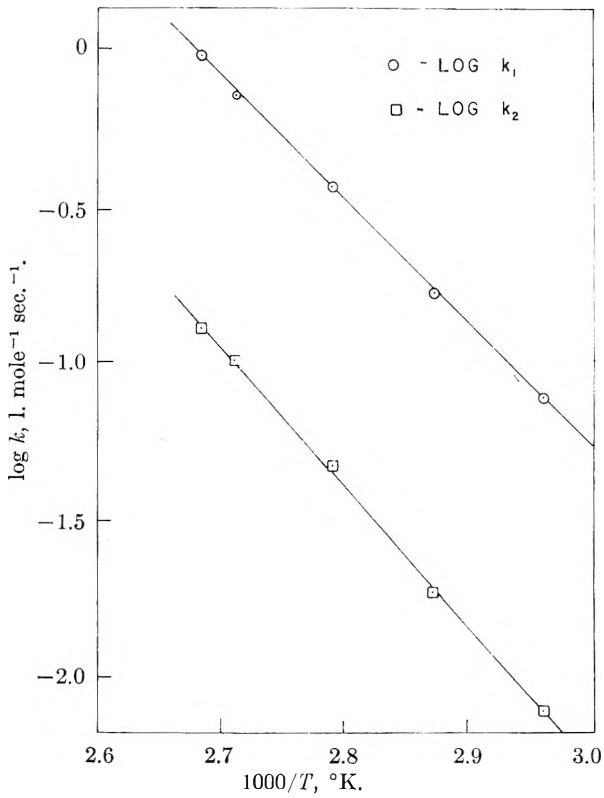

Fig. 3.—Arrhenius plots showing the temperature dependence of k_1 and k_2.

Acknowledgment.—Support of this work through a grant from the National Research Council of Canada is gratefully acknowledged.

(9) G. Schwarzenbach and G. Anderegg, *Helv. Chim. Acta*, **37**, 1289 (1954).

(10) P. Mahapatra, S. Aditya and B. Prasad, *J. Ind. Chem. Soc.*, **30**, 509 (1953).

VISCOSITIES AND DYNAMIC MECHANICAL PROPERTIES OF THE SYSTEM CELLULOSE TRINITRATE–ISOPHORONE[1]

BY D. J. PLAZEK AND JOHN D. FERRY

Contribution from the Department of Chemistry, University of Wisconsin, Madison, Wis.

Received July 25, 1955

Concentrated solutions of a cellulose trinitrate fraction (M_n = 145,000) in isophorone have been studied by the capillary and falling sphere methods to determine steady flow viscosities, and by the wave propagation and single transducer methods to determine dynamic rigidities and viscosities in the audio frequency region. The ranges of concentration and temperature covered were 2.00 to 18.17% and 0 to 60°. The dependence of viscosity on concentration was similar to that observed for vinyl polymers. The apparent activation energy for viscous flow increased linearly with concentration after a very rapid increase over that of the solvent at low concentrations. The dynamic data, when reduced to unit concentration and viscosity by the usual method of reduced variables, all superposed to give single composite curves of dynamic rigidity and viscosity as functions of reduced frequency. From each of these curves, the distribution function of relaxation times was calculated, the two sources giving results in good agreement. The terminal zone of the distribution is close to the location predicted by the Rouse theory. The plateau zone has a slope of −0.15 on a logarithmic plot, and is intermediate in character between those of cellulose tributyrate and of vinyl polymers of comparable molecular weight in concentrated solutions.

Introduction

Recent measurements[2] of the dynamic rigidity and viscosity of concentrated cellulose tributyrate (CTB) solutions have shown that their dependence on temperature and concentration can be described over a considerable range by reduced variables, just as in solutions of vinyl polymers. These measurements have provided relaxation distribution functions for three CTB fractions. The CTB distribution function exhibits a longer and flatter plateau than those of vinyl polymers of comparable

(1) Part XXI of a series on Mechanical Properties of Substances of High Molecular Weight.

(2) R. F. Landel and J. D. Ferry, THIS JOURNAL, **59**, 658 (1955).

molecular weight,[3] indicating a stronger tendency to intermolecular coupling by entanglement.

We have now obtained similar data for another cellulose derivative, the trinitrate (CTN). Measurements of steady flow viscosity, dynamic rigidity and dynamic viscosity are reported here.

Materials

The CTN was specially prepared for this study at the Allegany Ballistics Laboratory by Drs. Seymour Newman and Paul Drechsel. Purified cottonseed hull shavings were nitrated with nitric acid and phosphorus pentoxide at 20°, washed, neutralized with sodium bicarbonate, and repeatedly washed with water followed by methanol. The nitrogen content was not determined but on the basis of similarly prepared materials was probably 13.8%.

A rough fractionation was made on several successive batches by precipitation with *n*-heptane from a 1% solution in acetone. High and low molecular weight cuts of approximately 25% each were discarded; the central portions were combined for subsequent measurements. The resulting sample had an intrinsic viscosity in ethyl acetate at 25° of 5.1 dl./g. From osmotic pressure measurements in ethyl acetate at 25°, its number-average molecular weight was calculated to be 145,000. The thermodynamic coefficient A_2 was 1.2×10^{-3} cm.^{3} mole g.$^{-2}$, in reasonable agreement with values of $0.9–1.0 \times 10^{-3}$ found for similar cellulose nitrates by Newman.[4] The weight-average molecular weight was estimated from light scattering[5]; the scattered intensity at 90° together with a measured 45/135 dissymmetry of 1.45 provided a value of 145,000 also. However, this figure is probably too low, in view of the expected polydispersity[6,7] of a rough fraction prepared as this was.

The solvent chosen for mechanical properties was isophorone[8] (3,5,5-trimethyl-2-cyclohexen-1-one, $CH_2C(CH_3)_2$-$CH_2C(CH_3):CHC:O$), in which fairly concentrated solutions can be prepared without gelation, and which is relatively high-boiling. It was redistilled at 5–10 mm. and 80°.

Before preparation of solutions, the fractionated CTN was dried *in vacuo* 15 hr. at 45°. The most concentrated solution (18.2%) was mixed first. A Teflon-covered piece of magnetized iron was imbedded in the mixture, while the container was very slowly rotated between the poles of a large permanent magnet and warmed to about 45° by an infrared lamp. After measurements of viscosity and dynamic mechanical properties at various temperatures, additional solvent was added and the mixing process was repeated. This sequence was followed through nine successive dilutions. Care was taken to avoid contamination with metal ions, though in the course of mechanical measurements the solutions were at times in contact with stainless steel or, very briefly, nickel. Concentrations were determined in two ways: from the original weights of the components, and by gravimetric analysis, precipitating the CTN from a diluted aliquot with petroleum ether. Densities (ρ) of all solutions were measured, using in most cases a small cup-shaped pycnometer with a flat ground glass cover. They followed the relation $1/\rho = 1.088 - 0.498\ w_2$, where w_2 is weight fraction of polymer; this was used to check the concentrations of the more dilute solutions.

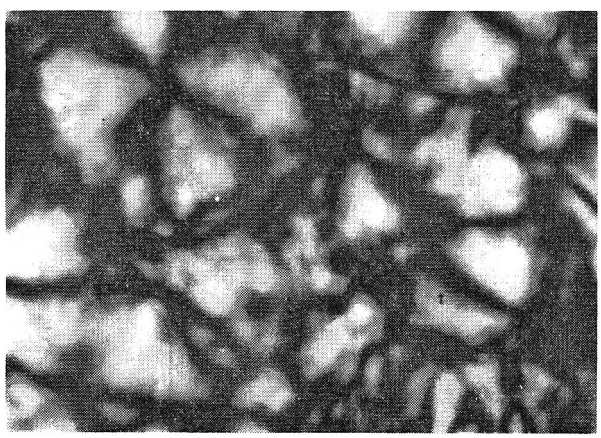

Fig. 1.—Photomicrograph between crossed Nicols of a sample of solution ($w_2 = 0.1448$) after melting at 60° and holding at room temperature 2 days, showing spherulites; magnification ×168.

At the end of the dilution sequence, which covered a period of 18 months, the intrinsic viscosity in isophorone was measured and compared with that of a portion of the original 18.2% solution which had been stored at −5°. The values were 3.76 and 4.27 dl./g., respectively, indicating that a small amount of degradation had occurred during the exposure of the sample, at various dilutions, to temperatures as high as 60°. This change throws some uncertainty on the concentration dependence of the steady flow viscosity, but none on the dynamic properties reduced to a standard reference state, as explained below.

Even in as effective a solvent as isophorone, crystallization occurred at high concentrations or low temperatures. When an 18.2% solution was stored at any temperature below 42°, transmitted light eventually revealed a rippled structure of discontinuities of the order of 1 mm. in size, recognizable between crossed polaroids as spherulites (*e.g.*, Fig. 1). Measurements of wave propagation and viscosity could be made for a brief period below this temperature before the crystallization progressed appreciably; later, abnormally high viscosity values were obtained, and eventually the birefringence of the spherulites completely prevented measurements of wave propagation by the strain double refraction method. At lower concentrations, the measurements could be carried to lower temperatures; below 9%, no crystallization occurred even at 0°.

Methods

Steady-flow viscosities were measured by the capillary and falling ball methods, as described in earlier papers.[9,10] Stainless steel balls were used. The container for falling ball measurements was sometimes the rectangular cell used in wave propagation measurements; in this case, the effective container radius used in the Faxén formula for viscosity was taken as the reciprocal mean of the reciprocal half-length and half-width of the cell.

The single transducer method of Smith, Ferry and Schremp,[11] in which the mechanical impedance of a needle vibrating along its axis in the solution is determined from measurements of the electrical impedance of the driving coil producing the motion, was used over the concentration range from 3.8 to 8.9% to determine the real part of the dynamic viscosity (η'). Measurements were made from 160 to 400 cycles/sec. at 20 and 35°. The associated measurements of the dynamic rigidity (G') were unsatisfactory, probably because of their greater sensitivity to inertial effects and other errors.

The wave propagation method[12,13] was used over the concentration range from 8.9 to 18.2%. Photoelastic measurements of wave length and damping of a transverse vibration set up in a rectangular cell were made between 250 and 3200 cycles/sec. at temperatures from 0 to 60°. Values of G' and η' were calculated by equations previously given.[12,13]

(3) L. D. Grandine, Jr., and J. D. Ferry, *J. Appl. Phys.*, **24**, 679 (1953).

(4) S. Newman, L. Loeb and C. M. Conrad, *J. Polymer Sci.*, **10**, 463 (1953).

(5) We are much indebted to Dr. Sidney Katz for these measurements.

(6) A. M. Holtzer, H. Benoit and P. Doty, THIS JOURNAL, **58**, 624 (1954).

(7) S. Newman, private communication.

(8) We are indebted to Mr. A. K. Doolittle, Carbide and Carbon Chemicals Company, for advice on the properties of solvents, and for generously supplying the isophorone.

(9) J. D. Ferry, E. L. Foster, G. V. Browning and W. M. Sawyer, *J. Colloid Sci.*, **6**, 377 (1951).

(10) J. D. Ferry, L. D. Grandine, Jr., and D. C. Udy, *ibid.*, **8**, 529 (1953).

(11) T. L. Smith, J. D. Ferry and F. W. Schremp, *J. Appl. Phys.*, **20**, 144 (1949).

(12) J. N. Ashworth and J. D. Ferry, *J. Am. Chem. Soc.*, **71**, 622 (1949).

(13) F. T. Adler, W. M. Sawyer and J. D. Ferry, *J. Appl. Phys.*, **20**, 1036 (1949).

Results

Viscosity.—The steady flow viscosity results are given in Table I and plotted logarithmically

TABLE I

STEADY FLOW VISCOSITIES

Capillary method for w_2 = 0, 0.0200, 0.0232 and 0.0384; falling ball method for all others.

w_2	Temp., °C.	log η	w_2	Temp., °C.	log η
0	25.0	−1.606	0.0887	0.0	3.075
	30.0	−1.654		20.1	2.543
	35.0	−1.702		40.2	2.107
0.0200	25.0	0.116		59.9	1.729
0.0232	25.0	0.301	0.1151	19.5	3.246
	35.0	0.114		39.3	2.783
0.0384	15.0	1.145		59.7	2.382
	20.0	1.053	0.1448	9.5	4.187
	25.0	0.952		19.5	3.854
	30.0	0.854		39.3	3.340
	35.0	0.761		59.7	2.906
0.0471	5.0	1.778	0.1770	29.5	4.167
	20.0	1.441		39.2	3.902
	35.0	1.137		49.7	3.658
0.0686	5.0	2.392		59.7	3.429
	20.0	2.031	0.1817	40.8	3.992
	35.0	1.717		48.8	3.809
				58.1	3.606

against the reciprocal absolute temperature in Fig. 2. The plots deviate somewhat from linearity, as expected from results on other polymers.[10]

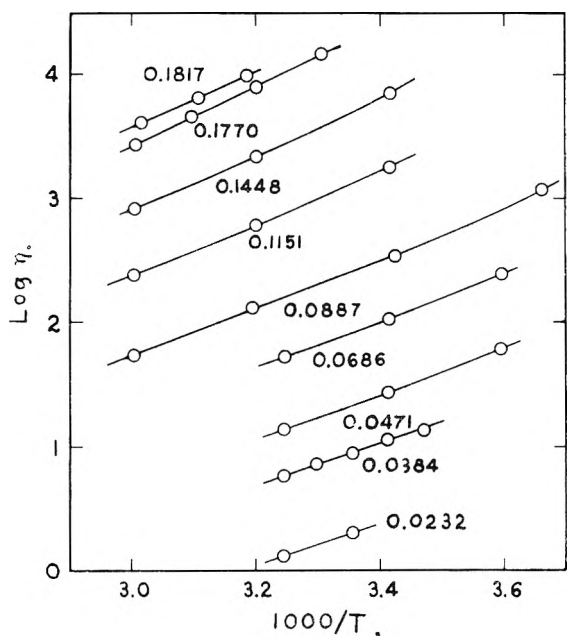

Fig. 2.—Logarithm of steady flow viscosity plotted against reciprocal absolute temperature for nine solutions. Figures denote weight fraction of polymer.

The degradation detected at the close of the dilution sequence from intrinsic viscosity measurements was also apparent from a comparison of the viscosity of the final 2.00% solution with that of a similar solution freshly diluted from the 18.2% stock which had been stored at −5°. The former was lower by a factor of 0.49. The gradual change over the total elapsed time of the experiments would not affect the temperature dependence, expressed logarithmically, at any one concentration, but it will exaggerate the apparent concentration dependence. The relative viscosities interpolated at 35° are plotted against concentration (c, in g. polymer per cc. solution) in Fig. 3 both as measured and also approximately corrected for the effect of degradation. For the latter purposes, a logarithmic correction has been added, assuming that log η changed due to degradation by an equal amount with each successive dilution. Figure 3 also includes two points at low concentrations (at 25°) from intrinsic viscosity measurements.

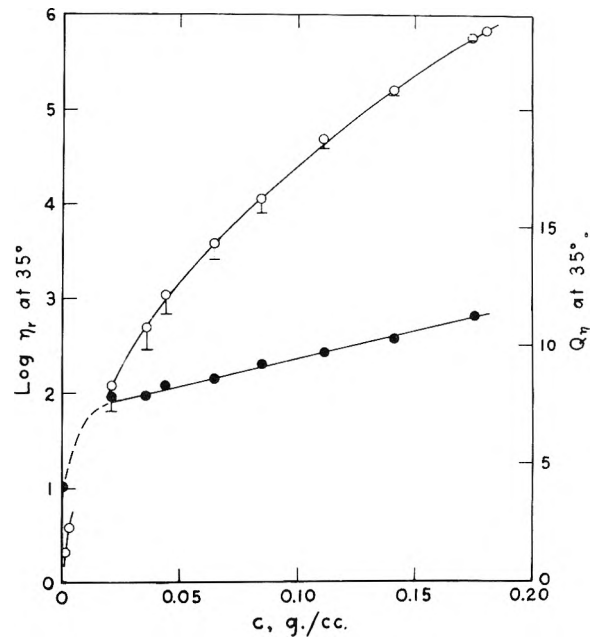

Fig. 3.—Logarithm of relative viscosity at 35° (open circles) and apparent activation energy for flow at 35° in kcal. (black circles) plotted against concentration (g. polymer per cc. solution). Horizontal bars denote viscosities before approximate correction for degradation. First two open circles are values at 25°.

The concentration dependence of the viscosity is very marked, as in all concentrated solutions of polymers; η is roughly proportional to c^5, an empirical relation which has also been found for polyisobutylene.[14]

The apparent activation energy for viscous flow, Q_η (= R d ln η/d(1/T)), calculated from tangents to the curves of Fig. 2 drawn at 35°, is given in Table II and also plotted in Fig. 3 against volume concentration. It increases linearly with c, as previously found for other polymers; however, it is notable that the linear plot extrapolates to an intercept of 7.1 kcal. at c = 0, considerably higher than that of the solvent (4.0 kcal.). For the vinyl polymers which we have studied[9,10,14] in several different solvents, such plots extrapolate rather closely into the respective pure solvent values. The abnormally high intercept seen here has been found also[15] for solutions of cellulose tributyrate in 1,2,3-trichloropropane, and may be characteristic of cellulose derivatives.

(14) M. F. Johnson, W. W. Evans, I. Jordan and J. D. Ferry, *J. Colloid Sci.*, **7**, 498 (1952).

(15) R. F. Landel, J. W. Berge and J. D. Ferry, unpublished experiments.

TABLE II

APPARENT ACTIVATION ENERGY FOR VISCOUS FLOW AT 35° (KCAL.)

w_1	Q_η	w_1	Q_η
0	4.03	0.0887	9.20
0.0232	7.85	.1151	9.75
.0384	7.91	.1448	10.30
.0471	8.33	.1770	11.21
.0686	8.60		

Dynamic Properties.– Values of G' and η' are not reported directly,[16] but have been reduced to standard reference states.[17] Wave propagation values of G' at different temperatures were reduced to 35° for each concentration by the formula $G'_p = G'T_0c_0/Tc$ and are plotted in Fig. 4 against the reduced frequency $\omega\eta T_0c_0/\eta_0Tc$. Here $T_0 = 308$°K.; c, c_0, η and η_0 are the concentrations (differing from each other due only to thermal expansion) and the steady flow viscosities at temperatures T and T_0, respectively. All the values at each concentration superpose within experimental error, showing that all the viscoelastic mechanisms concerned have the same temperature dependence.

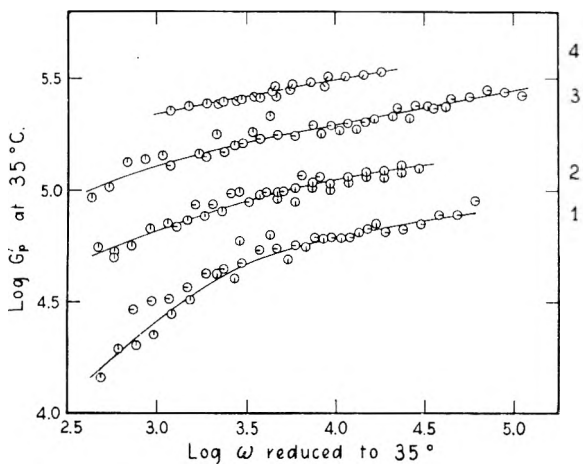

Fig. 4.—Real part of dynamic rigidity reduced to 35° and plotted logarithmically against reduced frequency for solutions with the following weight fractions of polymer: 1, 0.0887; 2, 0.1151; 3, 0.1448; 4, 0.1817. Key to temperatures: pip right, 0°; successive rotations clockwise, 20, 35, 40, 50 and 60°.

The same data further reduced to a reference state of unit viscosity and concentration are plotted in Fig. 5, where $G'_r = G'T_0/Tc$ and $\omega_r = \omega\eta T_0/Tc$. The points fall fairly well on a single curve, showing that all the mechanisms have the same concentration dependence. This is further demonstrated by the plot of reduced dynamic viscosity, η'/η, in Fig. 6. Here both wave propagation and transducer data are included; all the points fall quite satisfactorily along a single composite curve.

The data reduced in this way should not be perceptibly affected by the slight degradation apparent from the comparison of intrinsic and steady flow viscosities at the end of the dilution sequence. The actual measured viscosities were used in the reduction process; and dynamic properties, when

(16) The original data will appear in the Ph.D. Thesis of D. J. Plazek, University of Wisconsin, 1956.

(17) J. D. Ferry, *J. Am. Chem. Soc.*, **72**, 3746 (1950).

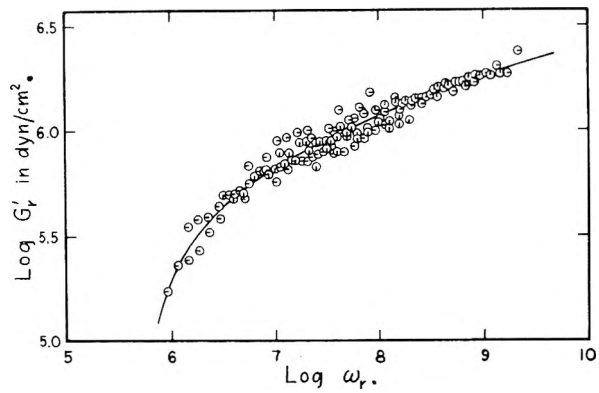

Fig. 5.—Real part of dynamic rigidity, reduced to unit viscosity and concentration at 35°, plotted logarithmically against reduced frequency: pip left, weight fraction of polymer 0.0887; successive 90° rotations counterclockwise, 0.1151, 0.1448 and 0.1817.

reduced to unit viscosity and concentration, depend on molecular weight only to a very minor degree in the range of time scale covered here.[2,18]

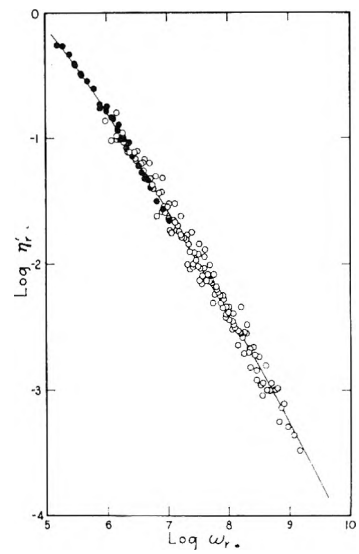

Fig. 6.—Real part of dynamic viscosity, reduced to unit viscosity and concentration at 35°, plotted logarithmically against reduced frequency: open circles, wave propagation data; black circles, single transducer data.

Relaxation Distribution Function.—The logarithmic distribution function of relaxation times, Φ_r, was calculated from the data of Figs. 5 and 6 by the usual second approximation formulas.[19] The results are plotted in Fig. 7. The agreement between values from G' and from η' is excellent.

The theoretical distribution function calculated from the Rouse theory,[20,18] for calculation of which (when reduced to the standard reference state) only the molecular weight is required, is also plotted in Fig. 7. The location of the terminal zone at the right appears to be correctly predicted by the theory, as it is in cellulose tributyrate solutions.[2] However, as usual in concentrated solutions, the remainder of the function within the time scale covered is a rather flat plateau instead of being proportional to $\tau^{-1/2}$ as provided by theory.

(18) J. D. Ferry, I. Jordan, W. W. Evans and M. F. Johnson, *J. Polymer Sci.*, **14**, 261 (1954).

(19) J. D. Ferry and M. L. Williams, *J. Colloid Sci.*, **7**, 347 (1952).

(20) P. E. Rouse, Jr., *J. Chem. Phys.*, **21**, 1272 (1953).

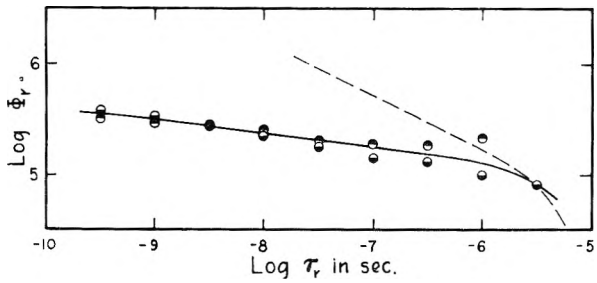

Fig. 7.—Relaxation distribution function reduced to unit viscosity and concentration at 35°: circles top black, calculated from G'; bottom black, from η'. Dashed line is the prediction of the Rouse theory.

Gelation Phenomena.—Some of the above data were obtained below the gel points of the solutions, by taking measurements soon after attainment of thermal equilibrium, before the slow crystallization processes had progressed appreciably. In one experiment, however, a 14.5% solution was kept below its gel point for 24 hours and wave propagation measurements were made repeatedly after gelation.

The solution was cooled from 60 to 20°, reaching thermal equilibrium within 0.5 hr. Wave propagation measurements over a frequency range from 300 to 2000 cycles/sec. at this point showed G' increasing with frequency from 1.5 to 1.8 $\times$ 10^5 dyne/cm.^{2}, in accordance with the dispersion shown in curve 3 of Fig. 4. At 4.5 hr. after changing the temperature, gelation had occurred; G' was now somewhat higher—3.4 $\times$ 10^5 dyne/cm.^{2}—and independent of frequency. With further storage at 20°, G' increased linearly with time to 7.8 $\times$ 10^5 dyne/cm.^{2} (Fig. 8), remaining independent of frequency.

The transverse waves appeared to be damped in this gel to an extent (damping index[12] λ/x_0 of the order of 1) incompatible with the absence of dispersion of G'. It is believed that the observed damping is spurious, due to the effect of the walls of the container as expected[13] when the inherent damping is small. The same effect has been observed in other gels.[21,22]

The absence of dispersion within experimental error means that $\Phi < 10^4$ dyne/cm.^{2} over a range of (unreduced) time scale from $10^{-2.5}$ to $10^{-3.3}$ sec., in contrast to its value of 4 $\times$ 10^4 in this solution before gelation. In this time range, which corresponds just to the middle of the reduced curve in Fig. 7, the elastic contributions are believed to be due to coöperative motions of groups of molecules coupled fairly tightly to each other by occasional entanglements.[18] Gelation evidently sharply depresses these contributions as neighboring molecules become still more tightly coupled by crystallite cross-links. The coöperative motions may be modified by the fact that the coupling is tighter or by a different spatial distribution of linkage points or both.

After gelation, G' as measured is probably not much different from the equilibrium modulus representing the rubber-like elasticity of the cross-linked network. Its increase with time no doubt reflects the lateral growth of crystallites. A linear increase of modulus with time has also been observed by Bisschops[23] in gels of polyacrylonitrile.

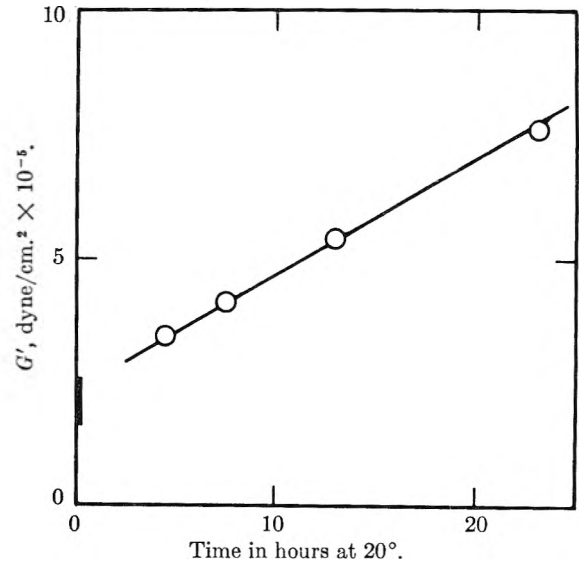

Fig. 8.—Increase in real part of dynamic rigidity with time for 14.5% gel at 20°. Vertical bar at left denotes range of G' between 300 and 2000 cycles/sec. before gelation.

Discussion

In Fig. 9, the relaxation distribution function of cellulose trinitrate is compared with those of several other cellulose derivatives: three fractions of cellulose tributyrate dissolved in 1,2,3-trichloropropane[2] and a cellulose acetate dissolved in dioxane (calculated by Smith[24] from data of Philippoff[25]). The other derivatives exhibit quite horizontal plateaus, while the plateau for cellulose trinitrate is inclined, with a slope of about −0.15. Vinyl polymers of comparable molecular weights[3] exhibit slopes of about −0.3, all thus deviating from the prediction of the simple Rouse theory of −0.5.

Such deviations from the Rouse slope are attributed to entanglement coupling,[18] and with respect to the latter cellulose trinitrate thus appears to be intermediate between cellulose tributyrate and vinyl polymers in character.[26] Without a more pre-

(21) J. D. Ferry and J. E. Eldridge, THIS JOURNAL, **53**, 184 (1949).

(22) G. E. Heckler, Ph.D. Thesis, University of Wisconsin, 1952.

(23) J. Bisschops, *J. Polymer Sci.*, **12**, 583 (1954); **17**, 89 (1955).

(24) T. L. Smith, *J. Polymer Sci.*, **14**, 37 (1954).

(25) W. Philippoff, *Physik. Z.*, **35**, 900 (1934).

(26) Another phenomenon in concentrated solutions has been attributed to entanglements by Hatfield and Rathmann[27] and by DeWitt,[28]—namely, an exaggerated concentration dependence of the magnitude of contributions to the relaxation spectrum, which makes it necessary to replace c by c^3 in the usual definitions for reduced variables—above a critical value of c. It should be emphasized that the Hatfield–DeWitt entanglements are not the same as the entanglements responsible for a plateau in the relaxation spectrum. In vinyl polymers[3,18] as well as in cellulose derivatives,[2] plateaus appear in the spectra of moderately concentrated solutions where the usual definitions for reduced variables give accurately superimposed composite curves. For example, the critical concentration for appearance of a plateau in solutions of polyisobutylene of molecular weight 10^6 is about 1%, as calculated from the average molecular weight between coupling entanglements in the undiluted polymer[29] and its anticipated inverse proportionality to concentration.[30] But the critical concentration for the onset of the c^2 concentration dependence observe by DeWitt is 8%.

(27) M. R. Hatfield and G. B. Rathmann, *J. Appl. Phys.*, **25**, 1082 (1954).

(28) T. W. DeWitt, H. Markovitz, F. J. Padden, Jr., and L. J. Zapas, *J. Colloid Sci.*, **8**, 174 (1955).

(29) J. D. Ferry, R. F. Landel and M. L. Williams, *J. Appl. Phys.*, **26**, 359 (1955).

(30) F. Bueche, *ibid.*, **26**, 738 (1955).

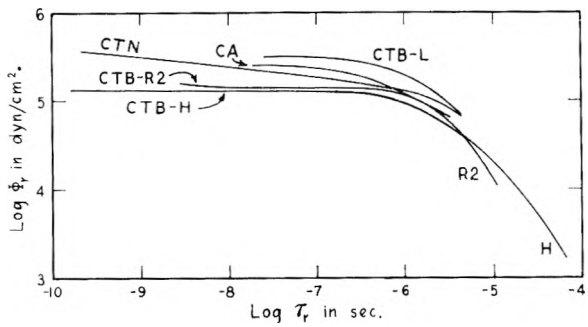

Fig. 9.—Comparison of relaxation distribution functions of cellulose derivatives: CTN, cellulose trinitrate (Fig. 7); CTB, cellulose tributyrate (reference 2), molecular weights of 55,000 (L), 152,000 (R2), and 300,000 (H); CA, cellulose acetate (references 23, 24).

cise concept of the nature of the entanglement coupling, however, it is difficult to interpret these differences. The CTB chain is certainly far more extended than those of vinyl polymers,[31] and the CTN chain appears to be even more so.[6] But there is some evidence that the cellulose units are actually more mobile than those of vinyl polymers, a feature perhaps associated with the free-draining character of the cellulose chain.[6] Thus, the internal viscosity parameter derived by Kuhn[32] for the resistance of the chain itself to deformation is much smaller for cellulose derivatives than for polystyrene. The differences in monomer structure must be responsible not only for the characteristic plateau shapes in Fig. 9 but also for other contrasting mechanical properties, such as the activation energies for viscous flow (Fig. 5) and the shapes of relaxation spectra in the transition region between rubber-like and glass-like consistency, which will be further discussed in later communications.[15,33]

Acknowledgment.—This work was part of a program of research on the physical structure and properties of cellulose derivatives and other polymers supported by the Allegany Ballistics Laboratory, Cumberland, Maryland, an establishment owned by the United States Navy and operated by the Hercules Powder Company under Contract NOrd 10431. It was also supported in part by a grant from Research Corporation and by the Research Committee of the Graduate School of the University of Wisconsin from funds supplied by the Wisconsin Alumni Research Foundation. We are indebted to Mrs. J. C. Alexander and Mrs. Garrett Droppers for assistance with calculations.

(31) L. Mandelkern and P. J. Flory, *J. Am. Chem. Soc.*, **74**, 2517 (1952).

(32) W. Kuhn and H. Kuhn, *Helv. chim. acta*, **29**, 609 (1946).

(33) R. F. Landel and J. D. Ferry, THIS JOURNAL, **60**, 294 (1956).

DYNAMIC MECHANICAL PROPERTIES OF THE SYSTEM CELLULOSE TRIBUTYRATE–DIMETHYL PHTHALATE[1]

BY ROBERT F. LANDEL AND JOHN D. FERRY

Contribution from the Department of Chemistry, University of Wisconsin, Madison, Wis.

Received August 10, 1955

The real and imaginary components of the complex compliance, J' and J'', have been measured between 30 and 4500 cycles/sec. for three gelatinous compositions of cellulose tributyrate (M_n = 300,000) and dimethyl phthalate containing 20.4, 42.6 and 57.5% polymer. The temperature range was from 25 to −52°. Data for the 20.4% gel were combined by the method of reduced variables to give composite curves of J' and J'' reduced to a standard temperature. Data for the 42.6% gel were similarly combined above −25° and separately below −25°; near −25° there was a change in properties attributable to a structural modification, probably increased crystallinity. Data for the 57.5% gel could not be combined by reduced variables, since there were progressive changes with decreasing temperature, attributable also to increases in crystallinity. Where reduced variables were applicable, the temperature shift factors followed a recently proposed equation of Williams, Landel and Ferry. The equilibrium rigidity approached at low frequencies at 25° was proportional to the 2.8 power of polymer concentration. The loss tangent passed through a maximum with increasing frequency; with increasing concentration (at constant temperature) this maximum became lower and broader and shifted to lower frequencies. The retardation distribution functions exhibited maxima whose heights were directly proportional to the equilibrium compliances. Increased crystallinity evidently depresses the retardation distribution, especially at long times; depresses J''; and depresses J' somewhat less, at the same time flattening the slope of the latter. The relaxation distribution function of the 20.4% gel followed the slope prescribed by the Rouse theory remarkably well. The more concentrated gels showed somewhat flatter slopes in a region where vinyl polymer systems show steeper slopes than that predicted by the Rouse theory.

Introduction

Recent studies of the dynamic rigidities and viscosities, at audiofrequencies, of concentrated solutions of cellulose tributyrate in trichloropropane[2] and of cellulose trinitrate in isophorone[3] have delineated the relaxation distribution functions of these systems in the plateau zone of soft viscoelastic consistency. These investigations provided no information, however, about the transition from soft to glass-like consistency which appears in shorter regions of time scale. The transition zone can be made accessible to audiofrequency methods by increasing the solvent viscosity and lowering the temperature.

Measurements of dynamic mechanical properties in the transition zone are now reported for solutions of cellulose tributyrate in dimethyl phthalate. Such solutions are partly crystalline, and hence cross-linked (*i.e.*, gelatinous), at the temperatures of measurement. When the concentration of polymer is not too high (*e.g.*, 20%), the crystallinity does not interfere with interpretation of the results, but at

(1) Part XXII of a series on Mechanical Properties of Substances of High Molecular Weight.

(2) R. F. Landel and J. D. Ferry, THIS JOURNAL, **59**, 658 (1955).

(3) D. J. Plazek and J. D. Ferry, *ibid.*, **59**, 289 (1956).

higher concentrations it introduces some complications. The relaxation and retardation distribution functions derived from these measurements exhibit some unusual features, which are attributed partly to the presence of crystallite cross-linking and partly to characteristics of the cellulose chain structure.

Materials

The cellulose tributyrate was generously provided by Dr. C. J. Malm of the Eastman Kodak Company. Its chemical characterization and fractionation have been described previously.[2] Fraction H, with a viscosity-average molecular weight of 300,000, was used in the present study. It was dried *in vacuo* at room temperature before solutions were prepared. The dimethyl phthalate, Eastman Kodak Co. practical grade, was redistilled under reduced pressure (boiling at 142–143°).

Solutions containing 20.4, 42.6 and 57.5% polymer by weight were prepared by mixing weighed amounts of polymer and solvent at 120°, with further heating to 150–180° for brief periods. Nitrogen (bubbled through solvent to minimize vaporization losses) was passed over the mixtures to prevent oxidation. Any air bubbles introduced during mixing were removed by aspiration at 120° before cooling to room temperature. The slight solvent losses were determined by reweighing, and the concentrations were calculated on the basis of residual solvent. In color the resulting gels ranged from almost colorless (20.4%) to light straw (57.5%).

The disc-shaped samples for the transducer were molded for the 20.4% gel by remelting the system and pouring directly into the preheated mold at 85°. The more concentrated gels were removed from the glass mixing tubes (by breaking the glass) and sliced into slightly oversize discs, which were then molded to exact size under pressure at 125°.

The melting points of the gels were not measured, but were calculated to be 72, 92 and 102° for concentrations of 20.4, 42.6 and 57.5%, respectively, using the theory of Flory[4] together with constants determined by Mandelkern and Flory[5] for the cellulose tributyrate–dimethyl phthalate system at higher concentrations (50 to 100% polymer). The melting point calculated in this way for another gel of concentration 13.4% was 67°, in fair agreement with an observed value of 75–78°, considering the magnitude of extrapolation.

Since the calculated melting points were so high, it was expected that prolonged annealing at room temperature would allow the extent of crystallinity to approach a stable state which would not be greatly affected by subsequent cooling to lower temperatures. Accordingly, the 20.4% samples were annealed at room temperature for 4.5 months, and the more concentrated samples were annealed for periods from 2 to 9 weeks. The expectation of stability was not entirely fulfilled, however, as will be seen below.

Method

Measurements of the complex shear compliance ($J^* = J' - iJ''$) were made at frequencies between 30 and 4500 cycles/sec. with the double transducer of Fitzgerald and Ferry.[6,7] The disc-shaped samples were compressed 5 to 10% between the floating mass and the driving tube of the instrument. The sizes and shapes of the samples used are summarized as follows.

Concentration 20.4%.—Only one pair of samples was employed, $^{11}/_{16}$ in. (diameter) by $^{1}/_{32}$ in. (thickness), with a sample coefficient[6,8] of 67.4 cm. after compression.

Concentration 42.6%.—Three pairs of samples were employed. Samples 60, $^{5}/_{16}$ in. by $^{3}/_{16}$ in., had a sample coefficient of 3.77 cm. Samples 59 and 66, both $^{11}/_{16}$ in. by $^{3}/_{32}$ in., had nominal sample coefficients of 20.6 and 22.4, respectively. However, neither of these sample pairs appeared to have adhered perfectly to the driving tube surfaces, as evidenced by values of J' and J'' higher than those obtained from samples 60 at several overlapping temperatures, whereas the ratio J''/J' was in good agreement for all three sample pairs. Imperfect adherence may have been due to slight irregularities in the surface which for these cross-linked gels are not smoothed out by flow under compression. Samples 60 were well sandpapered for smoothness and had the smallest cross-section area, and their adherence is assumed therefore to have been complete. Empirical correction factors of 0.51 for samples 59, 0.90 for samples 66 above −25°, and 0.70 for 66 below −25° were applied to bring their J' and J'' values into agreement.

Concentration 57.5%.—Three pairs of samples were employed. Samples 68, $^{5}/_{16}$" by $^{3}/_{16}$", had a sample coefficient of 3.77; their surfaces were carefully smoothed by sandpaper. Samples 52, $^{5}/_{16}$" by $^{1}/_{4}$", had a nominal sample coefficient of 2.67, but it was necessary to apply an empirical factor of 0.72 to bring J' and J'' values into agreement with those of samples 68 at overlapping temperatures. Samples 53, $^{11}/_{16}$" by $^{3}/_{32}$", had a nominal coefficient of 19.7, but required an empirical correction factor of 0.84. Both these corrections were attributed to incomplete adherence.

All these gels resembled those of polyvinyl chloride[6] in that there was no tendency toward the lateral bulging observed with sticky polymers such as polyisobutylene.[6] Absence of bulging was readily demonstrated by compression of samples outside the transducer. It is believed, therefore, that there are no errors in the sample coefficients attributable to bulging.

Sample coefficients above and below room temperature were calculated as usual,[6,5] assuming the thermal expansion coefficients of the gels to be 0.1% per degree.

Results

Concentration 20.4%.—Measurements at various frequencies were made at progressively decreasing temperatures from 25 to −52° and then at −40°, −25 and 25°. The latter check measurements agreed well with the corresponding values on the downward temperature sequence except for the final run at 25°. Here J'' was slightly lower; the differences were scarcely beyond experimental error, but they reveal an effect which became much more apparent in the gels of higher concentration. Values of J' and J'' are plotted logarithmically in Figs. 1 and 2.

Concentration 42.6%.—Measurements at various frequencies were made on samples 59 at progressively decreasing temperatures from 25 to −50° and then at −25°. The

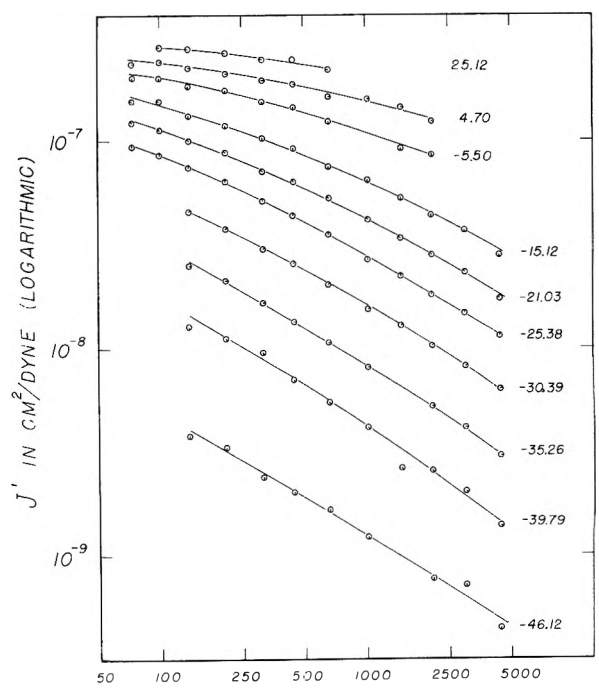

Fig. 1.—Variation of the real component of complex compliance with frequency for 20.4% gel at 10 temperatures as shown.

(4) P. J. Flory, *J. Chem. Phys.*, **17**, 223 (1949).

(5) L. Mandelkern and P. J. Flory, *J. Am. Chem. Soc.*, **73**, 3206 (1951).

(6) E. R. Fitzgerald and J. D. Ferry, *J. Colloid Sci.*, **8**, 1 (1953).

(7) We are much indebted to Professor Fitzgerald, Pennsylvania State University, for supervising maintenance of the apparatus and making certain modifications.[8]

(8) M. L. Williams and J. D. Ferry, *J. Colloid Sci.*, **9**, 479 (1954).

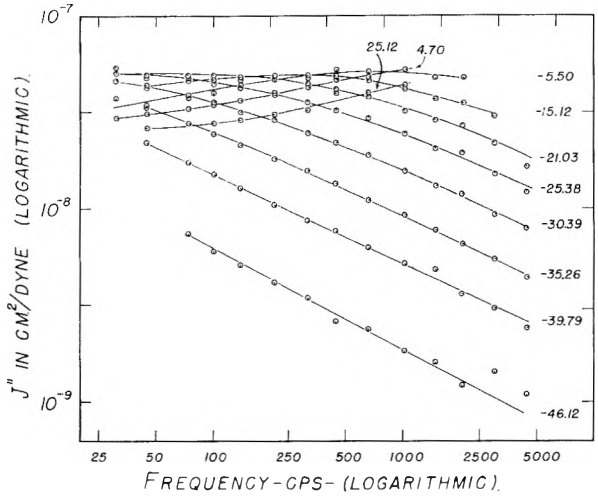

Fig. 2.—Variation of the imaginary component of complex compliance with frequency for 20.4% gel at 10 temperatures as shown.

latter check run disagreed with the corresponding −25° run on the downward temperature sequence; J'' had decreased considerably during the time spent at lower temperatures, and J' somewhat less so. Samples 60 were measured at 25° and then cooled immediately to −25°, with measurements there and at intervals down to −52°. A check run at −35° agreed with that on the downward sequence, but one at −25° showed again a lower compliance, with J'' affected more than J'. Samples 66 were measured from 25° down to −40°.

It was evident that a change in internal structure, probably an increase in crystallinity, occurred with decreasing temperature, and that the most marked change occurred near −25°. As a first approximation, the samples could be considered as existing in one state above −25° and in another, more highly crystalline or annealed, stable below −25°; the properties at −25° were distinctly different depending on whether the samples had been cooled below this temperature for an extended period. Values of J' and J'' are plotted logarithmically in Figs. 3 and 4, where the two states are separated by dashed curves.

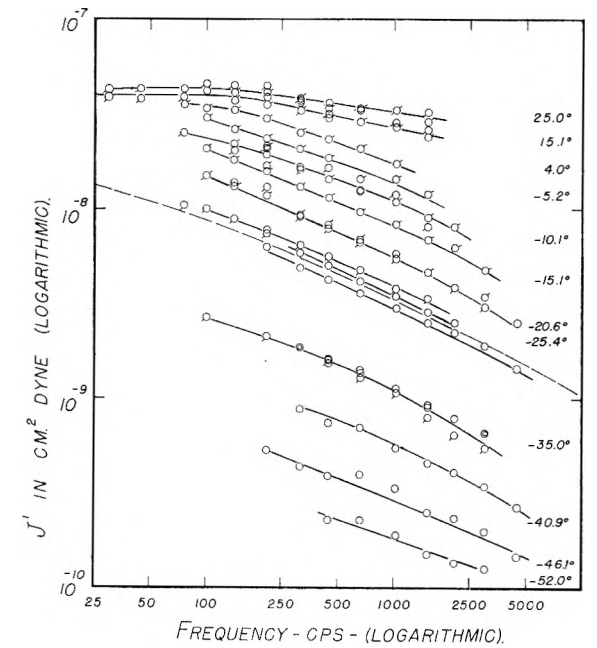

Fig. 3.—Variation of the real component of complex compliance with frequency for 42.6% gel at 12 temperatures as shown: above dashed line, before cooling below −25°; below dashed line, after cooling below −25°; tag up, samples 59; no tag, samples 60; tag down, samples 66.

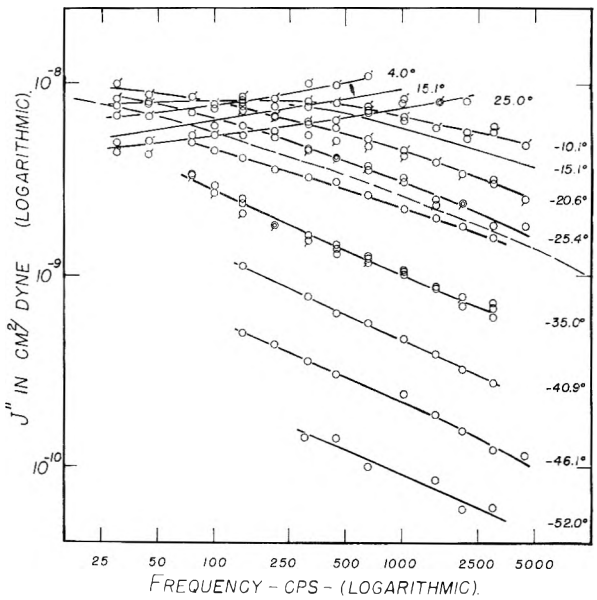

Fig. 4.—Variation of the imaginary component of complex compliance with frequency for 42.6% gel at 11 temperatures as shown. Key to samples and significance of dashed line same as in Fig. 3.

Concentration 57.5%.—Measurements at various frequencies were made on samples 68 at progressively decreasing temperatures from 25 to −46° and then at −30, −25, −15 and 25°. All the latter check runs agreed fairly well with those on the downward temperature sequence. Samples 52 were measured from 15° down to −34°. Samples 53 were measured from 25° down to −30°, with a check run at 25° which agreed fairly well. Although the state of the material appeared to be reproducible after a temperature cycle, attempts to apply the method of reduced variables (see below) indicated that the structure had changed reversibly with temperature, the crystallinity probably increasing upon cooling and then reverting to approximately its original state upon warming. Values of J' and J'' are plotted logarithmically in Figs. 5 and 6.

Application of Reduced Variables

Logarithmic plots of $J_p' = J'[T_0/T_0\rho_0 + (J_\infty/J')(1 - T\rho/T_0\rho_0)]$ and $J''_p = J''(T\rho/T_0\rho_0)$ were

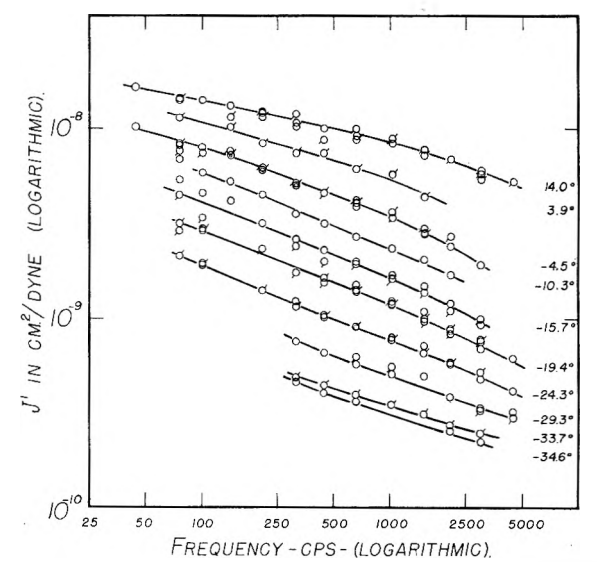

Fig. 5.—Variation of the real component of complex compliance with frequency for 57.5% gel at 10 temperatures as shown: tag up, samples 52; tag down, samples 53; no tag, samples 68.

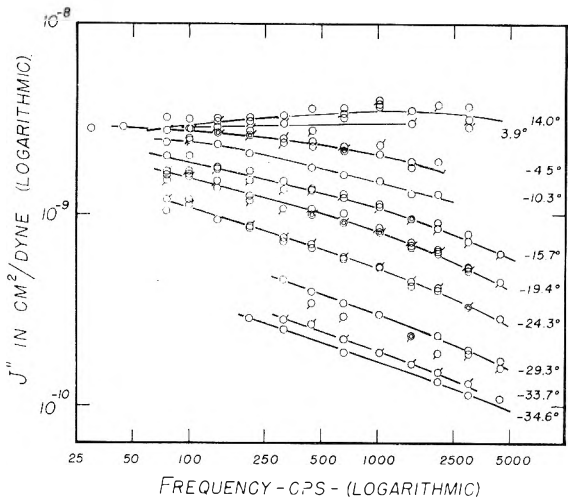

Fig. 6.—Variation of the imaginary component of complex compliance with frequency for 57.5% gel at 10 temperatures as shown. Key to samples same as in Fig. 5.

prepared to test the method of reduced variables.[9] Here ρ and ρ_0 are the densities at the absolute temperature of measurement, T, and a standard temperature, T_0. The limiting high frequency compliance, J_∞, was assumed to be 1.0×10^{-10} cm.²/dyne, and T_0 was chosen as 298°K. for the 20.4% gel and 248°K. for the other two. If all relaxation times depend identically on temperature, then such curves should be parallel and superposable by horizontal shifts on the logarithmic frequency scale; and the shifts should be identical for J'_p and J''_p.

For the 20.4% gel, the criteria for superposition were fulfilled. It was concluded, just as for the polyvinyl chloride gels previously studied,[6,9] that the proportion of crystalline material was small in this system; and that even if some changes in crystallinity occurred with changing temperature, the structure of the amorphous regions was essentially unmodified and the dynamic mechanical properties were dominated by the latter. The shift factors a_T are given in Table I, and composite curves of J'_p and J''_p are plotted logarithmically against the reduced circular frequency ωa_T in Figs. 7 and 8.

For the 42.6% gel, the a_T factors obtained from J'_p and J''_p agreed fairly well except near −25°. In this more concentrated system, the structural change already apparent in the dependence on thermal history near −25° affected J'' more than J', and the resulting shifts in J'_p and J''_p could not be attributed solely to prolongation of relaxation times. Nevertheless, reasonable superposition was obtained by combining the original −25° measurements with those at higher temperatures up to 4° and the subsequent "annealed" −25° measurements with those at lower temperatures. The necessary a_T factors are also given in Table I, and the composite curves for J'_p and J''_p are plotted in Figs. 9 and 10.

For the 57.5% gel, the J''_p curves were approximately parallel, but the J'_p curves became flatter

TABLE I

TEMPERATURE REDUCTION FACTORS

Concn. 20.4%, ref. 25° t, °C.	log a_T	Concn. 42.6%, ref. −25° t, °C.	log a_T
25.1	0.00	4.1	−1.87
4.7	0.58	− 5.2	−1.50
− 5.5	1.08	−10.1	−1.23
−15.1	1.68	−15.1	−0.88
−21.0	2.05	−20.6	−0.42
−25.4	2.44	−25.4	0.04
−30.4	2.87	−30.2	0.64
−35.3	3.39	−35.0	1.30
−39.8	3.94	−40.9	2.12
−46.1	4.80	−46.1	2.88
		−52.0	3.73

(9) J. D. Ferry and E. R. Fitzgerald, *J. Colloid Sci.*, **8**, 224 (1953).

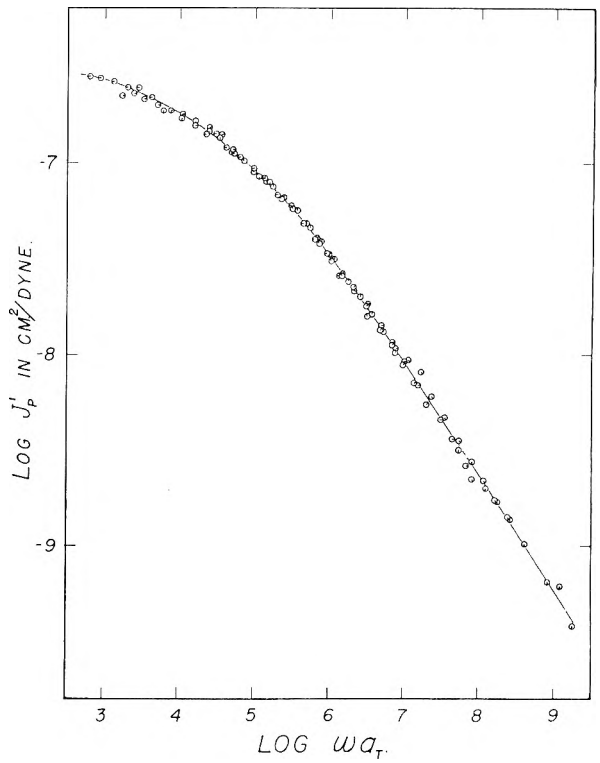

Fig. 7.—Real part of complex compliance of 20.4% gel reduced to 25°, plotted logarithmically against reduced frequency. Temperature key same as in Fig. 1.

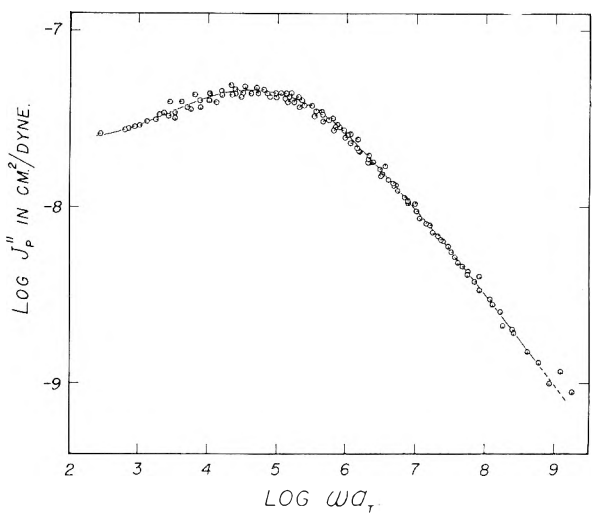

Fig. 8.—Imaginary part of complex compliance of 20.4% gel reduced to 25°, plotted logarithmically against reduced frequency. Temperature key same as in Fig. 2.

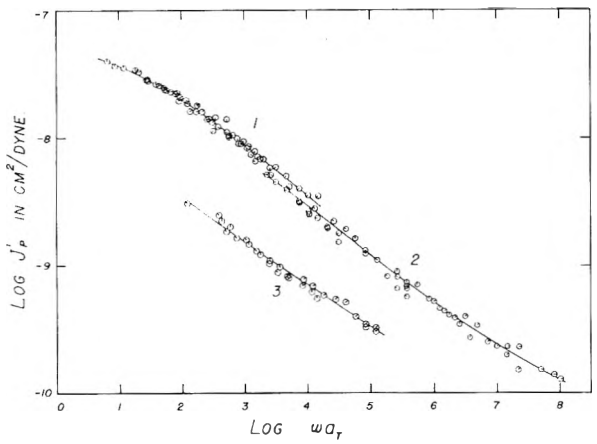

Fig. 9.—Real part of complex compliance reduced to −25°, plotted logarithmically against reduced frequency. Curve 1, 42.6% gel before cooling below −25°; pip up, 4.0°; successive 45° rotations clockwise, decreasing temperatures as shown in Fig. 3. Curve 2, 42.6% gel after cooling below −25°; pip right, −25°; successive 45° rotations clockwise, decreasing temperatures as shown in Fig. 3. Curve 3, 57.5% gel; pip 45° left, −19.4°; up, −24.3°; 45° right, −29.3°.

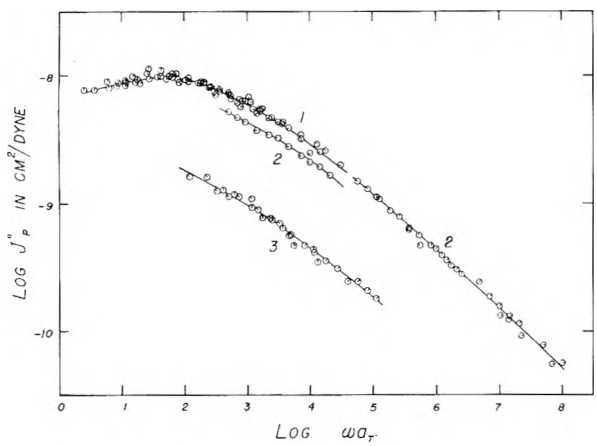

Fig. 10.—Imaginary part of complex compliance reduced to −25°, plotted logarithmically against reduced frequency. Key to concentrations and temperatures same as in Fig. 9.

with decreasing temperature so that superposition was impossible. When the retardation distribution function,[9] L, was calculated at each individual temperature by the usual second approximation formulas,[10] the values from J' and J'' were in good agreement. It was evident that the usual shift of L along the logarithmic time scale with decreasing temperature was accompanied by a decrease in magnitude. The latter change was manifested in a corresponding drop in magnitude of J'' (which in zero approximation equals L) but was manifested in J' primarily by a change in slope. This is consistent with the expected effects of increasing crystallinity in a concentrated system (see below).

To obtain a limited comparison of the 57.5% gel with the others, 248°K. was chosen as a standard temperature and data at the three nearest temperatures were superposed by choosing a_T values of −0.67, −0.07 and 0.62 at −19.4, −24.3 and −29.3° respectively. The resulting composite curves of J'_p and J''_p, shown also in Figs. 9 and 10, are probably not seriously distorted within such a narrow temperature range, but it would be useless to attempt superposition over wider ranges.

(10) M. L. Williams and J. D. Ferry, *J. Polymer Sci.*, **11**, 169 (1953).

Discussion

Analysis of Temperature Dependence.—For comparison of the temperature dependence of a_T with that prescribed by a recently proposed equation[11]

$$\log a_T = -8.86(T - T_s)/(101.6 + T - T_s)$$

the values in Table I were reduced to separate reference temperatures T_s, chosen as 247° for the 20.4% gel, 251° for the 42.6% gel in its state above −25°, and 256° for the latter in its more annealed state below −25°. These values are plotted in Fig. 11; they show quite good agreement with the curve given by the above empirical equation, except at the highest temperatures. For many polymer systems, T_s lies approximately 50° above the glass transition temperature T_g. The glass transition temperatures implied from this relationship are very low, and evidently correspond to the $T_g(1)$ measured by Mandelkern and Flory[5] rather than to their $T_g(2)$. It is hoped that measured T_g values for these systems will be available in the future for direct comparison.

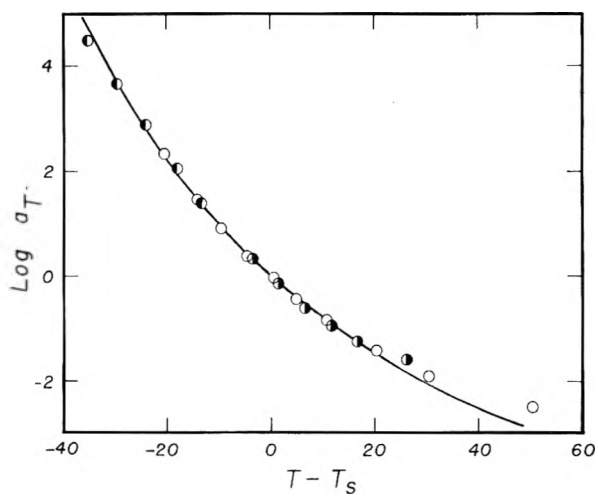

Fig. 11.—Temperature reduction factors reduced to T_s, plotted logarithmically against $T - T_s$: open circles, 20.4% gel (T_s = 247°K.); right black, 42.6% gel before cooling below −25° (T_s = 251°K.); left black, 42.6% gel after cooling below −25° (T_s = 256°K.). Curve is from equation of Williams, Landel and Ferry.[11]

Magnitudes of Mechanical Properties.—The maximum values of J' approached at room temperature and low frequencies are about 3×10^{-7}, 4.2×10^{-8} and 1.8×10^{-8} cm.²/dyne. respectively, for the 20.4, 42.6 and 57.5% gels. These values are probably not far from the equilibrium compliances of these cross-linked systems, and the losses are so small here that the reciprocals of J' represent the corresponding real components of the shear modulus, G'—practically, the equilibrium modulus G. A logarithmic plot against weight fraction of polymer (which is nearly the same as volume fraction, since the densities of the gels differ little from that of the solvent) shows that the modulus is propor-

(11) M. L. Williams, R. F. Landel and J. D. Ferry, *J. Am. Chem. Soc.*, **77**, 3701 (1955).

tional to the 2.8 power of polymer concentration. This figure may be compared with exponents of slightly over 3 obtained by Walter[12] from static measurements on polyvinyl chloride gels in several rather poor solvents, and suggests that the features of the crystallite cross-linking are similar in the two types of systems. (The two polyvinyl chloride gels at concentrations of 10 and 40% by volume whose dynamic properties were previously measured in this Laboratory[6,9] yield, from comparison of limiting low-frequency values of G', a corresponding exponent of 3.0.)

The measurements do not extend to high enough frequencies to furnish the limiting values of J_∞ for the gels, but the curves appear to be consistent with the assumption made earlier that this quantity is approximately 10^{-10} for all three, as expected from results on other polymer systems.

The real part of the complex shear modulus, G', was calculated from the composite curves of Figs. 7–10 and is plotted logarithmically against frequency in Fig. 12 for all three gels. Here the

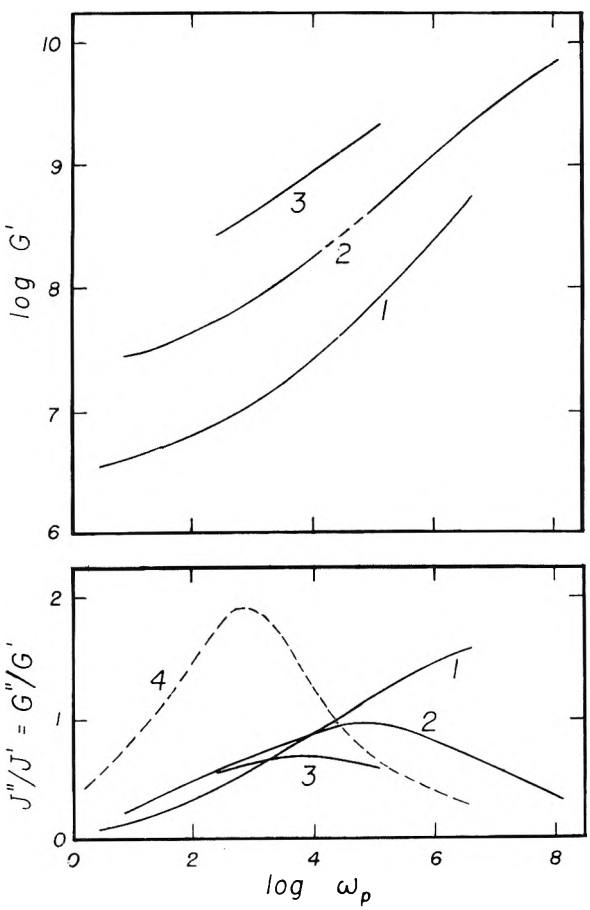

Fig. 12.—Logarithm of real part of complex shear modulus (above) and loss tangent (below) reduced to −25°: 1, 20.4%; 2, 42.6%; 3, 57.5%; 4, comparative data for a 40% polyvinyl chloride gel in dimethylthianthrene[9] reduced to 25°.

data for the 20.4% composition have been reduced to −25° for comparison with the other two. The slope evidently becomes smaller with increasing concentration, as the modulus, starting from different equilibrium (low frequency) values, must reach approximately the same value at high frequencies.

The loss tangent G''/G' ($= J''/J'$) is also plotted in Fig. 12, reduced to −25° for each gel. The loss maximum flattens with increasing concentration and shifts to lower frequencies. Actually, for the 20.4% gel, the maximum is not encompassed in the range of reduced frequencies covered. The loss tangent is considerably lower and broader for the 42.6% cellulose tributyrate gel than for a 40% (by volume) gel of polyvinyl chloride previously studied,[6,9] designated by a dashed curve for comparison. In their low maxima and breadth, these loss tangents differ from those of vinyl polymers previously studied[13]; the only one of the latter which at all resembles the curves in Fig. 11 is polyisobutylene, which however has an oddly shaped hump not present here.

Retardation Distribution Functions.—The distribution function of retardation times, L, was calculated from the composite curves of Figs. 7–10 by the usual second approximation formulas[10]; it is given in Table II and plotted in Fig. 13 for the three gels reduced to −25°. The values obtained separately from J' and J'' are mostly in good agreement. (The maximum in L at 57.5%, denoted by a dashed curve, is estimated from the maximum value of J'' at higher temperatures in Fig. 6.)

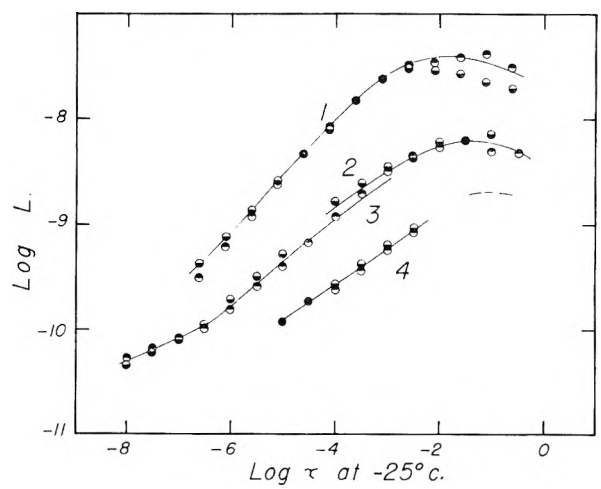

Fig. 13.—Logarithm of retardation distribution function reduced to −25°: 1, 20.4%; 2, 42.6% before cooling below −25°; 3, 42.6% after cooling below −25°; 4, 57.5%; circles top black, calculated from J'; bottom black, from J''.

The level of L decreases with increasing concentration, at constant τ. This may be partly due to a shift in logarithmic time scale occasioned by an increase in the local monomeric friction coefficient.[14,15] However, at long times (where L is flat and a shift in time scale would have no effect) it is almost entirely due to a decrease in the magnitude of the individual contributions to compliance in the retardation spectrum, no doubt associated with increased cross-linking as revealed by the drop

(12) A. T. Walter, *J. Polymer Sci.*, **13**, 207 (1954).

(13) J. D. Ferry, Chapter VI in Stuart, "Die Physik der Hochpolymeren," Vol. IV, Springer, Berlin, in press.

(14) F. Bueche, *J. Chem. Phys.*, **22**, 603 (1954).

(15) J. D. Ferry, R. F. Landel and M. L. Williams, *J. Appl. Phys.*, **26**, 359 (1955).

TABLE II

RETARDATION AND RELAXATION DISTRIBUTION FUNCTIONS, REDUCED TO −25°

Log τ	Log L From J'	Log L From J''	Log Φ From G'	Log Φ From G''
	Concn. 20.4%			
−6.6	−9.46	−9.31	...	...
−6.1	−9.16	−9.06	8.04	8.13
−5.6	−8.86	−8.80	7.75	7.83
−5.1	−8.56	−8.52	7.49	7.54
−4.6	−8.28	−8.26	7.24	7.27
−4.1	−8.00	−8.03	6.99	6.99
−3.6	−7.77	−7.76	6.74	6.71
−3.1	−7.55	−7.55	6.50	6.46
−2.6	−7.42	−7.46	6.29	6.19
−2.1	−7.41	−7.48	6.07	5.94
−1.6	−7.36	−7.50	5.93	5.71
−1.1	−7.31	−7.59	5.76	5.44
−0.6	−7.46	−7.65	...	...
	Concn. 42.6% (above −25°)			
−4.0	−8.92	−8.83	7.82	7.88
−3.5	−8.71	−8.61	7.57	7.66
−3.0	−8.50	−8.45	7.36	7.43
−2.5	−8.36	−8.33	7.14	7.26
−2.0	−8.26	−8.21	6.97	7.06
−1.5	−8.18	−8.19	6.77	6.80
−1.0	−8.14	−8.30	...	6.58
−0.5	...	−8.32	...	...
	Concn. 42.6% (below −25°)			
−8.0	−10.55	−10.67	9.35	9.31
−7.5	−10.37	−10.43	9.19	9.19
−7.0	−10.17	−10.20	9.06	9.05
−6.5	−9.99	−9.95	8.90	8.93
−6.0	−9.81	−9.72	8.69	8.75
−5.5	−9.58	−9.50	8.47	8.54
−5.0	−9.40	−9.28	8.26	8.37
−4.5	−9.17	...	...	...
−4.0	−8.97	−8.97	7.94	7.99
−3.5	−8.78	−8.74	7.81	7.80
−3.0	...	−8.59	...	...
	Concn. 57.5%			
−5.0	−9.93	−9.93	8.80	8.90
−4.5	−9.77	−9.75	8.64	8.73
−4.0	−9.62	−9.56	8.46	8.55
−3.5	−9.44	−9.37	8.29	8.33
−3.0	−9.25	−9.20	8.12	8.10
−2.5	−9.07	−9.04	7.92	7.91

in the equilibrium compliance. In the more familiar uncrossed-linked systems,[2,3] the steady-state compliance is inversely proportional to the first power of polymer concentration,[16] as provided by the theories of Rouse[17] and Bueche.[14] But in these gels cross-linked by crystallites, the equilibrium compliance J is inversely proportional to about the third power of the concentration, as shown above. According to the Bueche theory,[14] each contribution to compliance in the retardation spectrum should in turn be proportional to J. Although the observed form of the spectrum is not the same as in the theory (which is based on equal spacings between cross-links), the maximum in L is in fact found to be directly proportional to J not only for these cellulose tributyrate gels but also for the polyvinyl chloride gels previously studied (Table III).

(16) J. D. Ferry, M. L. Williams and D. M. Stern, THIS JOURNAL, **58**, 987 (1954).

(17) P. E. Rouse, Jr., *J. Chem. Phys.*, **21**, 1272 (1953).

TABLE III

RELATION BETWEEN EQUILIBRIUM COMPLIANCE AND MAXIMUM IN RETARDATION DISTRIBUTION FUNCTION

System	Polymer concn.	log L_{max}	Log J	log L_{max}/J
Cellulose tributyrate–dimethyl phthalate[a]	20.4	−7.4	−6.5	−0.9
	42.6	−8.2	−7.3	−0.9
	57.5	−8.6	−7.7	−0.9
Polyvinyl chloride–dimethyl thianthrene[b]	10.0	−5.9	−5.0	−0.9
	40.0	−7.7	−6.8	−0.9

[a] Concentrations weight per cent. (nearly equal to volume per cent.). [b] Concentrations volume per cent. (references 6, 9, 10).

The form of L in the neighborhood of its maximum, in a cross-linked system, is determined by the disposition of the cross-links and the distribution of chain lengths among them. The fact that at its maximum $L = 0.13J$ for all these systems suggests that the distribution of chain lengths is similar in all, and that the arrangement of crystallites is similar, as already inferred from the fact that the dependence of J (or G) on concentration is nearly the same for both polymers. It may be noted that for uncross-linked systems a distinctly greater ratio L_{max}/J has been observed; for example, it is about 0.2 for unfractionated polyisobutylenes of both low[18] and high[19] molecular weights. Here it is determined by the distribution of molecular lengths.

Accordingly, the interpretation given for the drop in L for the 42.6% gel upon cooling through −25°, as an increase in cross-linking, seems reasonable. Such a drop would be most prominent near the maximum in L—at long times—and hence would affect J'' (dominated by the long times, $\tau > 1/\omega$) more than J' (dominated by the short times, $\tau < 1/\omega$); though the *slope* of J' *vs.* ω would be strongly influenced. This is exactly what is observed (Figs. 3 and 4). Similar changes evidently occur in the 57.5% gel with each progressive temperature decrease.

Relaxation Distribution Functions.—The distribution function of relaxation times, Φ, was calculated from the composite curves for G' in Fig. 12 and similar curves for G'' by the usual second approximation formulas. The values are also given in Table II and are plotted in Fig. 14, and again the results from the real and imaginary components of the measured modulus are in good agreement.

According to the theory of Rouse,[15,17] a logarithmic plot of Φ should have a slope of $-1/2$ in a range of time scale where the coöperative motions of molecular segments are sufficiently long-range to be oblivious of local steric effects or other short-range interactions but not so long-range that they are influenced by entanglements, cross-links, or free

(18) H. Leaderman, R. G. Smith and R. W. Jones, *J. Polymer Sci.*, **14**, 47 (1954).

(19) R. S. Marvin, "Proc. 2nd Intern. Congress Rheology," London, p. 156,

ends. The curve for the 20.4% cellulose tributyrate gel follows the theoretical slope quite well over several decades of time scale; in fact, it is by far the most satisfactory fit to the theory that has ever been observed. It may be concluded that the cellulose chain, in a diluted system of this sort, behaves more like the model postulated by Rouse than does a simple carbon chain. The agreement may be associated with the fact that the Rouse model is a free-draining coil; in frictional properties in dilute solution, cellulose derivatives approach this more closely than do vinyl polymers.[20]

For vinyl polymers, whether undiluted, in concentrated solution, or as cross-linked gels, plots of Φ usually follow the Rouse slope at fairly long times (where log $\Phi \cong 6$) but at shorter times curve upward more steeply, as shown by the plot for a polyvinyl chloride gel reproduced as a dashed curve in Fig. 14. The curves for the more concentrated cellulose tributyrate gels, on the other hand, have slopes everywhere somewhat *flatter* than $-1/2$, thus deviating in the opposite direction from that characteristic of vinyl polymers. This is probably due to the presence of rather closely spaced cross-links rather than any feature of the chain structure itself. From the preceding discussion of the L functions, it seems clear that the effects of cross-links on the coöperative motions extend to quite short times in these more concentrated systems. The effect of crystallite cross-links on the shape of Φ can be seen to an exaggerated degree in densely cross-linked systems like polyethylene, where Φ may have a zero slope over many decades of logarithmic time.[13]

The local friction coefficient per monomer unit, ζ_0, can be calculated for the 20.4% gel; log $\zeta_0 = -4.6$ at 25°, or -2.3 at $-25°$. It cannot be obtained for the other two systems. However, it can perhaps be very roughly estimated from the separation of the curves at their upper ends that ζ_0 is higher by about a power of ten at 42.6% and by two powers of ten at 57.5%.

None of the curves extends to sufficiently short times to reach the maximum in Φ which is usually found in systems of vinyl polymers.[13,15]

Conclusions.—The outstanding characteristic of the cellulose chain backbone revealed in these measurements is the absence of upward curvature in the relaxation spectrum of the 20.4% gel. This behavior may be related to the free-draining properties of the anhydroglucose chain. The effects of crystallite cross-linking, and its increase with decreasing temperature and increasing concentration, are apparent in the shapes of the retardation and relaxation spectra, especially of the more concentrated gels. They are accompanied by characteristic changes in J', J'', G' and G''/G', which should be recognizable in other cross-linked systems.

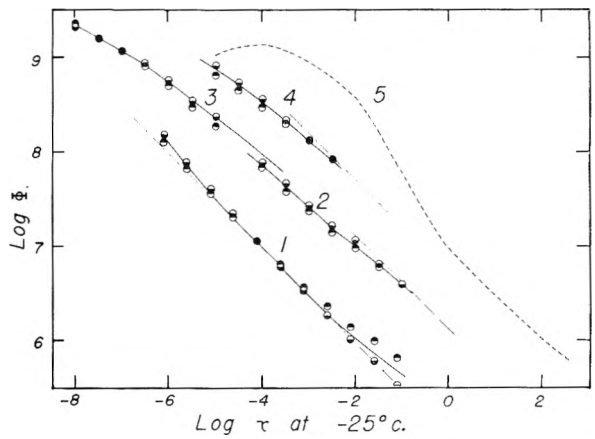

Fig. 14.—Logarithm of relaxation distribution function reduced to −25°: 1, 20.4%; 2, 42.6% before cooling below −25°; 3, 42.6% after cooling below −25°; 4, 57.5%; 5, comparative curve for a 40% gel of polyvinyl chloride in dimethylthianthrene[9] reduced to 11°; circles top black, calculated from G'; bottom black, from G''. Dashed lines denote slope prescribed by the Rouse theory.

Acknowledgments.—This work was part of a program of research on the physical structure and properties of cellulose derivatives and other polymers supported by the Allegany Ballistics Laboratory, Cumberland, Maryland, an establishment owned by the United States Navy and operated by the Hercules Powder Company under Contract NOrd 10431. It was also supported in part by a grant from Research Corporation and by the Research Committee of the Graduate School of the University of Wisconsin from funds supplied by the Wisconsin Alumni Research Foundation. We are indebted to Mrs. Garrett Droppers for assistance in calculation, and to Mr. Donald M. Stern and Mr. D. J. Plazek for help with some of the measurements.

(20) A. M. Holtzer, H. Benoit and P. Doty, THIS JOURNAL, **58**, 624 (1954).

THE BARIUM–STRONTIUM EQUILIBRIUM SYSTEM

BY R. G. HIRST,[1] A. J. KING AND F. A. KANDA

Contribution from the Department of Chemistry, Syracuse University, Syracuse, N. Y.

Received August 11, 1955

The barium–strontium phase diagram has been investigated in the liquid and solid state over the entire range of compositions. The liquidus and solidus curves were determined by thermal analysis whereas the solid state equilibria were investigated by X-ray diffraction methods. The system displays complete miscibility in both the liquid and solid states at all temperatures above 602 ± 8°. Alloys containing less than 69.3 atomic % strontium appear only in the B.C.C. form from room temperature to the melting point. Alloys containing more than 69.3 at. % strontium undergo solid state transformations and may assume B.C.C., H.C.P. or F.C.C. crystalline forms or equilibrium mixtures of these depending upon the temperature and composition. Between the compositions 72.3 and 76.9 at. % strontium the alloys on cooling undergo the eutectoid reaction β (H.C.P.) $\rightleftarrows$ γ (B.C.C.) and α (F.C.C.) at 171 ± 3°. The eutectoid composition corresponds to 73.2 at. % strontium.

Introduction

Equilibrium systems of the alkaline earth metals have been an object of research in this Laboratory for several years. Suitable techniques have been developed for handling and obtaining reliable data for these highly reactive metals.

Preliminary evidence obtained by Sheldon and King[2] using high temperature X-ray techniques, showed that strontium is polymorphic and exists in three crystalline modifications: B.C.C. above 605°, H.C.P. from 215–605 and F.C.C. below 215 all ±10°. Klemm and Mika[3] found the strontium and barium system at room temperature to consist of two series of terminal solid solutions. A phase which was F.C.C. appeared between 0 and 24 at. % barium. Another phase, B.C.C. extended from 30 to 100 at. % barium and the intermediate region consisted of a mixture of these two phases.

Rinck[4] concluded from electrical resistance, dilatometric and thermoelectric measurements that allotropic transformations of strontium occur at 235 and 540°. Although the temperature of the lower transition is in fair agreement, the higher transition is considerably at variance with that observed in the present investigation.

Sheldon[5] investigated the calcium–barium phase diagram by thermal and X-ray methods and found complete miscibility in the liquid and the solid state. He found that calcium can exist in three polymorphic forms with the transitions, F. C. C. → H.C.P. occurring at 335° and H.C.P. → B.C.C. at 610°. The calcium-rich alloys displayed the eutectoid decomposition: H.C.P. → B.C.C. + F.C.C. He also observed thermal evidence for solid state transitions in the calcium-rich alloys which could not be verified by X-ray data.

Since calcium and strontium exhibit similar polymorphic transformations it was expected that the strontium–barium system would be very similar to the calcium–barium system investigated by Sheldon. The investigation proved this assumption to be correct.

Experimental

Purity of the Metals and Alloys.—The barium and strontium were of the highest purity available and were obtained from King Laboratories, Inc., of Syracuse, N. Y. A gravimetric analysis of their content of barium and strontium showed a purity of 99.3 and 99.5%, respectively. The metals were selected from the middle fractions of 2–3 lb. vacuum sublimed charges. The melting point of the strontium was found to be 768° whereas the melting point of barium was 714°. Spectrographic analysis showed the strontium to contain 0.3% barium and traces of Ca, Al, Mn, Sn and Fe. The impurities found in the barium consisted of 0.4% strontium and traces of Ca, Mg and Na. There were minor traces of several other metallic elements in each metal.

Alloy samples of approximately 60 g. each were made by weighing, to within 0.01 g., appropriate amounts of the metals in an argon atmosphere. After fusion, a chemical analysis of the samples agreed within ±1% of the make-up composition. The liquidus and solidus curves sloped so slightly that a shift of composition by as much as 2% did not shift the temperature by an amount exceeding the observed accuracy of the temperature measurements. The compositions given in the equilibrium plot correspond to make-up compositions and are reliable to within ±1%.

Since the metals and alloys used in this investigation react rapidly with ordinary atmospheric gases, special precautions were observed in handling them. Whenever feasible the metals and alloys were handled in a dry box in an atmosphere of purified argon. X-Ray powder specimens were prepared in a unit which allowed for maintenance of an argon atmosphere during the preparation of the alloy powder and the loading and sealing of the powder into capillary tubes.

Studies of the Liquidus–Solidus Equilibrium.—The crucible assembly utilized for this phase of the investigation consisted of a seamless iron tube, containing the sample, fitted into a water-cooled brass head. The brass head was suitably constructed to allow for introduction of the thermocouple and connections for vacuum and argon flushing lines. The thermocouple protection shield consisted of a thin walled iron tube which also served as a stirring device for the alloys. The crucible assembly was alternately evacuated and flushed several times before each run with barium-purified argon. An argon atmosphere slightly greater than room pressure was maintained in the system during a run by means of a rubber balloon reservoir.

Heating and cooling of the wire wound electric furnace was maintained at a rate of 4°/min. by means of a specially constructed program controller which was actuated by a control thermocouple.

Thermal data were recorded on a Brown variable range recorder[6] from the output of the recording chromel–alumel thermocouple. The recording thermocouple was calibrated and checked frequently against a standard Pt–90% Pt, 10% Rh thermocouple certified by the National Bureau of Standards. The usual temperature–time curves were adequate for points on the liquidus curve but were unreliable for obtaining reproducible values of points on the solidus curve. Samples were re-investigated using two recorders plotting temperature differential *vs.* time on one while simultaneously plotting temperature *vs.* time on the other. The temperature differential was obtained by submerging the charge zone of the crucible in copper powder and recording the difference in temperature between the

(1) Abstracted from the thesis of R. G. Hirst submitted to the Chemistry Department of Syracuse University in partial fulfillment of the requirements for the Ph.D. degree, January, 1953.

(2) E. A. Sheldon and A. J. King, *Acta Cryst.*, **6**, 100 (1953).

(3) W. Klemm and G. Mika, *Z. anorg. allgem. Chem.*, **248**, 155 (1941).

(4) E. Rinck, *Compt. rend.*, **234**, 1845 (1952).

(5) E. A. Sheldon, Thesis, Syracuse University, 1952.

(6) F. A. Kanda and R. C. Shaver, *J. Am. Ceramic Soc.*, **36**, 101 (1953).

TABLE I

	This Work	Sheldon and King
αSr (F.C.C.)	$a_0 = 6.076 \pm 0.005$ Å. (25°)	6.0849 ± 0.0005 Å. (25°)
βSr (H.C.P.)	$a_0 = 4.28 \pm 0.02$ Å. (225°)	4.32 ± 0.01 Å. (248°)
	$c_0 = 7.05 \pm 0.02$ Å.	7.06 ± 0.01 Å.
γSr (B.C.C.)	$a_0 = 4.87 \pm 0.02$ Å. (628°)	4.87 ± 0.01 Å. (614°)
Ba (B.C.C.)	$a_0 = 5.013 \pm 0.005$ Å. (25°)	5.0126[7] ± 0.0001 Å. (25°)

charge in the crucible and the copper powder. Later in the investigation a two function variable-range recorder was constructed which directly plotted the temperature differential against the temperature. From the temperature differential plots liquidus points could be duplicated to within ±1° and solidus points to within ±2° in both heating and cooling cycles. None of these techniques were used for obtaining the data for the solid state transformations.

Solid State Investigations.—Room temperature and high temperature X-ray diffraction methods were applied in this portion of the study. The Debye–Scherrer type high temperature camera, used in the investigation, was constructed in our laboratory. The entire unit, including the temperature controller and recorder, was calibrated by observing melting points of standardized salt mixtures in capillaries mounted in the camera and by X-ray measurement of the coefficient of expansion of silver. On the basis of these calibrations the reliability of the temperature data is estimated to be within ±3° up to 500°, decreasing to ±8° at 650°.

A total of nearly 300 X-ray photographs were taken to establish the points and boundaries in the solid state region as shown in Fig. 1. Lattice spacings were determined by the Straumanis technique. At high temperatures accurate measurement of the lattice spacings was difficult and even impossible for some specimens due to reaction of the alloys with the Vycor capillaries, grain growth which produced diffraction spots instead of lines and the diffuse character of lines due to thermal vibration. In general none of these interfered with the application of the disappearing phase technique which was used as a method of identification of the phases present at the various temperatures.

Lattice Dimensions.—The unit cell dimensions of the various lattices observed for the component metals are given in Table I. Also listed for comparison are the data of Sheldon and King.[2]

Nature of the Transitions.—Although the transitions were reversible it was found that they were usually sluggish. On heating for example, the transition of (α) F.C.C. → (β) H.C.P. required 4 hours whereas (β) H.C.P. → (γ) B.C.C. required 2 hours at 300° and 30 minutes at 500–600°. On cooling, the transition (β) H.C.P. → (α) F.C.C. required eight days for completion at 130°.

Discussion of Experimental Results

The two metals form a continuous series of solid solutions (Fig. 1) as would be expected of metals with identical crystal lattices, similar lattice constants and melting points. The solid state region of the strontium-rich alloys is complicated due to the polymorphic character of strontium.

The existence of the polymorphic forms of strontium was confirmed and the transition temperatures: B.C.C. → H.C.P. (602 ± 8°) and H.C.P. → F.C.C. (213 ± 3°) found to be in good agreement with the values found by Sheldon.[2]

The transitions most difficult to follow in the alloys were those which on heating involved the disappearance of the F.C.C. phase from a mixture of the F.C.C. and H.C.P. phases. This was due to the fact that most of the lines of the F.C.C. pattern were almost superimposed by those of the H.C.P. pattern. The (200) reflection of the F.C.C. pattern was an exception, and was the only one with sufficient intensity to be of use in identifying this phase in the presence of the H.C.P. phase. However, its d-value is so close to that of the (111)-reflection of SrO that in some instances the presence of the latter rendered the results uncertain. However, with the establishment of the transition temperature of pure strontium and the eutectoid triple point, in addition to two reliable temperature determinations for the disappearance of the F.C.C. lattice, it was felt that enough points were fixed to construct the upper boundary of this two phase region. The course of the lower boundary line of this region was not so difficult to bracket because the H.C.P. diffraction pattern contains almost twice as many lines as the F.C.C. and its appearance in a two phase mixture was easily recognized.

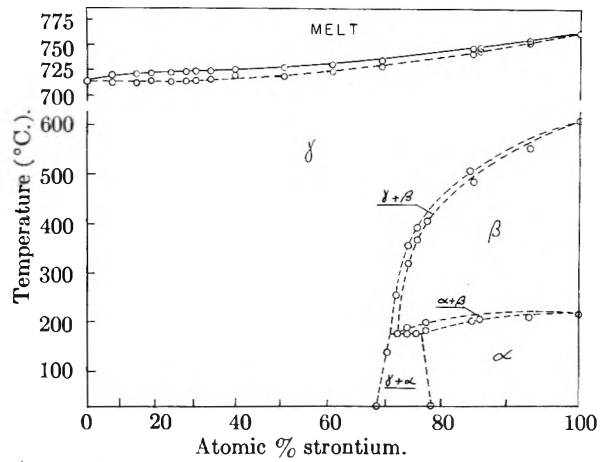

Fig. 1.—Temperature *vs.* composition plot of the phase regions of the system.

Three compositions fixed the eutectoid temperature as 171 ± 3°. The eutectoid reaction: H.C.P. ⇆ F.C.C. + B.C.C. occurs over the composition range 72.3–76.9 atomic % strontium with the eutectoid composition corresponding to 73.2 atomic % strontium. Since the investigation of the eutectoid boundary regions was made at 1% (by weight) increments in composition, it is felt that the limits are reliable to within 0.5–1.0%.

The limits of the B.C.C.-F.C.C. two phase region at room temperature were found by application of the parametric method for solid solutions to extend from 69.3–78.0 atomic % strontium. The variation of the unit cell parameters with composition is shown graphically in Figs. 2 and 3. The point of inflection, where the unit cell parameter no longer changes with composition, designates the boundary of a two-phase region. These limits are in good agreement with those reported by Klemm and Mika.[3] It will be noted in Fig. 2 that by extrapolation a B.C.C. cell parameter of 4.812 Å. is indicated for pure strontium at room temperature although only the F.C.C. form actually exists at this temperature under atmospheric pressure. The atomic radius of B.C.C. strontium calculated

(7) A. J. King, unpublished result of a precision determination of a_0 for specially purified barium.

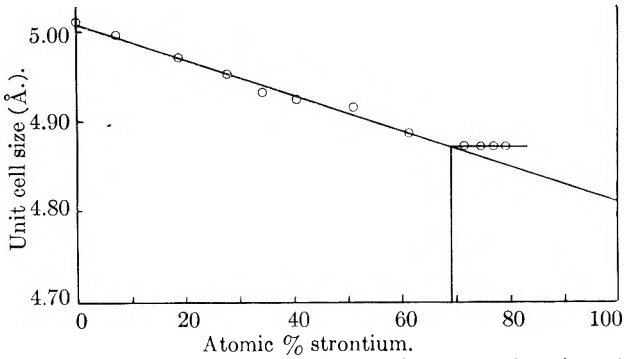

Fig. 2.—a_0 values of the B.C.C. (γ) phase as a function of composition at room temperature.

from this cell size is 2.083 Å. as compared with 2.148 Å. for that of the F.C.C. form. This represents a difference of 3% between the radii of the atoms in the two structures, a magnitude in good agreement with that predicted for these.[8]

(8) L. Pauling, "Nature of the Chemical Bond," Cornell Univ. Press, Ithaca, N. Y., 1945, p. 406.

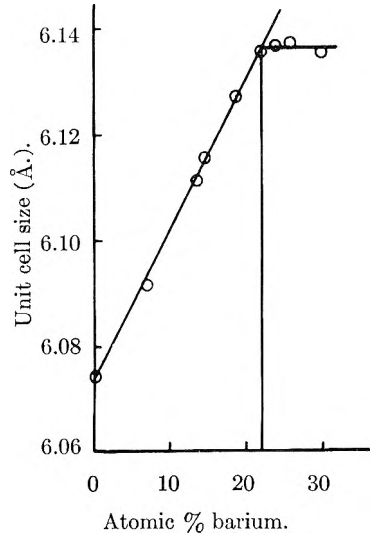

Fig. 3.—a_0 values of the F.C.C. (α) phase as a function of composition at room temperature.

PHYSICAL PROPERTIES OF EIGHT HIGH-PURITY NITROPARAFFINS

BY EMORY E. TOOPS, JR.

Commercial Solvents Corporation, Terre Haute, Indiana

Received August 11, 1955

The boiling point, vapor pressure, freezing point, density and refractive index have been determined for the eight mononitroparaffins from nitromethane through the four isomeric nitrobutanes. The measurements were made on highly purified samples, characterized by both ebullioscopic and cryoscopic methods. The vapor pressure data have been fitted to the Antoine equation by the method of least squares.

Introduction

Physical properties of the mononitroparaffins have been appearing in the literature during the past 80 years. Few reliable data are available, with the exception of nitromethane, whose properties were carefully measured by Timmermans and Hennaut-Roland.[1] Measurements made during the past 20 years are particularly liable to error because commercial products have been used without adequate purification.

Nitromethane, nitroethane and 1- and 2-nitropropane are made commercially by the vapor phase nitration of propane.[2] These materials are available containing 90–95% w. of the specified product with a total nitroparaffin content of at least 99%. A careful fractional distillation is essential to obtain a high purity nitroparaffin. A summary of physical data on these compounds recently has been published.[3]

Whenever possible the nitroparaffins were prepared by synthesis as well as by purifying the commercial product. The primary nitroparaffins can be prepared in good yields from the corresponding alkyl bromide or iodide by the Victor Meyer reaction.[4] They may also be prepared in satisfactory yields from the corresponding α-halogenated acid by the Kolbe synthesis.[5] This method is an excellent laboratory preparation of nitromethane from chloroacetic acid.[6]

All purifications of both the synthetic and commercial nitroparaffins were made by careful fractional distillation, except for nitromethane where both fractional distillation and fractional crystallization were used. The products were collected in 100-ml. fractions during the distillation and preliminary purity measurements made by mass spectra analysis.

Preparation and Purification of the Nitroparaffins

Nitromethane was prepared from the commercial product by fractional distillation in a Podbielniak Hyer-Cal column at 100 mm. pressure, followed by a fractional crystallization in which one-half of the sample was discarded as mother liquor. A material of equivalent purity was prepared from chloroacetic acid and sodium nitrite.

(1) J. Timmermans and M. Hennaut-Roland, *J. chim. phys.*, **29**, 529 (1932).

(2) C. L. Gabriel, *Ind. Eng. Chem.*, **32**, 887 (1940); S. D. Kirkpatrick, *Chem. & Met. Eng.*, **49** [9], 129 (1942).

(3) A. Weissberger, "Technique of Organic Chemistry," Vol. VII, Interscience Publishers, Inc., New York, N. Y., 1955.

(4) V. Meyer, *Ber.*, **5**, 203, 399, 514, 1029, 1034 (1872); N. Kornblum, N. Lichtin, *et al.*, *J. Am. Chem. Soc.*, **69**, 307 (1947); N. Kornblum, J. T. Patton and J. B. Nordmann, *ibid.*, **70**, 746 (1948); C. W. Plummer and N. L. Drake, *ibid.*, **76**, 2720 (1954).

(5) H. Kolbe, *J. prakt. Chem.*, **5**, 427 (1872); W. Steinkopf and G. Kirchhoff, *Ber.*, **42**, 3438 (1909); A. Wahl, *Bull. soc. chim.*, **5**, 180 (1909).

(6) H. Gilman and A. H. Blatt, "Organic Syntheses," Coll. Vol. I. John Wiley and Sons, Inc., New York, N. Y., 1941, p. 401.

Nitroethane was prepared by the Victor Meyer reaction from purified bromoethane. Purification was done in a 30 plate Penn State-type column at 100 mm. pressure. It was not possible to prepare nitroethane of a purity greater than 99.8% mole by fractional distillation of the commercial product.

1-Nitropropane was prepared by both the Victor Meyer reaction and fractional distillation of the commercial product in a 60 plate Penn State-type column at 100 mm. pressure. A reflux ratio of 75:1 was used. Both methods gave material of equal purity.

2-Nitropropane was prepared by fractional distillation of commercial material in the same manner as 1-nitropropane.

1-Nitrobutane, prepared by nitrating butane, was fractionally distilled in a Podbielniak Hyer-Cal column at 100 mm. pressure using a 100:1 reflux ratio. Its purity was equivalent to material prepared by the Victor Meyer reaction.

2-Nitrobutane was prepared and purified by the same procedure as 1-nitrobutane.

1-Nitro-2-methylpropane was prepared from 1-bromo-2-methylpropane by the Victor Meyer reaction. The yield was low and purification was difficult. Two fractional distillations in 30 plate Penn State-type columns at 50 mm. pressure and a redistillation in a Podbielniak Hyer-Cal column were required to obtain a product of acceptable purity.

2-Nitro-2-methylpropane was prepared from *t*-butylamine by the method of Kornblum and Clutter.[7] The crude product was dried with Drierite overnight and fractionally distilled in a 30 plate Penn State column at atmospheric pressure.

Experimental

All temperature measurements were made with platinum resistance thermometers connected to a Leeds and Northrup type G-2 Mueller bridge through a mercury switch of negligible resistance. The thermometers were compared against one calibrated by the National Bureau of Standards. Measurements were made to ±0.001° but in this paper have been rounded off to the nearest 0.01°.

Purity measurements were made by both cryoscopic[8] and ebullioscopic methods.[9] The cryoscopic and ebullioscopic purities are tabulated in Table I. The Roman numerals are the Swietoslawski purity class[9] and Δt is the difference between the boiling point of the liquid and the condensing temperature of the vapor.

TABLE I

PURITY OF THE NITROPARAFFINS

Compound	Purity: From freezing curve, mole %	From boiling point: Class	From boiling point: Δt, °C.
Nitromethane	99.99	IV	0.007
Nitroethane	99.9+	IV	.013
1-Nitropropane	99.9+	IV	.007
2-Nitropropane	99.99	III	.046
1-Nitrobutane	99.96	III	.022
2-Nitrobutane	Indeterminable	III	.023
1-Nitro-2-methylpropane	99.82	III	.021
2-Nitro-2-methylpropane	Indeterminable	IV	.008

The freezing points are tabulated in Table II. Calculated values for zero impurity are given for nitromethane, 2-nitropropane, 1-nitrobutane and 1-nitro-2-methylpropane. The freezing points of the other nitroparaffins are experimental values since exact calculations could not be made.

The boiling points, degree of purity and vapor pressure were measured in Swietoslawski differential ebulliometers. The ebulliometers were constructed from the improved Swietoslawski design, adapted to electrical heating.[10] The original design was followed except for decreasing the diameter of the thermometer well to better accommodate the Leeds and Northrup Type 8160 resistance thermometers.

TABLE II

FREEZING POINTS OF THE NITROPARAFFINS

Compound	Freezing point, °C.
Nitromethane	− 28.55
Nitroethane	− 89.52
1-Nitropropane	−103.99
2-Nitropropane	− 91.32
1-Nitrobutane	− 81.33
2-Nitrobutane	Glass
1-Nitro-2-methylpropane	− 76.85
2-Nitro-2-methylpropane	26.23

The vapor pressures were measured in two Swietoslawski ebulliometers connected to a five-gallon reservoir following the arrangement of Smith and Matheson.[11] A vacuum pump and open end manometer were connected to the reservoir. The nitroparaffin was placed in one ebulliometer and water, distilled from an alkaline permanganate solution, placed in the other. The two ebulliometers were separated by a cold trap. The ebulliometers were evacuated to approximately the lowest pressure desired and simultaneous measurements made of the boiling points of the nitroparaffin and water. Dry air was then bled into the system to raise the pressure and the boiling points again measured. This procedure was repeated until the desired number of points had been obtained. Fifteen to twenty observations were made on each compound starting at about 80 mm.

The experimental vapor pressure data consisted of the boiling points of the nitroparaffin and water for each individual pressure in terms of ohms. After correcting for lead resistance, bridge zero and individual resistance errors they were converted to temperature by use of the Callendar formula. The pressure for each point was then calculated from the boiling point of water, using the data of Osborne and Meyers.[12] The data were fitted to the Antoine equation by the method of least squares.

The boiling points at 760 mm. were calculated from the vapor pressure equation and are tabulated in Table III, together with the pressure coefficients of temperature. The Antoine constants are given in Table IV. The average deviation between the calculated and experimental pressure ranged from ±0.03 mm. for nitromethane to ±0.06 mm. for 2-nitrobutane. The maximum deviation was 0.10 mm. for nitromethane and 0.15 mm. for 2-nitrobutane.

TABLE III

BOILING POINTS AND PRESSURE COEFFICIENTS OF TEMPERATURE OF THE NITROPARAFFINS

Compound	B.p., °C. (760 mm.)	dt/dp, °C./mm.
Nitromethane	101.20	0.0427
Nitroethane	114.07	.0445
1-Nitropropane	131.18	.0467
2-Nitropropane	120.25	.0460
1-Nitrobutane	152.77	.0490
2-Nitrobutane	139.50	.0485
1-Nitro-2-methylpropane	141.72	.0482
2-Nitro-2-methylpropane	127.16	.0473

Density measurements were made in a Sprengel-type pycnometer having a capacity of about 17 ml. Calibrations were made with freshly boiled redistilled water. The weighing procedure used was adapted to 5th decimal place accuracy. Measurements were made at 20, 25 and 30° for all compounds except 2-nitro-2-methylpropane. The precision of the measurements was checked by comparing

(7) N. Kornblum and R. J. Clutter, *J. Am. Chem. Soc.*, **76**, 4494 (1954).

(8) B. J. Mair, A. R. Glasgow and F. D. Rossini, *J. Research Natl. Bur. Standards*, **26**, 591 (1941).

(9) W. Swietoslawski, "Ebulliometric Measurements," Reinhold Publ. Corp., New York, N. Y., 1945, p. 80.

(10) W. E. Barr and V. J. Anhorn, *Instruments*, **20**, 822 (1947); A. Weissberger, "Technique of Organic Chemistry," Vol. I, pt. 1, Interscience Publishers, Inc., New York, N. Y., 1949, p. 107.

(11) E. R. Smith and H. Matheson, *J. Research Natl. Bur. Standards*, **20**, 641 (1938).

(12) N. S. Osborne and C. H. Meyers, *ibid.*, **13**, 1 (1934).

TABLE IV

CONSTANTS OF THE ANTOINE EQUATION

$$\log p = A - \frac{B}{t + C}$$

Compound	A	B	C
Nitromethane	7.274170	1441.610	226.939
Nitroethane	7.175154	1435.402	220.184
1-Nitropropane	7.127539	1474.299	215.986
2-Nitropropane	7.083240	1422.898	218.341
1-Nitrobutane	7.095500	1523.797	208.778
2-Nitrobutane	7.077892	1494.318	216.542
1-Nitro-2-methylpropane	7.074141	1483.643	212.095
2-Nitro-2-methylpropane	6.987722	1396.948	212.989

values of dd/dt calculated between 20 and 25°, 25 and 30° and 20 and 30°. The precision was ±0.00002 g./ml. and the estimated accuracy ±0.00004 g./ml. These data are tabulated in Table V.

TABLE V

DENSITIES OF THE NITROPARAFFINS

Compound	Density 20°	25°	30°	dd/dt
Nitromethane	1.13816	1.13128	1.12439	0.001377
Nitroethane	1.05057	1.04464	1.03870	.001187
1-Nitropropane	1.00144	0.99609	0.99073	.001071
2-Nitropropane	0.98839	.98290	.97740	.001099
1-Nitrobutane	.97344	.96848	.96352	.000992
2-Nitrobutane	.96535	.96036	.95536	.000999
1-Nitro-2-methylpropane	.96349	.95848	.95347	.001002
2-Nitro-2-methylpropane	Solid	Solid	.95028[a]	.001128

[a] d^{35}_4 0.94464.

A dipping refractometer was used to measure refractive index. The prisms were calibrated with either distilled water, sodium chloride solutions of known refractive index or fluorite test plates. The precision of measurement, estimated from values of dn/dt, is about ±0.000025 unit with an estimated accuracy of ±0.00005.

Discussion

It was not possible to calculate the cryoscopic purity for 2-nitro-2-methylpropane or 2-nitrobutane. The latter compound did not freeze but became glassy at about −111° while the freezing curve of the former exhibited a plateau in the cooling curve close to the freezing point. This plateau resembled an eutectic mixture, though it could also be caused by a transformation to a polymorphic form. The high degree of purity indicated by the ebullioscopic measurements would indicate that polymorphism was occurring. However, replicates of the cooling curve all exhibited the plateau regardless of the cooling rate.

TABLE VI

REFRACTIVE INDICES OF THE NITROPARAFFINS

Compound	Refractive index 20°	25°	30°	dn/dt
Nitromethane	1.38188	1.37964	1.37738	0.000450
Nitroethane	1.39193	1.38973	1.38754	.000439
1-Nitropropane	1.40160	1.39956	1.39755	.000405
2-Nitropropane	1.39439	1.39235	1.39028	.000411
1-Nitrobutane	1.41019	1.40801	1.40593	.000426
2-Nitrobutane	1.40407	1.40189	1.39979	.000428
1-Nitro-2-methylpropane	1.40642	1.40436	1.40232	.000410
2-Nitro-2-methylpropane	Solid	Solid	1.39715[a]	.000400

[a] $n^{35}D$ 1.39515.

Exact purity calculations could not be made on nitroethane or 1-nitropropane. These compounds gave a sharp freezing curve but one in which equilibrium was never reached. After 45 minutes of freezing the freezing curves were showing a small, steady rise in temperature. However, the sharpness of the freezing curves, together with the ebullioscopic degrees of purity, indicate that these compounds are at least 99.9% mole.

The ebullioscopic purity measurement is sensitive to traces of water. This is apparent from Table I when the ebullioscopic Δt is compared to the mole % purity calculated from the freezing curve. Freshly distilled nitroparaffins all showed a Δt of between 0.04 to 0.06°, even when elaborate precautions were taken to exclude moisture during the distillation. The Δt for nitromethane, nitroethane, 1-nitropropane and 2-nitro-2-methylpropane all dropped to a low value after these compounds were dried with Drierite. Treatment with Drierite was less effective for 2-nitrobutane, 1-nitro-2-methylpropane and 1-nitrobutane. The Δt's for these compounds were only reduced to about 0.02°. 2-Nitropropane decomposed when in contact with Drierite. The Δt rose from about 0.04 to 0.12°.

THE SORPTION OF BORON COMPOUNDS BY PALLADIUM AND CHARCOAL

BY HAROLD C. BEACHELL AND KLAUS R. LANGE[1]

Contribution from the Department of Chemistry, University of Delaware, Newark, Delaware

Received August 15, 1955

Charcoal and palladium black have been found to sorb diborane and other gaseous boron compounds. In studying the sorption of diborane, deuterodiborane and trimethylborane evidence is obtained for the nature of the sorption process. Palladium shows typical van der Waals adsorption. Charcoal is at the upper limit of physical adsorption in the range studied.

Until recently no work had been done concerning the sorption of boron compounds on solid surfaces. Veloric[2] began a program of investigations that includes the sorption of diborane gas on charcoal. This work has been repeated, along with some investigations as to pretreatment of the sorbents. In addition deuterodiborane and trimethylborane have been investigated in order to determine the magnitude of the isotope effect and to gain some insight into the nature of the sorption process.

Materials.—All adsorbates were prepared in this Laboratory, their purity being checked by vapor pressure measurements and infrared analysis.

Palladium black and coconut charcoal are available commercially.

Experimental

A conventional high-vacuum adsorption apparatus was used. Incorporated with it was an automatic Töpler pump used to desorb the gases for infrared analysis and to determine the reversibility of the various processes.

The manometer could be read to ±0.5 mm., the jacketed buret to ±0.05 cc. The values reported are the average of those obtained with increasing and decreasing pressure. Dead spaces were determined with He gas.

Pretreatment.—Untreated palladium black decomposes a small quantity of diborane rapidly with no further evolution of gas after 3 hours. Pretreatment by heating at 350° *in vacuo* or in a hydrogen atmosphere reduces the amount of diborane decomposed. However, since the amount of diborane affected is small compared to the total surface area it was found that treating the surface with diborane as a "scavenger" gave a reproducible sample that did not give a further evolution of gas in the temperature ranges reported below and completely reversible sorption.

The surface area of the sample was 5 m.²/g. by the method of Brunauer, Emmett and Teller.

Coconut charcoal, evacuated at room temperature, does not cause decomposition of diborane. However, the sorption of diborane is not completely reversible. This indicates that chemisorbed gases such as oxygen or water interact with the diborane in some way. Since no hydrogen is given off as shown by condensation of the diborane with liquid nitrogen after contact, times varying from one to five hours. Since all the diborane was not recovered, this interaction is probably a coördination of oxygen and boron analogous to etherate formation. No further work has been done as yet to study this effect.

It was found, finally, that heating the charcoal at 350° in a hydrogen atmosphere for four hours and at 10^{-6} mm. pressure for an additional four hours eliminated this effect and gave reproducible, reversible sorption. The surface area of the sample, by the method of Brunauer, Emmett and Teller was 1130 m.²/g.

Data.—All x/m (cc./g.) values given are reduced to one atmosphere and 20°. It was found that the adsorption by palladium follows the Freundlich isotherm: $x/m = kp^{1/n}$ more closely than the Langmuir Isotherm: $x/m = kp/(1 + k'p)$. However adsorption by charcoal gives good agreement when the latter is applied. Plots of diborane are accordingly represented in Figs. 1 and 2.

P (cm.)	t (°C.) −61	−20	0	29	46
	B_2H_6 on Pd Black				
20	2.30	1.03	0.50	0.50	0.00
30	4.10	2.05	1.80	1.02	0.00
40	4.86	3.32	2.56	1.80	0.28
50	6.15	4.10	3.34	2.30	0.56
60	7.20	5.13	4.10	2.82	1.11

P (cm.)	t (°C.) −60	−20	0	30
	B_2D_6 on Pd Black			
20	3.48	1.88	0.81	0.00
30	4.95	2.41	1.34	0.00
40	5.78	2.68	1.88	0.00
50	6.16	2.95	2.14	0.00
60	7.24	3.22	2.42	0.00

P (cm.)	t (°C.) 0	25	35
	$B(CH_3)_3$ on Pd Black		
20	2.72	2.18	1.09
30	3.28	2.72	1.36
40	4.35	3.27	1.64
50	4.62	3.28	1.65
60	5.45	3.28	1.65

P (cm.)	t (°C.) −59	−22	0	20	40	60[a]
	B_2H_6 on Charcoal					
10	112	83.1	..	..	..	..
15	118	85.0	65.3	51.9	..	..
20	122	90.4	71.5	55.4	43.0	32.2
25	125	93.5	74.6	60.8	45.6	34.9
30	..	96.1	78.7	61.7	47.5	36.6
35	..	98.8	81.4	66.1	51.0	39.8
40	..	103.0	83.2	68.0	54.1	41.6
45	..	..	86.0	71.0	55.5	43.4
50	..	..	..	72.0	58.1	44.7
55	..	..	..	..	59.0	46.5

P (cm.)	t (°C.) −59	−22	0	20	40	60[a]
	B_2D_6 on Charcoal					
10	105	..	..	..	..	..
15	113	78.7	59.0	..	..	..
20	117	84.5	64.5	48.4	37.6	26.8
25	121	87.2	68.0	51.9	42.0	30.4
30	..	90.8	71.5	55.0	43.9	32.2
35	..	93.9	75.1	58.6	48.4	35.8
40	..	96.6	77.8	60.9	49.1	37.6
45	..	..	80.0	63.5	52.8	39.4
50	..	..	82.3	64.9	53.6	40.6
55	..	..	..	67.1	56.4	44.7

(1) Part of a thesis presented in partial fulfillment for the degree of Doctor of Philosophy.

(2) H. S. Veloric, Ph.D. Thesis, Univ. of Delaware.

TABLE (*Continued*)

P (cm.)	*t* (°C.) 0	29	51	70
	$B(CH_3)_3$ on Charcoal			
30	103	..	..	..
35	..	..	76.0	64.6
40	104	89.0	78.5	64.6
50	109	92.1	81.4	68.8
60	112	96.4	84.8	70.4
70	114	99.0	88.6	72.7
75	115	99.4	91.3	75.1

[a] Measurable decomposition of diborane occurs above 60°.

Nature of the Sorption Process.—Calculation of the isosteric heats of adsorption according to the formula

$$\frac{\mathrm{d} \ln p}{\mathrm{d}(1/T)} = \frac{\Delta H_{iso}}{R}$$

shows values for diborane on palladium black to be from 1–2 kcal. over all ranges of coverage measured. On coconut charcoal, however, the values are between 5–10 kcal. The heat of liquefaction of diborane is 3.45 kcal. at its boiling point.[3]

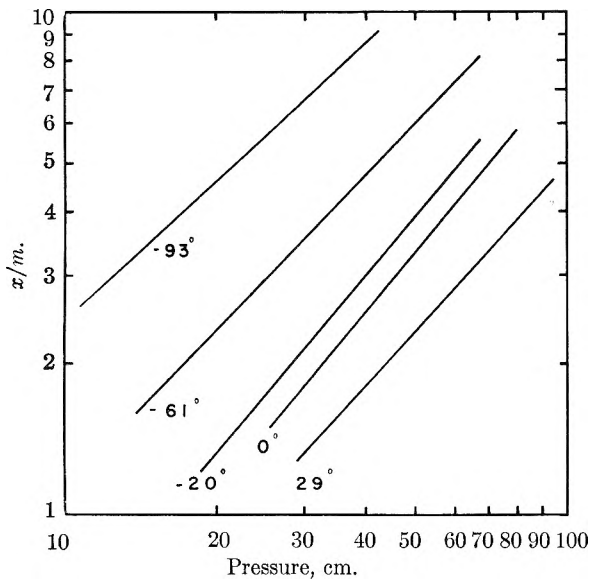

Fig. 1.—Freundlich isotherms, diborane on palladium black (x/m in cc. gas at 20° per g. adsorbent).

Conclusions

Palladium black presents a case of purely physical adsorption within the range studied. This is indicated by the extent of adsorption and the low heat involved.

In the case of charcoal it will be noted that the difference in adsorption between diborane and deuterodiborane is of a much lower magnitude then with palladium when compared with the total amount adsorbed. Apparently the sorption is also physical in spite of the high heats involved. Calculation of the theoretical maximum heat of adsorption of diborane on charcoal was made according to the equation[4,5]

$$5.5RT \geq q_1 - q_L \geq -2.3RT$$

By extrapolation of the diborane isobars it appears that physical adsorption should end at 115°. Using this value $q_1 - q_L = 4.25$ kcal. Therefore the maximum heat of physical adsorption ought to be 7.70 kcal. Unfortunately reliable data cannot be obtained at 115° due to the error introduced by decomposition of diborane. Although the isosteric heats of adsorption are inherently inaccurate, their mean value is in the vicinity of the calculated, indicating that the molecules are still adsorbed physically but are on the borderline between physical adsorption and chemisorption. The term "activated physical adsorption" might well apply in this case.

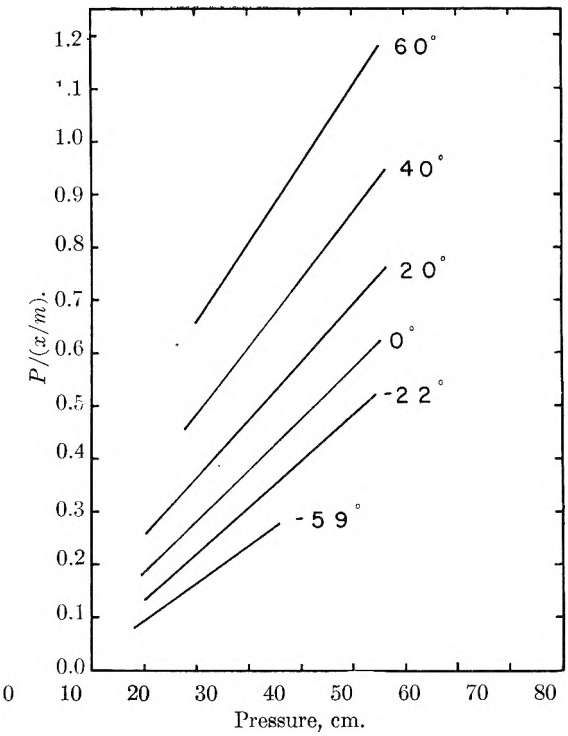

Fig. 2.—Langmuir isotherms, diborane on coconut charcoal ($P/(x/m)$ in cm. per cc. at 20° per g. adsorbent).

Acknowledgment.—We wish to thank Dr. L. N. Leum of the Atlantic Refining Co. and Dr. G. A. Mills of the Houdry Process Company for providing the surface area of palladium black and charcoal, respectively.

(3) D. T. Hurd, "Chemistry of the Hydrides," John Wiley and Sons, Inc., New York, N. Y., 1952.

(4) S. Brunauer, P. H. Emmett and E. Teller, *J. Am. Chem. Soc.*, **60**, 309 (1938).

(5) B. M. W. Trapnell, "Chemisorption," Academic Press, Inc., New York, N. Y., 1955, p. 143.

THERMODYNAMICS OF THE TITANIUM CHLORIDES. I. HEAT OF FORMATION OF TITANIUM TRICHLORIDE[1]

By David G. Clifton[2] and George E. MacWood

Contribution from the McPherson Chemical Laboratory, The Ohio State University, Columbus 10, Ohio

Received August 15, 1955

The heat of formation of titanium trichloride has been determined by measuring the heats of solution of $TiCl_4$(l) and $TiCl_3$(s) in a solvent of HCl–$FeCl_3$ in an ice calorimeter. The heat of formation of the trichloride is based upon the heat of formation for $TiCl_4$(l) of -192.1 ± 0.6 kcal./mole. The value obtained for the heat of formation of $TiCl_3$(s) at 298°K. is -172.2 ± 0.7 kcal./mole.

Introduction

There are few references in the literature for the heats of formation of the lower titanium chlorides. Brewer[3] gives estimated values for the trichloride and the dichloride. Also, Kubaschewski[4] reported estimated values for the tri- and dichlorides. In the light of recent work by Schaffer, Breil and Pfeffer,[5] and by Skinner and Ruehrwein,[6] these previously reported estimates are low.

This research provides an independent determination of the difference between the heats of formation of $TiCl_4$(l) and $TiCl_3$(s). With these results and the results on the heat of formation of $TiCl_2$(s),[7] an attempt is made to give consistency to the heats of formation of the titanium chlorides.

Apparatus

The heats of solution measurements were made using an ice calorimeter. The calorimeter, shown in Fig. 1, was a modification of the calorimeters developed by the National Bureau of Standards.[8,9] The main alteration was in the method of determining the volume change in the calorimeter. A dilatometer was used instead of the weight method employed by the Bureau.

The calorimeter was calibrated electrically for the purpose of comparison with the Bureau's calibration factor. The factor obtained was 878.08 ± 0.09% cal./cm.[3] This agrees within its precision with the value found by the National Bureau of Standards.

Materials

Titanium Tetrachloride.—The titanium tetrachloride used in the heat of solution determinations was provided by the Inorganic Chemical Section of the National Bureau of Standards. Their analysis gave the material a purity of 99.9991%. Samples were handled in sealed Pyrex bulbs and exposed only to dry nitrogen. The actual purity of the experimental samples was therefore not as high as the original, but any contamination was not appreciable.

Titanium Trichloride.—The titanium trichloride was prepared in this Laboratory by the method of Sherfey[10] as modified by Reed. The trichloride was formed by hydrogen reduction of titanium tetrachloride on a hot tungsten filament. After removal of any tetrachloride from the trichloride by pumping, the trichloride was further purified by sublimation.

The trichloride was analyzed for total titanium using the method of Rahm.[11] Analysis gave an empirical formula of $TiCl_{3.005}$.

Analysis of the reducing power was also made. The trichloride was dissolved in a solution of $FeCl_3$ and H_2SO_4 and the ferrous ion produced was determined by titration with ceric sulfate solution. The ceric sulfate was standardized against As_2O_3. An inert gas atmosphere was found necessary for precision.

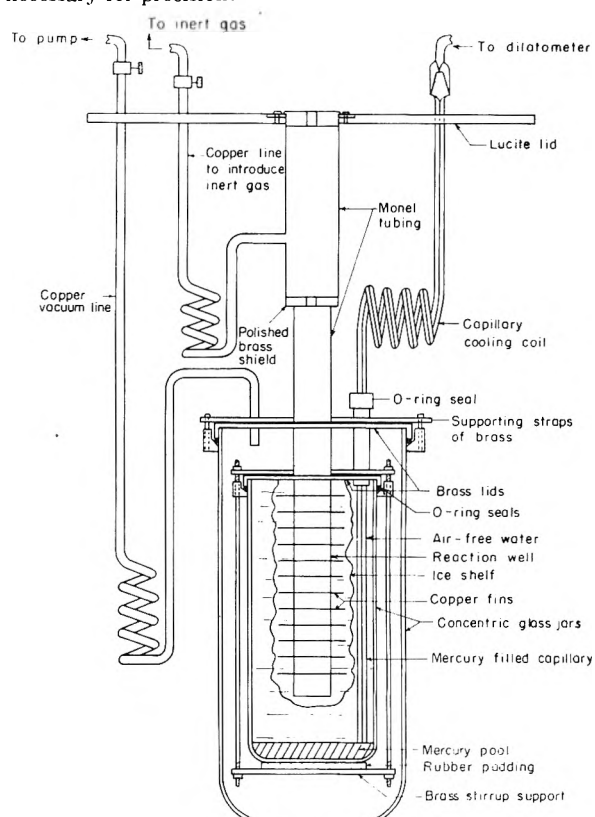

Fig. 1.—Ice calorimeter.

The reducing power analysis gave an empirical formula of $TiCl_{3.004}$.

The formula obtained by the total titanium analysis was used for the calculations on the heats of solution of the trichloride. The contaminant was assumed to be $TiCl_4$.

Solvent.—The solvent used was a solution of HCl and $FeCl_3$. In preparing this solvent an HCl solution, HCl·$8.859H_2O$, and 370 g. of $FeCl_3 \cdot 6H_2O$ were mixed to form 2 liters of solution. This concentration was chosen to duplicate a solvent used by Biltz and Fendius[12] as they have re-

(1) Work performed under the Office of Naval Research, Contract No. Nonr-495(06).

(2) Taken in part from the dissertation submitted by David G. Clifton in partial fulfillment of the requirements for the Ph.D. degree at The Ohio State University, March, 1955.

(3) L. Brewer, Paper 6, "National Nuclear Energy Series," Vol. IV-19B, edited by L. L. Quill, McGraw-Hill Book Co., New York, N. Y., 1950.

(4) O. Kubaschewski, "Metallurgical Thermochemistry," Academic Press Inc., New York, N. Y., 1951.

(5) H. Schaffer, G. Breil and G. Pfeffer, *Z. anorg. Chem.*, **276**, 325 (1954).

(6) G. B. Skinner and R. A. Ruehrwein, This Journal, **59**, 113 (1955).

(7) D. G. Clifton and G. E. MacWood, This Journal, **60**, 311 (1956).

(8) D. C. Ginnings and R. J. Corruccini, *J. Research Natl. Bur. Standards*, **38**, 583 (1947).

(9) D. C. Ginnings, T. B. Douglas and A. F. Ball, *ibid.*, **45**, 23 (1950).

(10) J. M. Sherfey, *ibid.*, **46**, 299 (1951).

(11) J. A. Rahm, *Anal. Chem.*, **24**, 1832 (1952).

(12) W. Biltz and C. Fendius, *Z. anorg. Chem.*, **176**, 49 (1928).

ported, for a solvent of this concentration, results which are used in subsequent calculations.

The density of the solvent at 27° was determined to be 1.1588 g./ml. This was used for calculations of the Ti-to-solvent weight ratios.

Initially, an arbitrary weight ratio of Ti ion to solvent was established in the heat of solution measurements of the $TiCl_4$. This same ratio was maintained throughout the heat of solution measurements, at 123.19 g. of solvent per g. Ti.

Heat of Formation of Titanium Trichloride

The heat of formation of $TiCl_3$ can be obtained if one has the heats of the reactions

$$TiCl_4(l) + \text{solvent} = \text{end soln. 1} \quad (1)$$

$$TiCl(s) + \text{solvent} = \text{end soln. 2} \quad (2)$$

$$Ti(s) + 2Cl_2(g) = TiCl_4(l) \quad (3)$$

$$FeCl_2(\text{soln. 2}) + {}^1/_2Cl_2(g) = FeCl_3(\text{soln. 1}) \quad (4)$$

Adding together the heats for reactions (1) and (3) and subtracting those for reactions (2) and (4), one obtains the heat of the reaction

$$Ti(s) + {}^3/_2Cl_2(g) = TiCl_3(s) \quad (5)$$

The heats of reactions (1) and (2) were measured experimentally. The heat of reaction (3) is the heat of formation of $TiCl_4(l)$. The heat of reaction (4) was taken from the literature. Biltz and Fendius[12] made a direct determination of the heat for reaction (4) and found it to be -21.4 ± 0.1 kcal./mole. This same heat of reaction was also determined by MacWood[13] in an HCl-$FeCl_3$ solution of stronger concentrations as -21.0 ± 0.2 kcal./mole. Since the solvent used here is the same as that of Biltz, his value will be used.

The results of the heat of solution measurements are listed in Tables I and II. Corrections were made on the $TiCl_3$ heats of solution for the $TiCl_4$ contamination as shown in Table II.

TABLE I

HEAT OF SOLUTION OF $TiCl_4$ IN SOLVENT

Run No.	Sample wt., g.	Heat measured, cal.	$-\Delta H_1$, kcal./mole
1	0.5775	123.3	40.5
2	.5028	107.5	40.6
3	.5774	123.3	40.5
4	.5232	111.1	40.3
5	.5411	114.9	40.3
6	.6100	130.6	40.6
7	.5592	118.7	40.3
8	.5722	121.9	40.4
9	.5792	123.9	40.6
10	.5685	119.8	40.0
11	.6064	127.9	40.0

Av. $\Delta H_1 = -40.4 \pm 0.2$ kcal./mole

TABLE II

HEAT OF SOLUTION OF $TiCl_3$ IN SOLVENT

Run No.	Sample wt., g.	$TiCl_3$ wt., g.	Heat measured, cal.	Cor. for $TiCl_4$, cal.	$-\Delta H_2$, kcal./mole
1	0.4568	0.4513	115.7	1.2	39.1
2	.4053	.4004	103.3	1.0	39.4
3	.3788	.3742	95.9	1.0	39.1
4	.3787	.3741	96.0	1.0	39.2
5	.3814	.3768	96.7	1.0	39.2

Av. $\Delta H_2 = -39.2 \pm 0.12$ kcal./mole

The combination of the measured heats of solution, ΔH_1 and ΔH_2, with the literature value for ΔH_4, -21.4 ± 0.1 kcal./mole, gives the heat of formation of $TiCl_3$, ΔH_5, in terms of the heat formation of $TiCl_4(l)$

$$\Delta H_5 = 20.2 + \Delta H_3 \pm 0.3 \text{ kcal./mole}$$

Therefore the heat for the reaction

$$TiCl_3(s) + {}^1/_2Cl_2(g) = TiCl_4(l) \quad (6)$$

at 0° is $\Delta H_6 = \Delta H_3 - \Delta H_5 = -20.2 \pm 0.3$ kcal./mole.

With the aid of heat capacity data, this heat of reaction can be corrected to 298°K. The heat capacities used are

$$C_{p_{TiCl_4(l)}} = 37.0 \text{ cal./deg. mole},$$

$$C_{p_{Cl_2(g)}} = 8.82 + 0.06 \times 10^{-3} T - 0.68 \times 10^5 T^{-2} \text{ cal./deg. mole}$$

$$C_{p_{TiCl_3(s)}} = 23.0 + 4.0 \times 10^{-3} T - 1.7 \times 10^5 T^{-2} \text{ cal./deg. mole}$$

The heat capacity of liquid $TiCl_4$ is taken as the average of the values reported by Gmelin[14] and the National Bureau of Standards.[15]

The heat capacity of gaseous chlorine is that given by Kelley.[16]

The heat capacity of the trichloride is not reported. The expression used above is the rounded-off value reported for vanadium trichloride by Kelley,[16] and should be a fair estimate because of the similarity of the compounds.

The change in heat capacity for reaction (6) is

$$\Delta C_p = 9.59 - 4.03 \times 10^{-3} T + 2.04 \times 10^5 T^{-2} \text{ cal./deg. mole}$$

and, therefore

$$\Delta H_6(298°) = -19.9 \pm 0.3 \text{ kcal./mole}$$

Thus the heat of formation of titanium trichloride at 298°K. is 19.9 ± 0.3 kcal./mole more positive than the heat of formation of titanium tetrachloride.

Recently, Johnson, Nelson and Prosen[17] have reported the heat of formation of $TiCl_4(l)$ as -192.1 ± 0.6 kcal./mole. Using this value and the heat of reaction (6) at 298°K. the heat of formation of $TiCl_3(s)$ is obtained

$$\Delta H_{f_{TiCl_3(s)}} = -172.2 \pm 0.7 \text{ kcal./mole}$$

Discussion

Schaffer, Breil and Pfeffer[5] reported two independently determined values for the heat of formation of $TiCl_3$. Effectively, they measured the difference between the heats of formation of $TiCl_4(l)$ and $TiCl_3(s)$, and in reporting the heat of formation of $TiCl_3$ based their calculations on the Bichowsky and Rossini[18] value of -181.4 kcal./mole for the $TiCl_4(l)$. By combining their difference values with the lately reported heat of formation of $TiCl_4(l)$, the heats of formation of $TiCl_3(s)$ reported by Pfeffer can be recalculated. They are -172.3 ± 0.8 and -172.8 ± 0.8 kcal./mole.

(13) Unpublished.

(14) Gmelin, "Handbuch der Anorganischen Chemie, Titan," Weinheim, 1951.

(15) "Selected Values of Chemical Thermodynamic Properties," Circular No. 500, National Bureau of Standards, 1952.

(16) K. K. Kelley, United States Bureau of Mines, Bulletin 476.

(17) W. H. Johnson, R. A. Nelson and E. J. Prosen, unpublished results, Reported to the Office of Naval Research in National Bureau of Standards Report No. 3663 revised (1955).

(18) F. R. Bichowsky and F. D. Rossini, "Thermochemistry of Chemical Substances," Reinhold Publ. Corp., New York, N. Y., 1936.

Skinner and Ruehrwein[6] determined the heat of formation of $TiCl_3(s)$ by a direct method, reporting the value of -170.0 ± 0.8 kcal./mole.

In view of the agreement between the present results and those of Pfeffer and co-workers by two independent methods, the difference between the heat of formation of $TiCl_4$ and $TiCl_3$ appears to be fixed within ± 0.3 kcal./mole. Therefore, unless there were an error in the heat of formation of $TiCl_4$, which is rather improbable, the heat of formation of $TiCl_3$ at 298.16 is -172.2 ± 0.7 kcal./mole.

Acknowledgment.—D.G.C. would like to express his appreciation to the Eastman Kodak Company for a fellowship which he held during part of this investigation.

THERMODYNAMICS OF THE TITANIUM CHLORIDES. II. HEAT OF FORMATION OF TITANIUM DICHLORIDE[1]

BY DAVID G. CLIFTON[2] AND GEORGE E. MACWOOD

Contribution from the McPherson Chemical Laboratory, The Ohio State University, Columbus 10, Ohio

Received August 15, 1955

The heat of formation of titanium dichloride has been determined by two independent methods. In the first method the heats of solution of $TiCl_4(l)$ and $TiCl_2(s)$ in a solvent of HCl–$FeCl_3$ were measured. In the second method the heats of solution of $TiCl_3(s)$ and $TiCl_2(s)$ in an HCl solution were used. The two values obtained are -123.3 ± 0.7 and -123.7 ± 1.0 kcal./mole, based on -192.1 ± 0.6 kcal./mole for the heat of formation of $TiCl_4(l)$.

I. Introduction

Brewer[3] and Kubaschewski[4] report estimated values for the heat of formation of titanium dichloride. Skinner and Ruehrwein[5] recently have reported a value for the heat of formation of the dichloride, calculated from disproportionation data.

This research gives the differences between the heats of formation of $TiCl_4$ and $TiCl_2$ and between $TiCl_3$ and $TiCl_2$. This information and that reported for $TiCl_3$[6] can then be used to give consistency to the heats of formation of the titanium chlorides.

II. Apparatus and Materials

The apparatus and some of the materials used for the measurements are described in the previous paper on $TiCl_3$.[6]

The titanium dichloride was prepared by disproportionation of sublimed titanium trichloride.[7] The trichloride was placed in a nickel boat which was put in a Vycor tube in a furnace. The heating chamber was evacuated using a mercury diffusion pump backed by a mechanical pump. The trichloride was held at 485° for 8 hours and then at 470° for 10.5 hours. The titanium tetrachloride formed during the reaction was condensed out in a liquid air trap.

Chloride analysis of the product gave an empirical formula of $TiCl_{2.004}$. Total titanium analysis of the sample gave an empirical formula of $TiCl_{1.999}$.

The sample dissolved completely in distilled water with slow evolution of hydrogen. This indicates that there was no appreciable metallic titanium impurity.

Since the chloride analysis afforded the greater precision, the empirical formula used in all calculations was $TiCl_{2.004}$. The contaminant was assumed to be $TiCl_3$, and the necessary corrections on the measured heats were made.

The same HCl–$FeCl_3$ solvent as previously reported[6] was used. The same weight-ratio of solvent to Ti-ion was maintained as in the previous experiments (123.19 g. of solvent per g. Ti). The water-to-HCl ratio in this solvent was 9.69.

The HCl solution used in the heat of dilution measurements of the solvent analyzed as $HCl \cdot 9.60H_2O$. The water-to-HCl ratio in the solution is not exactly the same as that in the solvent. However, this slight difference between the two ratios does not result in an appreciable difference in the heats calculated. This same HCl solution was used to determine the heats of solution of $TiCl_3$ and $TiCl_2$ in hydrochloric acid.

The density of this solution was measured to be 1.0843 g./ml. at 27°. The weight-ratio of solution to Ti-ion used for the trichloride and dichloride heats of solution in hydrochloric acid was 104.32 g. of solution per g. Ti.

III. Theory

The heat of formation of titanium dichloride can be obtained by using the following set of reactions

$$TiCl_4(l) + \text{solvent} = \text{end soln. 1} \quad (1)$$

$$TiCl_2(s) + \text{solvent} = \text{end soln. 2} \quad (2)$$

$$Ti(s) + 2Cl_2(g) = TiCl_4(l) \quad (3)$$

$$FeCl_2(\text{end soln. 2}) + {}^1/_2Cl_2(g) = FeCl_3(\text{end soln. 1}) \quad (4)$$

Adding together the heat for (1) and (3) and subtracting those for (2) and (4), the heat of reaction (5) is obtained

$$Ti(s) + Cl_2(g) = TiCl_2(s) \quad (5)$$

i.e., the heat of formation of $TiCl_2$.

Practically, complications arise in the above scheme. Reaction (2) involves the evolution of hydrogen. In order to use the above series of reactions, a correction must be made for the hydrogen evolution so that the end-solution after correction corresponds to the end solution 2. This required knowing quantitatively the amount of hydrogen evolved.

If no hydrogen were evolved, one equivalent of ferrous ion would be formed for every equivalent of divalent Ti-ion introduced into the solvent. Hence, the difference between the number of equivalents of ferrous-ion in the end solution actually found by titration, and that calculated from the

(1) Work performed under the Office of Naval Research, Contract No. Nonr-495(06).

(2) Taken in part from the dissertation submitted by David G. Clifton in partial fulfillment of the requirements for the Ph.D. degree at The Ohio State University, March, 1955.

(3) L. Brewer, Paper 6, "National Nuclear Energy Series," Vol. IV-19B, edited by L. L. Quill, McGraw-Hill Book Co., New York, N. Y., 1950.

(4) O. Kubaschewski, "Metallurgical Thermochemistry," Academic Press Inc., New York, N. Y., 1951.

(5) G. B. Skinner and R. A. Ruehrwein, THIS JOURNAL, **59**, 113 (1955).

(6) D. G. Clifton and G. E. MacWood, THIS JOURNAL, **60**, 309 (1956).

(7) W. C. Schumb and R. F. Sundstrom, *J. Am. Chem. Soc.*, **55**, 596 (1933).

amount of divalent Ti added, gives a measure of the amount of hydrogen evolved. A small correction to the ferrous-ion concentration must be made to compensate for that which resulted from the trichloride contamination.

The heat of the following reaction is necessary for the hydrogen correction

$$FeCl_3(soln.) + {}^1/_2H_2(g) = HCl(soln.) + FeCl_2(soln.) \quad (6)$$

which can be obtained from the heats of the following reactions

$$FeCl_3(soln.) = {}^1/_2Cl_2(g) + FeCl_2(soln.) \quad (7)$$
$$ {}^1/_2H_2(g) + {}^1/_2Cl_2(g) = HCl(soln.) \quad (8)$$

The heat of reaction (7) is the negative of the heat of reaction (4). The heat of reaction (8) is equal to the partial molal enthalpy of HCl at the applicable concentration. Rather than assume that the partial molal enthalpy of HCl in an aqueous solution is the same as in an HCl-solution containing $FeCl_3$, it was established experimentally.

The following series of reactions was used to determine the heat of reaction (8)

$$ {}^1/_2H_2(g) + {}^1/_2Cl_2(g) + 9.69H_2O = HCl(9.69\ H_2O) \quad (9)$$
$$HCl(9.69H_2O) + solvent = end\ soln.\ 3 \quad (10)$$
$$solvent + 9.69H_2O = end\ soln.\ 3\text{-}HCl \quad (11)$$

Reaction (8) is obtained by adding (9) and (10) and subtracting (11).

A second method of establishing the heat of formation of titanium dichloride involves measuring the heats of the following reactions:

$$TiCl_3(s) + HCl(xH_2O) = end\ soln.\ 4 \quad (12)$$
$$TiCl_2(s) + HCl(xH_2O) = end\ soln.\ 5 + {}^1/_2H_2(g) \quad (13)$$
$$ {}^1/_2H_2(g) + {}^1/_2Cl_2(g) = HCl(soln.) \quad (14)$$

Adding reactions (13) and (14) and subtracting reaction (12) gives

$$TiCl_2(s) + {}^1/_2Cl_2(g) = TiCl_3(s) \quad (15)$$

Hence, knowing the heat of formation of $TiCl_3$ permits the calculation of the heat of formation of titanium dichloride.

IV. Results

The heat of solution measurements are listed in Tables I, II, III and IV.

TABLE I

HEAT OF SOLUTION OF $TiCl_2$ IN SOLVENT

Run no.	$TiCl_2$ wt., g.	Heat evolved, cal.	$-\Delta H_2$, kcal./mole
1	0.2463	138.1	66.6
2	.1816	102.6	67.1
3	.2166	120.7	66.2
4	.2157	120.8	66.5
5	.2207	124.7	67.1

Av. $\Delta H_2 = -66.7 \pm 0.4$ kcal./mole

TABLE II

CORRECTIONS FOR THE HEAT OF SOLUTION OF $TiCl_2$

Run	$TiCl_{2.004}$ wt., g.	Measured heat, cal.	TiCl cor., cal.	Hydrogen cor., cal.
1	0.2484	124.2	−0.5	14.4
2	.1831	94.4	− .4	8.6
3	.2185	110.1	− .5	11.1
4	.2177	113.2	− .5	8.1
5	.2227	111.8	− .5	13.4

TABLE III

HEAT OF SOLUTION OF $TiCl_3$ IN HCl SOLUTION

Run no.	$TiCl_3$ wt., g.	Measured heat, cal.	$-\Delta H_{12}$, kcal./mole
1	0.4764	105.5	34.2
2	.3466	78.3	34.9
3	.5415	121.9	34.7

Av. $\Delta H_{12} = -34.6 \pm 0.4$ kcal./mole

TABLE IV

HEAT OF SOLUTION OF $TiCl_2$ IN HCl SOLUTION

Run	$TiCl_{2.004}$ g.	$TiCl_2$, wt., g.	Measured heat, cal.	$TiCl_3$ cor., cal.	$-\Delta H_1$, kcal./mole
1	0.2534	0.2512	98.8	−0.5	46.4
2	.1736	.1722	68.5	− .4	47.0
3	.2189	.2170	84.0	− .5	45.7

Av. $\Delta H_{13} = -46.4 \pm 0.65$ kcal./mole

In Table I, the weight of $TiCl_2$ is that in the particular sample of $TiCl_{2.004}$ used for the measurement. This is calculated from the analysis. The third column lists the heat assigned to the dichloride sample after the corrections have been made to the measured heat.

Table II lists the measured heats, the corrections for the $TiCl_3$ contamination, and the corrections for hydrogen evolution, which were used to get the quantity "Heat evolved" in Table I.

The various other heats of reaction required for reduction of the present data are given in Table V.

TABLE V

Reaction	Heat, kcal.	Source
ΔH_1	-40.4 ± 0.2	6
ΔH_3	-192.1 ± 0.6	10
ΔH_4, $-\Delta H_7$	-21.4 ± 0.1	8
ΔH_9	-37.8 ± 0.01	9
ΔH_{10}	0.0	Measured
ΔH_{11}	-1.0 ± 0.04	Measured
ΔH_{14}	-36.7 ± 0.04	9
ΔH_{16}	-39.2 ± 0.12	6

In order to evaluate the hydrogen-correction, the heat of reaction (6) was determined using the scheme outlined in Section III.

$$\Delta H_6 = \Delta H_7 + \Delta H_9 + \Delta H_{10} - \Delta H_{11}$$
$$= -15.4 \pm 0.11 \text{ kcal./mole}$$

The correction to the $TiCl_2$ heats of solution for the $TiCl_3$-impurity was made using the heat of the reaction

$$TiCl_3(s) + solvent = end\ solvent\ 1 \quad (16)$$

given in Table V.

V. Discussion

The difference between the heats of formation of $TiCl_4(s)$ and $TiCl_2(s)$ at 0° is obtained by using the heats of reactions (1), (2), (3) and (4)

$$\Delta H_{f_{TiCl_3(l)}} - \Delta H_{f_{TiCl_2(s)}} = \Delta H_2 + 2\Delta H_4 - \Delta H_1$$
$$= -69.1 \pm 0.5 \text{ kcal./mole}$$

(8) W. Biltz and C. Fendius, *Z. anorg. Chem.*, **176**, 49 (1928).

(9) F. D. Rossini, *J. Research Natl. Bur. Standards*, **9**, 679 (1932); **3**, 313 (1930).

(10) W. H. Johnson, R. A. Nelson and E. J. Prosen, unpublished results, Reported to the Office of Naval Research in National Bureau of Standards Report No. 3663 revised (1955).

The difference between the heat of formation of $TiCl_3(l)$ and $TiCl_2(s)$ at 0° is obtained by using the heats of reactions (12), (13) and (14).

$$\Delta H_{f_{TiCl_3(s)}} - \Delta H_{f_{TiCl_2(s)}} = \Delta H_{13} + \Delta H_{14} - \Delta H_{12}$$
$$= -48.5 \pm 0.85 \text{ kcal./mole}$$

To obtain the above differences in the heats of formation at 298°K., the following heat capacities were used

$$C_{p_{TiCl_4(l)}} = 37.0 \text{ cal./deg. mole}$$

$$C_{p_{Cl_2(g)}} = 8.82 + 0.06 \times 10^{-3} T - 0.68 \times 10^{5} T^{-2} \text{ cal./deg. mole}$$

$$C_{p_{TiCl_3(s)}} = 23.0 + 4.0 \times 10^{-3} T - 1.7 \times 10^{5} T^{-2} \text{ cal./deg. mole}$$

$$C_{p_{TiCl_2(s)}} = 17.0 + 2.7 \times 10^{-3} T - 0.7 \times 10^{5} T^{-2} \text{ cal./deg. mole}$$

The heat capacity of liquid titanium tetrachloride is the average of the values reported by Gmelin[11] and by the National Bureau of Standards.[12]

The heat capacity of gaseous chlorine is that given by Kelley.[13]

There are no reported heat capacities for titanium tri- and dichloride. The estimates used above are the rounded-off values of those reported for vanadium trichloride and vanadium dichloride, as given by Kelley.[13]

The differences corrected to 298°K. are

$$\Delta H_{f_{TiCl_4(l)}} - \Delta H_{f_{TiCl_2(s)}} = -68.8 \pm 0.5 \text{ kcal./mole}$$
$$\Delta H_{f_{TiCl_3(s)}} - \Delta H_{f_{TiCl_2(s)}} = -48.5 \pm 0.85 \text{ kcal./mole}$$

Combining the first difference with the heat of formation of $TiCl_4(l)$, -192.1 ± 0.6 kcal./mole, and the second difference with the heat of formation of $TiCl_3(s)$, -172.2 ± 0.7 kcal./mole, one gets

$$\Delta H_{f_{TiCl_2(s)}} = -123.3 \pm 0.8 \text{ kcal./mole}$$
$$\Delta H_{f_{TiCl_2(s)}} = -123.7 \pm 1.0 \text{ kcal./mole}$$

Even though the present determinations of the heat of formation of titanium dichloride and that previously reported for titanium trichloride[6] both involve the heat of formation of $TiCl_4(l)$ one can obtain the heat of the disproportionation reaction

$$2TiCl_3(s) = TiCl_2(s) + TiCl_4(l) \qquad (17)$$

from the heat of solution measurements, independently of the heat of formation of $TiCl_4(l)$, giving

$$\Delta H_{17}^{298^\circ} = 29.0 \pm 0.8 \text{ kcal./mole}$$

This agrees well with the heat of this reaction determined from disproportionation–pressure studies made by Sanderson and MacWood (29.2),[14] Skinner and Ruehrwein (29),[5] and Farber and Darnell (28.3).[15] In making the comparison 9.7 kcal./mole was used for the heat of vaporization of $TiCl_4(l)$.

In view of the agreement, between the various investigators, with respect to the heat of disproportionation, it must be concluded that the reported values of the heats of formation of Skinner and Ruehrwein are in error due to a discrepancy of approximately 2 kcal./mole in the heat of formation of $TiCl_3$. If the heat of formation of $TiCl_3$ is taken as -172.2 kcal./mole,[6] then, using their heat of disproportionation, the heat of formation of $TiCl_2$ becomes -123.3 in excellent agreement with the value reported here.

In conclusion the following features are emphasized: (1) the difference between the heats of formation of titanium tetrachloride and titanium trichloride measured by three independent methods is about 20.0 kcal./mole at 298°K.; (2) the heat of the disproportionation reaction has been found to be about 29.0 kcal./mole at 298°K. in four different investigations; and (3) the difference between the heats of formation of titanium trichloride and titanium dichloride measured in two independent ways was found to be about 48.9 kcal./mole.

Taking -192.1 ± 0.6 kcal./mole as the best value of the heat of formation for $TiCl_4(l)$,[10] the recommended heats of formation for the lower titanium chlorides are

$$\Delta H_{f_{TiCl_3(s)}} = -172.2 \pm 0.7 \text{ kcal./mole}$$
$$\Delta H_{f_{TiCl_2(s)}} = -123.3 \pm 0.8 \text{ kcal./mole}$$

(11) Gmelin, "Handbuch der Anorganischen Chemie, Titan," Weinheim, 1951.

(12) NBS, "Selected Values of Chemical Thermodynamic Properties," Circular No. 500, National Bureau of Standards, 1952.

(13) K. K. Kelley, United States Bureau of Mines, Bulletin **476**.

(14) B. S. Sanderson and G. E. MacWood, THIS JOURNAL, **60**, 316 (1956).

(15) M. Farber and A. J. Darnell, *ibid.*, **59**, 156 (1955).

THERMODYNAMICS OF THE TITANIUM CHLORIDES. III. THE SUBLIMATION PRESSURE OF TITANIUM TRICHLORIDE[1,2]

BY BENJAMIN S. SANDERSON AND GEORGE E. MACWOOD

Contribution from the McPherson Chemical Laboratory, The Ohio State University, Columbus, Ohio

Received August 15, 1955

Experimental measurements have been made of the sublimation pressure of $TiCl_3$ over the temperature range 628–823°K. by the transpiration method. From these results, the heat and free-energy of sublimation of 298°K. are found to be 42.0 ± 0.5 kcal./mole and 29.6 ± 1.0 kcal./mole. The heat of formation at 298°K. of gaseous $TiCl_3$ based on this work and the previously reported heat of formation of the solid is −130.2 ± 1.4 kcal./mole.

I. Introduction

As part of a program on the thermodynamic properties of the chlorides of titanium, the sublimation pressure of $TiCl_3$ has been studied by the transpiration method.[3–5]

Originally, it had been planned to use this experimental method to measure both the sublimation equilibrium

$$TiCl_3(s) = TiCl_3(g) \qquad (1)$$

and the disproportionation equilibrium

$$2TiCl_3(s) = TiCl_4(g) + TiCl_2(s) \qquad (2)$$

It was found that the transpiration method, though inadequate for the study of the disproportionation equilibrium,[6] gave very good results for the sublimation pressure of $TiCl_3$.

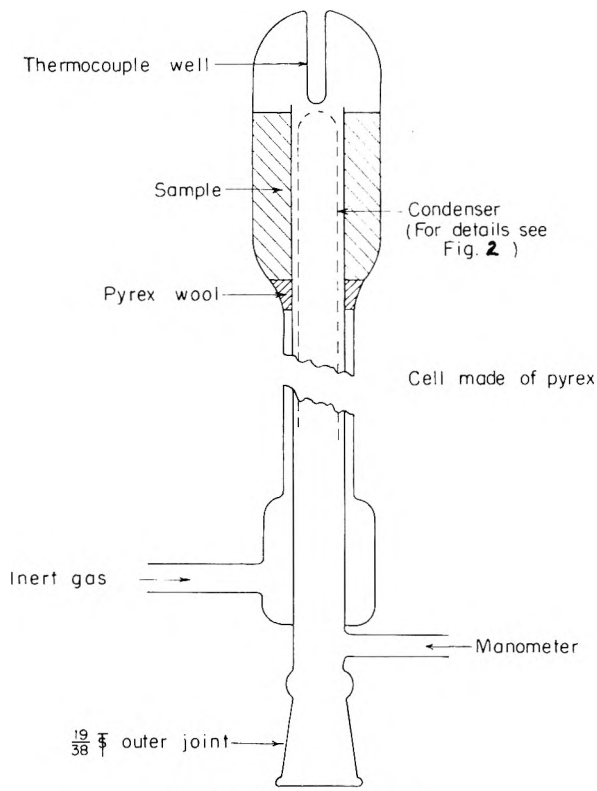

Fig. 1.—Transpiration cell.

II. Experimental Method

The apparatus used was a modification of that of Treadwell and Werner.[7] The transpiration cell is shown in Fig. 1 and the condenser for $TiCl_3$ and trap for $TiCl_4$ are shown in Fig. 2.

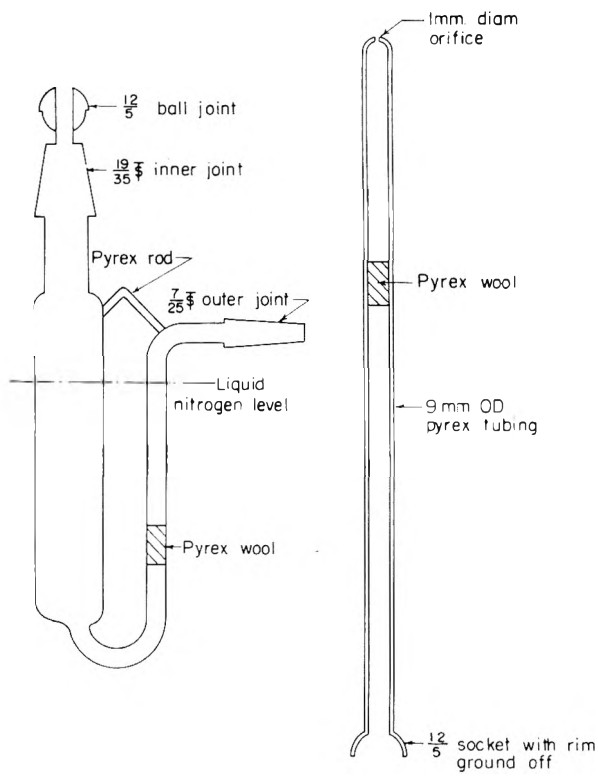

Fig. 2.—Trap and condenser.

Helium was used as the carrier gas. It was purified by flow through a train containing Drierite, hot copper turnings and then activated charcoal held at liquid nitrogen temperatures.

The purified helium entered the cell as indicated in Fig. 1, passed through the charge, and then the saturated gas passed out through the $TiCl_3$-condenser into the $TiCl_4$-trap. From the trap, the helium passed through a drying tube (to prevent back-diffusion of water vapor) into a 5-gallon flask where the helium was collected over water. The volume of displaced water was measured by collecting it in a two-liter volumetric flask from which the volume of helium was determined.

The furnace was of the nichrome resistance-type arranged so that it could be raised and lowered over the cell. This allowed the furnace to be brought to temperature before

(1) This paper presents the results of one phase of a program sponsored by the Department of Navy, Office of Naval Research, under Contract No. Nonr-495(06).

(2) Taken in part from the dissertation submitted by Benjamin S. Sanderson in partial fulfillment of the requirements for the Ph.D. degree at the Ohio State University, March, 1955.

(3) H. von Wartenburg, *Z. Elektrochem.*, **19**, 485 (1913).

(4) E. Thiele, *Ann. Physik*, **14**, 937 (1932).

(5) K. Jellinek and G. A. Rosner, *Z. physik. Chem.*, **A143**, 51 (1929).

(6) B. S. Sanderson and G. E. MacWood, THIS JOURNAL, **60**, 316 (1956).

(7) W. D. Treadwell and W. Werner, *Helv. Chim. Acta*, **36**, 1436 (1953).

lowering it into position over the cell. A Foxboro controller maintained the temperature of the charge within ±0.5°. The cell temperature was measured with an iron-constantan thermocouple, calibrated *in situ*.

The amount of $TiCl_3$ condensed out was determined either by weighing or by spectrophotometric analysis using the titanium–thymol complex described by Griel and Robinson.[8] The amount of $TiCl_4$ collected in the trap was determined by weighing.

III. Material

The $TiCl_3$ was made by an adaptation of the method of Sherfey[9] developed in this Laboratory by Mr. John Reed. In this method, titanium tetrachloride was refluxed over a red-hot tungsten filament while hydrogen was passed through the apparatus. The tetrachloride was reduced to trichloride and condensed on the walls of the apparatus. The refluxing tetrachloride washed the solid trichloride into a vessel with a fritted-glass bottom. After most of the tetrachloride had been filtered off the solid, the trichloride was transferred to Pyrex tubes about two inches in diameter and ten inches long. These tubes, after filling with crude charge, were pumped down and sealed off. They were then heated in a resistance furnace to 500°. The $TiCl_3$ sublimed to the cooler portion of the tube. Samples of both the crude and resublimed $TiCl_3$ were analyzed at the National Bureau of Standards for heavy metals. Neither sample contained metal impurities in excess of 15 p.p.m. Titanium and chlorine analyses of the trichloride gave an average empirical formula of $TiCl_{3.006}$, indicating the presence of a small amount of $TiCl_4$.

IV. Procedure

The $TiCl_3$ was loaded into the transpiration cell with the aid of a polyethylene "dry bag." A current of dry argon was circulated through the bag which was tied over the standard taper of the cell. All of the equipment required for loading the cell, as well as the $TiCl_3$, was put inside the bag before closing it.

After loading the cell, it was inverted and the $TiCl_3$ manipulated into its proper position as shown in Fig. 1. The cell was weighed and the weight of sample determined. Then the cell was mounted in place and connected to the helium gas train. The weighed condenser and trap were put into place while a current of helium passed through the system.

The furnace was brought to temperature in a position above the cell after which it was lowered around the cell. Thirty minutes was allowed for the sample to reach temperature equilibrium before the helium flow was started. By proper adjustments, the total pressure and the flow rate were rapidly established at the desired values.

At the end of a run, the furnace was lifted away from the cell. While the cell was cooling, the current through the heating tape around its lower end was continued in order to prevent $TiCl_4$ from condensing in the $TiCl_3$-condenser. When the cell had cooled, the condenser was removed and the amount of $TiCl_3$ collected determined either by weighing or spectrophotometric analysis. The amount of $TiCl_4$ collected in the trap was determined by weighing.

V. Results

The results of the sublimation measurements are summarized in Table I. The values for the weight of $TiCl_3$ collected reported to 0.1 mg. were determined by weighing, while those reported to 0.1 μg. were determined by spectrophotometric analysis. The average Cl/Ti ratios given in the table were calculated from the amounts of titanium and chlorine which were lost in each run.

The logarithms of the sublimation pressures are plotted against the reciprocal of the absolute temperature in Fig. 3. The straight line drawn through the points was determined by least squares and is given by the empirical equation

$$\log p(\text{mm.}) = -\frac{8296}{T} + 10.401 \qquad (3)$$

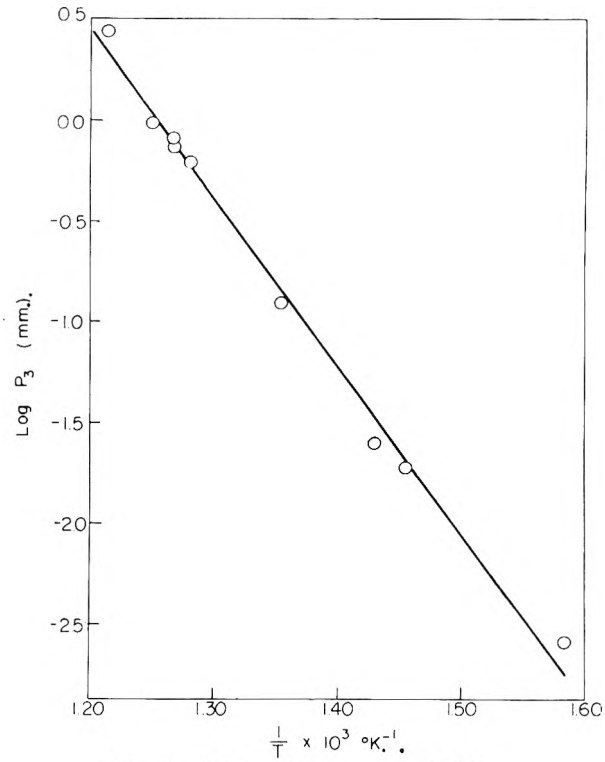

Fig. 3.—Sublimation pressure of $TiCl_3$.

The standard error of the slope is ±380, that of the intercept is ±0.51.

The average heat of sublimation for the temperature range 628 to 823°K., calculated from (3), is 38.0 ± 1.7 kcal./mole.

Heat and free energy of sublimation calculations were made, after the manner of Kelley,[10] based on the present measurements and the following estimated heat capacity equations for solid and gaseous $TiCl_3$

$$C_p(s) = 23 + 4 \times 10^{-3}\,T - 1.7 \times 10^5\,T^{-2} \qquad (4)$$
$$C_p(g) = 19.1 + 0.18 \times 10^3\,T - 1.7 \times 10^5\,T^{-2} \qquad (5)$$

The results of these calculations for the sublimation equilibrium are

$$\Delta C_p = -3.9 - 3.8 \times 10^{-3}T \qquad (6)$$
$$\Delta H^0 = 43300 - 3.9T - 1.9 \times 10^{-3}T^2 \qquad (7)$$
$$\Delta F^0 = 43300 + 3.9T \ln T + 1.9 \times 10^{-3}T^2 - 68.71T \qquad (8)$$
$$\Delta H^0_{298} = 42.0 \text{ kcal./mole } \Delta F^0_{298} = 29.6 \text{ kcal./mole}$$
$$\Delta S^0_{298} = 41.6 \text{ cal./deg. mole}$$

TABLE I

SUBLIMATION PRESSURE OF $TiCl_3$

T, °K.	Flow rate, cc./min.	Wt. $TiCl_3$, mg.	Vol. He, cc.	Moles $TiCl_4$ × 10^4	P, $TiCl_3$, mm.	Cl/Ti
628	11.0	0.0128	6007.0	4.7	2.58×10^{-3}	2.996
686	13.0	0.0917	6007.1	4.3	1.85×10^{-2}	2.267
699	19.6	16.7	8008.3	17.9	2.67×10^{-2}	2.735
738	15.0	6.2	6006.8	33.9	1.23×10^{-1}	2.644
780	13.0	31.4	6010.7	32.1	6.18×10^{-1}	2.546
788	27.0	37.4	5929.0	44.7	7.14×10^{-1}	2.939
789	13.6	40.9	6006.9	33.3	8.13×10^{-1}	2.413
800	14.0	48.2	5865.0	45.5	9.75×10^{-1}	2.779
823	14.0	95.2	4030.6	28.4	2.78	2.283

(8) J. V. Griel and R. J. Robinson, *Anal. Chem.*, **23**, 1871 (1951).

(9) J. M. Sherfey, *J. Research Natl. Bur. Stands.*, **46**, 299 (1951).

(10) K. K. Kelley, United States Bureau of Mines, Bulletin, 476 (1949).

The following thermodynamic constants for $TiCl_3$ obtained from the present results, heat of formation[11] and disproportionation data[6] are considered as the most reliable values at present available

$$\Delta H_f^0{}_{298}(g) = -130.2 \pm 1.4 \text{ kcal./mole}$$
$$\Delta H_f^0{}_{298}(s) = -172.2 \pm 0.8 \text{ kcal./mole}$$
$$S^0{}_{298}(g) = 73.8 \pm 2 \text{ cal./deg. mole}$$
$$S^0{}_{298}(s) = 33.3 \pm 2 \text{ cal./deg. mole}$$

VI. Discussion

Recently Farber and Darnell[12] have reported values for the sublimation pressure of $TiCl_3$ determined by the Knudsen method. Their values are considerably lower than those reported here. On the basis of work done in this Laboratory on the disproportionation equilibrium of $TiCl_3$[6], it appears probable that these low values are due to a low accommodation coefficient for gaseous $TiCl_3$. The agreement between the values of the heat of sublimation obtained by the two methods may imply that the temperature coefficient of the accommodation coefficient is very small as has been observed for gaseous $TiCl_4$ in study of the disproportionation of $TiCl_3$ by the Knudsen method.[12]

Skinner and Ruehrwein,[13] have reported measurements using the transpiration method. Their experimental values, although admittedly low, are of the same order of magnitude as those reported here. Their pressures, obtained by estimating the degree of saturation of the carrier gas, appear to be high. This results in a slightly higher entropy of sublimation at 298°K., 43.3 compared with 41.6, since the heats of sublimation at 298°K. agree within the precision of measurements.

(11) D. G. Clifton and G. E. MacWood, THIS JOURNAL, **60**, 309 (1956).

(12) M. Farber and A. G. Darnell, *ibid.*, **59**, 156 (1955).

(13) G. B. Skinner and R. A. Ruehrwein, *ibid.*, **59**, 113 (1955).

THERMODYNAMICS OF THE TITANIUM CHLORIDES. IV. THE DISPROPORTIONATION OF TITANIUM TRICHLORIDES[1,2]

BY BENJAMIN S. SANDERSON AND GEORGE E. MACWOOD

Contribution from the McPherson Chemical Laboratory, The Ohio State University, Columbus, Ohio

Received August 15, 1955

The disproportionation equilibrium of $TiCl_3$ was studied in the temperature range 593–821°K. by an effusion and static method. The two sets of measurements do not agree and indicate that the vaporization coefficient of $TiCl_4(g)$ is of the order of 10^{-4}. On the basis of the static measurements and previous work, a consistent set of thermodynamic properties of $TiCl_2$ and $TiCl_3$ are given.

I. Introduction

This is the fourth paper on the thermodynamic properties of titanium chlorides being investigated in this Laboratory[3-5] and gives the results of the investigation of the disproportionation equilibrium of $TiCl_3$

$$2TiCl_3(s) = TiCl_2(s) + TiCl_4(g) \qquad (1)$$

The course of the equilibrium as a function of temperature was studied by following the pressure of the titanium tetrachloride. The usual methods for measuring vapor pressures may be employed and, in this investigation, an effusion and static method were used.

II. Experimental

1. **Materials.**—The $TiCl_3$ and $TiCl_2$ were prepared as previously described.[3-5]

2. **Apparatus. (a) Knudsen Method.**—The apparatus is shown in Fig. 1. The body of the cell, shown in Fig. 2, was machined from stainless steel. The diaphragm, which contained the orifice, was made of 3-mil nickel sheet. It was held firmly in place by a screw-collar, a stainless steel washer being used to prevent tearing of the thin diaphragm. The weight loss of the cell was determined by following the change in length of a quartz helical spring, by comparison with a standard meter bar and cathetometer. The cathetometer has a Filar-micrometer eyepiece which could be read to 0.008 mm. The spring, obtained from the Houston Technical Laboratories, had a sensitivity of 5.092 cm./g. It had a maximum load capacity of ten grams. The cell was suspended from the spring by a 1-mil molybdenum wire. The portion of the apparatus housing the helix was protected on three sides to minimize random temperature fluctuations.

The cell was heated in a vertical resistance furnace, controlled by means of a Thyratron regulator. The sensing element for the regulator was B and S No. 30 platinum wire wound around the central portion of a nichrome tube which fitted between the glass tube containing the cell and the inside wall of the furnace. The wire was wound non-inductively and had a resistance of 35 ohms at room temperature. The resulting temperature regulation was within ±0.5°. The cell temperature was determined by means of a chromel–alumel thermocouple, placed about 1 cm. below the cell. From this measurement and preliminary calibration of the furnace temperature gradient as a function of position and temperature, a corrected value of the cell temperature was obtained.

The system was connected to a conventional high-vacuum system for maintaining low pressures during measurement.

(b) **Static Method.**—The Pyrex apparatus used for the static pressure determinations is shown in Fig. 3. The stopcocks were lubricated with a special fluorinated hydrocarbon grease. The tube for measuring the liquid $TiCl_4$ was calibrated against water with the aid of a weight-buret.

The gage used to measure pressures inside the system was a "Spoon-gage." In order to increase its sensitivity, while still maintaining mechanical strength, three "spoons" in series were used. A number of these gages were used during the course of the investigations. Their average sensitivity was about 0.03 mm. The outside jacket of the gage was connected through a two-way stopcock to vacuum pump or a supply of dry argon. The balancing argon pressure was measured with a tipping McLeod gage in the range

(1) This paper presents the results of one phase of a program sponsored by the Department of Navy, Office of Naval Research, under Contract No. Nonr-495(06).

(2) Taken in part from the dissertation submitted by B. S. S. in partial fulfillment of the requirements for the Ph.D. degree at The Ohio State University, March, 1955.

(3) I, D. G. Clifton and G. E. MacWood, THIS JOURNAL, **60**, 309 (1956).

(4) II, D. G. Clifton and G. E. MacWood, *ibid.*, **60**, 311 (1956).

(5) III, B. S. Sanderson and G. E. MacWood, *ibid.*, **60**, 314 (1956).

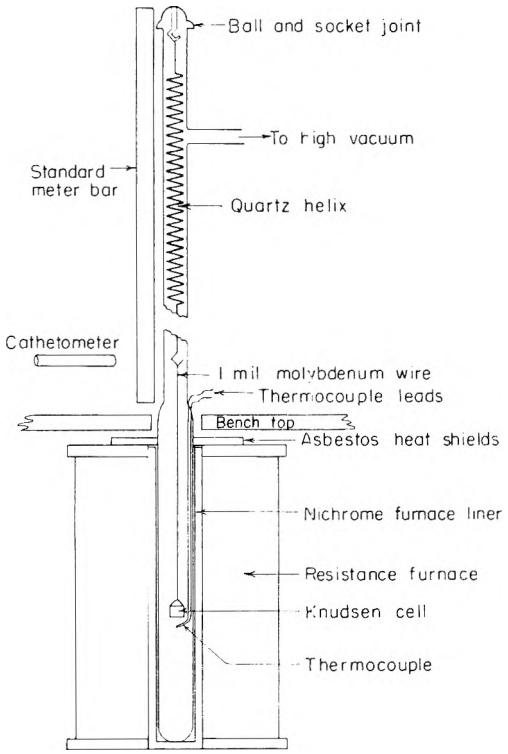

Fig. 1.—Knudsen apparatus.

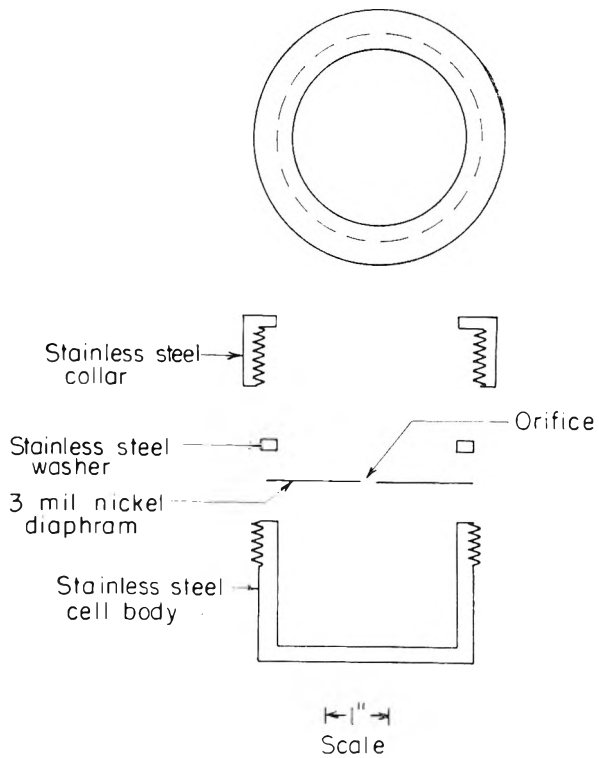

Fig. 2.—Knudsen cell.

0.001 to 5 mm. and with a Zimmerli gage for the range above 5 mm.

III. Procedure

(a) **Knudsen Method.**—A Lucite dry box was used in loading the cell with $TiCl_3$. A dry nitrogen atmosphere was used in the box. While the filled cell was being put into the effusion system dry argon was passed through the system.

When the system had been assembled, it was evacuated, then the furnace temperature raised to about 200°, and maintained at this temperature for 12 hours. After the furnace had been at the desired temperature for some time, the length of the helix was measured. A temperature correction, which varied with the load, was applied to each extension-measurement. The corrected extension was plotted against the time and the run continued until enough points had been determined to calculate an accurate slope.

(b) **Static Method.**—Before loading the cell for the static runs, it was outgassed at 590°. Then the cell was filled with dry argon, weighed and loaded with either titanium trichloride or dichloride. As shown in Fig. 3, a plug of Pyrex wool was inserted into the entrance to the cell to cut down the rate of diffusion of $TiCl_3$ vapor out of the constant temperature zone. After connecting the cell to the apparatus, the system was evacuated and the cell temperature raised to 200°. The cell and its charge were outgassed at this temperature for 12 hours.

The $TiCl_4$ was distilled into the reservoir at low pressure. After introduction into the system, it alternately was melted and frozen, followed by removal of gas by pumping until completely outgassed.

In the course of making a run, the temperature was allowed to reach a constant value and pressure readings were taken until a constant value obtained. In a few cases, it was necessary to plot the pressure against the time and extrapolate to large times to obtain the equilibrium pressure. When the pressure was approached either from above or below, the time to reach equilibrium varied, but the final pressures were the same within the precision of measurements.

The procedure for determining the pressure–composition isotherms was similar to that given above, except that the temperature was kept constant and the composition was varied by exchanging $TiCl_4$ between the system and reservoir. The amount of $TiCl_4$ which had been added to, or taken away from, the reservoir was followed with a catheto-

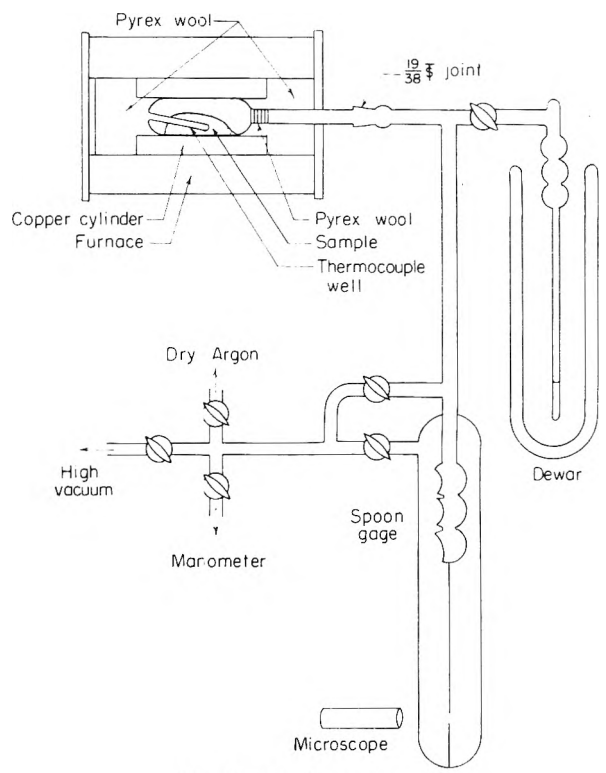

Fig. 3.—Static apparatus.

meter which measured the height of the meniscus to 0.1 mm., corresponding to 1.18×10^{-5} mole of $TiCl_4$.

IV. Results

1. **Knudsen Method.**—The results of the measurement of the disproportionation pressure of $TiCl_4$ by this method are summarized in Table I. A plot of the logarithm of the $TiCl_4$ pressure in

mm. against the reciprocal of the absolute temperature is given in Fig. 4. These data were fitted by least squares to the equation

$$\log p(\text{mm.}) = -\frac{6897}{T} + 8.407$$

TABLE I

SUMMARY OF $TiCl_4$ PRESSURES BY KNUDSEN METHOD

Run no.	T, °K.	p (mm.)	$-\log p$ (mm.)
28	593	0.000522	3.282
5	596	.000892	3.050
33	600	.00104	2.984
23	613	.00162	2.791
29	617	.00146	2.837
25	627	.00195	2.710
34	628	.00226	2.646
30	639	.00438	2.359
43	643	.00497	2.304
7	651	.00559	2.253
26	658	.00698	2.156
8	661	.00718	2.144
44	664	.0123	1.910
35	665	.0111	1.955
31	665	.0120	1.921
6	673	.0163	1.788
32	683	.0220	1.658
45	687	.0257	1.590
24	690	.0229	1.640
27	706	.0304	1.517
46	714	.0548	1.261
21	720	.0815	1.089

with a standard deviation of the slope of ±244 and of the intercept of ±0.374. This equation gives an average heat of reaction of 32 ± 1 kcal./mole for the temperature range 593 to 730°K.

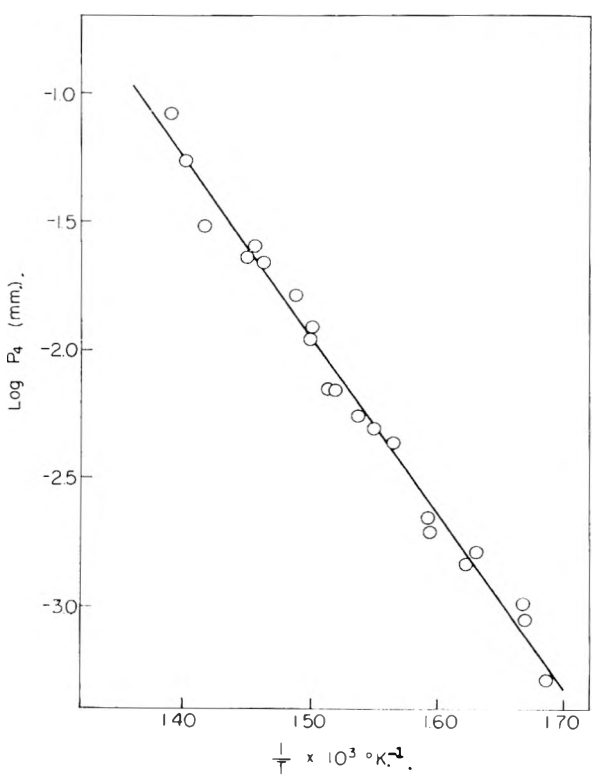

Fig. 4.—Disproportionation pressures of $TiCl_4$ by Knudsen method.

The values listed in the table were calculated from the observed total weight-loss by correcting for the amount of $TiCl_3$ effused using the reported $TiCl_3$ pressures of Darnell and Farber.[6] All of the pressures were corrected for the orifice thickness. The orifice used in runs 5 through 8 had a diameter of 0.1001 cm. The orifice used in runs 21 through 27 had a diameter of 0.0815 cm. Runs 28 through 46 were made with an orifice diameter of 0.1073 cm.

No values of the pressure are reported for which the Cl/Ti mole ratio is below 2.50.

2. Static Method.—The results of the static measurements of the equilibrium $TiCl_4$ pressure are summarized in Table II, Figs. 5 and 6.

TABLE II

SUMMARY OF $TiCl_4$ PRESSURES BY STATIC METHOD

T, °K.	p (mm.)	Cl/Ti
679.0	0.206	2.990
682.2	0.250	3.000
691.3	0.395	2.974
709.3	0.80	2.974
714.9	0.935	3.000
730.2	1.56	3.000
749.2	3.20	2.974
750.0	3.07	3.000
755.4	4.23	3.000
768.9	5.65	2.974
779.4	8.5	3.000
797.5	12.9	2.974
798.5	12.95	2.975
803.1	16.8	3.000
807.5	16.9	2.974
821.0	24.9	2.974

Using the static data, and the following heat capacities[3,4,7]

$$C_{p\,TiCl_4(g)} = 25.45 + 0.24 \times 10^{-3}T - 2.36 \times 10^5 T^{-2}$$
$$C_{p\,TiCl_3(s)} = 23 + 4 \times 10^{-3}T - 1.7 \times 10^5 T^{-2}$$
$$C_{p\,TiCl_2(s)} = 17 + 2.76 \times 10^{-3}T - 0.7 \times 10^5 T^{-2}$$

thermodynamic calculations were made. The results of the calculations for the disproportionation equilibrium of $TiCl_3$ are

$$\Delta C_p = -3.55 - 5 \times 10^{-3}T + 0.34 \times 10^5 T^{-2}$$
$$\Delta H^0 = 40000 - 3.55T - 2.5 \times 10^{-3}T^2 - 0.34 \times 10^5 T^{-2}$$
$$\Delta F^0 = 40000 + 3.55T \ln T + 2.5 \times 10^{-3}T^2 - 0.17 \times 10^5 T^{-1} - 67.75T$$
$$\Delta H^0_{298} = 38.6 \pm 0.4 \text{ kcal./mole}, \quad \Delta F^0_{298} = 25.9 \pm 0.8 \text{ kcal./mole}$$
$$\Delta S^0_{298} = 42.5 \pm 1.5 \text{ cal./mole deg.}$$

Discussion

Clifton and MacWood have determined the heat of formation of $TiCl_2(s)$[4] and $TiCl_3(s)$[3] relative to $TiCl_4(l)$. Using these measured differences and the heat of vaporization of $TiCl_4(l)$, they obtained for the heat of disproportionation at 298°K., 38.7 ± 0.8 kcal./mole. This agrees quite well with the 38.6 kcal./mole determined in this investigation.

Skinner and Ruehrwein[8] have made measurements on the $TiCl_3$ disproportionation equilibrium.

(6) M. Farber and A. J. Darnell, THIS JOURNAL, **59**, 156 (1955).

(7) K. K. Kelley, United States Bureau of Mines, Bulletin 383 (1935).

(8) G. B. Skinner and R. A. Ruehrwein, THIS JOURNAL, **59**, 110 (1955).

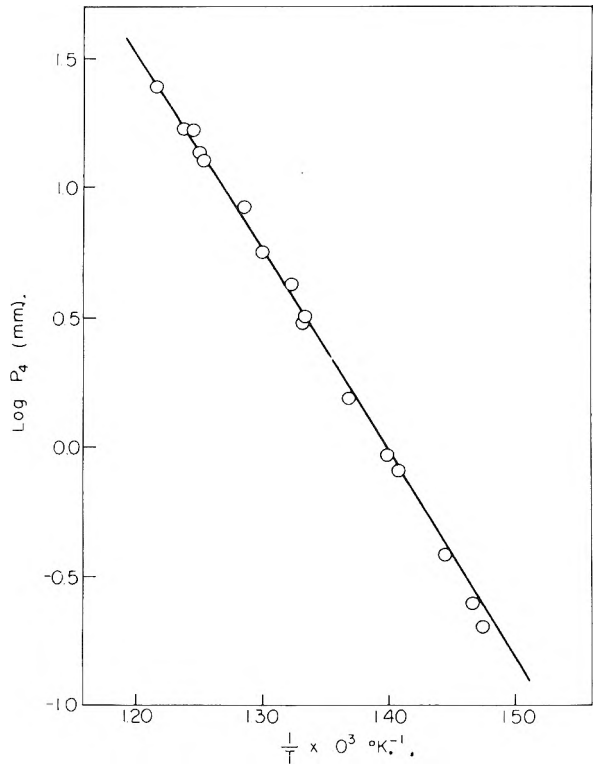

Fig. 5.—Disproportionation pressures of $TiCl_3$ by static method.

Using estimated free-energy functions they find, at 298°K.

ΔH^0_{298} = 38.7 kcal./mole, ΔF^0_{298} = 26.0 kcal./mole
ΔS^0_{298} = 42.6

in good agreement with the values reported here.

An examination of the $TiCl_4$ pressures determined by the effusion and static methods shows a large discrepancy. On the other hand, the measurements by either method are consistent and reproducible. This observation is supported, not only by the measurements reported here, but also by those of Farber and Darnell[6] and Skinner and Ruehrwein.[8]

It is suggested that the explanation of the above discrepancy is a low accommodation (vaporization) coefficient for $TiCl_4$ as recently suggested by Brewer and Kane.[9] If this is true, the accommodation coefficient can be calculated from $TiCl_4$ pressures determined by the two methods at the same temperature and the known orifice to surface ratio, using the relation given by Speiser and Johnston[10] for the observed pressure in the Knudsen method

$$p_{obs} = p_{true} \frac{\alpha}{\alpha + h/s}$$

where α is the accommodation coefficient, h/s the orifice to surface area ratio and p_{true} is taken as the pressure determined by the static method. On this basis, an accommodation coefficient of 2.4×10^{-4} is found for the temperature range 680 to 720°K.

It is evident from Fig. 6 that the isotherms observed do not correspond to those expected for a two-component, three-phase system, rather they

(9) Leo Brewer and J. S. Kane, *ibid.*, **59**, 105 (1955).

(10) R. Speiser and H. L. Johnston, *Trans. Am. Soc. Metals*, **42**, 283 (1956).

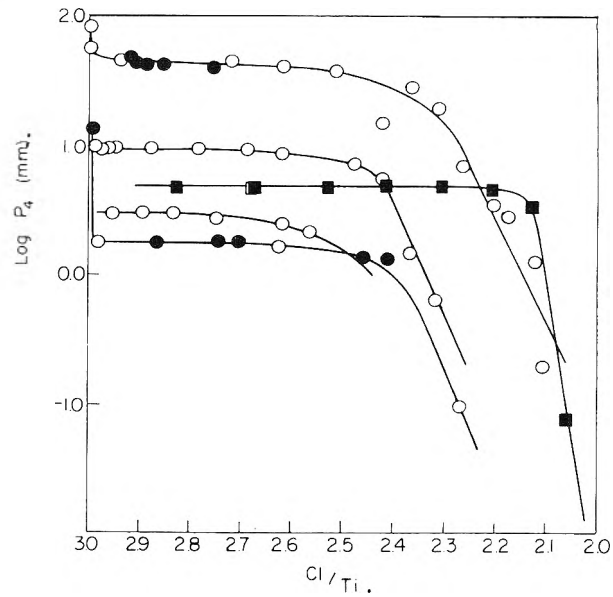

Fig. 6.—Isotherms of $TiCl_3$ disproportionation pressures.

indicate that in the $TiCl_2$-rich portion of the diagram there is solid solution of $TiCl_3$ in $TiCl_2$. Blitz and Juza[11] in their investigation of the platinum–sulfur system obtained similar isotherms, which they attributed to the existence of solid solution.

Clifton[12] in this Laboratory has determined the heat of solution of a mechanical mixture of pure $TiCl_3$ and $TiCl_2$, as well as the heat of solution of a partially disproportionated solid phase of the same average composition. He found a significant difference which can be interpreted as a heat of solid solution of 2.5 kcal./mole for an equimolal solution at 0°.

The observations suggest the existence of a miscibility gap. In the $TiCl_3$-rich region, the solubility of $TiCl_2$ in $TiCl_3$ is very small, *i.e.*, the solubility curve is very close to the $TiCl_3$-axis. While in the $TiCl_2$-rich region, the solubility of $TiCl_3$ in $TiCl_2$ is appreciable. In the previous calculations, it has been assumed that the mole fraction of $TiCl_2$ in the region of measurement, in the $TiCl_3$-rich range, is so small that the vapor pressure lowering due to it was insignificant and, furthermore, that the temperature coefficient of the solubility of $TiCl_2$ is small.[13]

In conclusion a consistent set of thermodynamic constants is given in Table III.

TABLE III

A CONSISTENT SET OF THERMODYNAMIC PROPERTIES OF TITANIUM CHLORIDES

Substance	ΔHf^0_{298}, kcal./mole	S^0_{298}, e.u.
$TiCl_4$(g)	−182.4 ± 0.7	84.4 ± 1.0
$TiCl_4$(l)	−192.1 ± 0.6	60.3 ± 1.5
$TiCl_3$(g)	−130.2 ± 0.7	73.8 ± 3.0
$TiCl_3$(s)	−172.2 ± 0.4	32.2 ± 1.0
$TiCl_2$(s)	−123.7 ± 0.4	22.6 ± 1.0

(11) W. Blitz and R. Juza, *Z. anorg. Chem.*, **190**, 161 (1930).

(12) D. G. Clifton, unpublished work.

(13) NOTE ADDED IN PROOF.—It appears that this system may be explained on the basis of a defect lattice as proposed by J. S. Anderson, *Proc. Roy. Soc.* (*London*), **A185**, 69 (1946).

INFRARED SPECTROGRAPHIC STUDIES OF PREFLAME REACTIONS OF *n*-BUTANE

BY JOHN T. NEU

Contribution from the California Research Corporation, Richmond, Cal.

Received August 15, 1955

This work reports the use of infrared spectroscopy to determine directly the behavior of the products and reactants as a reaction is occurring without the necessity of sampling. The method was applied to the oxidation of *n*-butane under conditions which caused a cool flame to occur as well as under slightly milder conditions which did not result in the formation of a cool flame. The products observed initially in both cases were formic acid, acetic acid, carbon monoxide, carbon dioxide and methyl alcohol. With the occurrence of a cool flame, ethylene, propene, butenes and acetylene formed, and formic and acetic acid were partially consumed. In the case in which no cool flame occurred, all products found initially increased throughout the reaction and in the latter stages of the reaction, methane formed. This work shows that infrared spectra can be used advantageously to study moderate temperature hydrocarbon oxidations and will be of considerable value as a complement to other methods of study.

Thomas and Crandall[1] employed a recording ultraviolet spectrophotometer to carry out kinetic studies of the reactions occurring during the preflame combustion of hydrocarbons. In this work, the reaction was conducted directly in the light path of the spectrophotometer. Barusch, *et al.*,[2,3] utilized similar techniques to identify products and intermediates of the preflame combustion reactions. This paper describes an analogous investigation of the formation of reaction products and intermediates, as determined by the infrared spectra of mixtures of *n*-butane and oxygen during preflame reactions.

The application of infrared spectroscopy to the analysis of certain fractions of butane oxidation products has been reported previously.[4] However, the procedures involved condensing and fractionating the products prior to subjecting them to analysis and suffer the disadvantage of allowing possible reactive and unstable combustion products to undergo further reaction prior to examination. Infrared spectroscopy has been used for the direct determination of intermediates in other types of reactions.[5] In general, the infrared spectral region is more useful than the ultraviolet because all pertinent molecular species, except the homonuclear diatomic molecules (O_2, H_2, N_2), absorb in the infrared region.

Experimental

A Perkin–Elmer Model 21 infrared spectrometer was used for these studies. A detailed description of the apparatus was published elsewhere.[6] The fuel in all experiments consisted of *n*-butane and oxygen in a 1:1 mole ratio. Phillips Research Grade *n*-butane (99% + pure) and Linde commercial oxygen were used without purification. Cancellation techniques, applicable to dual beam spectrometers,[6] were used to identify weak absorptions overlapped by spectra of known components and to measure quantitatively the gases known to be present in the sample cell. The quantitative analyses of products, with the exception of acetic acid and acetone, were made by this cancellation technique. Acetic acid and acetone were measured by conventional spectroscopic methods.

The first set of experiments was conducted at a temperature of 270° and an initial pressure of 500 mm. These conditions were too mild to produce a cool flame. The reaction proceeded over an interval of about 20 minutes, and this relatively slow rate permitted four scans of the entire rock salt region of the spectrum while the reaction was progressing. A scan from 5000 to 650 cm.$^{-1}$ and return to 5000 cm.$^{-1}$ required about five minutes.

In the second set of experiments, the same pressure and a slightly higher temperature (280°) were employed. Under these conditions the reaction resulted in the formation of a cool flame after an induction period of about two minutes. The scanning rate of the spectrometer was not high enough to allow scanning of the entire rock salt region during the two-minute induction period. To provide a representative picture of the kinetics of the reaction, it was necessary to survey this region several times during the reaction. Consequently, a number of combustion reactions were carried out under identical conditions, and the rock salt region was scanned by segments so that, during a given combustion reaction, several scans of a particular segment could be made. Each segment of the rock salt region was covered, and the scans were then pieced together to give a complete representation of the spectra during oxidation.

Table I shows the estimated detection limits of pertinent compounds in the presence of *n*-butane and also the estimated limits in the presence of *n*-butane combustion products. The increased difficulty of detection exhibited by the latter is caused by the overlapping of absorptions from the various products. The detection of water vapor is especially difficult because the water vapor spectrum is weak and because the sensitivity of the spectrograph in the water vapor region is limited due to the absorption caused by water in the atmosphere.

TABLE I

ESTIMATED LIMITS OF DETECTION OF COMPOUNDS AT 270° (EXCLUDING THE USE OF C=O AND C–H FREQUENCIES FOR IDENTIFICATION)

Compound	Pressure, mm. In presence of 250 mm. of *n*-butane	Pressure, mm. In presence of combustion products
Methane	5	10
Ethane	60	100
Formic acid	5	8
Acetic acid	1	5
Formaldehyde	25	50
Acetaldehyde	25	75
Acetone	5	5[a]
Methyl ethyl ketone	5	8[a]
Methyl alcohol	4	8
Ethylene	2	2
Ethyl alcohol	5	30
CO	8	8
CO_2	2	2
H_2O	100	150

[a] Using room temperature spectrum for identification.

(1) J. R. Thomas and H. W. Crandall, *Ind. Eng. Chem.*, **43**, 2761 (1951).

(2) M. R. Barusch, H. W. Crandall, J. Q. Payne and J. R. Thomas, *ibid.*, **43**, 2764 (1951).

(3) M. R. Barusch, J. T. Neu, J. Q. Payne and J. R. Thomas, *ibid.*, **43**, 2766 (1951).

(4) W. G. Appleby, W. H. Avery, W. K. Meerbott and A. F. Sarter, *J. Am. Chem. Soc.*, **75**, 1809 (1953).

(5) G. L. Simard, J. Steger, T. Mariuer, D. J. Salley and V. Z. Williams, *J. Chem. Phys.*, **16**, 836 (1948).

(6) J. T. Neu, *J. Opt. Soc. Am.*, **43**, 520 (1953).

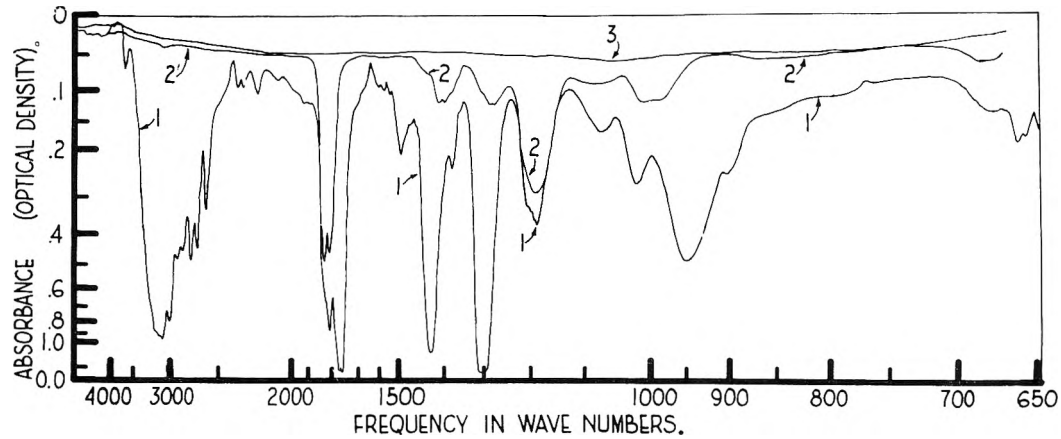

Fig. 1.—Acetic acid vapor: 1, T = 25°, P = 8 mm., cell length = 11.7 cm.; 2, T = 300°, P = 15 mm., cell length = 5.8 cm.; 3, background.

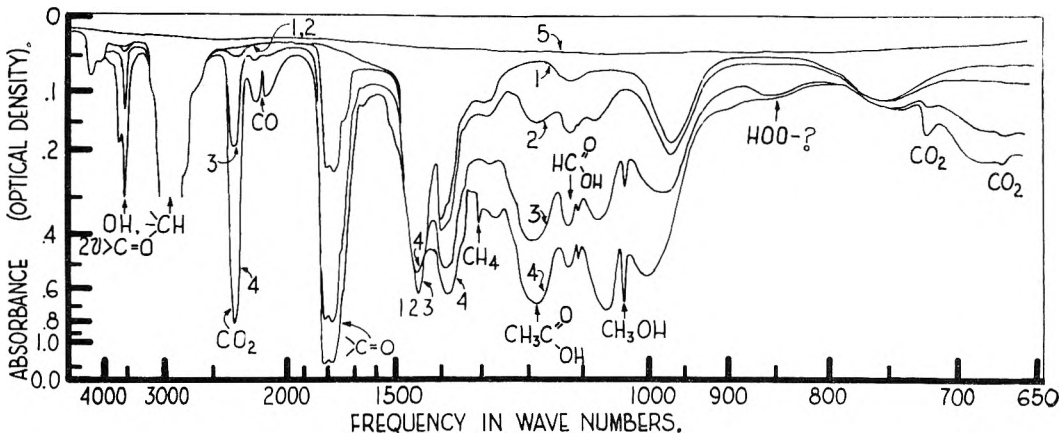

Fig. 2.—Oxidation in absence of a cool flame, successive spectra (T = 270°, initial P = 500 mm., final P = 525 mm.; fuel: 1:1 mixture *n*-butane–O_2, cell length = 5.8 cm.): 1, time 0 to 3.6 min.; 2, time 5 to 9.6 min.; 3, time 10.9 to 15.7 min.; 4, time 17 to 21.8 min.; 5, background.

Room temperature spectra of certain compounds may vary sharply from their elevated temperature spectra; and, consequently, elevated temperature reference spectra were required in some cases for identification of products. As an example, the contrast in the spectrum of acetic acid at 25° and at 300°, due to dimerization phenomena, is shown in Fig. 1.

Results

The general features characteristic of hydrocarbon oxidations carried out at moderate (250–350°) temperatures as discussed by Jost[7] were observed in these experiments. In all cases, there was an induction period during which little or no change was evident, followed by an autocatalytic reaction. In cases in which a cool flame did not occur, the rates of pressure rise reached maxima and then decreased to zero, giving the usual "S" shaped time–pressure curves. When cool flames occurred, the induction periods of the over-all oxidation reactions were shorter and were followed by accelerating pressure rises which apparently became discontinuous at the instant of cool flame occurrence. The heterogeneous nature of these reactions was indicated by the fact that a "conditioning" of the cell walls by several reactions was necessary before reproducible induction periods could be obtained.

The successive spectra of oxidation without a cool flame are shown in Fig. 2. For a period of several minutes after introduction of the gases into the heated cell, the only spectrum apparent was that of *n*-butane, as shown in Trace 1 of Fig. 2. It was noted that this spectrum differed from the room temperature spectrum of *n*-butane in that the absorption bands were somewhat broader, and there was a continuous absorption above the background. Trace 2 shows that formic acid (1100, 1780 cm.$^{-1}$), acetic acid (1186, 1780 cm.$^{-1}$), and carbon dioxide (2300 cm.$^{-1}$) were forming. The carbonyl absorption (1780 cm.$^{-1}$) due to the acids was so intense that it prevented the identification of carbonyl absorption caused by compounds expected in small concentrations, *e.g.*, formaldehyde and acetaldehyde. Trace 3 shows a general increase in absorption, and bands due to methyl alcohol (1034 cm.$^{-1}$) and carbon monoxide (about 2123 cm.$^{-1}$) appear. Trace 4 shows an increase of the products present, except formic acid which remains about the same. Methyl alcohol and carbon monoxide increased sharply, and a small amount of methane (1306 cm.$^{-1}$) appeared. Trace 3 shows a weak band centered at about 850 cm.$^{-1}$ which is not evident on trace 4. While this absorption is weak, it does indicate the transitory existence of an intermediate. The hydroperoxide group (–OOH) generally absorbs in this region, and an alkylhydroperoxide or peracid may account for this absorption; however, positive identification was not made. A

(7) W. Jost, "Explosion and Combustion Processes in Gases," McGraw-Hill Book Co., New York, N. Y., 1946, p. 367.

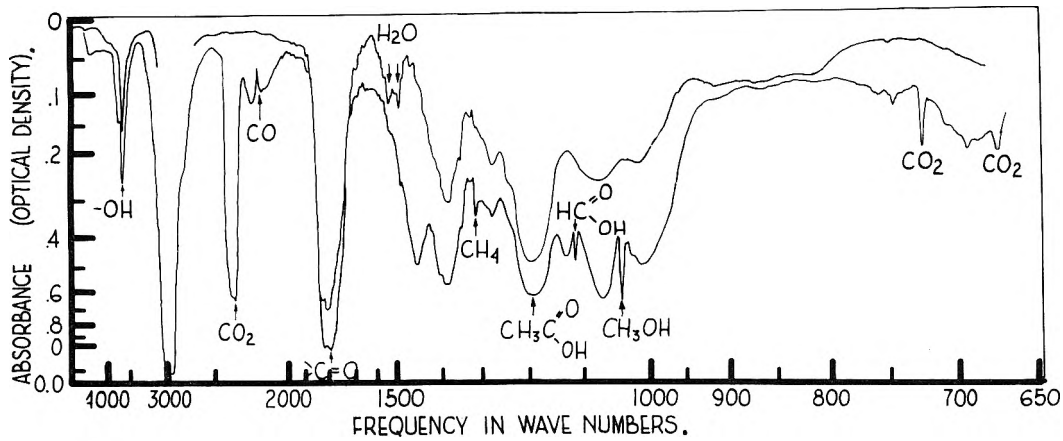

Fig. 3.—Oxidation in absence of a cool flame, high resolution scans (T = 270°, P = 525 mm., cell length = 5.8 cm.): 1, high resolution scan, vacuum in ref. cell; 2, high resolution scan, following gases in ref. cell

Formic acid	11	Methane	13	Carbon dioxide	65
Methyl alcohol	38	*n*-Butane	180	Nitrogen	138
		Carbon monoxide	68		

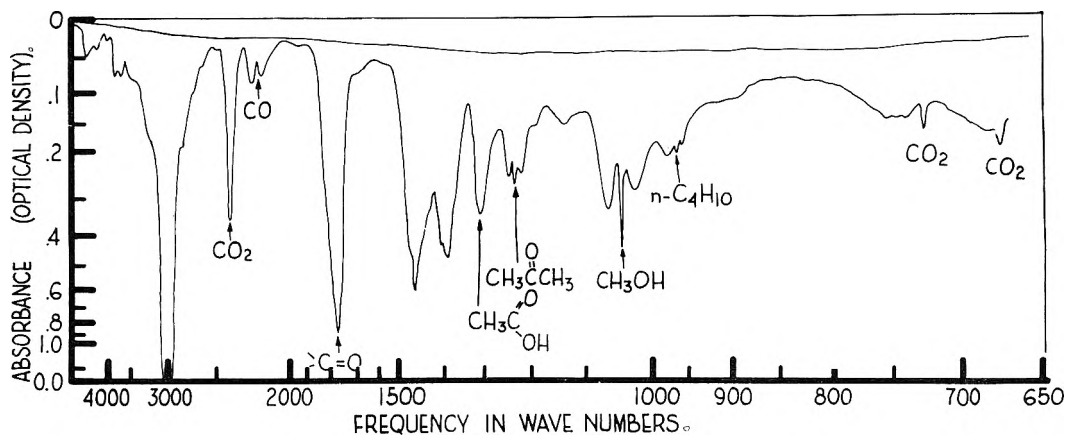

Fig. 4.—Oxidation in absence of cool flame, product spectrum at room temperature (T = 25°, cell length = 5.8 cm.).

subsequent scan, not represented on Fig. 2, established the fact that the reaction was essentially complete at the time scan 4 was taken. A slow, high resolution scan of the final products and also the spectrum recorded with certain products present in the reference cell are shown in Fig. 3. The high resolution scan shows definite but weak lines due to the presence of water vapor. In a separate but similar experiment after the reaction was complete, the cell was allowed to cool to room temperature. The spectrum of the product gases, as shown in Fig. 4, indicates the presence of acetone (1260 cm.$^{-1}$).

To check for any possible effects of the rock salt windows on the oxidation reactions, a combustion experiment was conducted in a Pyrex cell with Pyrex window under conditions otherwise comparable to the oxidation in the spectrometer cell. The spectrum at 25° of the gases removed from this cell was essentially the same as the room temperature spectrum noted above.

A summary of the combustion products from *n*-butane is shown in Table II. Formaldehyde was not detected by infrared absorption, and the value listed was taken from the data of similar experiments conducted in the ultraviolet spectrophotometer.[3] The water vapor spectrum was not strong enough to allow the determination of the amount of water vapor, and the value of 140 mm. was assumed so as to give an approximate material balance. The quantitative values in Table II are subject to some uncertainties but are useful to indicate the general distribution of products. Almost certainly, small amounts of other products, such as the β-dicarbonyl compounds, ethyl alcohol, acetaldehyde, etc., were present but not detected.

TABLE II

PRODUCTS OF OXIDATION IN ABSENCE OF A COOL FLAME

Compound	P, mm. at 270°	% of reactant elements found in products: Carbon	Oxygen	Hydrogen
n-Butane	180	72.0		72.0
Formic acid	11	1.1	4.4	0.9
Acetic acid	20	4.0	8.0	3.2
Methyl alcohol	38	3.8	7.6	6.1
Methane	13	1.3	0.0	2.1
Carbon monoxide	68	7.1	13.6	0.0
Carbon dioxide	65	6.5	26.0	0.0
Acetone	8	2.4	1.6	2.4
Water	140		28.0	11.2
Formaldehyde	(20)	(2.0)	(4.0)	(1.6)
Total	563	100.2	93.2	99.5

The products obtained prior to the occurrence of a cool flame are, so far as can be determined from the infrared absorption spectrum (Fig. 5), identical

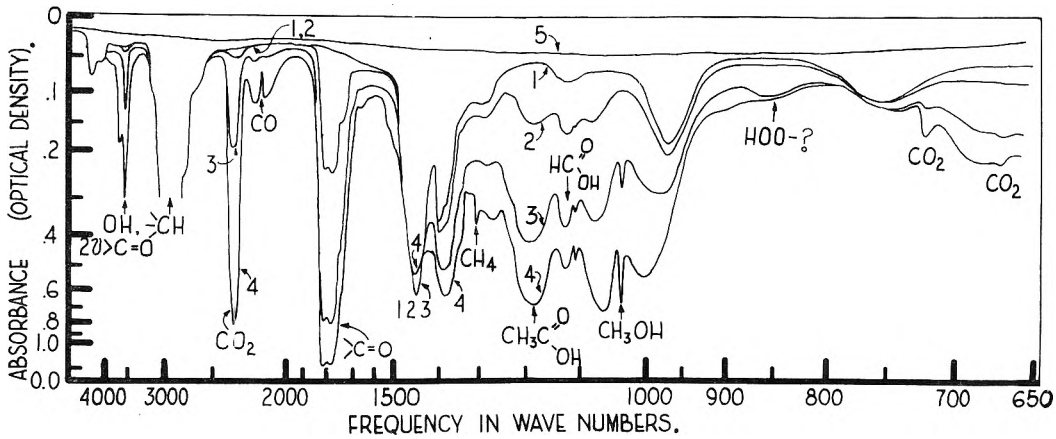

Fig. 5.—Spectra before and after a cool flame (T = 280°, initial P = 500 mm., final P = 580 mm.): 1, gases immediately after induction; 2, gases with induction period one-half expired; 3, gases directly before cool flame; 4, gases after cool flame occurred; 5, background.

to the products obtained when no cool flame occurs. The course of the changing spectrum, just prior to the cool flame, showed a general acceleration in infrared absorption, but there was no indication of a rapid build-up of a critical material, such as a peroxide. A comparison of the spectra recorded just before and just after the cool flame (Fig. 5) shows sharp differences. Some compounds appeared which were not observed prior to the occurrence of the cool flame. A relatively large amount of ethylene formed, together with propene, butenes, acetylene and methane. Coincident with the cool flame, there was a sharp drop in the concentrations of *n*-butane, formic and acetic acids, a large amount of carbon monoxide was formed, and the carbon dioxide concentration increased sharply. Following the occurrence of a cool flame, the spectrum showed essentially no change, as shown by subsequent scans.

Discussion

The large number of compounds formed and the order of appearance of the products suggest that no single mechanism is operative; rather, it is likely that several paths of degradation occur and that, as the population of the various molecular species changes, the predominant reactions change. The study of the reactions of certain simple oxy radicals[8,9] formed in peroxide decomposition and the researches on the mechanism of the oxidation of aldehydes[10] establish modes by which these radicals react. Applying this knowledge to the data obtained in these experiments permits the formulation of a reasonable explanation of the reaction mechanism for the oxidation of *n*-butane in the absence of a cool flame.

The occurrence of a number of the products formed in the absence of a cool flame is explained by assuming that methyl radicals are formed and react in the presence of a diminishing supply of oxygen. Raley and his co-workers[8] showed that the products formed from methyl radicals in the presence of oxygen are methyl alcohol, carbon monoxide, formaldehyde, formic acid, carbon dioxide, water and hydrogen, while the products formed in the absence of oxygen are methane and ethane. Although Raley's conditions differed somewhat from the conditions in the present work, there is a striking parallel between the products found. Apparently, in the presence of a high concentration of oxygen, the production of formic acid and carbon dioxide from methyl radicals predominates; but, as the oxygen concentration diminishes, oxygenated products containing less oxygen per molecule begin to form. Finally, when the oxygen concentration is low, methane forms. The mechanisms for the formation of these compounds are discussed by Raley.[8]

A possible mechanism for the formation of methyl radicals, as well as acetic acid and acetone, is of interest. It is considered that all of the products stem predominantly from the secondary butoxy radical, $CH_3\dot{C}HC_2H_5$ (O·). This radical is assumed to form through the intermediate of an alkyl peroxy radical, as

$$CH_3CH_2CH_2CH_3 + O_2 \longrightarrow CH_3\dot{C}HCH_2CH_3 + HO_2\cdot \quad (1)$$

$$CH_3\dot{C}HCH_2CH_3 + O_2 \longrightarrow CH_3CH(O{-}O\cdot)CH_2CH_3 \quad (2)$$

$$CH_3CH(O{-}O\cdot)CH_2CH_3 + RH \longrightarrow CH_3CH(O{-}OH)CH_2CH_3 + R\cdot \quad (3)$$

$$CH_3CH(O{-}OH)CH_2CH_3 \longrightarrow CH_3CH(O\cdot)CH_2CH_3 + \cdot OH \quad (4)$$

The formation of the alkyl peroxy radical (equations 1 and 2) is generally accepted as an initial step of the hydrocarbon oxidation chain reaction. The conversion of the peroxy radical to the butoxy radical was demonstrated in the case of the *t*-butyl group by Seubold and his collaborators,[11] though the mechanism for the conversion was not definitely established. The formation of the butoxy radical through an alkyl hydroperoxide (equations 3 and 4)

(8) J. H. Raley, L. M. Porter, F. F. Rust and W. E. Vaughan, *J. Am. Chem. Soc.*, **73**, 15 (1951).

(9) F. F. Rust, F. H. Seubold and W. E. Vaughan, *ibid.*, **72**, 338 (1950).

(10) J. Grumer, "Abstract of Papers Fifth Symposium (International on Combustion)" University of Pittsburgh, 1954, p. 41.

(11) F. H. Seubold, F. F. Rust and W. E. Vaughan, *ibid.*, **73**, 18 (1951).

is probable in oxidation reactions. On the basis of the products determined, the butoxy radical is thought to decompose according to the equations

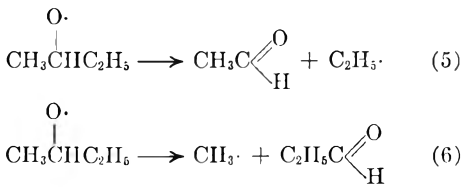

(5)

(6)

The other possible products of butoxy radical reactions, *i.e.*, methyl ethyl ketone, and secondary butyl alcohol, were not observed in this work. Aldehydes, in general, oxidize faster than hydrocarbons; and, under the conditions prevailing in this oxidation, the aldehydes would be expected to react further, as

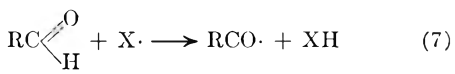

(7)

(The X· group could be any one of a number of hydrogen acceptors.) In the case of propionaldehyde, decomposition to ethyl radicals and carbon monoxide would be expected as

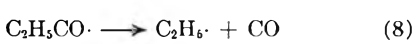

(8)

The conversion of the propionyl radical to propionic acid through perpropionic acid intermediate may occur to a small extent; however sufficient propionic acid was not present to allow detection by infrared spectroscopy. In the case of acetaldehyde, both decomposition to methyl radicals and CO and the formation of acetic acid through a peracid intermediate could occur.[10]

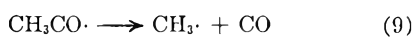

(9)

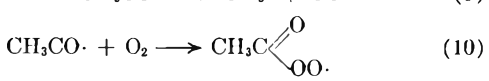

(10)

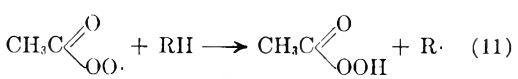

(11)

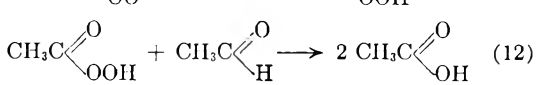

(12)

The ethyl radicals formed in the above steps (equations 5 and 8) would be expected to form ethoxy radicals (in a fashion analogous to the formation of butoxy radicals, equations 1, 2, 3, 4) and, ultimately, reaction products of ethoxy radicals. Ethanol, methanol, acetic acid, formic acid and CO were found experimentally to be the products of ethoxy radical decomposition carried out at 180° in the presence of oxygen by Bell and his coworkers.[12] At the higher temperature of the present combustion reactions, the decomposition products might be expected to increase at the expense of ethyl alcohol formation.

The formation of acetone can be postulated as occurring by the reaction of methyl and acetyl radicals

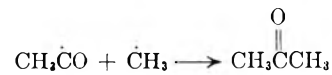

(13)

As in the case of the formation of methane, the supply of oxygen must be very low before this reaction occurs, because methyl radicals preferentially react with oxygen.[8]

Other paths of degradation probably exist. The β-dicarbonyl compound, found in oxidation experiments on *n*-butane in the ultraviolet work,[1,2] undoubtedly is produced in the infrared cell but not in sufficient amounts for detection. Using the proposed mechanism[3] for the formation of the β-diketone, an alternative method of formation of acetone can be advanced as follows, starting with the alkyl peroxy radical

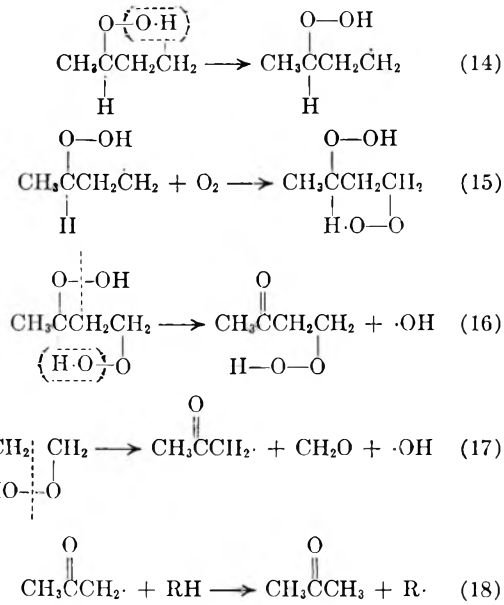

(14)

(15)

(16)

(17)

(18)

The last step in this mechanism, as is the case in equation 13, would only be expected to occur at low oxygen concentrations.

It is evident from the products formed that the reactions occurring in the cool flame are not just accelerated continuations of the processes occurring prior to the cool flame; completely different types of processes occur coincident with the cool flame. Hydrocarbon products, typical of thermal cracking reactions, are produced in the cool flame; whereas none of these hydrocarbons, except possibly methane, occurs before the cool flame. The reason for the change in the type of products is probably associated with the increased temperature and limited oxygen supply.

(12) E. R. Bell, J. H. Raley, F. F. Rust, F. H. Seubold and W. E. Vaughan, *Disc. Faraday Soc.*, No. 10, 242 (1954).

THE CHEMISORPTION OF CALCIUM HYDROXIDE BY SILICA

BY SIDNEY A. GREENBERG[1]

Johns-Manville Research Center, Manville, New Jersey

Received August 15, 1955

The chemisorption of calcium hydroxide from solution by silica was studied by measuring the immediate decrease in electrical conductance of calcium hydroxide solutions on the addition of silica. In this study the chemisorption properties of six varieties of silica were examined. The surface areas of the silicas ranged from less than one to 750 sq. m./g. SiO_2 and the water contents varied from almost zero (quartz) to 19.2%. The results indicate that the initial reaction of calcium hydroxide is with the surface SiOH groups on the silicas. This conclusion is substantiated by the data which show that the amount of calcium hydroxide removed from solution is proportional to the surface area and to the chemically-combined water in the silica.

The sorption of calcium hydroxide in solution by silica has been studied many times.[2] However, the nature of the process was described first as chemisorption by Maffei and his co-workers.[3] In many of the earlier studies the times allowed for equilibrium to be established were quite long and no allowance was made for the chemical reaction which can take place at room temperature between the matrix of the silica particle and the calcium hydroxide.[4] In the present study only the sorption occurring immediately on the mixing of the calcium hydroxide and silica was measured.

It is now generally agreed[5-9] that the surfaces of silica gels and quartz are covered with acidic SiOH groups which dissociate in this way

$$\text{—Si—OH} \rightleftarrows \text{—Si—O}^- + \text{H}^+ \qquad (1)$$

In addition, a small amount of monomeric silicic acid and its ions and colloidal silica are found in solution.[10-12] The interactions of the polysilicic acid surfaces with bases and neutral salts have been examined extensively.[13] According to recent theory the reaction of calcium hydroxide and the SiOH surface would be expected to be that of a weak acid ($K_1 = 10^{-9.8}$)[14] and a strong base

$$2\ \text{—SiOH} + \text{Ca(OH)}_2 \rightleftarrows (\text{—SiO})_2\text{Ca} + 2\text{H}_2\text{O} \qquad (2)$$

Although calcium silicates are relatively insoluble,[13,15] a certain amount of hydrolysis (reverse reaction of eq. 2) will take place in two steps

$$(\text{—SiO})_2\text{Ca} \rightleftarrows 2\text{—SiO}^- + \text{Ca}^{++} \qquad (3)$$

$$2\text{—SiO}^- + 2\text{H}_2\text{O} \rightleftarrows 2\text{—SiOH} + 2\text{OH}^- \qquad (4)$$

The hydrolysis of surface SiO^- would proceed because of the low ionization constant of silicic acid. Also when silica is allowed to react with neutral salts a decrease in *p*H results, which is explained[13] by this reaction

$$\text{—SiOH} + \text{MX} \rightleftarrows \text{—SiOM} + \text{H}^+ + \text{X}^- \qquad (5)$$

salt insoluble

In the present study the interaction of silica surfaces with calcium hydroxide and nitrate solutions was studied by measuring the decrease in conductance or *p*H of solutions of calcium hydroxide or nitrate on the addition of silica. Five varieties of amorphous silica and α-quartz were examined. Adsorption isotherms at 30 and 82° were obtained on silicas with surface areas varying from less than one to 750 sq.m./g. SiO_2 and water contents ranging from almost zero (quartz) to 19.2%. In addition, a comparison was made between the interactions of silica with sodium and with calcium hydroxide in solution.

Experimental

Equipment.—The *p*H determinations were made with a Beckman model H-2 meter. A constant temperature bath (±0.03°) regulated by a Thermocap relay (Niagara Electron Laboratories, Andover, N. Y.) was used for all experiments carried out at 30° and above. Electrical conductivity measurements were taken with an Industrial Instruments RC1B bridge and dip conductivity cells with constants of approximately one $cm.^{-1}$. Calcium hydroxide solutions were passed through Millipore HA filters (Millipore Filter Co., Watertown, Mass.) to clarify them. The dehydration curves of the silicas were obtained with a Chevenard thermobalance[16,17] at a constant heating rate of 8°/min. In a previous paper[17] the nitrogen adsorption measurements by the B.E.T. method were described.

Materials.—Mallinckrodt standard luminescent (S.L.), special bulky (Sp.B.), and aerogel (Santocel A) silicas were examined. (An excellent review of the properties of silica is given by Iler in a recent book.[9]) The du Pont Ludox (30% SiO_2) was diluted to 15% and small portions of this concentration were used in the sorption studies. A calculation of the amount of sulfate and hydroxyl ions present in the 60 ml. of calcium hydroxide solutions used, on the addition of small amounts of 15% Ludox sols, indicated a negligible concentration of these ions. Eimer and Amend $Ca(NO_3)_2 \cdot 4H_2O$ of tested purity was used. Well characterized mineral samples of α-quartz and opaline silica were

(1) Laboratory for Physical and Inorganic Chemistry, Leiden University, Holland.

(2) For review see H. H. Steinour, *Chem. Revs.*, **40**, 391 (1947).

(3) (a) A. Maffei and A. Battaglia, *Ann. Chem. Applicata*, **25**, 309 (1935); (b) A. Maffei, *Gazz. chim. ital.*, **66**, 197 (1936).

(4) H. F. W. Taylor, *J. Chem. Soc.*, 3682 (1950); L. Heller and H. F. W. Taylor, *ibid.*, 2397 (1951).

(5) M. W. Tamele in "Chemical Architecture, Frontiers of Chemistry," Vol. V, Interscience Publ. Inc., New York, N. Y., 1948.

(6) I. Shapiro and H. G. Weiss, THIS JOURNAL, **57**, 219 (1953).

(7) W. A. Weyl, *Research*, **3**, 230 (1950); *J. Am. Cer. Soc.*, **32**, 367 (1949).

(8) P. L. deBruyn, *Mining Eng.*, **7**, 291 (1955).

(9) For an excellent discussion see R. K. Iler, "The Colloid Chemistry of Silica and Silicates," Cornell Univ. Press, Ithaca, N. Y., 1955.

(10) G. B. Alexander, W. M. Heston and R. K. Iler, THIS JOURNAL, **58**, 453 (1954).

(11) F. G. Straub, Univ. Ill. Bull., 43, No. 59, Eng. Exp. Station, Bulletin Series No. 364, 1946.

(12) G. C. Kennedy, *Econ. Geol.*, **45**, 629 (1950).

(13) For review see J. N. Mukherjee and B. Chatterjee, *Nature*, **155**, 85 (1945).

(14) P. S. Roller and G. Erwin, *J. Am. Chem. Soc.*, **62**, 461 (1940).

(15) I. M. Kolthoff and V. A. Stenger, THIS JOURNAL, **38**, 475 (1934).

(16) C. Duval, "Inorganic Thermogravimetric Analysis," Elsevier Publ. Co., New York, N. Y., 1953.

(17) S. A. Greenberg, THIS JOURNAL, **58**, 362 (1954).

available for this study. The ignited opaline silica contained 95% SiO_2 and 5% impurities. Baker A.R. calcium hydroxide was found to be superior for the preparation of the solutions. Saturated solutions were made by shaking calcium hydroxide with distilled water at 26° and passing the solutions through a Millipore filter. Non-turbid solutions were prepared by this procedure. The concentration of the solutions was found to be 1.12 g. CaO/l. at 26° which compares very well with previously reported values.[18-20] The concentrations at 30 and 82° are 1.11 g. and 0.65 g. CaO/l., respectively, according to these authors, and solutions of such concentrations were made from the 1.12 g. CaO/l. solution.

Experimental Procedures and Theory.—The procedure used to determine the amount of calcium hydroxide in solution was employed previously by Cummins and Miller,[21] Beitlich,[22] and Budnikov[23] for similar purposes. In this procedure the changes in concentration of electrolytes in solution are determined by conductivity measurements.

It was first established in this study that the conductivities L of the calcium hydroxide solutions were directly proportional to the concentrations C at 30 and 82°. In addition, a plot was made of equivalent conductance *versus* the square root of concentration according to the Onsager equation[24]

$$\Lambda = \Lambda_0 - k\sqrt{C} \qquad (6)$$

where C is the concentration in equivalents/l. The equivalent conductance at infinite dilution Λ_0 was obtained from this plot. The value found was 259 $ohms^{-1}$ (25°) as compared to the 246 $ohms^{-1}$ (25°) reported by Lea and Bessey.[18] These authors point out that the value for Λ_0 derived from ionic mobility data at 25° is 256 $ohms^{-1}$.

Because of the linear relationship of specific conductance and concentration, it is possible to measure changes in concentration by resistance measurements. In this study, silica was added to calcium hydroxide solutions of known initial concentration C_{in}. By measuring the initial and final conductances L_{in} and L_f, respectively, C_f was found from the relationship

$$\frac{L_{in}}{L_f} = \frac{C_{in}}{C_f} \qquad (7)$$

With a knowledge of C_{in} and C_f, the amount of CaO sorbed in grams x by m grams of SiO_2 was calculated.

Two types of isotherms were obtained. In one case silica samples containing 0.075 g. of SiO_2 were added to 60 ml. of solutions of calcium hydroxide ranging from saturated at 30° (1.11 g. CaO/l.) and at 82° (0.35 g. CaO/l.) to very dilute solutions. The quantities x and m were calculated and x/m values were plotted as a function of the concentration of calcium hydroxide remaining in solution at equilibrium as is shown in Figs. 1 and 2. In the second kind of isotherm, samples of silica containing SiO_2 in the quantities shown in Fig. 3 were added to 60 ml. of saturated calcium hydroxide solutions at 30 and 82°. It was found that equilibrium was reached in the reaction between surface SiOH groups and calcium hydroxide in 15 seconds, except in the case of S.L. silica at 30° where one minute was allowed for equilibrium to be established. The x/m values of silica aerogel, opaline silica and α-quartz were measured in a similar manner.

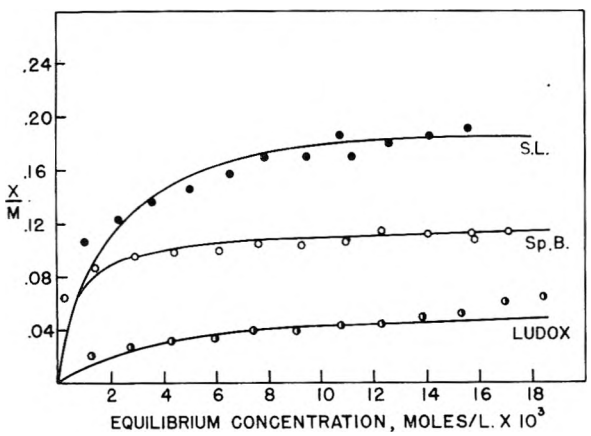

Fig. 1.—Sorption isotherms (30°) of calcium hydroxide by S.L., Sp.B. and Ludox silicas. The curves fit the Langmuir adsorption isotherm equation.

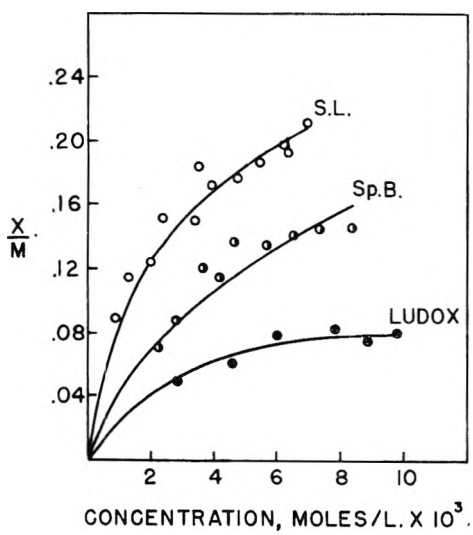

Fig. 2.—Sorption isotherms (82°) of calcium hydroxide by S.L., Sp.B. and Ludox silicas. The curves fit the Langmuir adsorption isotherm equation.

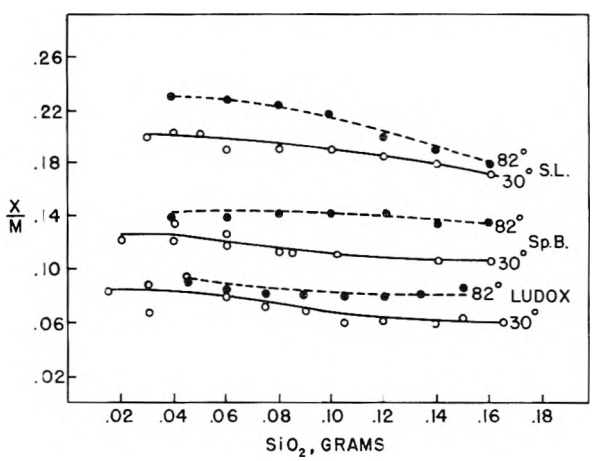

Fig. 3.—Dependence of x/m values on amount of S.L., Sp.B. and Ludox silicas added to equal concentrations of calcium hydroxide solutions.

To compare the removal by silica of calcium ions from hydroxyl and nitrate solutions, pH measurements were made before and after the addition of silica. The reagents used at 30° were 60 ml. of calcium hydroxide and of nitrate solutions to which were added 0.08 g. of Sp.B. silica. In the 82° experiments 60-ml. solutions and 0.10-g. samples of silica were used. The concentrations of the solutions are given in Figs. 7 and 8.

Results

Sorption Isotherms.—Figures 1 and 2 show the ratios of the grams of calcium oxide sorbed x per m grams of SiO_2 plotted as a function of the equilib-

(18) F. M. Lea and G. E. Bessey, *J. Chem. Soc.*, 1612 (1937).

(19) H. Bassett, *ibid.*, Pt. II, 1270 (1934).

(20) R. B. Peppler and L. S. Wells, *J. Research Natl. Bur. Standards*, **52**, 75 (1954).

(21) A. B. Cummins and L. B. Miller, *Ind. Eng. Chem.*, **26**, 688 (1934).

(22) A. E. Beitlich, *J. Am. Chem. Soc.*, **60**, 1832 (1938).

(23) P. P. Budnikov and M. I. Khigerovich, *Doklady Akad. Nauk, S.S.S.R.*, **96**, 141 (1954).

(24) For discussion see S. Glasstone, "Textbook of Physical Chemistry," D. Van Nostrand Co., Inc., New York, N. Y., 1946.

TABLE I

x/m VALUES AND SURFACE AREAS OF SILICAS

Silica	SiO_2, %	$(x/m)_{max}$ 30°	$(x/m)_m$ 30°	Surface area, sq. m./g. SiO_2 (nitrogen ads.)	Surface area, sq. m./g. SiO_2 (x/m values)
S.L.	80.8	0.20	0.20	750	660
Sp. B.	84.8	.13	.11	383	410
Aerogel	93.5	.095	...	247	215
Ludox	94.0	.080	.060	147 (dried)	225
Opaline	87.8	.015	...	23	46
Quartz	99.7	.004	...	<1	0

rium concentrations of calcium hydroxide for S.L., Sp.B. and Ludox silicas at 30 and 82°. The curves fit the Langmuir isotherm equation.[24] It may be noted that the x/m values increase with concentration toward a maximum at both temperatures. The higher x/m values obtained at 82° may be attributed to the small amount of chemical reaction with the matrix silica which begins almost immediately at the higher temperature.

The reduction in x/m values with decreased concentration of calcium hydroxide as shown in Figs. 1 and 2 may be attributed to the increased dissociation of the $(\equiv SiO)_2Ca$ groups and the increase in hydrolysis of $\equiv SiO^-$ ions at the lower concentrations of calcium and hydroxyl ions (eq. 3 and 4).

It may be seen in Fig. 3 that the x/m values at 30 and 82° of S.L., Sp.B. and Ludox silicas do not change markedly with an increase in SiO_2 additions. A small decrease may, however, be noted for the larger additions of silica. Higher values were obtained at 82° than those observed at 30° for the reason given previously.

In Table I are listed the maximum x/m values at 30° shown in Fig. 3. These values were considered maximum because the highest equilibrium concentrations of calcium hydroxide were obtained in these experiments by reducing the amount of silica added to the saturated calcium hydroxide solutions. In the experiments performed with equal SiO_2 additions (Figs. 1 and 2), a fairly large amount of SiO_2 (0.075 g.) was added in order to obtain a reasonable change in conductance on the addition of silica. Therefore, by using the saturated solutions and decreasing the amounts of silica added as shown in Fig. 3, it was possible to extrapolate back to almost saturation concentrations.

The maximum x/m values for aerogel, opaline and quartz silicas are listed in Table I. The $(x/m)_{max}$ value for quartz is approximate because of the small changes in the resistances of the calcium hydroxide solutions on the addition of quartz.

At the suggestion of Dr. Stephen Brunauer the maximum x/m values ($(x/m)_m$) were also calculated from the equation[25]

$$\frac{C}{x/m} = -\frac{1}{(x/m)_m b} + \frac{C}{(x/m)_m} \qquad (8)$$

where $(x/m)_m$ is the maximum x/m value, C is the equilibrium concentration of calcium hydroxide, b is a constant, and x is the grams of CaO adsorbed by m grams of SiO_2. It may be noted that the absolute magnitudes of the values of $(x/m)_{max}$ and $(x/m)_m$ (Table I) are not very different.

Surface Areas.—The correlation between the nitrogen adsorption surface areas[25] and maximum x/m values of the six varieties of silica may be seen in Fig. 4 and Table I. Ludox with an $(x/m)_{max}$ value of 0.08 should show according to the curve a surface area of 260 sq. m./g. SiO_2, which is somewhat higher than the values found by Alexander and Iler[26] on silica in suspension with unreported SiO_2 contents. However, a nitrogen adsorption area of 147 sq.m./g. SiO_2 was found for the precipitated and vacuum dried Ludox sample. The same value was obtained on samples of Ludox dried under different conditions. Either during the drying process unavailable pores are formed or the small amount of hydroxyl and sulfate ion impurities in the Ludox may account for the discrepancy.

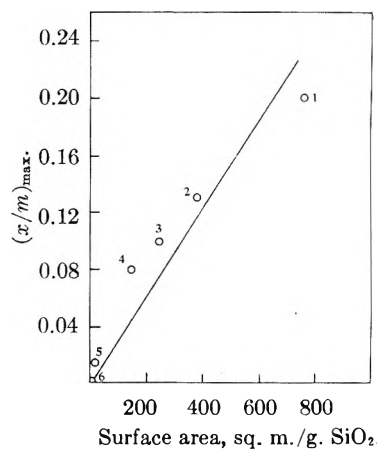

Fig. 4.—The relationship of $(x/m)_{max}$ values and the nitrogen adsorption surface areas of: 1, S.L.; 2, Sp.B.; 3, aerogel; 4, Ludox; 5, opaline silica; 6, quartz.

Since calcium hydroxide is dihydroxic, each molecule will react with two hydroxyl groups. The two hydroxyls may be on the same or different silicon atoms

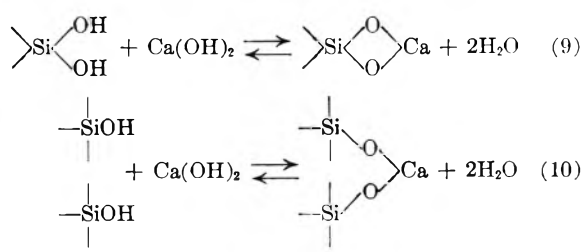

(25) S. Brunauer, "The Adsorption of Gases and Vapors," Princeton University Press, Princeton, N. J., 1945, p. 71.

(26) G. B. Alexander and R. K. Iler, THIS JOURNAL, **57**, 932 (1953).

TABLE II

WATER CONTENTS OF SILICAS

Type	Total, %	"Free" (115°), %	"Bound" (>115°), %	"Bound" (T.B.), %	"Bound" (>115°)/ 100 g. SiO_2	"Bound" (T.B.)/ 100 g. SiO_2	$H_2O(x/m)$/ 100 g. SiO_2
S.L.	19.2	11.9	7.3	6.6	9.0	8.3	7.9
Sp.B.	15.2	9.2	6.0	5.5	7.1	6.6	4.9
Aerogel	5.0	2.0	3.0	..	3.2	..	2.6
Ludox	6.8	4.5	2.3	2.1	2.5	2.2	2.7
Opaline	6.5	3.2	3.3	3.1	3.8	3.6	0.55
Quartz	0.1	0.03	0.07	..	0.07	..	0.71

Iler[9] predicts the first arrangement of hydroxyls if the surface of amorphous silica is like that of β-cristobalite and the second if it resembles that of β-tridymite. It seems reasonable to assume that all the hydroxyl groups can be made to react with calcium hydroxide if the concentration of the latter is sufficiently high and the silica surface is available to the ions. Therefore, assuming that each molecule of calcium hydroxide reacts with two hydroxyl groups, eight of which occupy one sq. mμ (calculated by Iler from the arrangement on the surface of β-cristobalite) then the surface area in sq.m./g. SiO_2 can be calculated and the values are listed in the last column of Table I. These values, it may be seen, are reasonably close to those obtained by nitrogen adsorption except in the case of Ludox.

Water Contents.—The nature of the water in the silica samples was examined by direct ignition, thermobalance and sorption techniques. In this study it is assumed that the total water in hydrated silica consists of "free," physically sorbed water and of "bound," chemically-combined water. The results are summarized in Table II.

1. The total water in the samples was determined by direct ignition at temperatures higher than 1000° and the results are given in column 1 of Table II. Similarly the "free"[27] water content was determined by measuring the weight loss on samples at 115°. Columns 2 and 3 list the "free" water and "bound" (total minus free) water for the samples. In Fig. 5 the relationship of the "bound" water contents and the $(x/m)_{max}$ values is shown graphically.

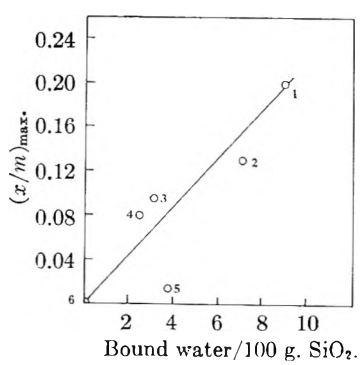

Fig. 5.—The relationship of $(x/m)_{max}$ values and "bound water" (>115°) contents of: 1, S.L.; 2, Sp.B.; 3, aerogel; 4, Ludox; 5, opaline silica; 6, quartz silica.

2. Dehydration curves were made with a Chevenard thermobalance and three may be seen in Fig. 6. From these curves it was possible to calculate the total water content of the samples. In addition the assumption was made that a sample heated under these conditions (8°/min.) begins to show the loss of "bound" water at the sharp change in the slope at approximately 225°. The weight loss above 225° of each silica was calculated and the results are listed in the column labeled "bound" (T.B.).

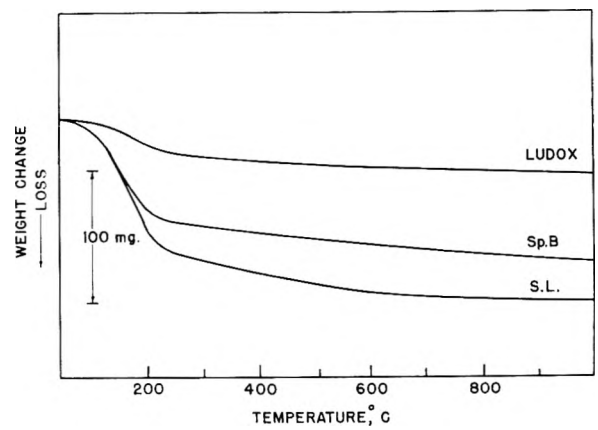

Fig. 6.—Dehydration curves of S.L., Sp.B. and Ludox silicas.

In the following two columns the "bound" water contents are converted to the amounts per 100 g. SiO_2. It may be noted that the values for "bound" water found by the ignition and thermobalance techniques are approximately the same.

3. In the last method for estimating the water contents, the $(x/m)_{max}$ values were used. Equations 8 and 9 show that the reaction of one molecule of calcium hydroxide with two hydroxyl groups corresponds to the liberation of one molecule of water. Hence, if the $(x/m)_{max}$ values correspond to a completely reacted SiOH surface then the amount of "bound" water in SiOH groups can be calculated. In the last column of Table I the results are listed.

It may be noted that the water contents (last three columns of Table II) found by the three methods show differences, but are of the same order of magnitude. An exception may be observed in the difference between the water content of opaline silica obtained from the $(x/m)_{max}$ value and the water content determined by weight loss measurements. In general, the "bound" water contents measured by ignition methods are higher than those calculated from sorption experiments. These higher values may be attributable to the difficulty in removing strongly-sorbed water at 115°. Therefore, the "bound" water determined by ignition meth-

(27) I. Shapiro and I. M. Kolthoff, *J. Am. Chem. Soc.*, **72**, 776 (1950).

ods may include a certain amount of sorbed water in addition to the water in SiOH groups.

Interaction of Silica with Calcium Nitrate.—The reaction would be expected to proceed according to this equation

$$2\text{—SiOH} + Ca(NO_3)_2 \rightleftharpoons (\text{—SiO})_2Ca + 2HNO_3 \quad (11)$$

Because both the reactants and products contribute to the conductance of solutions, the amount of reaction was determined by *p*H measurements. It may readily be seen in Figs. 7 and 8 that the decreases in *p*H on addition of Sp.B. silica to calcium hydroxide solutions were small and may be attributed to the decrease in hydroxyl ion concentration. Equation 11 serves to explain the larger drop in *p*H found in the calcium nitrate solutions. It should be pointed out that the change in concentration of the saturated solution of calcium hydroxide at 30° on the addition of silica is from 0.020 to 0.016 mole/l. according to the conductivity measurements and corresponds to a hydrogen ion change of 7.2×10^{-3} equivalent/l. However, the *p*H change on addition of silica to the calcium nitrate solution corresponds to a change of hydrogen ion concentration of only 3.7×10^{-6} equivalent/l. This could be expected because of the larger degree of hydrolysis of $(\text{—SiO})_2Ca$ at the lower *p*H in the calcium nitrate solution than at the *p*H of 12.5 found in the saturated calcium hydroxide solutions.

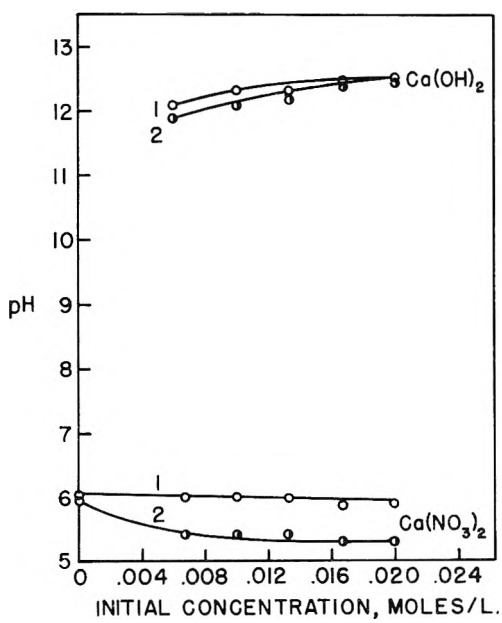

Fig. 7.—The *p*H of solutions (30°) of calcium hydroxide and nitrate before (1) and after (2) the addition of 0.08-g. samples of Sp.B. silica.

Sorption of Sodium Hydroxide.—A comparison was made of the milliequivalents of sodium hydroxide and calcium hydroxide sorbed by S.L., Sp.B. and Ludox silicas at room temperature. To 60 ml. of 0.04 *N* solutions, 0.075 g. of Ludox silica, and 0.10-g. samples of S.L. and Sp.B. silicas were added. In Table III the amount of each species sorbed is listed. It may be seen that the magnitude of the sorption of both ions is quite different.

TABLE III

CHEMISORPTION OF SODIUM AND CALCIUM HYDROXIDES

Silica type	Na(OH) meq. sorbed/g. SiO_2	$Ca(OH)_2$ meq. sorbed/g. SiO_2
S.L.	0.0048	0.0074
Sp.B.	.0033	.0053
Ludox	.00053	.0018

More calcium ions than sodium ions are removed from solution. This is consistent with the results of Mukherjee and Chatterjee[13] who found that the hydroxyl ion concentrations of solutions of calcium hydroxide containing silica sol were lower than those with equivalent concentrations of sodium hydroxide. This may, perhaps, be attributed to the greater degree of dissociation of $(\text{—SiO})Na$ than $(\text{—SiO})_2Ca$ groups. The order in which the silicas remove sodium ions is the same as for the removal of calcium ions.

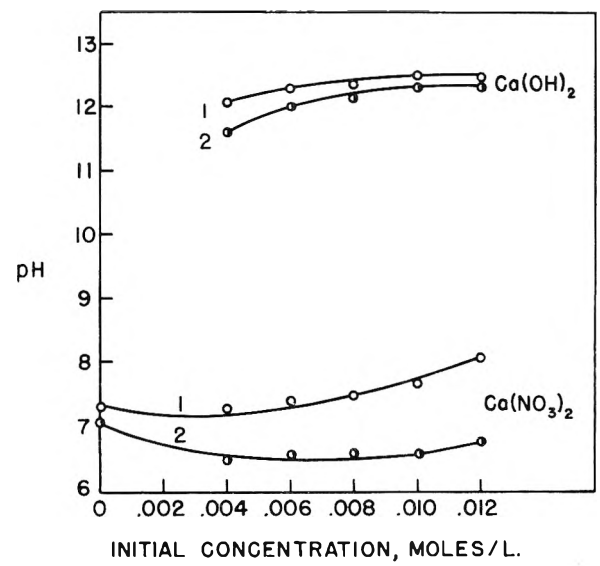

Fig. 8.—The *p*H of solutions (82°) of calcium hydroxide and of nitrate before (1) and after (2) the addition of 0.10-g. samples of Sp.B. silica.

Discussion

On the basis of the results, several conclusions can be drawn concerning the initial interaction between calcium ions and silica, and the nature of silica.

1. The results confirm the hypothesis that chemisorption of calcium ions by acidic SiOH groups is the initial step in the reaction of these two substances. The correlation between the amount of sorption and the surface areas and the "bound" water contents is strong evidence. In addition, the presence of limiting x/m values shows that only a monolayer forms.

2. The presence of SiOH groups on the surface and in the pores of the amorphous silicas provides evidence that silica is a condensation polymer of silicic acid.

3. The effect of *p*H on the hydrolysis of the SiO–Ca bond is clearly indicated by the results of this study. Additional evidence also is offered that

the hydrogen ion in SiOH groups can be replaced by calcium ions in solutions of *p*H greater than five and less than thirteen (Fig. 7).

4. The similarity between the surface areas determined by nitrogen adsorption and those found by sorption measurements assuming a β-cristobalite structure indicates that the local order of amorphous silicas is that of β-cristobalite. The lack of correlation between the surface areas of dried Ludox (measured by nitrogen adsorption) and the sol (determined by the sorption method) may be due to the change in orientation of the silica structure on dehydration.

Additional study is necessary to establish the cause of the difference between the "bound" water content of opaline silica found in the sorption experiment and the content measured by the ignition methods (Table II).

It might be suggested as an alternate mechanism that the calcium hydroxide in solution reacts with soluble monomeric $Si(OH)_4$ (silicic acid), which goes into solution at a rate proportional to the surface areas and water contents. Two pieces of evidence refute this mechanism. First, the similarity of $(x/m)_{max}$ values at 30 and 82° is inconsistent with the difference in the solubility of silica at the two temperatures. Second, it frequently has been reported that silicic acid goes into solution slowly.[10,12] Alexander, *et al.*,[10] found that it was necessary to wait 20 days to reach the equilibrium concentration at room temperature.

Acknowledgments.—The author wishes to acknowledge the assistance of Mr. J. Pellicane of this Laboratory in making the measurements reported in this study. Thanks are due to Dr. F. Pundsack for the well-characterized opaline silica and the stimulating discussions on the nature of the surface of silica. The nitrogen adsorption measurements were made by Mr. G. Reimschussel and Miss M. Cronin of this Laboratory. The author also wishes to thank Dr. Stephen Brunauer (Portland Cement Association, Skokie, Ill.) for his helpful comments on the manuscript.

CONDUCTANCES OF SOME ELECTROLYTES IN 1-PROPANOL AT 25°[1]

BY THOMAS A. GOVER AND PAUL G. SEARS

Contribution from the Department of Chemistry, University of Kentucky, Lexington, Kentucky

Received August 15, 1955

Conductances of sodium and potassium iodides and thiocyanates and of tetraethylammonium and tetra-*n*-propylammonium bromides and iodides in 1-propanol have been determined at 25° for concentrations in the range 8–300 × 10^{-5} *N*. Limiting equivalent conductances and dissociation constants have been determined by the Shedlovsky extrapolation method. The results indicate that limiting ionic conductances are additive in 1-propanol.

Introduction

Although many studies[2] have been made concerning the properties of solutions of electrolytes in methanol and in ethanol, very few data have been reported regarding the behavior of electrolytes in 1-propanol. Hovorka and Simms[3] have reported the most systematic previous study regarding 1-propanol solutions; however, their results indicate that the Kohlrausch law of independent ion migration does not apply to electrolytic solutions in this solvent. Inasmuch as this law has been found to be applicable to solutions of electrolytes in methanol, ethanol and most other solvents, their results appear questionable. The purpose of this study, therefore, has been to re-examine the additivity of ionic mobilities in 1-propanol.

Experimental

1. **Purification of Solvent.**—1-Propanol (Eastman Kodak Co. White Label) was fractionated at atmospheric pressure through a 120-cm. vacuum-jacketed column packed with glass helices. Traces of water were removed as a minimum-boiling ternary azeotrope using benzene as the third component. The retained middle fractions had conductivities of 2 × 10^{-8} ohm^{-1} $cm.^{-1}$ or less.

2. **Salts.**—The salts were purified as described previously[4,5] and were dried to constant weight in a vacuum oven at 70° prior to using.

3. **Apparatus and Procedure.**—Resistances of the solutions were measured at 500, 1000 and 2000 cycles with an assembly consisting of the following parts having the designated numbers according to the Leeds and Northrup Catalog EN-95: Jones conductivity bridge (4666), tuned audio frequency amplifier (9847), audio frequency oscillator (9842) and telephone receiver (9874).

The conductance cells, the constant temperature bath and the experimental procedure have been described adequately in previous papers.[5,6]

In converting concentrations from a weight to a volume basis, it was assumed that the densities of the solutions were equal to that of the solvent. All weights were corrected to vacuum. The conductivity of a salt was obtained by subtracting the conductivity of the solvent from that of the solution.

The following data for 1-propanol at 25° were determined by using several samples of the solvent: density, 0.8008 g./ml.; viscosity, 0.0193 poise; dielectric constant, 20.4. The values for the density compare favorably with those which have been reported by Dunstan and Thole.[6] The value for the dielectric constant agrees with the data reported by Maryott and Smith.[7] The values of the fundamental constants which were used in the calculation of the Onsager constants were taken from the latest report of the Subcommittee on Fundamental Constants.[8]

(1) Based in part upon a report submitted by Thomas A. Gover in an undergraduate independent work course in chemistry.

(2) D. A. MacInnes, "The Principles of Electrochemistry," Reinhold Publ. Corp., New York, N. Y., p. 356.

(3) F. Hovorka and J. C. Simms, *J. Am. Chem. Soc.*, **59**, 92 (1937).

(4) D. P. Ames and P. G. Sears, THIS JOURNAL, **59**, 16 (1955).

(5) P. G. Sears, E. D. Wilhoit and L. R. Dawson, *ibid.*, **59**, 373 (1955).

(6) A. E. Dustan and F. B. Thole, *J. Chem. Soc.*, **95**, 1556 (1909).

(7) A. A. Maryott and E. R. Smith, NBS Circular 514, August 10, 1951.

(8) F. D. Rossini, F. T. Gucker, Jr., H. L. Johnston, L. Pauling and G. W. Vinal, *J. Am. Chem. Soc.*, **74**, 2699 (1952).

Results

Corresponding values of the equivalent conductance, Λ, and of the molar concentration, C, are given in Table I. Confirmatory data for another series of solutions for each salt have been omitted for conciseness. However, the data for the two series of solutions in each case agreed within the estimated error of 0.2%.

TABLE I

EQUIVALENT CONDUCTANCES OF SOME SALTS IN 1-PROPANOL AT 25°

$c \times 10^4$	Λ	$c \times 10^4$	Λ
(a) Sodium thiocyanate		(e) Tetraethylammonium bromide	
1.333	22.83	0.6134	25.69
3.200	21.81	1.243	24.88
6.254	20.68	2.482	23.69
11.04	19.37	4.036	22.59
18.13	18.12	6.313	21.33
26.48	17.01	8.907	20.22
		13.86	18.70
(b) Potassium thiocyanate		(f) Tetraethylammonium iodide	
1.109	24.47	0.7544	26.71
2.534	23.34	1.405	25.82
5.726	21.68	2 522	24.61
8.524	20.64	3.923	23.44
11.64	19.75	6.789	21.70
15.95	18.74	10.91	19.99
(c) Sodium iodide		(g) Tetra-*n*-propylammonium bromide	
0.8605	22.78	0.6610	23.23
1.666	22.20	1.509	22.27
3.716	21.28	3.189	21.14
7.550	20.01	5.737	19.86
12.55	18.96	9.763	18.41
19.33	17.84	14.95	17.11
(d) Potassium iodide		(h) Tetra-*n*-propylammonium iodide	
0.5946	24.60	0.6031	24.45
1.334	23.82	1.513	23.36
2.403	23.04	3.216	21.86
4.199	21.97	5.653	20.44
7.292	20.61	9.541	18.79
11.60	19.31	15.13	17.19

Discussion

Figure 1 shows Kohlrausch plots for the potassium and sodium thiocyanates and iodides in 1-propanol. The plots for the potassium salts are approximately parallel and have limiting slopes which are slightly more than 100% greater than the calculated Onsager slopes. In like manner, the plots for the sodium salt exhibit parallelism and have slopes which are about 60% numerically greater than the corresponding Onsager slopes. Owing to their nature, one would expect the plots for the potassium and sodium salts with a common anion to intersect at about 0.0025 N. Since the slopes of the Kohlrausch plots for the quaternary ammonium bromides and iodides were found also to be considerably greater than those calculated by the Onsager equation, values of the limiting equivalent conductance, Λ_0, and the dissociation constant, K, for

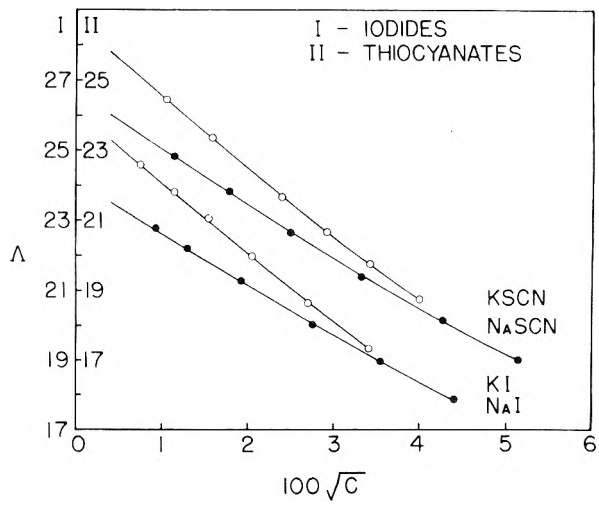

Fig. 1.—Kohlrausch plots for potassium and sodium iodides and thiocyanates in 1-propanol at 25°.

each salt were calculated by the Fuoss–Shedlovsky method.[9] Figure 2 shows linear plots of $S\Lambda$ *versus* $cf^2S^2\Lambda^2$ for the quaternary ammonium salts in 1-propanol. Plots for the potassium sodium salts are very similar. Table II contains the values of Λ_0 and K which were obtained for each salt by this method.

The results indicate that dissociation occurs to a greater extent for sodium than for corresponding potassium salts and for bromides than for corresponding iodides. This may be explained on the basis that the greater charge densities of the sodium and the bromide ions probably enhance solvation effects. If the sodium and the bromide ions are more solvated than the potassium and the iodide ions, respectively, in 1-propanol, the Bjerrum "a" parameter (or distance of closest approach) should be greater for the salts containing the sodium and the bromide ions. Inasmuch as the energy required for dissociation varies inversely with the "a" parameter, the salts characterized by the larger "a" values should be more dissociated. Supporting experimental verification of this appears in the data showing that the tetra-*n*-propylammonium salts are more dissociated than the corresponding tetraethylammonium salts.

TABLE II

LIMITING EQUIVALENT CONDUCTANCES AND DISSOCIATION CONSTANTS FOR SOME SALTS IN 1-PROPANOL AT 25°

Salt	Λ_0	$K \times 10^3$	Salt	Λ_0	$K \times 10^3$
KI	25.75	3.0	Et_4NI	28.55	1.7
NaI	23.92	5.3	Et_3NBr	27.10	2.0
KSCN	26.12	3.1	Pr_4NI	25.88	2.0
NaSCN	24.40	4.1	Pr_4NBr	24.50	2.6

The difference between the conductances of corresponding potassium and sodium salts was found to be 1.83 ± 0.10 and 1.72 ± 0.10 ohm^{-1} cm.^{2} equiv.$^{-1}$, respectively, for the iodides and the thiocyanates. The difference between the conductances of corresponding iodides and bromides was found to be 1.45 ± 0.11 and 1.38 ± 0.10 ohm^{-1} cm.^{2} equiv.$^{-1}$, respectively, for the tetraethylammonium and tetra-*n*-propylammonium salts. The

(9) R. M. Fuoss and T. Shedlovsky, *J. Am. Chem. Soc.*, **71**, 1496(1949).

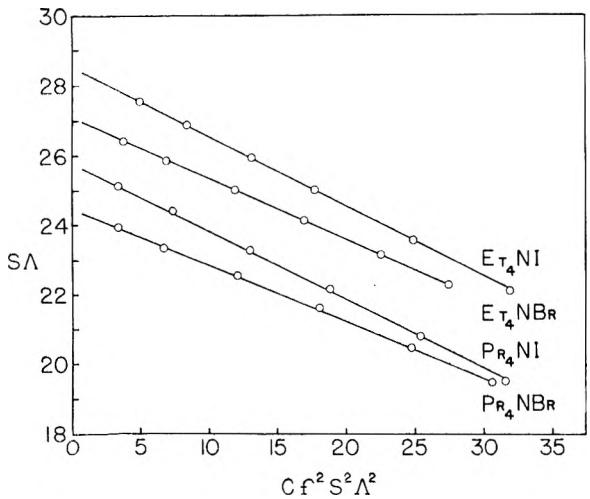

Fig. 2.—Shedlovsky plots for some quaternary ammonium salts in 1-propanol at 25°.

uncertainties designated for the differences are based upon the estimation that the combined experimental and extrapolation errors do not exceed 0.2%. The above corresponding differences show good agreement within the limits of the estimated error and provide convincing evidence that the Kohlrausch law of independent ion migration applies to solutions of salts in 1-propanol.

For a comparison with previous studies, Hovorka and Simms[4] have reported values of 25.42 and 24.12 ohm^{-1} cm.^{2} equiv.$^{-1}$ for limiting equivalent conductances of potassium and sodium iodides respectively in 1-propanol at 25°. These values are 1.2% less for potassium iodide and 0.8% greater for sodium iodide than the corresponding values listed in Table II. The difference between the limiting equivalent conductances of corresponding potassium and sodium salts which can be determined from their data is 1.30 and 5.36 ohm^{-1} cm.^{2} equiv.$^{-1}$, respectively, for the iodides and bromides. Their data also indicate that the difference between the limiting equivalent conductances of the corresponding iodides and bromides is 2.23 and 5.63 ohm^{-1} cm.^{2} equiv.$^{-1}$, respectively, for the potassium and the sodium salts. Their findings and those presented in this paper obviously differ appreciably. Owing to the very limited solubilities of the alkali metal bromides in 1-propanol, an extremely difficult problem exists in obtaining accurate conductance data for a concentration range sufficiently broad to permit a good extrapolation to the the limiting equivalent conductance value.

The $\Lambda_0\eta_0$ product varies from 0.46 to 0.55 ohm^{-1} cm.^{2} equiv.$^{-1}$ poise for the salts in 1-propanol and is of smaller magnitude than that which is found for most other non-aqueous systems. For the potassium and sodium salts it is interesting to note that the $\Lambda_0\eta_0$ product has approximate relative values of 1.00, 0.89 and 0.80 for methanol, ethanol and 1-propanol, respectively. For this homologous series it appears that the product for many salts decreases as the size of the molecules and the molecular weight of the solvent increases. A similar effect has been observed for a homologous series of monomethyl acid amides.[10]

Acknowledgment.—The authors of this paper wish to express their appreciation to the Kentucky Research Foundation and to the Signal Corps for the use of several items of equipment in the performance of this research.

(10) R. H. Graves, Dissertation, University of Kentucky, 1953.

THE SPECTROPHOTOMETRIC DETERMINATION OF THE SOLUBILITY OF CUMENE IN WATER BY A KINETIC METHOD

BY D. N. GLEW[1a] AND R. E. ROBERTSON

Division of Pure Chemistry, National Research Council,[1b] *Ottawa, Canada*

Received August 15, 1955

A continuous circulation cell is described for the spectrophotometric determination of reactions in solution at constant temperature. The saturation solubility of cumene in water between 25 and 80° and the reaction velocity constants for the transfer of cumene to and from the aqueous phase have been determined by a kinetic method. The solubility and thermodynamic functions of aqueous cumene are discussed in terms of a model, generally applicable to all non-ionized aqueous solutions.

Introduction

A continuous circulation cell is described for the spectrophotometric study of reactions in solution. The solubility of cumene in water between 25 and 80° has been determined by a direct method which eliminates the inconvenience of extraction[2] and dilution[3] techniques. Theory for the kinetic approach to equilibrium is given and a method is developed for the determination of equilibrium constants from kinetic measurements. Thermodynamic functions for the equilibria have been calculated and are discussed in terms of a model applicable to all non-ionized aqueous solutions.

Liquid ⇄ saturated aqueous solution ⇄ vapor

Apparatus.—A general description of the apparatus used in the determination has been given elsewhere.[4] The cumene was floated on the surface of the main body of the water and the aqueous solution was pumped steadily by a small induction motor[5] in a closed circuit through the quartz adsorption cell where its optical density was measured and on return swept over the hydrocarbon-water interface.

(1) (a) National Research Council of Canada Postdoctorate Fellow, 1952–1954. (b) N.R.C. Contribution No. 3857.

(2) L. J. Andrews and R. M. Keefer, *J. Am. Chem. Soc.*, **72**, 5034 (1950).

(3) R. L. Bohon and W. P. Claussen, *ibid.*, **73**, 1571 (1951).

(4) D. N. Glew and R. E. Robertson, *J. Sci. Instr.*, in press.

(5) D. Michell, *J. Applied Chem.*, **1**, Supplement No. 1, S8 (1951).

The apparatus is kept at constant temperature by pumping water from a large thermostat through the outer jacket of the circulation cell and through the inner surface of a metal box surrounding the quartz absorption cell. To reduce radiation losses from the upper part of the circulation cell including the magnetic motor, the apparatus is provided with a split Dural block incorporating heater windings and control thermometer. Below the Dural block and above the water jacket, the neck of the circulation cell, containing filling ports, is wound with heating wire and provided with a thermojunction. The lower part of the circulation cell, insulated by a wrapping of glass wool, is enclosed in an asbestos paper shell. The glass apparatus is mounted on the thermostated box which replaces the cell carrier of the standard Beckman DU spectrophotometer. This thermostated box is moved laterally by a screw, enabling either the quartz absorption cell or a blank to be moved into the spectrophotometer beam.

Materials.—Eastman Kodak Co. White Label cumene was distilled through a 15-plate Fenske-packed glass column in an atmosphere of nitrogen and the middle third, boiling over a 0.2° range, was retained in darkened bottles. Before each experiment, sufficient cumene was passed repeatedly through a fresh column of Fisher activated alumina to remove traces of oxidation products. The purity of this cumene was evident from the constancy of the saturation optical density of aqueous solutions in replicate experiments.

The water used in the experiments was obtained by passing distilled water through a three-foot mixed-bed demineralizing column.

Experimental

Concentration Dependence of D.—Aqueous solutions of cumene show ultraviolet absorption between 2560 and 2630 Å. with a flat maximum at 2595 Å. The position of this maximum was found to be independent of temperature in the range 25 to 80° and the spectral measurements reported were all made at this wave length with a slit width of 1.00 mm. and cell length of approximately 1 cm.

Oxidation of the cumene was avoided by weighing the 0.2–0.6 g. sample of outgassed cumene in a thin walled capsule. This capsule, together with a 2 cm. glass ball, was placed in a tube containing 50 ml. of ethyl alcohol. After the latter was outgassed, the tube was sealed and weighed. The cumene was then released to form an alcoholic solution by shattering the capsule with the glass ball. The sealed tube containing the cumene solution and a 500-g. stainless steel cylinder were placed in a 10-liter serum bottle filled with water. After the water was out-gassed, the tube was broken, releasing a fine cloud of cumene which rapidly dissolved. Since the vapor phase volume was less than 20 ml. the possible loss of cumene from the solution was reduced to less than 0.15%. The solution was made homogeneous on a motor driven roller, after which the aqueous solution was siphoned into the circulation cell, sufficient solution being allowed to flow to sweep out air-contaminated solution. The presence of 0.002 mole fraction of ethanol should not change the optical density of cumene in aqueous solution.

Table I shows the dependence of the optical density of aqueous cumene on concentration at 25°, where c is the concentration of cumene in water in g./l., d_{25} is the absorption of the water–alcohol solvent and the quartz cell faces measured against an air blank and D_{25} is the optical density of the cumene dissolved in water, the number of determinations of $(D_{25} + d_{25})$ being given in parentheses.

TABLE I

DEPENDENCE OF OPTICAL DENSITY ON CONCENTRATION AT 25°

c (g./l.)	$D_{25} + d_{25}$
0.0	0.0643 (15)
.02172	.1053 (12)
.04940	.1517 (13)
.05058	.1550 (13)
.06450	.1769 (6)

The results in Table I are expressed by the equation

$$c = (0.5643 \pm 0.0056)D_{25} \qquad (1)$$

or transforming to mole fractions

$$x_2 = 8.485 \times 10^{-5} D_{25} \qquad (2)$$

where x_2 is the mole fraction of cumene in water.

Temperature Dependence of D.—A standard solution of cumene in out-gassed water was passed into the continuous circulation cell *via* a filling port until all the air was displaced; further solution was then passed to remove traces of air-contaminated solution. The circulation cell was isolated by a mercury trap to allow for thermal expansion. A series of optical density measurements was made at temperatures between 25 and 75°.

Table II gives corresponding pairs of average values of D at approximately 25 and 75°, which are obtained by successive dilution: these values are corrected for d, the optical absorption of the water and the quartz cell faces at the respective experimental temperatures. Experiments over the range 25 to 75° have shown that within experimental error the molar extinction coefficient is linearly dependent on temperature. The final column of Table II shows the values of the temperature coefficient K, defined by the equation

$$K = \frac{1}{D_{25}/\rho_{25}} \frac{(D/\rho - D_{25}/\rho_{25})}{(T - 25)} \qquad (3)$$

and calculated from the corresponding optical density and temperature values. ρ and ρ_{25} are the bulk densities of water at the temperatures $T°$ and 25°, respectively, which allow for the expansion of the water and the corresponding reduction of cumene molecule concentration in the spectrophotometer beam. The average value of K is $(1.628 \pm 0.148) \times 10^{-3}$ deg.$^{-1}$, the error corresponding to a deviation of ± 0.00042 on D. Equations 2 and 3 are combined to give the equation

$$x_2 = \frac{D\rho_{25}}{\rho} \frac{8.485 \times 10^{-5}}{(1 + (T - 25)\,0.001628)} \qquad (4)$$

by which x_2, the mole fraction of cumene in the solution, is calculated from D, the optical density of cumene at $T°$.

TABLE II

TEMPERATURE DEPENDENCE OF OPTICAL DENSITY

T, °C.	D	T, °C.	D	K (deg.$^{-1}$) $\times 10^3$
26.5	0.12333 (6)	75.0	0.12943 (3)	1.506
28.0	.12272 (3)	74.0	.12838 (11)	1.494
28.0	.11936 (9)	76.0	.12714 (6)	1.869
27.0	.11737 (9)	75.0	.12312 (10)	1.510
26.0	.11596 (6)	75.0	.12231 (10)	1.604
26.0	.11280 (8)	71.0	.11953 (11)	1.789
26.0	.11224 (5)	74.0	.11838 (8)	1.624

The combined errors of the constants in equation 4 lead to the standard deviations of 1.00% in x_2 for D determined near 25° and of 1.25% in x_2 for D determined near 80°.

Determination of D_0.—Prior to each determination of D_0, the optical density of cumene in a saturated solution at any temperature, the cell was cleaned with hot chromic acid and repeatedly washed with water to give a constant value of d_{25}. The cell filled with water and swept with nitrogen was heated to the experimental temperature and maintained to within ±0.002° throughout the run. When thermal equilibrium had been established the circulating motor was stopped and 2 ml. of freshly prepared cumene injected onto the surface of the water inside the circulation cell. As soon as thermal equilibrium was re-established, circulation was commenced and readings of $(D + d)$ taken at 5-minute intervals for three hours. The circulation of water and flow of nitrogen continued overnight and equilibrium values of $(D_0 + d)$ were determined directly. A detailed discussion of a kinetic method for determining D_0 is given, since it constitutes a new approach to the measurement of such equilibria.

Kinetic Analysis of Cumene Transfer and Equilibrium.—The kinetics of the transfer of cumene from the pure liquid cumene phase through a con-

stant area interface to an aqueous solution is represented by the equation

$$\underset{\text{(liq.)}}{\text{cumene}} \underset{k_1 D}{\overset{k_0}{\rightleftharpoons}} \underset{\substack{\text{(soln.)} \\ D}}{\text{cumene aq.}} \qquad (5)$$

The rate of increase of D, the optical density of the cumene in the aqueous solution is expressed by the equation

$$dD/dt = k_0 - k_1 D \qquad (6)$$

where k_0 is a zero-order velocity constant and k_1 the opposing first-order velocity constant, the units of these constants involving the geometrical factors of the circulation cell and the effective stirring. At equilibrium, equation 6 reduces to

$$k_0 = k_1 D_0 \qquad (7)$$

where D_0 is the saturation value of the optical density of cumene in the solution.

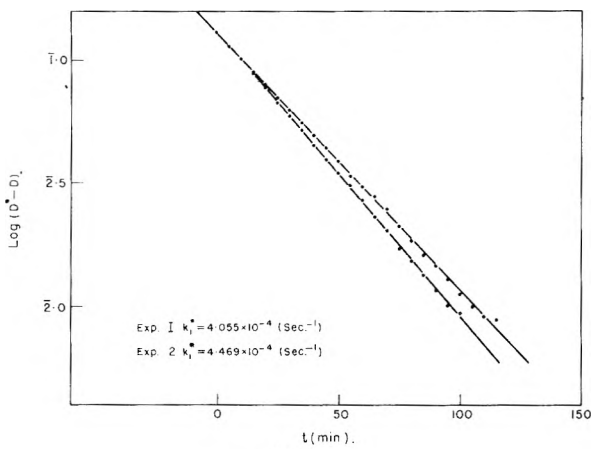

Fig. 1.

Calculation of k_1.—The method of determination of k_1 is an adaptation of the treatment given by Guggenheim[6] for first-order kinetics. The instantaneous rate of transfer of cumene into the aqueous solution is given by (6). Integration of (6) between the limits $D = 0$ at $t = 0$ and the optical density D at time t gives the equation

$$k_0 - k_1 D = k_0 e^{-k_1 t} \qquad (8)$$

Similarly, if the optical density is D^* at time $t + t^*$, the integration of (6) leads to the equation

$$k_0 - k_1 D^* = k_0 e^{-k_1 (t + t^*)} \qquad (9)$$

Subtracting (9) from (8) and dividing the difference by k_1 gives the equation

$$D^* - D = C e^{-k_1 t} \qquad (10)$$

where

$$C = (1 - e^{-k_1 t^*}) k_0 / k_1 \qquad (11)$$

Rearrangement of (10) yields the equation

$$\log (D^* - D) = \log C - k_1 t / 2.3026 \qquad (12)$$

which is used in the experimental determination of k_1.

A series of differences $(D^* + d) - (D + d)$ are determined for $t^* = 3600$ sec. and a set of 24 differences are obtained for $t = 0$ to $t = 7200$ sec. The slope of the plot of $\log (D^* - D)$ against the time, t, yields k_1 according to (12). Figure 1 shows the results of two different experiments at 49.892 ± 0.002°, the values of k_1 being 4.055 and 4.469 × 10^{-4} sec.$^{-1}$. The experimental points extend from $D = 7.06\%$ of the total change when $t = 0$, to $D^* = 99 = 1\%$ change from $t + t^* = 10{,}800$ sec. The linearity of these and all similar plots at other temperatures confirms the proposed kinetic analysis and the validity of Beer's law at all temperatures.

Calculation of D_0.—Substitution for k_0 in (8), using equation 7, gives the equation

$$D_0 - D = D_0 e^{-k_1 t} \qquad (13)$$

which expresses the time dependence of D in terms of D_0 and k_1 the dependence of D^* at time $t + t^*$ is given similarly by

$$D_0 - D^* = D_0 e^{-k_1 (t + t^*)} \qquad (14)$$

Division of (14) by (13) and rearrangement yields the equation

$$D_0 = (D^* - fD)/(1 - f) \qquad (15)$$

where

$$f = e^{-k_1 t^*} \qquad (16)$$

The 24 pairs of D^* and D values corresponding to the time interval $t^* = 3600$ sec. are used with the proper value of f to calculate 24 values of D_0 from equation 15. In practice, it is more convenient to use the experimental values for $(D^* + d)$ and $(D + d)$ in place of D^* and D in (15), giving $(D_0 + d)$ in place of D_0. In Table III are shown the values of $(D_0 + d)$ calculated for the two experiments already described. The columns $(D_0 + d)$ observed show the values of the saturation optical density measured directly after 24 hours.

The agreement between the kinetic calculated and directly observed values of $(D_0 + d)$ confirms the validity of the kinetic analysis, agreement between the two experiments giving a measure of the reproducibility, notwithstanding the differing values for k_1. Calculation of D_0 gives a final weighted mean value of 0.1827 ± 0.0003 for the saturation optical density of the cumene at 49.892°.

Temperature Variation of Solubility.—The change of x_2°, the saturation mole fraction of cumene in water, between 25 and 80°, is given by the equation

$$\log x_2^\circ = 4298.88/T + 34.6369 \log T - 105.04408 \qquad (17)$$

where T is the absolute temperature (0°C. = 273.16°K.).

In Table IV are shown the absolute temperatures, the average values of the D_0 determinations, and in parentheses, the number of determinations made at each temperature. The fourth column gives the values of $x_{2\,\text{obsd}}^\circ$, which are calculated from D_0 and t^0 in equation 4; these values have been used to calculate equation 17. The values of $x_{2\,\text{calcd}}^\circ$ in the final column are computed by substituting the experimental temperatures into equation 17.

Analysis of the differences of $x_{2\,\text{obsd}}^\circ$ and $x_{2\,\text{calcd}}^\circ$ gives a standard error of ±0.13% on the experimental values of D_0. The standard errors on the values for x_2° at 25 and 80° are ±1.00 and ±1.25%, respectively, the first of which arises from the error in the constant of equation 1 and the second from the errors in the constants of equations 1 and 3.

(6) E. A. Guggenheim, *Phil. Mag.*, **2**, 17] 538 (1926).

TABLE III

COMPARISON OF KINETIC AND DIRECT DETERMINATION OF D_0 AT 49.892° ± 0.002°

Experiment 1					Experiment 2				
$k_1 = 4.055 \times 10^{-4}$ (sec.$^{-1}$)					$k_1 = 4.469 \times 10^{-4}$ (sec.$^{-1}$)				
$d = 0.0635 \pm 0.0002$					$d = 0.0638 \pm 0.0002$				
t, min.	$D_0 + d$, calcd.	t, min.	$D_0 + d$ Calcd.	$D_0 + d$ Obsd.	t, min.	$D_0 + d$, calcd.	t, min.	$D_0 + d$ Calcd.	$D_0 + d$ Obsd.
0	0.2461	60	0.2464	0.2465	0	0.2464	60	0.2468	0.2463
5	.2449	65	.2467	.2465	5	.2465	65	.2463	.2460
10	.2456	70	.2467	.2466	10	.2462	70	.2464	.2464
15	.2462	75	.2464	.2468	15	.2469	75	.2461	.2463
20	.2463	80	.2460	.2465	20	.2466	80	.2463	.2464
25	.2464	85	.2458	.2465	25	.2464	85	.2464	.2462
30	.2461	90	.2461	.2466	30	.2468	90	.2464	
35	.2466	95	.2465		35	.2469	95	.2464	
40	.2467	100	.2463		40	.2463	100	.2469	
45	.2468	105	.2464		45	.2460	105	.2469	
50	.2466	110	.2468		50	.2463	110	.2467	
55	.2459	115	.2473		55	.2469	115	.2465	
		mean	0.2463 ± .0002	0.2466 ± .0002			mean	0.2465 ± .0001	0.2463 ± .0002

TABLE IV

VARIATION OF SOLUBILITY OF CUMENE WITH TEMPERATURE

T, °K.	D_0	$x_2^\circ \times 10^5$ Obsd.	Calcd.
298.086	0.14201 (46)	1.2050	1.2052
303.134	.14731 (77)	1.2416	1.2402
308.068	.15314 (72)	1.2825	1.2860
313.108	.16154 (60)	1.3446	1.3450
318.055	.17114 (65)	1.4162	1.4158
323.052	.18274 (60)	1.5037	1.5011
328.066	.19565 (49)	1.6011	1.6022
333.133	.21155 (52)	1.7221	1.7217
338.315	.22996 (26)	1.8624	1.8642
343.470	.25192 (32)	2.0302	2.0289
348.247	.27499 (49)	2.2064	2.2047
353.359	.30310 (35)	2.4212	2.4209

The only other value for the solubility of cumene in water at any temperature is that of Andrews and Keefer,[2] who have obtained 0.073 g. cumene/1000 g. solution at 25° which compares with the value of 0.0804 g. cumene/1000 g. solution calculated from Table IV through equation 1.

Thermodynamic Functions for Cumene–Water Equilibrium.—The thermodynamic functions at 298.16°K. for the change represented by the equation

$$\underset{\text{(liq.)}}{\text{cumene}} \underset{x_2^\circ}{\rightleftharpoons} \underset{\text{(soln.)}}{\text{cumene aq}} \qquad (18)$$

are calculated from (17) and are shown with their standard errors in Table V.

TABLE V

THERMODYNAMIC FUNCTIONS FOR CUMENE–WATER EQUILIBRIUM

T	= 298.16°K.
x_2°	= 1.206 ± 0.012 × 10^{-5}
ΔG_1°	= +6708 ± 6 cal./mole
ΔH_1	= +852 ± 84 cal./mole
ΔS_1°	= −19.64 + 0.25 cal./deg. mole
ΔC_{p_1}	= +68.80 ± cal./deg. mole

ΔG_1° and ΔS_1° are the standard changes of free energy and entropy for the transfer of one mole of liquid cumene to an aqueous solution at unit cumene mole fraction, ΔH_1 and ΔC_{p_1} being the corresponding changes of heat content and heat capacity.

The changes of ΔS_1° and ΔH_1 with temperature are given by the equations

$$\Delta S_1^\circ = -411.66 + 68.8027 \ln T \qquad (19)$$

and

$$\Delta H_1 = -19{,}663 + 68.8027T \qquad (20)$$

respectively, which relations are derived from (17) with the gas constant R = 1.9864 cal./deg. mole. Table VI gives the values of $\Delta S_{1\,\text{obsd}}^\circ$ and $\Delta H_{1\,\text{obsd}}^\circ$ calculated from adjacent values of $x_{2\,\text{obsd}}^\circ$ through the relations $\Delta G_1^\circ = -RT \ln x_2^\circ$, $\Delta S_1^\circ = -\partial \Delta G_1^\circ / \partial T$ and $\Delta H_1 = -\partial(\Delta G_1^\circ/T)/\partial(1/T)$; the values of $\Delta S_{1\,\text{calcd}}^\circ$ and $\Delta H_{1\,\text{calcd}}$ are computed from equations 19 and 20.

The standard errors in ΔS_1° and ΔH_1 are ±0.254 cal./deg. mole and ±83.6 cal./mole, respectively, of which ±0.236 cal./deg. mole and 78.6 cal./mole arise from random errors in D_0 and the remainder from the error in the constant of equation 3. The value of ΔC_{p_1} = +68.8027 cal./deg. mole is calculated by the method of least squares from the values of $\Delta H_{1\,\text{obsd}}$ and the temperatures given in Table VI. The standard error on ΔC_{p_1} is ±3.037 cal./deg. mole, which arises only

TABLE VI

TEMPERATURE VARIATION OF ENTROPY AND HEAT CONTENT

T, °K.	$-\Delta S_1^\circ$, cal./deg. mole Obsd.	Calcd.	ΔH_1, cal./mole Obsd.	Calcd.
300.610	18.93	19.08	1064	1020
305.601	18.42	17.95	1219	1364
310.588	16.54	16.83	1798	1707
315.582	15.66	15.73	2075	2050
320.554	14.48	14.66	2449	2392
325.559	13.90	13.59	2635	2737
330.600	12.42	12.54	3121	3084
335.724	11.63	11.48	3384	3436
340.893	10.22	10.43	3863	3792
345.859	9.41	9.43	4140	4133
350.803	8.54	8.45	4442	4474

from errors in D_0, since errors in equation 3 add constant values to $\Delta H_{1\,\mathrm{obsd}}$ at 25 and 80°.

Deviations from Raoult's Law.—Aqueous solutions of cumene between 25 and 80° show large positive deviations from Raoult's law. At 298.16° K. the positive deviation, or positive value of ΔG_1° in Table V is seen to derive mainly from the large negative value of −19.64 cal./deg. mole for ΔS_1°, rather than from the positive value of +852 cal./mole for ΔH_1. A minimum value for x_2° occurs at 285.78°K. when $\Delta H_1 = 0$ and $\Delta S_1^\circ = -22.56$ cal./deg. mole; at this temperature the Raoult law activity coefficient, f_2, passes through its maximum value of $8.554 + 10^4$. At 396.67°K. $\Delta S_1^\circ = 0$ and the positive value of ΔG_1 is due only to the +7629 cal./mole of ΔH_1.

The large negative values for ΔS_1° at the lower temperatures are ascribed to the restricting influence that the cumene molecule exerts on the rotational degrees of freedom of the water molecules within its coördination shell; the large positive value of ΔC_{p_1} is evidence of the thermal breakdown of these restrictions by molecular agitation. At higher temperatures the positive values of ΔH_1 are due to the energy required to form a cavity in the hydrogen bonded liquid against internal pressure of the usual type.

Temperature Variation of Saturation Vapor Pressure.—Calculation of the Henry law constants from the saturation solubility data already requires the values of the thermodynamic functions for the evaporation of liquid cumene. The temperature variation of p_2°, the saturation vapor pressure of liquid cumene in mm., between 25 and 80°, is given by the equation

$$\log p_2^\circ = -3464.84/T - 8.2846 \log T + 32.78027 \quad (21)$$

which has been calculated from recent data.[7] Table VII shows the values of the thermodynamic functions at 298.16°K. for the change

$$\underset{\text{(liq.)}}{\text{Cumene}} \rightleftharpoons \underset{\substack{\text{(vapor)}\\ p_2^\circ \text{ mm.}}}{\text{Cumene}} \quad (22)$$

which have been calculated from equation 21. ΔG_2° and ΔS_2° are the standard changes of free energy and entropy accompanying the transfer of one mole of cumene from the liquid to the vapor phase at one mm. pressure and ΔH_2 and ΔC_{p_2} are the corresponding changes of heat content and heat capacity, respectively.

TABLE VII

VAPORIZATION AND HENRY LAW THERMODYNAMIC FUNCTIONS

$T = 298.16$°K.

p_2°	= 4.568 mm.	p_2°/x_2°	= 3.789×10^5 mm.
ΔG_2°	= −900	ΔG_3°	= −7608 cal./mole
ΔH_2	= +10,941	ΔH_3	= +10,089 cal./mole
ΔS_2°	= +39.71	ΔS_3°	= +59.35 cal./deg. mole
ΔC_{p_2}	= −16.46	ΔC_{p_3}	= −85.26 cal./deg. mole

Temperature Variation of Henry Law Constant.—The temperature variation of p_2°/x_2°, the Henry law constant for cumene in water, is given by the equation

$$\log p_2^\circ/x_2^\circ = -7763.72/T - 42.9215 \log T + 137.82435 \quad (23)$$

which is the difference of equations 21 and 17 and which neglects the effect of the water dissolved in the liquid cumene phase.

Table VII shows the thermodynamic functions at 298.16°K. for the change represented by the equation

$$\underset{\substack{\text{(soln.)}\\ x_2^\circ}}{\text{cumene aq}} \rightleftharpoons \underset{\substack{\text{(vapor)}\\ p_2^\circ \text{ mm.}}}{\text{cumene}} \quad (24)$$

which equation is the difference of equations 22 and 18.

ΔG_3° and ΔS_3° are the standard changes of free energy and entropy for the transfer of one mole of cumene from the aqueous solution phase at unit cumene mole fraction to the vapor phase at one mm. pressure at 298.16°K.; ΔH_3 and ΔC_{p_3} are the respective changes of heat content and heat capacity.

Discussion of Henry Law Constants.—The value of ΔH_3 for the evolution of cumene from aqueous solution at lower temperatures is nearly equal to that for the evaporation of the pure liquid. Calculations based on the normal dimensions of the water and cumene molecules show that a coördination number of approximately thirty water molecules is required and this value accounts for the observed change of heat content. Smaller coördination numbers lead to unrealistically small values for both the intermolecular distances and the heat change.

ΔC_{p_3} for cumene has the value of −85.26 cal./deg. mole, which is near to the values −87.39, −78.06 and −83.10 cal./deg. mole found for the corresponding Henry law constants of aqueous methyl iodide,[8] benzene and toluene,[3] respectively, in spite of the considerable differences of the molar volumes of the four compounds.

A comparison of the solubility of cumene at 298.16°K. with that of the other alkyl benzenes[3] shows that as the number and size of the alkyl groups increase, the Henry law constants increase, that is, the solute mole fractions at unit partial pressure decrease, an effect noted by Butler[9] for aqueous solutions of aliphatic alcohols. Similarly, the linear relationship that Butler observed between ΔS_3° and ΔH_3 for the alcohols is again shown by cumene and the other aqueous alkyl benzenes. Figure 2 shows plots of ΔS_3° and ΔH for benzene, toluene, ethylbenzene, *m*- and *p*-xylenes[3] and cumene in comparison with the values for the alcohols taken from Butler's paper.[3]

An interesting fact arises in that the two lines are parallel within the experimental error, and that the slopes, $d\Delta S_3^\circ/d\Delta H_3$ are almost equal to 1/273.16; alkyl benzenes, $d\Delta S_3^\circ/d\Delta H_3 = 1/275.9 \pm 15.8$; aliphatic alcohols, $d\Delta S_3^\circ/d\Delta H_3 = 1/269.6 \pm 9.7$. The linear relationship for the alkyl benzenes not only holds at 298.16°K. but also at 273.16° and at 323.16°K. where the slopes, $d\Delta S_3^\circ/d\Delta H_3$ are 1/280.0

(7) Selected Values of Properties of Hydrocarbons, A.P.I. project 44, Natl. Bur. Standards (1947).

(8) D. N. Glew and E. A. Moelwyn-Hughes, *Faraday Soc. Disc.*, **15**, 150 (1953).

(9) J. A. V. Butler, *Faraday Soc. Disc.*, **33**, 229 (1937).

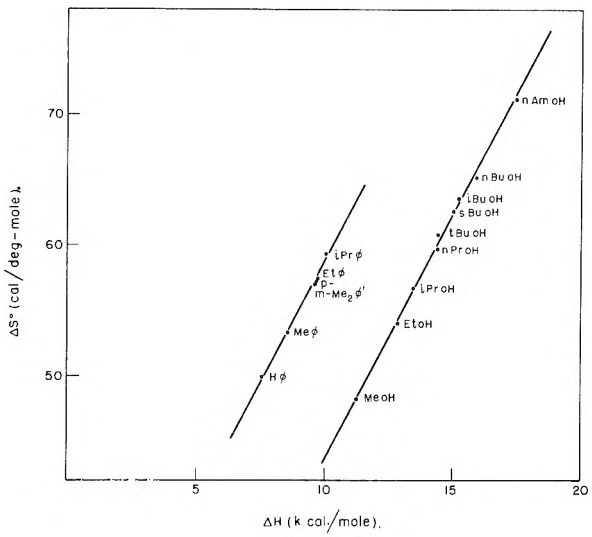

Fig. 2.

± 15.7 and 1/270.1 ± 13.9 deg.$^{-1}$, respectively. It is likely that when sufficient data become available, other aqueous solutions of aliphatic homologs will show similar linear $\Delta S_3^\circ - \Delta H_3$ relations, with the same slope.

The reason for the relationship would appear to depend on some type of "freezing" process of the water solvent itself, where the presence of the solute molecule causes the coördination water to lose certain degrees of freedom in such a manner that $d\Delta S_3^\circ / d\Delta H_3 = 1/273.16°$ deg.$^{-1}$. This "freezing" can be visualized such that the water coördination shell around the solute molecule is similar to the shells found in the solid gas hydrates,[8,10,11] except that no long range order exists in the solutions. The presence of the solute molecule in the water restricts the rotation of the coördination water molecules so that these, due to hydrogen bonding, are able to orient in fewer directions than formerly without large increases in energy. This reduction of the possible number of configurations of the coördinated water molecules, consistent with a given energy level, qualitatively explains the large entropy losses accompanying the formation of aqueous solutions. The rotational restriction on the coördination water molecules is primarily a function of the strength and directional nature of the hydrogen bonds of the water molecule,[12] the number of water molecules affected being a function of the size of the solute molecule.

The model proposed provides an explanation of the formation of low energy cavities within the water structure at lower temperatures which have been proposed by Eley.[13]

The surface tensional model proposed by Butler[9] can be rationalized in terms of the present model except that no water–water hydrogen bonds are broken on the formation of cavities for the solute molecule; alcohol, amine and acid groups are exceptions since these break down and are incorporated in the water structure itself.

In terms of a free volume theory,[14,15] a model of the type proposed leads to the "crystallization" of the coördination water molecules and the corresponding loss of free volume associated with these. From the work of Powell and Latimer[15] it would appear that the loss of free volume of the coördination water molecules more than compensates for the gain in free volume due to the extra solute molecule, so that the larger the solute molecule the larger the standard entropy change associated with dissolution.

The large values of the partial molar heat capacities for non-ionized aqueous solutes, are due to thermal agitation causing rotation and to a smaller extent, vibration and translation of the coördination water molecules of the solutes. At lower temperatures the nature of the external bulk water phase helps to maintain the "crystallinity" of the coördination molecules of the solute; compare the formation of the gas hydrates. As the temperature rises, thermal agitation breaks down the order within the coördination shell and increases both the entropy and heat content of the system, the heat capacity characteristics of the water coördination shell being reflected in the values of the thermodynamic functions of the enclosed solute molecule.

(10) D. N. Glew, Ph.D. Thesis, Cambridge University, 1952.
(11) W. F. Claussen and M. F. Polglase, *J. Am. Chem. Soc.*, **74**, 4817 (1952).
(12) J. A. Pople, *Proc. Roy. Soc. (London)*, **A205**, 163 (1951).
(13) D. D. Eley, *Trans. Faraday Soc.*, **35**, 1281 (1939).
(14) H. S. Frank and M. W. Evans, *J. Chem. Phys.*, **13**, 507 (1945).
(15) R. E. Powell and W. M. Latimer, *ibid.*, **19**, 1139 (1951).

THE CRYSTAL STRUCTURE OF CESIUM MONOXIDE[1]

BY KHI-RUEY TSAI, P. M. HARRIS AND E. N. LASSETTRE

Contribution from the Department of Chemistry, The Ohio State University, Columbus, Ohio

Received August 18, 1955

The *anti*-$CdCl_2$ type layer structure[2] (D_{3d}^5-$R\bar{3}m$) of dicesium monoxide (Cs_2O) has been confirmed by X-ray single-crystal work. The variable parameter for the positions of the cesium atoms is found to be $u = 0.256$, instead of $u = 1/4$ (powder work[2]), which fails to account for some of the weak powder lines.[3] The abnormally large cesium–cesium distance ($Cs^+ - Cs^+ = 4.19$ Å.) between layers and the slightly shortened cesium–oxygen distance ($Cs^+ - O^= = 2.86$ Å.) indicate that the cesium ions are highly polarized in this layer crystal.

Introduction

The monoxide of cesium, Cs_2O, is believed to play an important role in Cs–O–Ag photocathodes.[4] This oxide, orange yellow at room temperature, is also known to exhibit color changes upon heating and cooling.[3,5] It is the only compound which has been assigned an *anti*-$CdCl_2$ type layer structure.[2] However, there has been some doubt[3] about this assigned structure which is based upon X-ray powder data. A further study of the structure of this oxide by means of single crystal work thus appeared to be desirable.

Preparation of Dicesium Monoxide and Analysis of the Samples.—This monoxide was prepared by distilling a lower suboxide of cesium (Cs_7O_2) in a Pyrex vessel at 180–190° until no more cesium appeared to condense on the air-cooled trap. The suboxide (Cs_7O_2), in turn, was prepared by direct combination of pure cesium with the calculated amount of pure oxygen admixed with a small amount of argon, the procedure being the same as described for the preparation of tricesium monoxide, Cs_3O.[6]

The monoxide thus obtained was in the form of polycrystalline, laminated plates, orange yellow at room temperature, cherry red above 180°, and lemon yellow at Dry Ice temperature. It was readily pulverized by shaking with glass beads in a thoroughly degassed Pyrex tube.

On account of the small weight percentage (5.7%) of oxygen in dicesium monoxide, the composition of the sample cannot be accurately determined by alkalimetric determination of the cesium content alone. In the present investigation, the alkalimetric determination was supplemented by determination of excess cesium, or excess oxygen. The amount of gas evolved upon decomposition of the sample in thoroughly degassed Pyrex vessels was measured by means of a Töpler pump and a McLeod gage, and the resulting alkaline solution titrated. Any excess cesium in the sample would produce an equivalent amount of hydrogen, whereas the presence of peroxides would be indicated by the liberation of oxygen. A sample of dicesium monoxide (orange yellow, crystalline powder) thus analyzed gave 0.001 mole of gas for each mole of the monoxide, showing an almost stoichiometric compound. A separate preparation yielded a sample (also orange yellow, crystalline powder) which gave 0.014 mole of gas for each mole of the monoxide; the gas was not identified, but was assumed to be oxygen due to a small leakage of atmospheric oxygen into the sample tube. This latter sample showed five extra powder-lines (weak), which were also present in X-ray powder photographs of other Cs_2O samples known to be partially oxidized due to inadequate protection against atmospheric oxygen. However, both the pure and the partially oxidized sample were found to be diamagnetic, $\chi_g = -0.20 \times 10^{-6}$ c.g.s. unit per gram.

(1) This work was supported by the U. S. Army Engineer Corps under contract DA-44-009-eng-405 and by the University Committee for Allocation of Research Foundation Grants.

(2) A. Helms and W. Klemm, *Z. anorg. Chem.*, **242**, 33 (1939).

(3) V. G. Brauer, *ibid.*, **255**, 101 (1947).

(4) V. K. Zworykin and E. G. Ramberg, "Photo-electricity and Its Applications," John Wiley and Sons, Inc., New York, N. Y., 1949, p. 46.

(5) E. Rengade, *Ann. Chem. Phys.*, **11**, 348 (1907); *Bull. soc. chim. phys.*, **69**, 667 (1907).

(6) Recent investigation in this Laboratory, to be reported in a separate article.

Re-examination of the Powder Pattern.—The X-ray powder pattern of dicesium monoxide was first re-examined, using Cu Kα radiation and an 11.4-cm. camera, the finely pulverized sample being sealed in a thin-walled Pyrex capillary tube of about 0.2 mm. diameter. The higher resolution of the camera made it possible to observe many weak powder lines besides those observed by Brauer.[3] However, the powder pattern could still be indexed by the rhombohedral system with a hexagonal c/a ratio of 4.46 instead of 2.30 as employed by Helms and Klemm.[2] (Helms and Klemm's reported c/a ratio is for a hexagonal pseudo cell containing 3Cs; those weak powder lines which cannot be indexed by employing this c/a ratio have odd l-indices (hexagonal).) This shows that the 2Cs cannot be in a body-centered rhombohedral setting; in other words, the parameter, $u = 1/4$, given by Helms and Klemm is not quite correct.

When a freshly pulverized sample was used, the powder lines derived from lattice planes parallel, or nearly parallel to the c-axis (*i.e.*, those lattice planes with small l-indices) became considerably weakened, indicating a shearing disorder in the directions parallel to the basal plane. If the sample was annealed by heating for about an hour at 150°, or simply was allowed to stand at room temperature for a few days, and then photographed, the intensity distribution of the powder lines became normal, indicating that the shearing disorder resulting from mechanical disturbance could be removed by annealing. This together with the fact that the monoxide tends to crystallize in laminated plates with more or less perfect basal cleavage leaves little doubt that a layer structure is correct.

The present powder data give $a = 4.256 \pm 0.004$ Å., $c = 18.99 \pm 0.02$ Å., for a hexagonal unit cell containing three Cs_2O "molecules." The calculated density is 4.71 g./cc. as compared with 4.60 g./cc. observed by Helms and Klemm.[2] Based upon an *anti*-$CdCl_2$ type structure (D_{3d}^5; $2Cs^+$ at uuu and $\bar{u}\bar{u}\bar{u}$, $O^=$ at 000.), the relative intensities of the powder lines were calculated from the expression

$$I_{\text{calc}} \propto \frac{1 + \cos^2 2\theta}{\sin^2 \theta \cos \theta} p(f_0 + 2f_{Cs} \cos 2\pi lu)^2$$

no corrections for the absorption and temperature factors being made. As shown in Table I, with $u = 0.256$, the agreement between the observed and the calculated intensities is quite satisfactory. However, the ($hk.0$)-reflections (or ($hk.l$)-reflections with small l) appear to have a slightly higher temperature factor (B_T) than the (00.l)-reflection (or ($h0.l$)-reflections with small h and large l), indicating that there might still be an appreciable shearing disorder in the powder sample. Helms and Klemm[2] and Brauer[3] reported the (10.2)-, (00.6)-, and (10.4)-powder line intensities as about equal; this indicates that they must have used freshly pulverized powder samples. In interpreting the intensity data from the powder sample of a layer crystal, special attention should be paid to the mechanical treatment of the sample.

Single Crystal Work.—Single crystals of dicesium monoxide were obtained by distillation-decomposition of a suboxide (Cs_7O_2) in Pyrex capillaries at 170–180°. The orange-yellow crystal used in the present investigation was a thin, almost rectangular plate with the dimensions and crystallographic geometry shown in Fig. 1.

The following rotation photographs were taken: (a) Cu Kα radiation with the hexagonal base diagonal [11.0] as the rotation axis; (b) Cu Kα ra-

TABLE I

X-RAY POWDER DATA FOR CESIUM MONOXIDE

Hexagonal indices				Rhombohedal indices			Planar spacings, d		Obsd.	Relative intensities	
h	k	i		H	K	L	Obsd.	Calcd.[a]		Calcd. $u = 0.255$	Calcd. $u = 0.256$
0	0	0	3	1	1	1	6.33	6.330	5	5.0	6.2
1	0	$\bar{1}$	1	1	0	0		3.620	..	0.3	0.2
1	0	$\bar{1}$	$\bar{2}$	1	1	0	3.433	3.435	100	100	100
0	0	0	6	2	2	2	3.159	3.165	25	27	26
1	0	$\bar{1}$	4	2	1	1	2.911	2.911	100	88	88
1	0	$\bar{1}$	$\bar{5}$	2	2	1	2.638	2.643	1	0.5	0.9
1	0	$\bar{1}$	7	3	2	2	2.177	2.185	3	2.6	3.5
1	1	$\bar{2}$	0	1	0	$\bar{1}$	2.124	2.128	25	35	35
0	0	0	9	3	3	3		2.110	..	0.5	0.8
1	1	$\bar{2}$	3	2	1	0		2.017	..	1.1	1.4
1	0	$\bar{1}$	$\bar{8}$	3	3	2	1.995	1.995	20	25	24
2	0	$\bar{2}$	$\bar{1}$	1	1	$\bar{1}$		1.835	..	0.1	0
2	0	$\bar{2}$	2	2	0	0	1.806	1.810	10	16	16
1	1	$\bar{2}$	6	3	2	1	1.766	1.766	20	29	29
2	0	$\bar{2}$	$\bar{4}$	2	2	0	1.717	1.718	10	17	17
1	0	$\bar{1}$	10	4	3	3	1.688	1.688	10	11	11
2	0	$\bar{2}$	5	3	1	1		1.684		0.2	0.3
0	0	0	12	4	4	4	1.580	1.583	5	3.8	3.5
1	0	$\bar{1}$	$\bar{1}1$	4	4	3	1.559	1.563	2	1.8	2.4
2	0	$\bar{2}$	$\bar{7}$	3	3	1		1.525	..	0.7	1.0
1	1	$\bar{2}$	9	4	3	2	1.497	1.498	1	1.1	1.7
2	0	$\bar{2}$	8	4	2	2	1.457	1.456	5	9.2	8.8
2	1	$\bar{3}$	1	2	0	$\bar{1}$		1.390	..	0	0
2	1	$\bar{3}$	$\bar{2}$	2	1	$\bar{1}$	1.378	1.379	10	14	14
1	0	$\bar{1}$	13	5	4	4	1.359	1.359	1	0.9	1.3
2	1	$\bar{3}$	4	3	1	0	1.336	1.337	10	14	14
2	0	$\bar{2}$	$\bar{1}0$	4	4	2	1.324	1.323	3	5.1	4.9
2	1	$\bar{3}$	5	3	2	0		1.308	..	0.2	0.3
1	0	$\bar{1}$	$\bar{1}4$	5	5	4	1.269	1.273	20	4.3	3.9
1	1	$\bar{2}$	12	5	4	3		1.270		11	10
0	0	0	15	5	5	5		1.266	..	0.4	0.6
2	0	$\bar{2}$	11	5	3	3		1.260	..	0.8	1.1
2	1	$\bar{3}$	7	4	2	1		1.239	..	0.7	1.0
3	0	$\bar{3}$	0	2	$\bar{1}$	$\bar{1}$	1.229	1.229	3	5.6	5.6
3	0	$\bar{3}$	3	3	0	0		1.206	..	0.1	0.2
0	3	$\bar{3}$	3	2	2	$\bar{1}$					
2	1	$\bar{3}$	$\bar{8}$	4	3	1	1.201	1.202	10	9.4	9.1
3	0	$\bar{3}$	6	4	1	1		1.146		7.1	7.0
0	3	$\bar{3}$	6	3	3	0	1.144		5		
2	0	$\bar{2}$	$\bar{1}3$	5	5	3		1.145		0.6	0.8
1	0	$\bar{1}$	16	6	5	5	1.125	1.129	2	3.2	2.8
2	1	$\bar{3}$	10	5	3	2		1.123		6.4	6.1
2	0	$\bar{2}$	14	6	4	4	1.093	1.093	1	2.6	2.4
1	1	$\bar{2}$	15	6	5	4		1.088		1.8	2.5
2	1	$\bar{3}$	11	5	4	2		1.085	..	1.1	1.5
1	0	$\bar{1}$	$\bar{1}7$	6	6	5	1.069	1.069	1	0.8	1.2
2	2	$\bar{4}$	0	2	0	$\bar{2}$		1.064		3.8	3.8
3	0	$\bar{3}$	9	5	2	2					
								1.062	..	0.4	0.6
0	3	$\bar{3}$	9	4	4	1					
0	0	0	18	6	6	6		1.055	..	0.7	0.6
2	2	$\bar{4}$	3	3	1	$\bar{1}$		1.049	..	0.2	0.2
3	1	$\bar{4}$	$\bar{1}$	2	1	$\bar{2}$		1.021	..	0	0
3	1	$\bar{4}$	2	3	0	$\bar{1}$	1.015	1.017	1	6.0	6.0
2	2	$\bar{4}$	6	4	2	0		1.009	..	5.7	5.6
2	1	$\bar{3}$	13	6	4	3		1.009	..	0.9	1.3
3	1	$\bar{4}$	$\bar{4}$	3	2	$\bar{1}$	0.998	0.999	2	6.9	6.9
2	0	$\bar{2}$	$\bar{1}6$	6	6	4		0.998		2.7	2.4

[a] Based upon $a = 4.256$ Å., $c = 18.99$ Å.

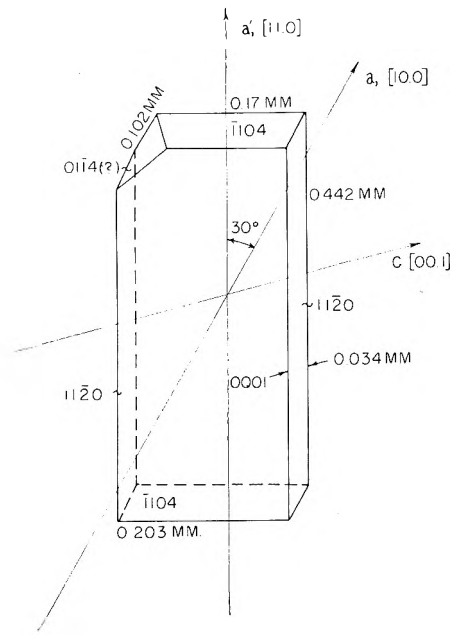

Fig. 1.—Diagram of single crystal employed.

diation with the hexagonal a-axis [10.0] as the rotation axis; and (c) Mo Kα radiation with the hexagonal a-axis [10.0] as the rotation axis. The rotation spots were readily indexed, the hexagonal base diagonal being equivalent to the a-axis of a larger hexagonal unit cell ($h' = 2h + k$, $k' = k - h$, $l' = l$; $a' = \sqrt{3}a$). The relative intensities were estimated visually by comparison with a blackening scale and measurement of the areas of the rotation spots.

The rotation photographs exhibit layer disorder similar to that recently described by Brindley and Ogilvie[7] for brucite, a CdI_2-type layer crystal. On both the [10.0] rotation photograph and the [11.0] rotation photograph, the ($hk.0$)-reflections appear as sharp spots, while the ($00.l$)-reflections appear as extended arcs. According to Brindley's interpretation the resulting angular displacement of the c-axis is approximately 2°.

Laue photographs taken along the c-axis, consisting essentially of streaks because of the slight disorder, indicate a D_{3d} diffraction symmetry. This confirms the D_{3d}^5-R$\bar{3}$m rhombohedral space group, there being only one Cs_2O "molecule" in the rhombohedral unit cell.

Treatment of the Single Crystal Data. (A) The Absorption Factor.—For a crystal containing a high percentage of heavy atoms, the absorption correction becomes very important even though the crystal is very thin. Hendershot[8] has described an analytical method for computing the absorption factor for a rotating crystal bounded by polygonal faces. The formulas apply to the zero-layer reflections only. The graphical method recently described by Howells[9] is rather time-consuming.

For a thin crystal plate with rectangular cross-section and high absorbing power, the estimation of the absorption factor can be done analytically with much less labor than that required for a graphical computation. The crystal employed in the present experiment can be treated as a thin rectangular plate with wedge-like top and bottom sections. For the case of rotation about the [11.0] axis, the major portion of the crystal is one of constant cross-section perpendicular to the rotation axis. This cross-section may be divided by the projections of the incident and reflected X-ray beams into appropriate regions for integrations of the absorption integral. For fixed hk, the absorption factor A_{hkl} can be plotted as a function of the l-indices. This is illustrated in Fig. 2. An abrupt change in the slope of the curve indicates a change in the type of reflection.

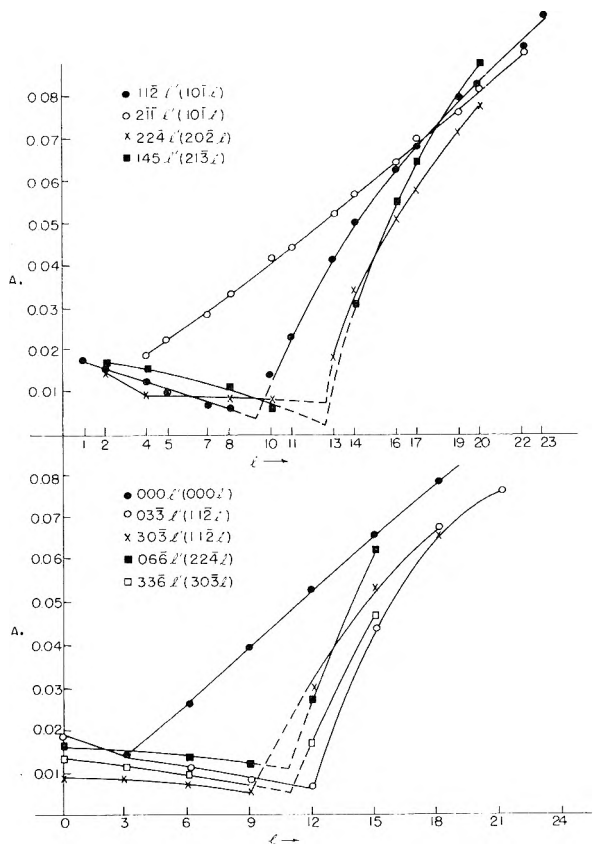

Fig. 2.—Calculated absorption factors *versus* l-indices for the [11.0] rotation photograph taken with CuK_α radiation.

In the case of Mo Kα radiation ($\mu = 192$ cm.$^{-1}$) and rotation about the [10.0]-axis, the crystal can be treated as a thin rectangular plate, contribution from the wedge-like edges being negligible. The crystal is divided into one parallelopiped (central) section and two triangular prismatic sections since the rotation axis is now inclined 30° to the [11.0] edges. However, in the case of internal reflection through both major faces of the crystal plate, good approximation can usually be obtained by merely integrating through the thickness of the crystal plate.

(B) The Temperature Factor and the Scale Factor.—The *anti*-$CdCl_2$ structure (D_{3d}^5) has only one variable parameter, u, which has been shown by the powder data to be about 0.256. From the single-crystal intensity data, the observed structure amplitudes (including the inherent tempera-

(7) G. W. Brindley and G. J. Ogilvie, *Acta Cryst.*, **5**, 412 (1952).
(8) O. P. Hendershot, *Rev. Sci. Instr.*, **8**, 324 (1937).
(9) R. G. Howells, *Acta Cryst.*, **3**, 366 (1950).

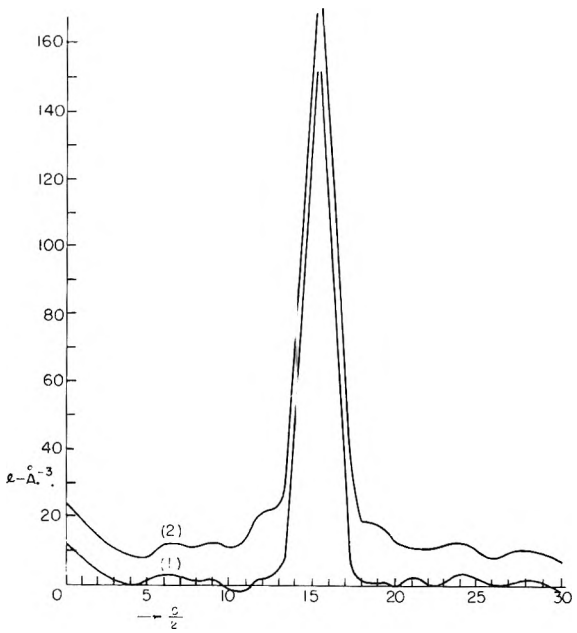

Fig. 3.—Electron density line-sections along c-axis from the observed and calculated structure factors: 1, P_0 (00Z); 2, P_3 (00Z) + 10.

ture factor) were calculated, taking $^1/_3\ \phi_{11.0} = 85$ ($F_{11.0}$ is independent of u) as an arbitrary basis in order to give a scale factor, K, close to unity. Based upon these values of ϕ, an electron density line-section along the c-axis was constructed; from the position of the Cs peak, u was again found to be close to 0.256. The structure factors, F_c, for $u = 0.255$ and $u = 0.256$ were then calculated using Thomas-Fermi scattering factor for the cesium atom (for $\sin\theta/\lambda > 0.2$) and Hartree scattering factor for the oxide ion as given in the International Tabellen. F_c based upon $u = 0.256$ gave a slightly better agreement with the observed structure factors. A least-squares treatment of the values of $\log_{10}(\phi/F_c)$ *versus* corresponding values of $\sin^2\theta/\lambda^2$ gave $K = 0.829$ and $\bar{B}_T = 3.24 \times 10^{-16}$ cm.^{2}. Using these values of K and $\bar{B}_T$, the observed structure factors, F_0, were calculated from ϕ by means of the expression: $\phi = KF_0 \exp(-\bar{B}_T(\sin^2\theta/\lambda^2))$. The reliability factor, $\Sigma(|F_0| - |F_c|) \div \Sigma|F_c|$, was found to be 0.13.

(C) Electron Density Maps.—Figure 3 shows the calculated and the observed electron density line section along the c-axis. $\rho_c(00z)$ was constructed from the calculated structure amplitudes, $F_c' = F_c \exp(-\bar{B}_T(\sin^2\theta/\lambda^2))$, based upon $u = 0.256$, $\bar{B}_T = 3.24 \times 10^{-16}$ cm.^{2}, and Thomas-Fermi atomic scattering factors; while $\rho_0(00z)$ was constructed from the observed structure amplitudes $F_0' = \phi/K = F_0 \exp(-\bar{B}_T(\sin^2\theta/\lambda^2))$, given in Table II, together with interpolated values of F_0' (assumed equal to F_c') for the weak, unobserved reflections. The weak, unobserved reflections, however, can be neglected without producing significant changes in the essential feature of the $\rho_0(00z)$ curve. Both sets of structure amplitudes, F_c' and F_0', cover the same region in the reciprocal lattice corresponding to $\sin^2\theta/\lambda^2 = 0$ to 0.642, so that the series termination errors in $\rho_c(00z)$ and $\rho_0(00z)$ may be assumed to be approximately the same.

A plane-section of electron-density, $\sigma(x0z)$, based upon the observed structure amplitude, F_0', alone (Fig. 4), shows that: (1) the outer-shell of the cesium ion appears to be elongated along the c-axis; and that (2) the lower electron density region, between zero and 3e/Å.^{3}, also appears to be more extended on the side toward the neighboring Cs^+-layer, than on the side toward the neighboring $O^=$-layer. These two points also can be seen readily from Fig. 3, by comparing the values of the electron density difference function, $\rho_0(00z) - \rho_c(00z)$, on both sides of the cesium nucleus. Their significance will be discussed presently.

(D) Interionic Distances.—With $u = 0.256 \pm 0.001$, $a = 4.256 \pm 0.004$ Å., and $c = 18.99 \pm 0.002$ Å., the observed interionic distances were found to be Cs^+–$O^=$ = 2.86 ± 0.01 Å. and Cs^+–Cs^+ = 4.19 ± 0.02 A., as compared with 3.09 and 3.38 Å.,

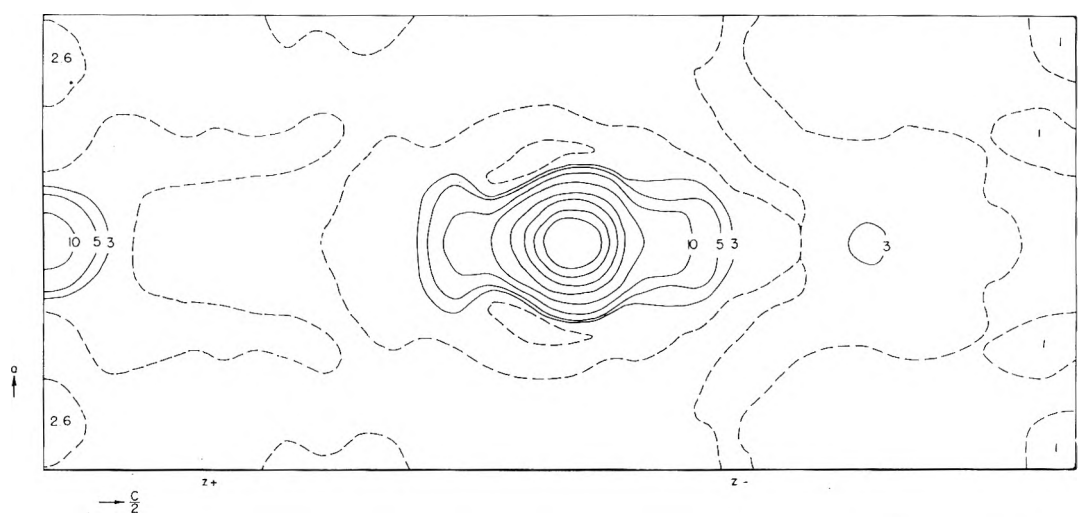

Fig. 4.—Electron density (XOY) section. The zero contours are dotted; maximum depths of the negative valleys are −2.7 to −3.0 e-Å.$^{-3}$ Unlabeled contours around the cesium nucleus are 100, 80, 60, 40 and 20 e-Å.$^{-3}$ The z-coördinate of the adjacent Cs^+ layer is indicated by $z+$; that of the adjacent $O^=$ layer by $z-$. The cell constants are $a = 4.256$ Å. and $c = 18.99$ Å.

TABLE II

OBSERVED AND CALCULATED STRUCTURE FACTORS

Hexagona indices				Intensity,	Layer, rotation	Absorption factor,	Structure factors	
h	k	i		$I_{obs.}$	photograph	A	Obsd. $^1/_3F_0$	Calcd. $^1/_3F_c$ (u = 0.256)
0	0	0	3	1.8	0, (a)	0.0136	8.6	20
1	0	$\bar{1}$	1	...			...	3.3
1	0	1	2	200	1, (a)	.0154	114	−87
				122	0, (b)	.54		
0	0	0	6	100	0, (a)	.026	70	−84
				100	0, (c)			
1	0	$\bar{1}$	4	92	1, (a)	.014	109	96
				92	0, (b)	.48		
1	0	$\bar{1}$	$\bar{5}$	...			...	−11
1	0	$\bar{1}$	7	2.2	2, (a)	.028	24	27
				2.9	0, (b)	.38		
1	1	$\bar{2}$	0	141	0, (a)	.019	123	88
				134	3, (a)	.0086		
				93	1, (b)	.57		
0	0	0	9	9.0	0, (a)	.040	22	−23
1	1	$\bar{2}$	3	3.1	0, (a)	.0136	18	14
				3.4	3, (a)	.0086		
1	0	$\bar{1}$	$\bar{8}$	7.5	1, (a)	.0061	69	82
				32	2, (a)	.033		
				18	0, (b)	.35		
2	0	$\bar{2}$	$\bar{1}$	...			...	1.1
2	0	$\bar{2}$	2	45	2, (a)	.0146	96	−74
				34	0, (b)	.56		
1	1	$\bar{2}$	6	37	0, (a)	.0114	77	−71
				18	3, (a)	.0068		
				50	1, (b)	.46		
2	0	$\bar{2}$	$\bar{4}$	22	2, (a)	.0089	92	79
				28	0, (b)	.54		
1	0	$\bar{1}$	10	11	1, (a)	.0143	55	−67
				15	2, (a)	.040		
				4.6	1, (b)	.23		
2	0	$\bar{2}$	$\bar{5}$	...			...	−10
0	0	0	12	39	0, (a)	.053	62	70
				ca. 4.4	0, (b)	.24		
1	0	$\bar{1}$	$1\bar{1}$	3.9	1, (a)	.024	30	33
				4.1	2, (a)	.045		
				ca. 1.0	0, (b)	.27		
2	0	$\bar{2}$	$\bar{7}$	2	0, (c)		26	22
1	1	$\bar{2}$	$\bar{9}$	0.6	0, (a)	.0089	19	−21
				3.4	3, (a)	.0058 (?)		
				1.9	1, (b)	.39		
2	0	$\bar{2}$	8	5.0	2, (a)	.0089	65	70
				9.6	0, (b)	.46		
2	1	$\bar{3}$	1	...			...	0.4
2	1	$\bar{3}$	$\bar{2}$	17	1, (a)	.018	85	−65
				15	1, (b)	.55		
1	0	$\bar{1}$	13	4.9	1, (a)	.033	32	−29
				3.8	2, (a)	.053		
				0.6	0, (b)	.25		
2	1	3	4	11.4	1, (a)	.015	78	70
				11	1, (b)	.54		
2	0	2	10	4.1	0, (b)	.43	54	−60
				ca. 1.5	2, (a)	.0079 (?)		
2	1	$\bar{3}$	$\bar{5}$	...			...	−10
1	0	$\bar{1}$	$\bar{1}4$	16	1, (a)	.050	58	−54
				10	2, (a)	.057		
1	1	$\bar{2}$	12	*ca.* 3.6 (?)	0, (a)	.0064 (?)	60	62
				27	3, (a)	.030		
0	0	0	15	3.6	0, (c)	*ca.* .066	30	38
				ca. 3.6 (?)	0, (a)	.066		
				ca. 0.4	0, (b)	.29		
2	0	$\bar{2}$	11	*ca.* 0.5	0, (b)	.41	22	29

TABLE II (*Continued*)

Hexagonal indices h	k	i	l	Intensity, $I_{obs.}$	Layer, rotation photograph	Adsorption factor, A	Structure factors Obsd. $1/3F_o$	Calcd. $1/3F_c$ (u = 0.256)
2	1	$\bar{3}$	7	0.3	1, (a)	.50	22	19
				0.4	1, (b)	.50		
3	0	$\bar{3}$	0	7.7	3, (a)	.0136	74	67
				8.4	0, (b)	.55		
3	0	$\bar{3}$	3	0.7	0, (c)		11	10
2	1	$\bar{3}$	$\bar{8}$	3.5	1, (a)	.0107	63	63
				5.2	1, (b)	.49		
3	0	$\bar{3}$	6	6.1	3, (a)	.0093	58	−58
				6.2	0, (b)	.51		
2	0	$\bar{2}$	$\bar{1}3$	1.5	2, (a)	.019	31	−27
1	0	1	16	1.2	1, (a)	.063	55	53
				7.2	2, (a)	.064		
2	1	$\bar{3}$	10	1.3	1, (a)	.0064	55	−55
2	0	2	14	6.4	2, (a)	.035	52	−50
				1.3	0, (b)	.35		
2	1	$\bar{3}$	$\bar{1}1$	*ca.* 0.4	1, (b)	.44	24	27
1	1	2	15	*ca.* 0.6	1, (b)	(.25)		
				4.2	0, (a)	.044	36	35
				16	3, (a)	.054		
1	0	$\bar{1}$	17	6.3	1, (a)	.068	44	−34
				4.5	2, (a)	.070		
2	2	$\bar{4}$	0	3.8	0, (a)	.017	64	62
3	0	$\bar{3}$	9	...			...	−18
0	0	0	18	6.5	0, (a)	.079	40	−44
2	2	$\bar{4}$	3	...			...	9
3	1	$\bar{4}$	$\bar{1}$	...			...	− 0.2
3	1	$\bar{4}$	2	3.4	2, (a)	.016	63	−56
				2.3	1, (b)	.54		
2	2	$\bar{4}$	6	3.5	0, (a)	.014	48	−54
2	1	$\bar{3}$	13	...			...	−25
3	1	$\bar{4}$	$\bar{4}$	2.1	1, (b)	.54	60	59
2	0	$\bar{2}$	$\bar{1}6$	*ca.* 6	2, (a)	.051	46	49
3	1	$\bar{4}$	5	...			...	− 9
2	1	$\bar{3}$	$\bar{1}4$	3.3	1, (a)	.031	48	−47
3	0	$\bar{3}$	12	9.0	3, (a)	.017	57	53
				2.0	0, (b)	.45		
1	0	$\bar{1}$	19	6.6	1, (a)	.076	46	39
				4.4	2, (a)	.076		
3	1	$\bar{4}$	$\bar{7}$	...			...	17
2	0	$\bar{2}$	17	3.4	2, (a)	.059	32	−32
2	2	$\bar{4}$	9	...			...	−17
1	1	2	18	11	0, (a)	.068	45	−41
				16	3, (a)	.066		
3	1	$\bar{4}$	8	1.1	1, (b)	.50	51	55
4	0	$\bar{4}$	1	...			...	− 0.5
1	0	$\bar{1}$	20	7.5	1, (a)	.083	44	42
				4.0	2, (a)	.082		
4	0	$\bar{4}$	2	1.5	0, (b)	.54	60	−53
2	1	$\bar{3}$	16	6.5	1, (a)	.055	49	46
4	0	$\bar{4}$	4	1.4	0, (b)	.53	58	55
0	0	0	21	5.1	0, (a)	.091	36	−37
3	1	$\bar{4}$	$\bar{1}0$	0.8	1, (b)	.48	46	−49
$\bar{4}$	0	$\bar{4}$	5	...			...	− 8
2	2	$\bar{4}$	12	3.1	0, (a)	.028	37	50
3	0	$\bar{3}$	15	7.9	3, (a)	.048	34	30
3	1	$\bar{4}$	11	...			...	23
2	0	$\bar{2}$	19	4.5	2, (a)	.071	34	37
4	0	$\bar{4}$	7	...			...	16
2	1	$\bar{3}$	$\bar{1}7$	2.9	1, (a)	.065	32	−30
4	0	$\bar{4}$	8	1.0	0, (b)	.050	65	52
3	2	$\bar{5}$	1	...			...	− 0.3
2	0	$\bar{2}$	20	4.3	2, (a)	.078	31	40
3	2	$\bar{5}$	$\bar{2}$	*ca.* 1.6	1, (a)	.016	57	−50

TABLE II (*Continued*)

Hexagonal indices h	k	i	l	Intensity, $I_{obs.}$	Layer, rotation photograph	Adsorption factor, A	Structure factors Obsd. $^1/_3F_0$	Calcd. $^1/_3F_c$ (u = 0.256)
1	0	$\bar{1}$	22	*ca.* 5.4	2, (a)	.092	30	−33
				1.7	2, (a)	.091		
3	1	$\bar{4}$	$\bar{1}3$	1.1	2, (a)	.042	22	−23
3	2	$\bar{5}$	4	*ca.* 0.7	2, (b)	.50	58	53
1	1	2	21	11	0, (a)	.076	35	−35
				16	3, (a)	.079		
4	0	$\bar{4}$	10	0.7	0, (b)	.48	50	−46
				1.0	0, (c)			
3	2	$\bar{5}$	$\bar{5}$	...			...	− 8
3	1	$\bar{4}$	14	6.5	2, (a)	.054	41	−42
2	2	$\bar{4}$	15	3.9	0, (a)	.064	24	29
4	0	$\bar{4}$	$1\bar{1}$	...			...	22
2	1	$\bar{3}$	19	5.6	1, (a)	.080	35	35
3	2	$\bar{5}$	7	...			...	15
1	0	$\bar{1}$	$\bar{2}3$	8.5	1, (a)	.101	35	40
				5.1	2, (a)	.101		
4	1	$\bar{5}$	0	0.7	1, (b)	.54	63	52
3	0	$\bar{3}$	18	11	0, (c)		31	−38
4	1	$\bar{5}$	3	...			...	7
3	2	$\bar{5}$	8	*ca.* 2.5	1, (a)	.0143 (?)	52	49
4	0	$\bar{4}$	13	...			...	−22
0	0	0	24	6.5	0, (a)	.104	29	32
2	1	$\bar{3}$	20	8.2	1, (a)	.089	37	38
2	0	$\bar{2}$	$\bar{2}2$	8.0	0, (c)		32	−32
4	1	$\bar{5}$	6	0.5	1, (b)	.500	41	−46

respectively, calculated from Pauling crystal radii.[10]

(1) **Apparent Elongation of the Charge Distribution of the Cesium Ion along the *c*-Axis.**—This elongation of the charge distribution would seem to indicate that the thermal vibration in the direction of the *c*-axis is considerably greater than that in the directions of the *a*-axis, as would be expected for this type of layer crystal. However, the agreement between F_0 and F_c in the higher $\sin^2\theta/\lambda^2$ region appears to be generally good; in fact, better than that between F_0 and F_c in the lower $\sin^2\theta/\lambda^2$ region. Hence the "effective" temperature factor, which includes the effect due to any slight disorder of the crystal, cannot be very far from isotropic.

Since the observed values of $F^2_{00.l}$ are significantly too small at small values of $\sin\theta/\lambda$ and higher values of I_{obsd} relative to the observed values of $F^2_{hk.0}$, it is natural to suppose that this is a result of extinction due to higher degree of perfection of the crystal in the direction of the *c*-axis. This is consistent with a model of the crystal having a slight layer-shearing disorder perpendicular to the *c*-axis, or a dislocation disorder, which affects the alignment of the (*hk*,0)-planes more than it does that of the (00.1)-planes.

B. Polarization of the Cesium Ions in the Layer Lattice.—The abnormally large Cs^+–Cs^+ distance (4.19 Å. as compared with $2r_{Cs^+}$ = 3.38 Å.), the slight shortening of the Cs^+–$O^=$ distance (2.86 Å. as compared with $r_{Cs^+} + r_{O^-}$ = 1.69 Å. + 1.40 Å. = 3.09 Å.), and the appreciably higher electron density in the outer-shell of the cesium ion on the side toward the neighboring Cs^+-layer than on the side toward the neighboring $O^=$-layer, all indicate that the cesium ions must be highly polarized in the layer crystal of cesium monoxide. The observed parameter (u = 0.256) and interionic distances (Cs^+–$O^=$ = 2.86 Å., Cs^+–Cs^+ = 4.19 Å.) should correspond to a maximum lattice energy of the crystal consisting of the Madelung, the polarization, the van der Waals, and the repulsive energy terms. The result (to be published later) of a calculation of the lattice energy of the crystal as a function of the parameter, u, shows that this is actually the case.

It is to be noted that, in the case of the following $CdCl_2$-type layer crystals: $CdCl_2$, $CoCl_2$, $FeCl_2$, $MgCl_2$, $NiCl_2$, $ZnCl_2$, $NiBr_2$, $CdBr_2$, $MnCl_2$, the observed inter-layer halide–halide distances all appear to be about normal (Cl^-–Cl^- = 3.6 Å., Br^-–Br^- = 3.9 Å., based upon the cell constants and parameters given in Wyckoff's "Crystal Structures")[11]; and in the case of NiI_2, another $CdCl_2$-type layer crystal with a highly polarizable anion, the observed interlayer I^-–I^- distance (3.97 Å.) is even considerably smaller than that calculated from the crystal radius of the iodide ions ($2r_{I^-}$ = 4.32 Å.), in spite of the anionic contact. This is not surprising, however, in view of the fact that the polarizing fields (contributed mainly from three neighboring cations, M^{++}) acting on the halide ions in the $CdCl_2$-type layer crystals are in reversed directions to the polarizing field (contributed mainly from the three neighboring anions, $O^=$) acting on the cesium ions at corresponding positions in the *anti*-$CdCl_2$ type layer crystal, Cs_2O.

Acknowledgment.—The valuable help rendered by Dr. Donald Tuomi in connection with this work is acknowledged with great pleasure.

(10) L. Pauling, "The Nature of the Chemical Bond," 2nd ed., Cornell Univ. Press, Ithaca, N. Y., 1940, p. 346.

(11) R. W. G. Wyckoff, "Crystal Structures," Vol. I, Table IV, Interscience Publishers, New York, N. Y., 1948, p. 7.

THE CRYSTAL STRUCTURE OF TRICESIUM MONOXIDE[1]

BY KHI-RUEY TSAI, P. M. HARRIS AND E. N. LASSETTRE

Contribution from the Department of Chemistry, The Ohio State University, Columbus, Ohio

Received August 18, 1955

Tricesium monoxide, Cs_3O, has been prepared and found to possess many metallic properties, a D_{6h}^3-$C_{\bar{3}}$ cm structure with two molecules per unit cell. The observed interatomic distances indicate that the bond between cesium and oxygen is ionic as in the crystal of cesium monoxide, while the bond between cesium and cesium is metallic.

Introduction

The existence of four suboxides of cesium, Cs_7O, Cs_4O, Cs_7O_2 and Cs_3O, was first discovered by Rengade,[2] through thermal analysis of the cesium–oxygen system. Part of the phase diagram (from Cs to $CsO_{0.25}$) has been substantiated recently by Brauer[3] by means of X-ray powder diagrams and measurement of the resistivity–temperature coefficients of the samples. Brauer observed, however, that Cs_4O gave an abnormal X-ray powder pattern consisting of only two lines.

No structure work on any of these suboxides has been recorded in the literature, despite the fact that they are of great interest from the point of view of valency and structural chemistry.

Experimental

(a) **Preparation of Tricesium Monoxide, Cs_3O.**—The suboxide was prepared by direct combination of pure cesium with the calculated amount of pure oxygen admixed with a small amount of argon, which served as an inert gas to prevent excessive volatilization of the alkali metal. Toward the later stage of the oxidation, the reaction temperature was raised to 170° to decompose any higher oxides of cesium. The molten reaction product was allowed to solidify and cool to room temperature. It was pulverized in dried argon purified by passing through copper turnings at 350°.[3]

Crystalline samples of tricesium monoxide were also prepared by distilling small amounts of a lower suboxide, Cs_7O_2, in thin-walled Pyrex capillaries (sealed *in vacuo*) at 120–130°. In the distillation process, however, yellowish films of cesium monoxide were also formed above the dark greenish crystals of tricesium monoxide. The lower suboxide, Cs_7O_2, was prepared by direct combination of pure cesium and oxygen in the presence of a small amount of argon.

(b) **Study of the Crystal Properties.**—The tricesium monoxide prepared by direct combination of the elements was obtained as a dark greenish, translucent solid, with a metallic luster, soft and malleable, difficult to pulverize. Analyzed by decomposition with water, the sample gave 0.337 equivalent of hydrogen for each equivalent of total alkali; hence the composition was $CsO_{0.332}$. The method of analysis is similar to that recently described by Libowitz[4] for determining the excess of metallic barium in barium oxide crystals.

The following physical properties were observed:

(1) Dark greenish, translucent solid; m.p. *ca.* 165°, as observed in Pyrex capillary tube.

(2) Density: 2.73 ± 0.03 g./cc. at 30.2°, determined by displacement of dried, oxygen-free toluene in a pyknometer.

(3) Magnetic susceptibility at 30° $\chi_m = 61 \times 10^{-6}$ c.g.s./unit per mole, as compared with $\chi_m = (29 - 2 \times 35 - 10) \times 10^{-6} = -51 \times 10^{-6}$ c.g.s. unit calculated from Wiedeman's law for Cs_2O + Cs, and with $\chi_m = 29 \times 10^{-6}$ c.g.s. unit for metallic cesium. The magnetic measurement was done by the standard Gouy method.[5]

(4) Electrical resistivity at 30°: 7.21×10^{-5} ohm-cm. (as compared with 2.08×10^{-5} ohm-cm. for metallic cesium at 18°); resistivity–temperature coefficient: α = 0.0025 per degree. The measurement was done potentiometrically by determining the voltage-drop across a column of solidified suboxide in a conductivity pipet standardized with mercury. These observations definitely show that Cs_3O possesses the physical properties characteristic of an alkali metal.

(c) **X-Ray Diffraction Experiments.**—Debye–Scherrer diagrams of tricesium monoxide were obtained with Cu Kα radiation and with Mo Kα radiation in an 11.4-cm. camera at room temperature. The pattern was readily indexed graphically by the simple hexagonal system with a c/a ratio of 0.86.

A highly imperfect crystal of tricesium monoxide was obtained by melting a small sample in a thin-walled Pyrex capillary tube and allowing it to cool very slowly to 150°. The crystal was of irregular shape with one (hexagonal) a-axis approximately parallel to the length of the capillary. A rotation photograph taken with Cu Kα radiations and with an a-axis as the rotation axis confirmed the hexagonal symmetry with a glide extinction of the $(h0\cdot l)$- and $(0k\cdot l)$-type with odd l-indices. The cell constants are $a = 8.78 \pm 0.01$ Å. $c = 7.52 \pm 0.01$ Å. The calculated density for two molecules (Cs_3O, formula wt. = 414.73) per unit cell is $d_{calc.} = 2.74$ g./cc., as compared with $d_{obs.} = 2.73 \pm 0.03$ g./cc. at 30.2°.

Determination of the Structure.—The presence of strong hhl-reflections with off l-indices and the systematic absence of $(h0\cdot l)$- and $(0k\cdot l)$-reflections with odd indices show the presence of a $(1\bar{1}.0)$-glide, rather than a (11.0)-glide (equivalent to a (10.0)-glide). Hence the possible space group symmetries[6] are $D_{3d}^4 - D_{\bar{3}c}$, $C_{6v}^3 -$ C 6cm, $D_{6h}^3 -$ C6/mcm. The shortness of the c-axis and the strong (10.0)-reflection eliminate the possibility of putting the six cesium atoms at the combined two and four equivalent positions possible with these space-groups. Thus the cesium atoms must lie on six equivalent positions. This means that the six cesium atoms in the hexagonal unit cell of the suboxide are crystallographically alike.

The two space groups, D_{3d}^4 and D_{6h}^3, give the same set of six equivalent positions: $uu0$; $0\bar{u}0$; $\bar{u}00$; $\bar{u}\bar{u}1/2$; $0u1/2$; $u01/2$. The six equivalent positions possible with the space group C_{6h}^3 differ from this set only in the choice of the origin along the c-axis. The relative intensities of the (10.0)- and (11.0)-powder lines are approximately in the ratio of 5:1. This fixes u at about 0.24. With this approximate parameter for the positions of the cesium atoms, and assuming that the observed extinctions are true, the only reasonable positions for the two oxygen atoms are $00^1/_4$ and $00^3/_4$, corresponding to a D_{6h}^3 structure. Comparison of the observed and calculated intensities of the powder lines (Table I) gives $u = 0.250 \pm 0.001$. Based upon this structure and with $u = 1/4$ for the parameter of the cesium atoms, the calculated relative intensities of the rotation spots were also found to

(1) This work was supported both by the University Committee for Allocation of Research Foundation Grants and by the U. S. Army Engineer Corps under Contract DA 44-009-eng-405.

(2) E. Rengade, *Bull. soc. chim.*, **5**, 994 (1909).

(3) V. G. Brauer, *Z. anorg. Chem.*, **255**, 101 (1947).

(4) C. G. Libowitz, *J. Am. Chem. Soc.*, **75**, 1501 (1953).

(5) L. G. Gouy, *Compt. rend.*, **109**, 935 (1889).

(6) "International Tabellen zur Bestimmung von Kristallstrukturen," Bd. 1, Gebruder Borntraeger, Berlin, 1935.

TABLE I

OBSERVED AND CALCULATED INTENSITIES OF X-RAY POWDER LINES OF TRICESIUM MONOXIDE

Hexagonal indices, $hk\cdot l$	Planar spacings, d		Relative intensities $I_{obsd.}$	Relative intensities calcd., $I_{calcd.}$			
	Calcd.	Obsd.		$u = (1/4 - 1/360)$		$u = 1/4$	$u = (1/4 + 1/360)$
10.0	7.60	7.62	60	62.6		57.6	52.9
00.1	7.52			0		0	0
10.1	5.35			0		0	0
11.0	4.39	4.39	10	8.5		9.1	9.6
20.0	3.801			6.4			
11.1	3.793	3.80	100	69.3	100	100	100
00.2	3.760	(broad)		24.3			
20.1	3.393	3.37	10	0		0	0
10.2	3.371			10.2		9.2	8.2
21.0	2.875	2.87	15	6.9	17.4	17.2	17.0
11.2	2.857			10.5			
21.1	2.684	2.68	50	59.3	68.5	65.0	61.6
20.2	2.673			9.2			
30.0	2.535	2.54	2	3.0		3.8	4.4
00.3	2.507			0		0	0
30.1	2.402			0		0	0
10.3	2.380			0		0	0
21.2	2.283	2.28	5	12.0		11.2	10.2
22.0	2.195			1.5		1.5	1.4
11.3	2.176	2.175	5	15.3		15.5	15.7
31.0	2.109			4.1			
22.1	2.108	2.103	5	0	6.0	7.0	7.8
30.2	2.101			1.9			
20.3	2.092			0		0	0
31.1	2.031			0		0	0
40.0	1.901			12.2			
22.2	1.896			3.2			
21.3	1.889	1.891 (broad)	15	21.0	40.1	38.8	37.0
00.4	1.880			3.7			
40.1	1.844			0		0	0
31.2	1.840	1.833	2	3.4	6.4	6.4	6.3
10.4	1.826			3.0			
32.0	1.744	1.74 (?)	1 (?)	1.4	2.8	2.9	3.0
11.4	1.728			1.4			
32.1	1.699			13.3			
40.2	1.697	1.696	10	14.4	29.1	29.0	28.8
20.4	1.685			1.4			

be in good qualitative agreement with the observed values obtained by visual estimation with the triple-film technique. However, in some cases, such as the (11.0)-, (11.1)-, and (11.3)-reflections on the Cu Kα rotation photograph, the absorption (μ = 894 cm.$^{-1}$) appeared to be quite appreciable. Unfortunately, it was not possible to correct for absorption because of the irregular shape of the crystal.

Since the diffracting power of the oxygen atoms is very small compared with that of the cesium atoms, the possibilities of placing the two oxygen atoms at positions other than those required by the observed extinctions must be examined. Thus with $u = 1/4$ for the parameter of the cesium atoms, we still have to consider the possibilities of putting the two oxygen atoms at one of the following two sets of two equivalent positions: (1) $1/3$, $2/3$, $1/4$; $2/3$, $1/3$, $3/4$, for a D_6^5 — $C6_32$ structure, in which the Cs–O distance would be 3.84 Å.; or (2) $1/3$, $2/3$, 0; $2/3$, $1/3$, $1/2$; for a C_{6h}^2 – $C6_3/m$ structure, with Cs–O = 3.35 Å. However, comparison of the calculated (10.0)-, (10.1)-, (11.0)-, and (10.2)- powder-line intensities for these two structures with the observed intensities ((10.1)-reflection absent) shows that these two structures must be ruled out in favor of the D_{6h}^3 — C6/mcm structure.

The X-ray powder and single-crystal data are given in Tables I and II. The powder data indicate an abnormally high temperature factor, $\bar{B}_T$, of the order of 10×10^{-16} cm.^{2}, probably due to lattice defects. The absorption correction for the powder sample appeared to be small (from comparison of the Cu Kα and Mo Kα photographs), since the sample was spread out in a thin film of small crystallites on the wall by rapid melting and cooling in the capillary tube.

The observed interatomic distances are shown in Fig. 1. The Cs–O distance in tricesium monoxide, Cs_3O, is very close to the observed Cs^+–$O^=$ distance in the cesium monoxide (Cs_2O) layer crystal, indicating that the Cs–O bond in tricesium monoxide is ionic; while the Cs–Cs distance is about 8% higher than the interatomic distances in metallic cesium

TABLE II

OBSERVED AND CALCULATED INTENSITIES OF BRAGG SPOTS ON ROTATION PHOTOGRAPHS OF TRICESIUM MONOXIDE CRYSTAL

(Cu Kα radiation, a-axis rotation.)

Hexagonal Indices, $hk\cdot l$		Reciprocal lattice coordinates ζ (‖ to a)	ξ (⊥ to a)	Intensities, I Obsd.	Calcd. (u = 1/4)
01.0		0	2.0	50	37
02.0, 00.2	β	0		3	
02.0, 00.2		0	4.1	100	100
01.2		0	4.6	10	14
02.2		0	5.7	14	16
03.0		0	6.1	2	7
03.2		0	7.3	1	6
04.0		0	8.2	5	31
00.4		0	8.3	4	31
01.4		0	8.4	1	7
04.2, 02.4		0	9.1	6	46
10.0		1.76	1.0	75	76
11.0		1.76	3.0	4	14
11.1		1.76	3.6	63	100
10.2		1.76	4.2	17	15
12.0, 11.2		1.76	5.1	21	26
12.1		1.76	5.5	28	53
12.2		1.76	6.5	6	12
11.3		1.76	6.8	8	35
13.0		1.76	7.3	3	5
12.3		1.76	7.9	9	26
13.2, 10.4		1.76	8.2	3	12
$2\bar{1}.0$		(3.52)	i (out of range)	..	..
20.0, $2\bar{1}.1$		3.52	2.0	80	116
21.0, $2\bar{1}.2$		3.52	4.1	8	20
21.1, 20.2		3.52	4.6	54	86
21.2		3.52	5.7	5	14
22.0, $2\bar{1}.3$		3.52	6.2	9	24
22.2, 21.3		3.52	7.4	6	38
23.1, 20.4		3.52	8.4	7	26
$3\bar{1}.0$		(5.27)	i (out of range)	..	..
$3\bar{1}.1$		5.27	2.3	77	171
30.0		5.27	3.1	5	16
$3\bar{1}.2$		5.27	4.2	9	21
31.0, 30.2		5.27	5.1	3	17
$3\bar{1}.3$		5.27	6.3	7	36
31.2		5.27	6.6	2	6
32.1		5.27	7.4	6	26

(Cs–Cs = 5.36 Å., at room temperature), probably due to the polarizing effect of the oxide ions. In view of the observed metallic properties of the suboxide, the observed Cs–Cs distance suggests that the Cs–Cs bonds in Cs_3O crystals have metallic character. The structure can be regarded as consisting of hexagonal columns of Cs_3^+O (formed by piling up the hypothetical pyramidal tricesiumoxonium ions, Cs_3^+O, according to the symmetry of a 6_3 screw axis), the columns being bonded together by "metallic" electrons.

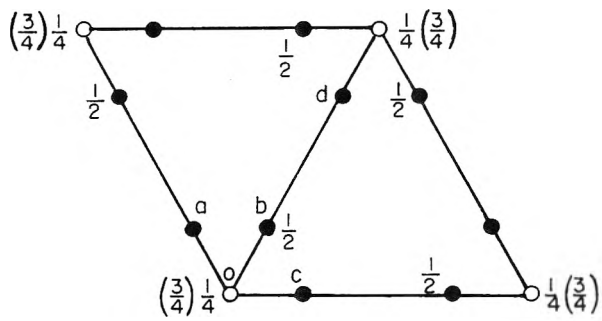

Fig. 1.—Diagram showing the positions of the cesium and the oxygen atoms (denoted, respectively, by the closed and the open circles) in the hexagonal unit cell of Cs_3O crystal at room temperature. The observed cell constants and internuclear distances are: a = 8.78 ± 0.01 Å., c = 7.52 ± 0.01 Å., u = 0.250 ± 0.001.; $\overline{ao}$ = 2.89 ± 0.02 Å. (*cf.* Cs^+–O^{--} = 2.86 ± 0.01 Å. in Cs_2O crystal)[7]; $\overline{ab}$ = 4.34 ± 0.03 Å. (*cf.* Cs^+–Cs^+ = 4.19 ± 0.02 Å. in Cs_2O crystal)[7]; $\overline{ad}$ = 5.80 ± 0.04 Å., $\overline{bd}$ = 5.78 ± 0.05 Å. (*cf.* Cs–Cs = 5.36 Å. in metallic cesium).

Brauer[3] has observed that the lower suboxides of cesium (Cs_4O, and other suboxides lower in oxygen content) are metallic (electrical) conductors. Probably these also possess partial metallic structures. Silver subfluoride, Ag_2F, has also been found by Terry and Diamond[7] to possess metallic properties and partial metallic structure (*anti*-CdI_2 structure) in which the Ag–F distance is about the same as that in silver fluoride (AgF) crystals and the Ag–Ag distance the same as that in metallic silver. Thus the metal suboxides and subhalides probably belong to the same class as far as structure chemistry is concerned. Further study of this class compounds appears to be desirable.

Our thanks are due Dr. D. Tuomi for his valuable help in connection with this work.

(7) H. Terry and H. Diamond, *J. Chem. Soc.*, 2820 (1928).

THE RATE OF EVAPORATION OF WATER THROUGH MONOLAYERS OF ESTERS, ACIDS AND ALCOHOLS

BY HENRI L. ROSANO AND VICTOR K. LA MER

Contribution from the Department of Chemistry, Columbia University, New York, N. Y.

Received August 23, 1955

In a previous communication, the rate of evaporation was investigated by employing monolayers of the C_{17}, C_{18}, C_{19} and C_{20} members of the saturated fatty acid series. The rate was independent of the surface pressure of these monolayers in the range 10–24 dyne/cm., provided the film was spread initially under pressure to prevent the entrance of impurities. This finding has been confirmed using a similar technique. The present investigation extends the study to nine pure substances, esters, acids, alcohols and one fluorinated alcohol. The surface area, the resistance to evaporation and the surface viscosity were measured for each substance as a function of the surface pressure. Certain of these films are highly compressible in the liquid phase, as compared to the incompressible saturated fatty acids. The compressible films are poor retardants of evaporation, whereas the incompressible films retard by a large factor. The specific conductances (reciprocal resistances to evaporation) are additive for a mixed film composed of substances of similar compressibility, for example, a 50-50 mol mixture of stearic and arachidic acids. A film composed of 80 mol arachidic acid (incompressible) and 20 mol ethyl palmitate (compressible) reduces the rate of evaporation. Additivity of the conductances is approached at very low pressures, whereas under high pressures the resistance approaches that of the incompressible component. No direct relationship was found between surface pressure, surface viscosity and specific resistance to evaporation. The correlation depends upon the compressibility of the film except for the fluorinated alcohol which is exceedingly viscous.

I. Introduction

The permeability of surface layers involves a physicochemical model and a process, whose study should aid in understanding many problems of biology, physics (liquid–gas interfaces) and technology (lowering of the rate of evaporation of water in reservoirs). The problem of permeability has been investigated since 1921 by Devaux,[1] with interesting results followed by many investigators.

Restricting our interest to the rate of evaporation of water through films, we find that three sets of conditions have been employed in the measurements: (a) a current of air is passed over the surface.[1–10] (b) The air above the surface is free of convection currents.[8–14] (c) A partial vacuum is created above the surface.[15–20] At first glance, the conditions under (2) would seem the most profitable under which to study evaporation since they most closely approximate the actual conditions under which water evaporates from a reservoir. However, from the viewpoint of a physical chemist, conditions (a) and (c) introduce an additional dynamic factor not present in (b) which complicates the interpretation of the data.

Archer and La Mer[11,12] employed the method of Langmuir and Schaefer[13] but obtained entirely different results in respect to the behavior of the fatty acid films as a function of the surface pressure. Whereas Langmuir and Schaefer found a marked dependence upon surface pressure and often a hysteresis type of curve on compression and expansion, Archer and La Mer controlled the technique of spreading the fatty acid film so that the resistance became a reproducible constant independent of the surface pressure in the range 10–24 dynes/cm. The upper limit exceeds 30 dynes/cm. as with arachidic acid, but collapse of the film with other monolayers may occur below 30 and above 24 dynes/cm.

The essential point was to spread the film from a highly volatile solvent (petroleum ether) and under an initially high pressure to prevent the entrance of impurities (solvent or foreign molecules) into the film during the spreading and measurement. They were thus able to obtain consistent results yielding simple relations in respect to chain length and the energy barrier to permeability. The energy barrier for the C_{19} acid was determined from the resistances at several temperatures.[12]

It is possible that a surface pressure–area isotherm as ordinarily measured may not be sensitive enough to show that the states of a film of low compressibility obtained under decompression may not lead to the same equilibrium states on compression in the liquid state. On the other hand, the resistance to evaporation is exceedingly sensitive to many factors of technique and molecular architecture.

Since the spreading technique of Archer and La Mer was quite different from that of any previously employed, and their conclusions are of far-reaching importance, our first task was to satisfy ourselves that the resistances of their fatty acid monolayers were actually independent of surface pressure. Their results have been confirmed for the C_{18} and C_{20} acids (Fig. 4, curves 6 and 5).

We investigated nine pure substances and two mixtures. In each case we measured the surface

(1) H. E. Devaux, "La permeabilite des lames minces. Etude de l'influence des vapeurs at des huiles sur les lames minces solides et liquides. Soc. Fr. de physique, 20 mai, 1921, et les lames tres minces at leurs proprietes physiques conference 5 juin 1930, Soc. Fr. de physique 23–24, Delmas Editeur, Bordeaux.

(2) G. Hedestrand, THIS JOURNAL, **28**, 1244 (1924).

(3) I. Langmuir and D. B. Langmuir, *ibid.*, **31**, 1719 (1927).

(4) H. N. Glazov, *J. Phys. Chem. USSR*, **11**, 484 (1938).

(5) A. C. Heinman, *ibid.*, **14**, 118 (1940).

(6) C. I. Sklaiarenko and M. K. Baranaiev, *ibid.*, **12**, 271 (1938).

(7) C. I. Sklaiarenko, M. K. Baranaiev and E. I. I. Miejouia, *ibid.*, **18**, 447 (1944).

(8) A. R. Docking, E. Heymann, L. F. Kerley and K. N. Mortensen, *Nature*, **146**, 265 (1940).

(9) E. Heymann and A. Yoffe, *Trans. Faraday Soc.*, **38**, 408 (1942).

(10) A. R. Gibby and E. Hyman, *Australian J. Sci. Res.*, Ser. A., 197–212 (1948).

(11) R. J. Archer and V. K. La Mer, *Ann. N. Y. Acad. Sci.*, **58**, 807 (1954).

(12) R. J. Archer and V. K. La Mer, THIS JOURNAL, **59**, 200 (1955).

(13) I. Langmuir and V. J. Schaefer, *J. Franklin Inst.*, **235**, 119 (1943).

(14) W. W. Mansfield, *Nature*, **172**, 1101 (1953).

(15) E. K. Rideal, THIS JOURNAL, **29**, 1585 (1927).

(16) M. K. Baranaiev, *J. Phys. Chem. USSR*, **9**, 69 (1937).

(17) F. Sebba and E. K. Rideal, *Trans. Faraday Soc.*, **37**, 273 1941).

(18) F. Sebba and N. Sutin, *J. Chem. Soc.*, 2513 (1952).

(19) J. F. Holliman, J. F. Largier and F. Sebba, *ibid.*, 738 (1954).

(20) F. Sebba and H. V. A. Briscoe, *J. Chem. Soc.*, 106 (1940).

area of the film (compression–area isotherm), the specific resistance to evaporation and the surface viscosity all as functions of surface pressure.

II. Experimental Methods

A technique analogous to that of Langmuir and Schaefer was used with modifications for measuring the specific resistance of the monolayers to the evaporation of water, taking advantage of the experience of Archer and La Mer. Figure 1 shows the trough and torsion balance of the present apparatus but equipped with oscillating mica rings V for the measurement of surface viscosity, to be described later. For the measure of rate of evaporation through the film the mica rings are replaced by the Lucite desiccant box used previously for collecting and weighing the evaporated water. This part of the apparatus has been described in detail in the previous papers,[11,12] and need not be repeated here. The torsion balance M firmly connected with an elevator (not shown in sketch) bears a wettable plate K of depolished mica or sand-blasted platinum which allows facile measurement of the surface pressure of a monolayer spread on water contained in the trough E. The steel torsion wire bears a mirror galvanometer, a damping plate immersed in oil, and a 20 mm. horizontal rod, at the edge of which is attached the wettable plate by a thin silk thread.

A narrow beam of light is reflected from the galvanometer mirror through a 4-meter optical path to a vertical mirror and then to a translucent scale, which acts as an image index. The sensitivity of the torsion balance is 0.1 dyne/cm.; for 0.289 g., we have 32.9 cm. of light displacement. Since the plate has a perimeter of 4 cm., we estimate visually the sensitivity (within $^1/_2$ mm.) as

$$\frac{980 \times 0.289 \times 0.5}{329 \times 4} = 0.1 \text{ dyne/cm.}$$

The water rests in a glass trough having the dimensions 66 × 16 × 2.5 cm. For the measurement of surface pressure the surface is delimited by a floating mica frame thinly coated with pure paraffin, and by two movable barriers, which are made either of glass or of mica and also coated with paraffin. The mica frame is kept in place by two glass rods F; it is free to move vertically but not horizontally. A given temperature is maintained by passing water from a thermostat through a glass coil immersed in the trough. At the edge of a Lucite platform, supported by the edges of the trough, is a steel pointed rod with which one can adjust the distance between the surface of the liquid and the bottom face of the desiccant box. This box, containing LiCl separated by a water permeable membrane fits into the platform through a circular hole 10 cm. in diameter. The trough is kept level by four adjusting screws.

The entire system is kept under a Vaseline-coated hood which serves to catch dust particles from the air and prevent them falling on the surface of the water. Guastalla's[21] technique of blowing air and creating suction for cleaning the water surface was used. This method consists of amassing in one corner of the water surface all the impurities which can be detected by dusting calcinated talcum powder onto the surface.

To avoid the rapid reappearance of impurities the water was distilled in a glass apparatus, cleaned with a mixture of H_2SO_4—$K_2Cr_2O_7$. The laboratory-distilled water was successively redistilled from acid permanganate (to oxidize organic products) and hydrated barium hydroxide added for neutralization. The edges of the trough and the barriers were coated with a minute amount of paraffin before each experiment. This paraffin was replaced as soon as there was any sign of surface activity. All parts of the apparatus that came into contact with the surface of the water were handled with tweezers. No other chemical research was permitted in the room.

Despite all these precautions, it was not possible to maintain a clean water surface for more than approximately one minute. The reappearance of impurities increased with time. It was not possible to evaluate the amount of such impurities, but everything possible was done to keep them at a minimum.

Measurement of Surface Area Isotherm.—The Wilhelmy (wettable plate) method was used.[22] If γ_0 is the surface tension of pure water and γ that of water covered by a film, the surface pressure p is defined as $\gamma_0 - \gamma$.

$\gamma_0 - \gamma$ represents for an insoluble film the work necessary to isothermally and reversibly increase by one cm.^{2} the free surface of a liquid covered. It can be broken into: (1) work against instantaneous surface tension of the pure liquid; (2) work gained by the spreading of surface active molecules to an equilibrium state.[26]

For a very dilute surface film, the instantaneous surface tension is very close to the surface tension of the pure liquid, so that

$$\gamma_{soln} = \gamma_0 - W_{adsorptn} = \gamma_0 - p$$

To measure this isotherm, the surface of the water is cleaned, then the wettable plate is put into the surface, noting where it registers on the scale. The surface active material, dissolved in petroleum ether, is introduced onto the water surface from a calibrated pipet. The petroleum ether was distilled in a glass apparatus (b.p. 40–55°) and was tested for purity by evaporating 20 drops on a clean water surface and noting the lack of any residue. Starting with a non-discernible surface pressure, the barrier J is gradually moved, thus decreasing or increasing the area of the film. The surface pressure is measured at each area by the displacement of the light on the scale.

Measurement of the Specific Resistance.—Starting with non-discernible surface pressure we obtained reproducible area isotherms on compression. It is impossible to measure an area isotherm by decompressing a monolayer containing micro-crystals; nevertheless, we have determined the specific resistance *vs.* surface pressure by spreading the film under high pressure and decompressing, because it seems to be the practical way to prevent impurities entering the monolayer.

Reproducible results can be obtained by the following technique: (1) the surface is cleaned many times with blowing air and suction technique. (2) We place the platform in position. (3) The surface water level is adjusted with the movable rod. (4) We remove the platform and the wettable plate K. (5) Barrier J is at F_1 and is pushed toward F_2. (6) The substance is spread as a film under high surface pressure. (7) We replace the platform and plate K. (8) We decompress the film to a certain surface pressure. (9) The desiccant box is opened and placed on the platform. Temperature of the box is noted. A stop watch is started. After a certain time (2 minutes, for example), the box is removed, closed and weighed. The temperature given is again noted. With this technique we have checked the results of Archer and La Mer using saturated fatty acids.

When we create a new water surface (operation No. 5) and immediately deposit the solution, it seems reasonable to suppose that the surface is cleaned by the spreading of the solvent. Since we have a film under high surface pressure the impurities cannot adsorb in surface. This explanation given by Archer and La Mer seems plausible.

Before adopting the technique just cited, we also measured the specific resistance *vs.* surface pressure starting with a non-discernible surface pressure and compressing. The resistance to evaporation under this procedure increased with surface pressure as was reported by Langmuir and Schaefer[13] and by Archer and La Mer (Fig. 3 of reference 12).

The explanation of Archer and La Mer was based primarily on the trapping of solvent molecules in the monolayer on compression. While we do not question the importance of trapping impurities, nevertheless, it is also possible that in the compression and decompression of a monolayer we may not have the same ratio of the several possible configurations in the liquid states of the film. We shall show later that the dependence of resistance upon surface pressure is governed by the compressibility ($dp/d\sigma$) of the substance forming the monolayer, *i.e.*, by the tangents to the area isotherm. To determine the compressibilities as a function of the time and surface pressure or area will require a more sensitive surface manometer than we have used. This means that the surface pressure–area isotherm is relatively insensitive as compared to the resistance–pressure isotherm, so that it may not be possible to detect significant differences in compressibility on compression and decompression.

Measure of the Surface Viscosity of Monolayers.—Figure 1 shows the apparatus as used to measure surface viscosity. It consists of a mica frame V coated with paraffin. A mica

(21) Thesis, Montpellier, France, 1948.

(22) H. L. Rosano, *Memorial Serv. Chem. Etat.*, **36**, 309–341 (1951).

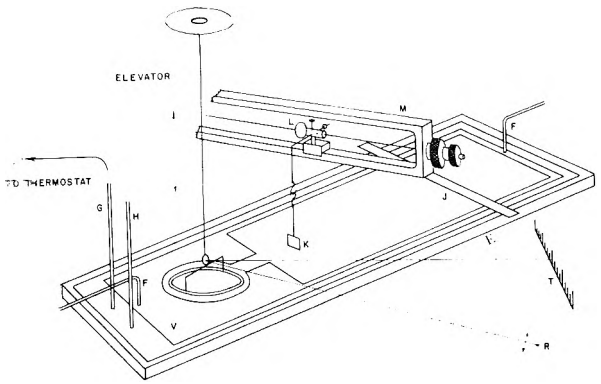

Fig. 1.—Sketch of apparatus for measuring surface viscosity of surface films by the damping of oscillations including the torsion type of Wilhelmy surface balance for measurement of surface pressure. Description of lettered parts in text.

ring floats on the surface of the water and is attached to a vertical torsion wire. Using a light beam reflected from a mirror on the wire, it is possible to measure the decrement of oscillations of the ring for the clean surface water and for the surface monolayer. The damping of the oscillations depends upon the concentration and nature of the surface film, whereby one calculates the surface viscosity of a monolayer. We have used a narrow mica ring coated with paraffin.[23] Surface viscosity can be calculated as

$$\mu = \frac{\sqrt{\Gamma I}}{2\pi} \times \frac{R_2^2 - R_1^2}{R_2^2 R_1^2} \left[\frac{\Delta}{7.4 \mp \Delta^2} - \frac{\Delta_0}{7.4 \mp \Delta_0^2} \right] \quad [1]$$

in which

Γ is the torsion module of the wire
I is the initial moment of the floating system
R_1 is the radius of the moving ring
R_2 is the radius of the fixed ring
Δ_0 is the decrement without film
Δ is the decrement with film

The method of damped oscillations is best adapted for viscous films.

III. Theoretical Basis for Calculating the Specific Resistance of the Monolayer to Evaporation

From diffusion theory, the rate of flow of water vapor through a column of air in a steady state can be expressed by

$$M/t = (w - w_0)/(b/D)(A) \quad (2)$$

where M is the mass of water (in g.) taken up by the solid absorbant in the time t (seconds), A is the cross-sectional area of the diffusion tube, b is the length of the diffusion path (in cm.), and D is the diffusion coefficient of the water vapor in air (in cm.^{2}/sec.), w is the concentration of the water vapor (in g./cm.^{3}) at the surface of the water just above the monolayer, and w_0 is the concentration in similar units at the lower surface of the silk gauze.

Equation 2 suggests an analogy to Ohm's law in the form

$$\text{Rate} = \text{driving force/specific resistance}$$

thus

$$M/t = (w - w_0)/r \quad (3)$$

where r is the sum of the resistance (by unit of cross-sectional area of the diffusion tube) of the water surface—the air column, the membrane and the desiccant surface acting in series. In these conditions two determinations are made of the rate of absorption, one with a monolayer on the water and one without. The specific resistance of the monolayer r is equal to

$$r = (w - w_0)t(A/M_{\text{film}}) - (w - w_0)t(A/M_{\text{no film}}) \quad (4)$$

The rigorous application of equation 2 is possible if we note the temperature of the water and the desiccant absorbant at the beginning and the end of each experiment.[11] The validity of the method has been established.[11,12] The value for w_0 of lithium chloride is taken from graphical data published by Bichowsky.[24] Following Archer and La Mer,[11,12] we have adopted a correction with regard to the additional contribution from water vapor in the surrounding air. For experimental convenience, it was necessary to establish the following relationships

$w = f$ (temperature)
$w_0 = f$ (temperature)
wt. of water absorbed by the surrounding air $= f$ (time)

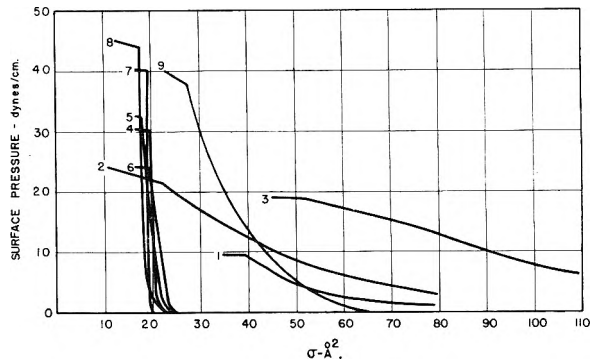

Fig. 2.—Surface pressure–surface area isotherms showing compressible (no. 1, 2, 3, 9) and non-compressible films (4, 8) for substances of Table I.

TABLE I[a]

1	Ethyl palmitate	$C_{15}H_{31}COOC_2H_5$	M.p. 24°
2	Ethyl linoleate	$C_{17}H_{31}COOC_2H_5$	$n^{27}D$ 1.4573
3	Ethyl elaidate	$C_{17}H_{33}COOC_2H_5$	$n^{28.9}D$ 1.4519
4	Ethyl stearate	$C_{17}H_{35}COOC_2H_5$	M.p. 34.4°
5	Arachidic acid	$CH_3(CH_2)_{18}COOH$	M.p. 76°
6	Stearic acid	$CH_3(CH_2)_{16}COOH$	M.p. 68.7°
7	1-Octadecanol	$CH_3(CH_2)_{16}CH_2OH$	M.p. 58.2°
8	Cetyl alcohol	$CH_3(CH_2)_{14}CH_2OH$	M.p. 49°
9	1,1,13-Trihydroperfluorotridecyl alcohol	$H(CF_2)_{12}CH_{20}H$	M.p. 110°

[a] The products 1, 2, 3, 4, 5, 6, 7 and 8 were dissolved in redistilled Merck petroleum ether (b.p. 45–55°) and the product 9 in methyl alcohol (boiling range 64.2–64.7°).

I. Experimental Results

A. Pure Substances. (1) Compression Area Isotherm.—Figure 2 shows the surface pressure–area isotherm for the above substances. The data fall into two categories, the compressible monolayers (substances number 1, 2, 3 and 9), and the relatively incompressible substances (4, 5, 6, 7, 8).

It is not surprising to find that substances with double bonds (nos. 2 and 3) give compressible monolayers. Neither is it surprising in the case of the fluorinated substance as shown by Klevens and Raison.[25] However, it is not always possible to predict *a priori* if a substance will give a compressible or an incompressible film, as in the con-

(23) M. July, *Kolloid Z.*, **126**, 35 (1952).

(24) F. R. Bichowsky, *Chem. Met. Eng.*, 302 (1940).

(25) H. B. Klevens and M. Raison, *J. chim. phys.*, **51**, 1–8 (1954).

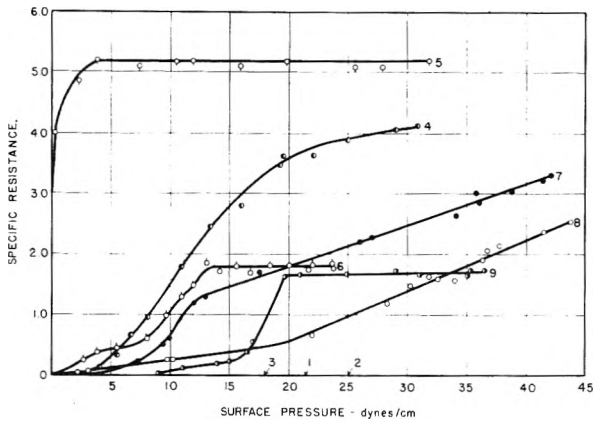

Fig. 3.—Reduction in rate of evaporation of water through a monolayer by substances listed in Table I in terms of the specific resistance to evaporation as a function of the surface pressure. Note the very low resistance of the esters 1, 2, 3 and the high resistance of saturated fatty acids—stearic and arachidic.

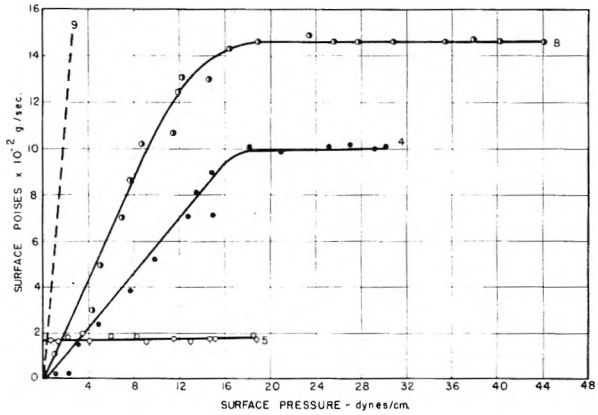

Fig. 4.—Surface viscosity (in 10^2 poises) as a function of surface pressure for substances of Table I.

trasting behavior of the two esters: ethyl palmitate and ethyl stearate.

(2) **Specific Resistance *vs.* Surface Pressure.**—Figure 3 gives the results of specific resistance measurements. The products 1, 2 and 3 are ineffective for reducing the rate of evaporation of water. These products also give compressible films (Fig. 2). The effective substances have relatively incompressible films. Except for the fluorinated alcohol, which we shall discuss later, we are led to the general conclusion that *for substances with hydrocarbon tails, the resistance to evaporation of a monolayer is determined by the compressibility.*

We have also checked the results of Archer and La Mer for the C_{18} and C_{20} acids in the range of 12 to 24 dynes/cm. where the specific resistance is independent of the surface pressure. When the surface pressure is below 12 dynes/cm. the data indicate that (a) in the case of the acid C_{20} the specific resistance of the monolayer remains practically independent of the surface pressure down to 3 dynes/cm., and (b) in the case of C_{18} acid below 13 dynes/cm. the specific resistance decreases with decreasing surface pressure.

From the other curves it can be seen that there are regions where the resistance is independent of surface pressure (no. 9 between 18 dynes/cm. and saturation) and also regions where the specific resistance is an increasing function of surface pressure (curves 4, 7, 8).

Generally the specific resistance is independent of the surface pressure only for certain substances and certain ranges of that pressure. Those substances exhibiting compressible films show little or no resistance to evaporation.

(3) **Surface Viscosity *vs.* Surface Pressure.**—Only three curves are given in Fig. 4 since the method used was not sensitive enough to determine the viscosity of the more fluid monolayers. The fluorinated alcohol (no. 9) has a high viscosity.

Even though there appears to be no relationship between specific resistance and surface viscosity, an examination of the two curves for any one product shows that both curves have approximately the same slope at any given pressure. The discontinuities in the slope of the surface viscosity *vs.* surface pressure curves have been ascribed by Joly[23,26] to changes of phases in the monolayers. Since these discontinuities in the slopes of the specific resistance *vs.* surface pressure curves occur at the same surface pressure, it seems highly plausible that a change in the specific resistance of a monolayer reflects a change in the structure of the film.

On comparing curves for products 6 (stearic acid) and 9 (fluorinated alcohol) we find that 6 is non-compressible and non-viscous, and 9 is compressible and very viscous. Yet we see that both 6 and 9 have approximately the same specific resistance in their most effective regions. This suggests that resistance to evaporation through a monolayer depends on two effects: (a) cohesive forces residing in the monolayers (compressible films are not effective); (b) adhesive forces between the monolayer and the sub-phase due to hydrogen bonding.

In product 9 even though this film is fairly compressible, the increase in cohesive forces, in the tails of the fluorinated compound, which are evident from the extremely high value of surface viscosity, lead to an appreciable specific resistance.

B. Mixtures.—Mixtures have been studied for two reasons: (a) to see the effect of impurities on the measurement of the specific resistance; (b) to see if it is possible to get mixtures that are still effective in reducing evaporation but which have properties that are more desirable than the pure substances alone (lower melting point of mixtures for practical purposes).

Under (a) we chose two substances of similar compressibility and under (b) a mixture of a compressible and a non-compressible substance.

(1) **Mixture of Arachidic and Stearic Acids: 50/50 Molecules.**—Figure 6 shows that this mixture obeys approximately the formula

$$1/r \text{ mixture} = 1/r \text{ arachidic acid} + 1/r \text{ stearic acid}$$

The conductances are additive as was suggested by Langmuir and Schaefer.

(2) **Mixture of Arachidic Acid and Ethyl Palmitate: 80/20 Molecules.**—The specific resistance *vs.* surface pressure for pure ethyl palmitate monolayers shows no appreciable decrease in the rate of evaporation (curve 1 of Fig. 3) of water. If the law of the additivity of reciprocal resistances is generally applicable, then any substance mixed

(26) M. Joly, *J. chim. phys.*, **44**, 215 (1947).

with ethyl palmitate should exhibit no appreciable effect on the rate of evaporation of water. However, an experiment with mixtures of (20 mole %) ethyl palmitate and (80 mole %) arachidic acid shows an appreciable effect on the rate of evaporation contrary to expectation (Fig. 7). This result can be understood in the following way.

Since the C_{18} and C_{20} fatty acids exhibit almost identical compression–area isotherms, a mixture of these two acids should exhibit a similar behavior (Fig. 5). Actually, the mixtures show slightly

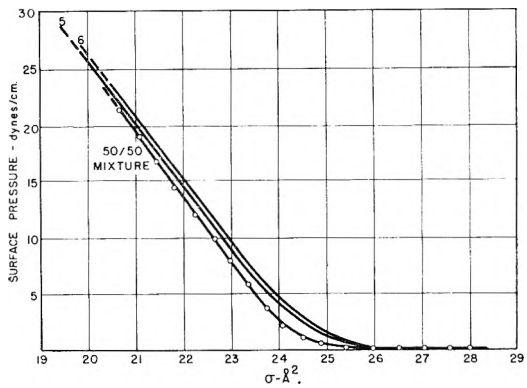

Fig. 5.—Surface pressure–surface area isotherm of the mixed film formed from a 50/50 mixture of pure stearic[4] and pure arachidic[15] acids.

smaller areas at given pressures, and likewise the measured resistance (Fig. 6) of the mixture is somewhat below the theoretical curve for the additivity of the reciprocal resistances. These minor effects may be within the experimental error.

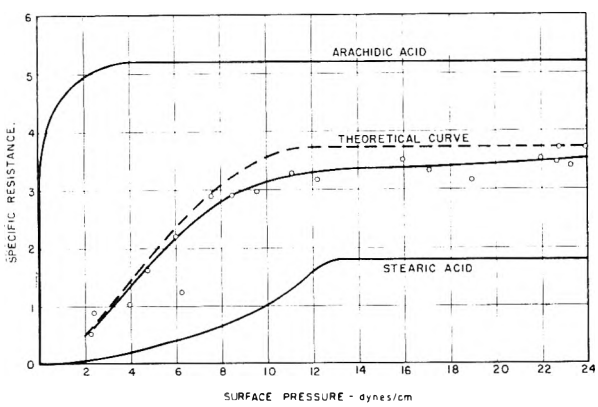

Fig. 6.—Specific surface resistance to evaporation through a mixed film composed of 50 mols stearic (C_{18}) acid and 50 mols arachidic (C_{20}) acid. The theoretical curve is computed on the basis of the additivity of the individual reciprocal resistances or conductances of the pure substances.

On the other hand, in the case of two substances of different chemical type (acid and ester), the reciprocal resistances are not additive for the mixed film (Fig. 7). The resistance of ethyl palmitate is so low that on the basis of this rule its conductance should dominate the conductance of any mixed film containing any appreciable amount of the ester.

Figure 8 shows the compression–area isotherms of the pure substances and their 80 acid/20 ester mixture. This mixture exhibits a compressibility very similar to that of the pure acid.

However, when we examine the evaporation resistance of this mixture (Fig. 7), we find that in the

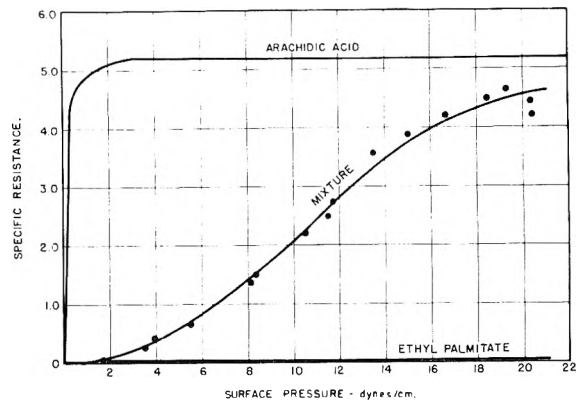

Fig. 7.—Specific surface resistance to evaporation as function of surface pressure of mixed film prepared from a mixture containing 80 mols of arachidic (C_{20}) acid and 20 mols of ethyl palmitate.

limit of low pressures, the resistance of the mixture approaches that predicted by the additivity of reciprocal resistances. In any case, the limiting tangent at low pressures approaches that of the ester and not that of the C_{20} acid.

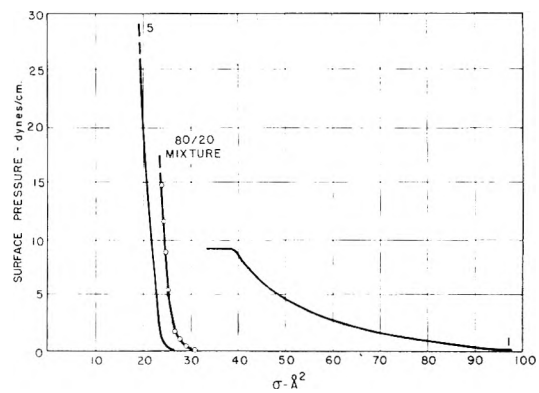

Fig. 8.—Surface pressure–area isotherm of the mixed film of 80 mols arachidic acid–20 mols ethyl palmitate corresponding to the resistance measurements of Fig. 7.

As the pressure is increased, the resistance of the film spread from the mixture rises rapidly and in the limit seems to approach the high resistance of the arachidic acid component.

This behavior is explicable. At low pressures the interaction forces between the molecules in the monolayer are weak with the result that every molecule more or less exhibits its own specific resistance which adds in parallel. On the other hand, with increasing pressure, the interaction forces increase rapidly with decrease in area, so that the additivity rule fails completely.

Near the pressure for the collapse of the mixed film, the ethyl palmitate molecules are squeezed out and the resistance approaches the high value for the arachidic acid component.

In practice this result has importance. A solid substance which has a pronounced effect on the rate of evaporation can be mixed with another product thereby making a liquid easier to spread without reducing the rate of evaporation, provided it is maintained under pressure.

C. Miscellaneous Observations.—Before adopting the decompression technique of measuring resistance to evaporation, a number of substances,

not listed in Table I, were tested by compressing the film spread at low pressures. Cyclohexyl myristate and also ethyl oleate gave easily compressible films producing very little reduction in the rate of evaporation. Methyl stearate on compression from 0.3 to 11 dynes/cm. reduced the rate of evaporation by a practically constant value of 12%. Lauryl alcohol gave a low resistance to evaporation which was practically constant (0.21 to 0.37) over a wide range of pressures (1.4 to 41 dynes/cm.).

With arachidic acid even at non-discernible pressures, there is a noticeable effect (reduction of 15%) on the rate of evaporation. On compressing this film the rate decreased rapidly as soon as discernible pressures were noted until at about 22 dynes/cm. the rate of evaporation becomes 60% of that of pure water.

Acknowledgment.—H. L. R. wishes to gratefully acknowledge the grant of a Fellowship from the International Cooperation Administration, Washington, D. C., which made this work possible.

ADSORPTION OF GASES ON A SILICON SURFACE

BY J. T. LAW AND E. E. FRANCOIS

Bell Telephone Laboratories, Incorporated, Murray Hill, New Jersey

Received August 23, 1955

An investigation of the adsorption of argon, nitrogen, carbon dioxide, carbon monoxide, hydrogen, oxygen and water vapor on a silicon surface has been carried out using a mass spectrometer and a flash filament technique. All measurements were made at 300°K. and gas pressures between 10^{-7} and 10^{-4} mm. The decomposition of carbon dioxide and water vapor at various temperatures has also been studied.

Introduction

The adsorption of gases on germanium has recently been studied[1,2] using the flash filament technique[3] but up to the present, no work has been done on silicon. It has been shown by various workers[4] that the state of the surface (*i.e.*, extent and nature of adsorbed material) can have a marked effect on the electrical properties of the semiconductor, so that a study of the adsorption of gases is a prerequisite to understanding the physics of the surface region.

The purpose of this paper is to present a survey of the adsorption properties of gases on silicon which have been investigated using a flash filament technique and a mass spectrometer as a pressure measuring device. Any initial study of this type must use a mass spectrometer to identify decomposition products of the adsorbed gas. The adsorption of argon, nitrogen, hydrogen, carbon monoxide, carbon dioxide, oxygen and water have been studied in this manner.

Experimental

Apparatus.—A filament having the dimensions 2 × 2 × 100 mm. was cut from a single crystal of 5 ohm cm. n-type silicon. It was lapped with 600 mesh carborundum and etched,[5] after which molybdenum leads were welded to the ends. The filament was then mounted in a glass jacket and connected to the inlet line of a Consolidated mass spectrometer as described previously. The tube containing the silicon filament was pumped through the ionization chamber of the mass spectrometer, from which the inlet leak had been removed. The heating current for the filament was supplied by means of a manually operated variac. Because of the large change in resistance of the filament in going from room temperature to 500°, very little control of temperature over this range was possible.

During a flash run the mass spectrometer was focused on the mass of an ion fragment of the gas being investigated and a record of the gas desorbed made on the recording oscillograph. At the same time the change in pressure was read on the ion gage. Temperatures within the range of visible radiation were determined with an optical pyrometer using an emissivity correction of 0.40 and at the same time the resistance of the filament was measured. Values of the conductivity obtained in this way are shown in Fig. 1 compared with data obtained by Morin and Maita[6] at lower temperatures. All the points fall on the same straight line and in fact the agreement is so good that it may

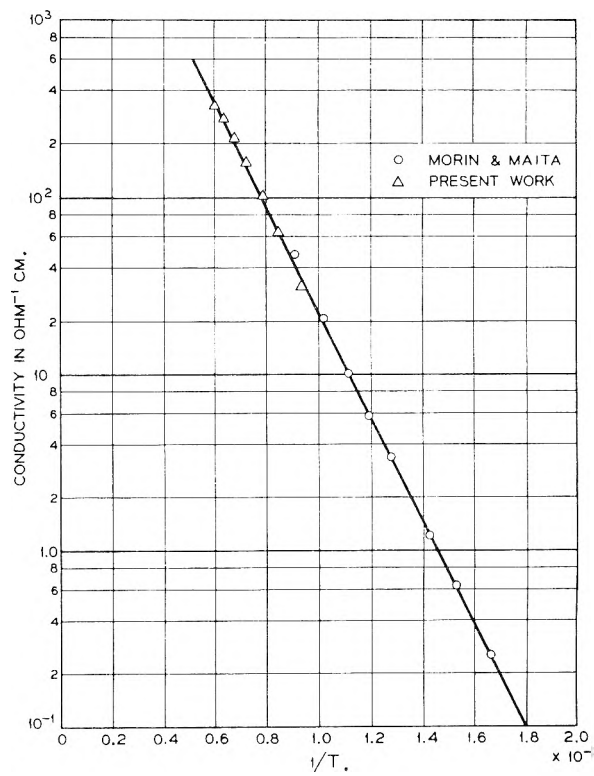

Fig. 1.—Conductivity of intrinsic silicon as a function of temperature.

(1) J. T. Law and E. E. Francois, *Ann. N. Y. Acad. Sci.*, **58**, 925 (1954).

(2) J. T. Law, THIS JOURNAL, **59**, 543 (1955).

(3) L. Apker, *Ind. Eng. Chem.*, **40**, 846 (1948); J. A. Becker and C. D. Hartman, THIS JOURNAL, **57**, 157 (1953).

(4) W. H. Brattain and J. Bardeen, *Bell System Tech. J.*, **32**, 1 (1953); E. N. Clarke, *Phys. Rev.*, **91**, 756 (1953); W. L. Brown, *ibid.*, **91**, 518 (1953).

(5) Twenty-five cc. of concd. nitric acid and 25 cc. of 48% HF.

(6) F. J. Morin and J. P. Maita, *Phys. Rev.*, **96**, 28 (1954).

be fortuitous. The determination of filament temperature with an optical pyrometer should not be much more accurate than ±5–10°.

Procedure.—The silicon filament was outgassed for several days in the best vacuum attainable in the system ($\sim 10^{-8}$ mm.). The most difficult species to remove from the surface is probably oxygen, but in the case of silicon, the stable oxide at high temperature is the monoxide. Its vapor pressure has been measured by Gel'd and Kochnev[7] and by Schäfer and Hörnle[8] who obtained values at 1200° of 8×10^{-2} and 4×10^{-1} mm., respectively. These values are sufficiently high that if the surface oxide behaves at all like the bulk oxide, it will be removed at temperatures close to the melting point of silicon. The data obtained in the present work were reproducible, in that if after adsorption the filament was flashed, it again adsorbed the same amount of gas as previously.

The principal methods used to investigate the adsorption and reaction of gases were as follows.

(1) The filament was flashed several times to 1200° (the melting point is 1420°) *in vacuo* and then the gas introduced to the filament volume while the silicon was cold. After varying time intervals, and with the gas still flowing, the filament was flashed focusing on a peak characteristic of the gas. When the silicon was heated the pressure rose sharply and then fell as the system pumped out. At the same time the pressure change was read on the ion gage. To test the reversibility of the isotherm the gas can be pumped out before the filament is flashed. In the pressure range 10^{-7}–10^{-4} mm. the change in pressure on flashing was between 10^{-6} and 10^{-5} mm. This method was used for argon, nitrogen, hydrogen, carbon monoxide, carbon dioxide and water.

(2) In cases where reaction occurred, the following method was used. The mass spectrometer was focused on an ion fragment of one of the reaction products with the gas flowing through the system and the filament cold. The silicon was now heated in steps of 100 or 50° and a continuous record obtained of the partial pressure of the decomposition product. The values obtained are steady state rather than equilibrium ones since gas is continuously flowing through the system. The decompositions of water and carbon dioxide were investigated in this way.

(3) The amount of oxygen adsorbed on the silicon surface cannot be determined by flashing the filament, since it will come off as a silicon oxide, which, because of its low volatility, will not reach the ionization chamber. However, there is an alternative way of obtaining the amount of adsorption. In Fig. 5 two curves are shown for pressure in the system as a function of time. Curve B was obtained after flashing the silicon in a high vacuum, allowing it to cool and then admitting oxygen. After the completion of this run, the system was pumped out with the filament remaining cold, and then oxygen readmitted giving curve A. The initial part of curve A is due to the time taken by the system to come to pressure equilibrium after gas is admitted into the vacuum. The difference between the two curves must be due to adsorption either on the glass walls or on the silicon. To eliminate the former possibility the filament was flashed *in vacuo* for a time which was insufficient to cause any heating of the glass walls (and therefore desorption of oxygen) and then oxygen was readmitted. Curve B was once more obtained so we must conclude that the adsorption observed is on the silicon filament. Becker and Hartman[3] have shown that it is possible to calculate the amount of gas adsorbed from curves of the type shown in Fig. 5. If the peak investigated was common to more than one gas, it was necessary to focus on another peak that was peculiar only to the gas investigated, in order to separate the effects. The purity of the gases used was checked by carrying out a sweep over the whole mass range in each case.

Calculation of Results

The peak heights observed on the mass spectrometer represent pressure readings in the ion chamber and the relationship between peak height and pressure differs from one gas to another. For this reason the instrument was calibrated for each gas by establishing a known pressure (usually 10^{-3} mm.) on the high pressure side of the leak and measuring the corresponding peak height obtained. The pressure drop across the leak is known for all the gases studied. The values obtained could be checked by measuring the pressure in the filament vessel with the ion gage at the same time as the peak height. The values never disagreed by more than 10%.

The volume of the system is known so that the number of molecules desorbed per unit area may be calculated from

$$N = \frac{KV\Delta P}{A}$$

where K is the number of molecules per liter for $p = 1$ mm. (at 300°K., $K = 3.2 \times 10^{19}$), V is the volume of the system, ΔP the change in pressure (in mm.) on flashing, and A is the area of the silicon in cm.^{2}.

The CP-4 etched filament has a highly polished surface and a geometrical area of 8 cm.^{2}. After the cleanup process was complete, it had the appearance of a sandblasted surface with a real area of greater than 8 cm.^{2}. From our work with germanium we know a sandblasted surface has a roughness factor of 3 because it adsorbs 3 times more gas than an etched surface. A study of the surface of a sandblasted silicon filament compared with one that had been through the cleanup process was made using the electron microscope. It was found that the surface of the filament from the cleanup process was slightly less rough than that from the sandblasted filament. A roughness factor of 2.5 was established giving a true surface area of 20 cm.^{2}. Hence, $N = 6.4 \times 10^{18}\ \Delta P$ for a volume of 4 liters.

Results

The adsorption of all the following gases was studied at 300°K. and at gas pressures between 10^{-7} and 10^{-4} mm.

Argon and Nitrogen.—Argon and nitrogen were introduced individually to the silicon filament. In each case no desorption was observed on flashing the filament to 600°. One may therefore assume that at 300°K. and at pressures below 10^{-4} mm. no adsorption of argon and nitrogen occurs. This is the same result that was obtained for germanium under the same conditions.

Hydrogen and Carbon Monoxide.—These two gases adsorbed appreciably and without reaction. The amount of gas adsorbed was measured as a function of the time for which the gas had been in contact with the silicon. From the first part of this type of curve it is possible to calculate a sticking probability or the fraction of molecules striking the surface that are adsorbed.

The number of molecules of a gas at rest that strike unit area per unit time is given by

$$\upsilon = 3.513 \times 10^{22} \frac{P_{mm}}{\sqrt{MT}}\ \text{cm.}^{-2}\ \text{sec.}^{-1}$$

For hydrogen at 300°K. and a pressure of 1 mm.

$$\upsilon = 1.43 \times 10^{21}\ \text{cm.}^{-2}\ \text{sec.}^{-1}$$

and for carbon monoxide $\upsilon = 3.8 \times 10^{20}$ cm.$^{-2}$ sec.$^{-1}$. The number of molecules adsorbed by the filament per second is given by $\upsilon p a_f s$ where p is the

(7) P. V. Gel'd and M. I. Kochnev, *Doklady Akad. Nauk SSSR*, **61**, 649 (1948).

(8) H. Schäfer and R. Hörnle, *Z. anorg. allgem. Chem.*, **263**, 261 (1950).

gas pressure in mm., a_f is the area of the filament in cm.^{2} and s is the sticking probability.

From the initial slopes of the curves obtained experimentally, s is found to be approximately 10^{-5} for both hydrogen and carbon monoxide. This means that only one molecule is adsorbed for every 10^5 that strike the surface. However, the value of s may be too low, because the filament takes a finite time to cool to room temperature after the flash which occurs at $t = 0$. This means that during the first part of the curve the adsorption is occurring on a surface which is at a temperature greater than 300°K. and as it is found that complete desorption occurs at temperatures close to 600°K. the low value of s obtained seems reasonable. In the previous work on germanium similar values were obtained for the sticking probability.

In Figs. 2 and 3 the number of molecule of hydrogen and carbon monoxide adsorbed per cm.^{2}

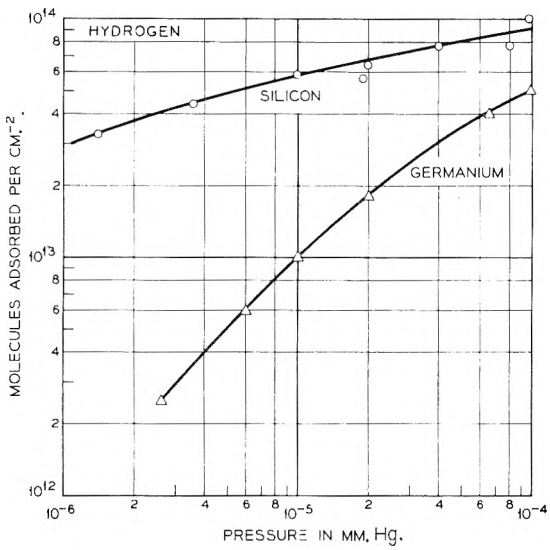

Fig. 2.—The adsorption isotherms for hydrogen on silicon and germanium at 300°K.

is shown as a function of the equilibrium gas pressure. In the same figures are included data obtained on germanium.[2] The agreement between the values of the number of molecules of carbon monoxide adsorbed, obtained from the ion gage and from the mass spectrometer was within 10%. The isotherms for hydrogen and carbon monoxide were not reversible, *i.e.*, the amount of material desorbed was independent of whether or not the pressure was reduced before flashing the filament. This would indicate that the adsorptive forces are stronger than purely van der Waals or dispersive forces. This conclusion is borne out in the case of hydrogen by the fact that although its boiling point is much lower than that of carbon monoxide, the amount of material adsorbed at a given pressure is greater by a factor of two or three.

Dyakonov and Samarin[9] have reported that hydrogen is weakly absorbed by silicon in the temperature range 300–1200°. If this had occurred during our measurements we should have seen a decrease in pressure on heating in this temperature range.

(9) I. A. Dyakonov and A. Samarin, "Bull. acad. sci. URSS," Class sci. tech. 1945, 813.

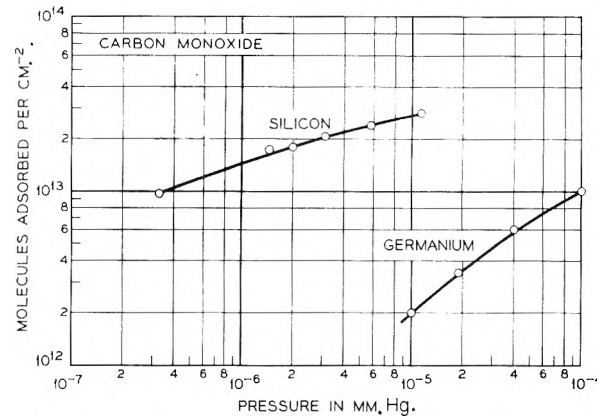

Fig. 3.—The adsorption isotherms for carbon monoxide on silicon and germanium at 300°K.

No such change was observed so that any absorption must be very small.

Carbon Dioxide.—When the filament was flashed after being left in contact with carbon dioxide at pressures up to 10^{-4} mm. no desorption of CO_2 occurred. The carbon monoxide peak was also investigated to determine whether any dissociation had occurred on the surface. None was found so that at room temperature (300°K.) and pressures below 10^{-4} mm. no dissociative or non-dissociative adsorption of carbon dioxide occurs.

When carbon dioxide was passed over the silicon filament, heated to temperatures above 800°, decomposition occurred to carbon monoxide and presumably an oxide of silicon

$$Si(s) + 2CO_2(g) \rightleftarrows SiO_2(s) + 2CO(g) \quad (1)$$

or

$$Si(s) + CO_2(g) \rightleftarrows SiO(g) + CO(g) \quad (2)$$

This decomposition was investigated by the method described above. In Fig. 4 the partial pressures of carbon monoxide and carbon dioxide are shown as a function of the silicon temperature.

Two runs were carried out varying the initial pressure of carbon dioxide by a factor of 3. The ratio $(CO)/(CO_2)$ for these two runs was identical. As the data were obtained under steady state rather than equilibrium conditions (a stream of gas was flowing through the system) no calculation of thermodynamic data is possible.

Oxygen.—The amount of oxygen adsorbed on the silicon surface was investigated as described above. From the curves shown in Fig. 5 it is possible to calculate the number of oxygen molecules adsorbed and also the sticking probability.

Let L be the number of oxygen molecules entering the system per second through the leak. The number of molecules leaving the system per second through the pump $= 3.6 \times 10^{20} p a_p$ where 3.6×10^{20} is the number of oxygen molecules striking one cm.^{2} per second when the pressure is one mm. and $T = 300$°K. p is the pressure in mm. and a_p is the area of the hole through which gases are pumped out. (In the present case $a_p = 6.7 \times 10^{-2}$ cm.^{2}.) The number of molecules removed from the volume per second by the filament $= 3.6 \times 10^{20} p a_f s$ where a_f is the area of the filament in cm.^{2} and s is the sticking probability. Let C be the number of molecules per second accumulating in the volume V.

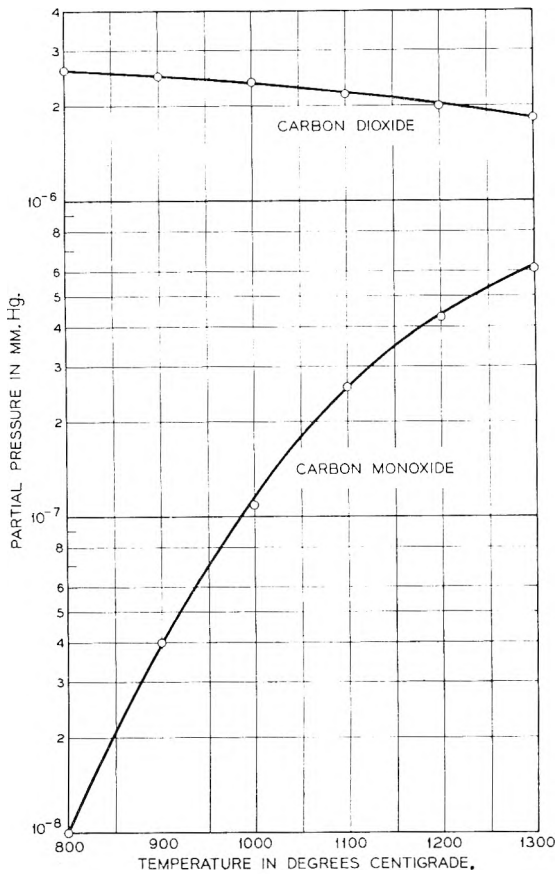

Fig. 4.—The partial pressures of carbon monoxide and carbon dioxide over silicon as a function of the temperature of the silicon filament.

Then $C = 3.2 \times 10^{19} V(\mathrm{d}p/\mathrm{d}t)$. Over most of the run C is small and may be neglected, as $\mathrm{d}p/\mathrm{d}t$ is small. At any time t in the experiment, the rate at which molecules enter the volume less the rate at which they leave must equal the rate of accumulation. Hence

$$L - 3.6 \times 10^{20}(pa_p + pa_f s) \approx 0$$

When s is small or zero

$$L = 3.6 \times 10^{20} p_0 a_p$$

where p_0 is the value of p when $s = 0$, *i.e.*, when the filament is saturated. Hence

$$s = \frac{a_p}{a_f} \times \frac{p_0 - p}{p}$$

Let N_a equal the number of molecules per cm.^{2} adsorbed on the silicon surface at time t, then

$$\frac{\mathrm{d}N_a}{\mathrm{d}t} = 3.6 \times 10^{20} ps = 3.6 \times 10^{20} \frac{a_p}{a_f}(p_0 - p)$$

and

$$N_a = 3.6 \times 10^{20} \frac{a_p}{a_f} \int_0^t (p_0 - p)\,\mathrm{d}t$$

This means that the number of molecules adsorbed per cm.^{2} of silicon is proportional to the area between curves A and B of Fig. 5 from 0 to t.

In the present apparatus

$$N_a = 1.21 \times 10^{18} \int_0^t (p_0 - p)\,\mathrm{d}t$$

The results obtained from this equation are given by the dashed line in Fig. 5. From the values of the

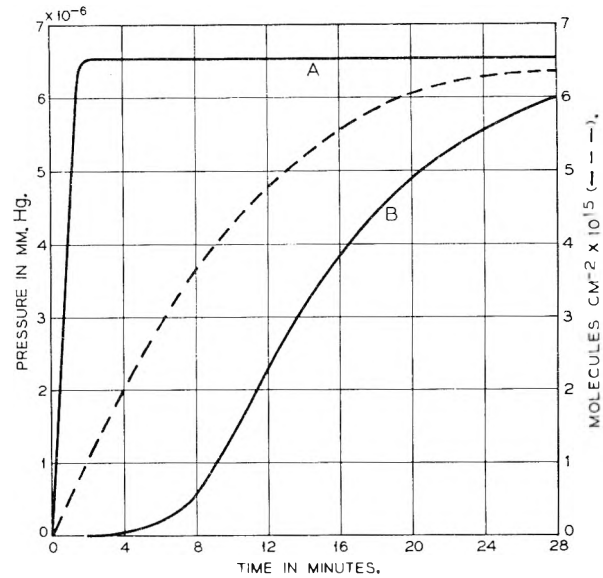

Fig. 5.—Pressure in the system as a function of time after admission of oxygen. Curve A shows no adsorption, curve B shows adsorption. Dashed curve shows number of molecules of oxygen adsorbed per cm.^{2} as a function of time.

amount of oxygen adsorbed and the gas pressure shown in Fig. 5, it is possible to calculate values of the sticking probability. If we assume that the rate of evaporation of oxygen atoms is negligible, then

$$s = \frac{N'}{\upsilon p}\frac{\mathrm{d}\theta}{\mathrm{d}t}$$

where $\upsilon = 3.6 \times 10^{20}$ molecules cm.$^{-2}$ sec.$^{-1}$, p is the gas pressure, N' is the number of molecules in a monolayer and $\mathrm{d}\theta/\mathrm{d}t$ is the variation in coverage with time. N' is equal to 10^{15} molecules cm.$^{-2}$ if we assume one oxygen *molecule* per surface silicon atom and average over the various crystal faces. Values of s calculated in this way are shown in Fig. 6 as a function of θ. The most striking thing about the curve is the rapid decrease in s after one layer of oxygen is adsorbed. In going from one to five layers of oxygen on the surface, s decreases by three orders of magnitude. During the adsorption of the first layer, s is close to unity, *i.e.*, almost every oxygen molecule that strikes the surface is adsorbed.

This marked decrease in s is what one would expect because only the first layer of oxygen can really be considered as chemisorbed. Beyond this we are forming an oxide film which is obviously quite a different process. The value of 6×10^{15} molecules taken up at room temperature agrees quite well with the data obtained by Allen and Mitchell[10] for oxygen on copper. They found that at 300°K. and an oxygen pressure of the order of 10^{-3} mm. an oxide film of 24 Å. thickness was formed in about 60 minutes.

It may be worthwhile to attempt a calculation of the heat of adsorption of oxygen on silicon and germanium. Eley[11] has shown that if one assumes that the chemisorptive bond is of the covalent type, the heat of adsorption can be calculated in terms of the bond energies $E_{(M-O)}$ and $E_{(O-O)}$ where $E_{(M-O)}$

(10) J. A. Allen and J. W. Mitchell, *Disc. Faraday Soc.*, **8**, 309 (1950).

(11) D. D. Eley, *ibid.*, **8**, 34 (1950).

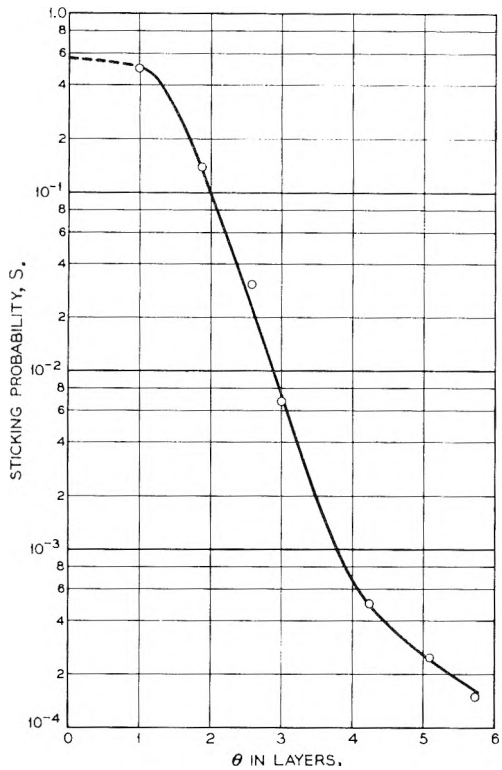

Fig. 6.—The sticking probability s of oxygen on a silicon surface as a function of coverage.

refers to the adsorbent–oxygen bond and $E_{(O-O)}$ is the dissociation energy of oxygen. He assumed that the energy of the surface M–O bond was given by Pauling's[12] equation

$$E_{(M-O)} = {}^1/_2(E_{(M-M)} + E_{(O-O)}) + 23.06\,(X_M - X_0)^2$$

Where $E_{(M-M)}$ is the adsorbent atom–adsorbent atom bond strength and X_M and X_O are the electronegativities of the adsorbent and oxygen atoms, respectively.

Hence the heat of adsorption, which was given by

$$\Delta H_{Ads} = -2E_{(M-O)} + E_{(O-O)}$$

becomes

$$\Delta H_{Ads} = -E_{(M-M)} - 46.12\,(X_M - X_0)^2$$

Stevenson[13] has obtained values of X_M from the work function φ_M of the adsorbent material ($X_M = 0.355\varphi_M$) and used Pauling's[12] assignment of electronegativities for the gas atoms. By this means he obtains values of the heat of chemisorption of hydrogen on a number of metals in good agreement with experiment.

The value of $E_{(M-M)}$ is a fraction ($^1/_4$) of the heat of vaporization of the adsorbent. The heat of vaporization of silicon is given by Ruff[14] as 105.5 kcal. mole^{-1} and that of germanium as 91.5 kcal. mole^{-1} by Searcy and Freeman.[15] Assuming a work function of 4.8 e.v. for both substances and X_0 equal to 3.5 the heats of adsorption (ΔH_{ads}) of oxygen are found to be: silicon, 173 kcal./mole; germanium, 170 kcal./mole.

If these values are at all correct it is not surprising that a monolayer of oxygen was adsorbed on silicon at pressures near 10^{-6} mm. It is disturbing, however, that a similar adsorption was not noticed on germanium. Recently Green and Kafalas[16] have shown that approximately 1–2 layers of oxygen are adsorbed on germanium at room temperature and pressures near 10^{-3} mm. so that both heats of adsorption may be nearly correct. In the previous work on germanium the adsorption of a monolayer or less of oxygen would not have been detected as the time required for the system to come to pressure equilibrium after the admission of gas would be quite short.

Water.—Both the desorption and decomposition of water vapor at a silicon surface have been investigated.

When water vapor was passed over the silicon filament heated to temperatures above 600°, decomposition occurred to give hydrogen and presumably an oxide of silicon

$$Si(s) + H_2O(g) \rightleftarrows SiO(g) + H_2(g)$$

or

$$Si(s) + 2H_2O(g) \rightleftarrows SiO_2(s) + 2H_2(g)$$

This reaction was investigated by the method described above, the partial pressures of water and hydrogen being measured as a function of the temperature of the silicon.

If the above equilibria exist one can define equilibrium constants by

$$K_1 = \frac{[SiO][H_2]}{[H_2O]} \text{ and } K_2 = \frac{[H_2]^2}{[H_2O]^2}$$

assuming that both Si and SiO_2 are present in the solid form, *i.e.*, their activities are unity.

In Fig. 7 the ratio $[H_2]^2/[H_2O]^2$ is plotted as a function of silicon temperature. It was shown above that the reaction measurements were not made under equilibrium conditions, so we will not attempt to calculate any thermodynamic quantities. It is worthwhile mentioning, however, that the corresponding reaction of water vapor with germanium was found[1] to begin at about the same temperature.

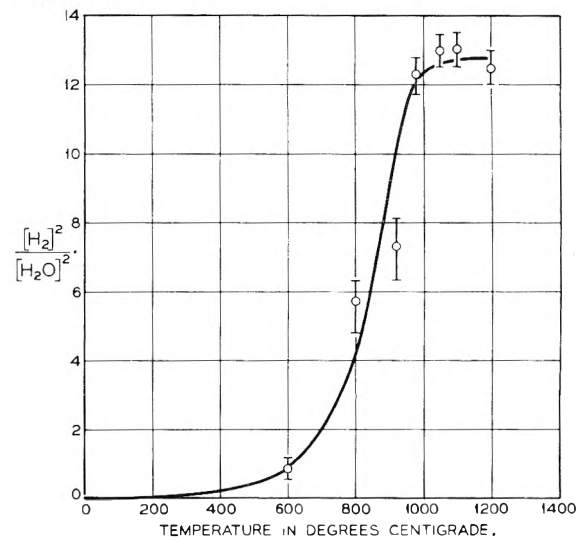

Fig. 7.—The ratio $[H_2]^2/[H_2O]^2$ as a function of filament temperature.

(12) L. Pauling, "The Nature of the Chemical Bond," Cornell Univ. Press, Ithaca, N. Y., 1939.

(13) D. P. Stevenson, *J. Chem. Phys.*, **23**, 203 (1955).

(14) O. Ruff, *Trans. Electrochem. Soc.*, **68**, 87 (1935).

(15) A. W. Searcy and R. D. Freeman, *J. Chem. Phys.*, **23**, 88 (1955).

(16) M. Green and J. A. Kafalas, The Electrochemical Society Meeting, Cincinnati, O., May, 1955.

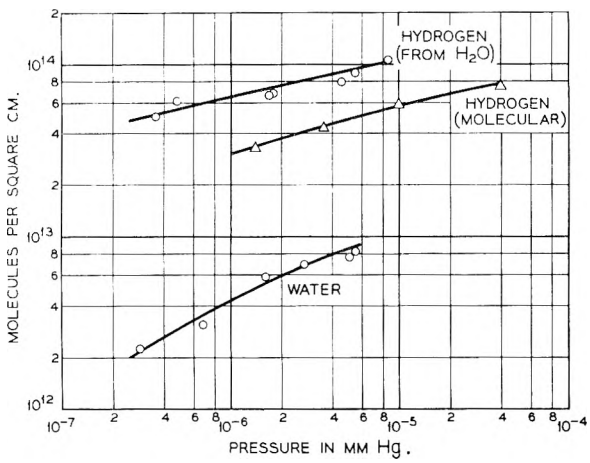

Fig. 8.—The adsorption isotherms for water and the hydrogen produced by decomposition on the surface compared to the isotherm for molecular hydrogen at 300°K.

The results obtained for the desorption of water are shown in Fig. 8. It was found that when the filament was flashed after the adsorption of water vapor, most of the gas desorbed was hydrogen, the ratio of hydrogen to water desorbed being approximately 10:1. In Fig. 8 curves are given for the number of molecules of hydrogen and water vapor desorbed as a function of the water vapor pressure with which the filament had been in contact. The curve obtained for the desorption of molecular hydrogen is also shown. Twice as much hydrogen is desorbed after the adsorption of water vapor as compared to the adsorption of molecular hydrogen. It is believed that the decomposition of the water molecule occurs at room temperature on the surface due to the formation of a strong silicon–oxygen bond. In the case of germanium, some hydrogen was also produced, but the amount of hydrogen desorbed was one-tenth of the amount of water vapor, the exact opposite to what we find with silicon. If one adds the amount of hydrogen and water desorbed one should get a measure of the number of molecules of water originally on the surface. At a pressure of 10^{-4} mm. this corresponds to about one-tenth of a monolayer, *i.e.*, much less than the amount of oxygen adsorbed at the corresponding pressure.

SWELLING OF PROTEIN MOLECULES IN SOLUTION AND THE α-β TRANSFORMATION

BY TERRELL L. HILL

Naval Medical Research Institute, Bethesda, Maryland

Received August 24, 1955

The suggestion of Yang and Foster that bovine serum albumin swells at low *p*H because of an α-β transformation is examined theoretically using a necessarily approximate treatment. The conclusion reached is that the Yang-Foster mechanism is a reasonable possibility. The theory, in its present form, predicts a salt effect of opposite sign to that found experimentally. Refinements in the theory will presumably remove this discrepancy.

Yang and Foster[1] have found evidence from viscosity and optical rotation measurements for molecular swelling in bovine serum albumin in the *p*H range 2–4. They suggest, as a tentative explanation, that the apparent swelling which occurs as the *p*H is lowered below about 4, is due to the increased positive charge on the molecule initiating an $\alpha \rightarrow \beta$ transformation in the peptide chains of the protein. The object here is to present a few calculations designed to test, qualitatively, the reasonableness of the above explanation from a theoretical point of view.

It should be pointed out that an α-β transition allows a long chain to increase its length essentially continuously; thus an α-β transition should not be considered an example of an "all-or-none" transition[1] for the whole chain or molecule. See, however, the discussion of Fig. 1.

The model used is necessarily quite approximate. Refinements of the model and more extensive calculations hardly seem justified until the Yang-Foster suggestion[2] is more firmly established. Incidentally, the recent deuterium exchange work of Linderström-Lang might be applied here to test the α-β hypothesis.

In earlier papers[3] the elasticity of sheets of peptide chains (involving an α-β transition) was investigated. The needs of the present problem can be met by making appropriate modifications in this earlier work.

The Model

As a model of a single protein molecule in solution, we use an equivalent sphere of somewhat cross-linked peptide chains (there are 16 disulfide linkages in a bovine serum albumin molecule).[1] In the *p*H range of interest here, the chains are assumed uncoiled in the usual polymer statistics sense.[4] But to the extent that the chains are in the α-helical form, they can be lengthened by going over into an extended (β) configuration. We visualize the molecule as essentially a small sphere of S-S cross linked isotropic gel, so that we are not

(1) J. T. Yang and J. F. Foster, *J. Amer. Chem. Soc.*, **76**, 1588 (1954); see also J. F. Foster and J. T. Yang, *Fed. Proc.*, **14**, 212 (1955).

(2) For other interpretations see C. Tanford, *Proc. Iowa Acad. Sci.*, **59**, 206 (1952); M. Laskowski and H. A. Scheraga, *J. Amer. Chem. Soc.*, **76**, 6305 (1954); H. A. Saroff, G. I. Loeb and H. A. Scheraga, *ibid.*, **77**, 2908 (1955).

(3) T. L. Hill, *J. Chem. Phys.*, **20**, 1259 (1952); *Faraday Soc. Discussion*, **13**, 125 (1953).

(4) In a more refined treatment, one might want to include both statistical uncoiling and the α-β transformation. The initial swelling would then be primarily at the expense of statistical uncoiling, with a gradual transition to the α-β mechanism as the swelling became more extensive. However, one would not expect changes in optical rotation to accompany statistical uncoiling.

dealing here with sheets of parallel α or β chains as in the previous papers.

Solvent, including electrolyte ions, can penetrate inside the protein molecule filling whatever space is available initially or made available by swelling. Every chain is assumed stretched ($\alpha \rightarrow \beta$) to the same degree, and the volume V through which the network of chains (the protein molecule) extends is assumed proportional to the third power of the individual chain length.

There are B° equivalent sites on a molecule for binding hydrogen ions. When N hydrogen ions are bound, the total charge is $n^*\epsilon = (n + N)\epsilon$, where ϵ is the charge on a proton and $n\epsilon$ is the charge on the molecule when $N = 0$. The B° sites are assumed distributed uniformly over the chains, and the average degree of ionization is assumed the same for all sites.[5]

The procedure we follow is to write down a complete approximate expression for the free energy A of a single protein molecule, including binding of hydrogen ions, stretching ($\alpha \rightarrow \beta$) of chains, and an electrostatic contribution. The equilibrium volume V is then found by minimizing A with respect to V. This volume represents a compromise between the electrostatic term which favors swelling, and the stretching term which resists it. The binding free energy is involved implicitly through the electrostatic term.

Some details can be omitted because the argument follows already published work[3] rather closely.

Derivation of Equations

We write[3]

$$A = A_1 + \Delta A_2 + \Delta A_3 \qquad (1)$$

where

A_1 = deformation free energy
ΔA_2 = binding free energy
ΔA_3 = electrostatic free energy

We do not include the usual heat and entropy of mixing terms of polymer solution theory because the chains of the network are assumed rigid and do not "mix" with solvent in a statistical sense.

In order to handle the α-β transformation, we assume as before[3] that α and β units (three amino acid residues per unit) are statistically scrambled along a chain with the statistics modified to take account of hydrogen bonds between nearest neighbor α units and van der Waals interactions between side chains of nearest neighbor $\alpha\alpha$, $\alpha\beta$ and $\beta\beta$ units. For simplicity we use here the Bragg-Williams approximation.[6] Then we have

$$Q = \frac{B!}{B_\alpha!(B - B_\alpha)!}\, y_{\alpha\alpha}^{\theta^2 B}\, y_{\alpha\beta}^{2\theta(1-\theta)B}\, y_{\beta\beta}^{(1-\theta)^2 B}\, J_\alpha^{B\alpha}\, J_\beta^{B-B\alpha} \qquad (2)$$

$$A_1 = -CkT \ln Q \qquad (3)$$

where B is the number of units in a single chain (between cross links) of which B_α are α units and $B - B_\alpha$ are β units, C is the number of chains in a single protein molecule, J_α and J_β are "intrinsic" or "internal" partition functions for α and β units,

(5) In a more refined treatment, the degree of ionization would be a function of distance from the center of the sphere. Calculations, which involve numerical solution of a non-linear integral equation, are in progress on this problem (without swelling). Also, several types of sites might be important in some cases, though not here.

(6) This one dimensional statistical problem (the "Ising model") can be treated exactly in a more refined analysis.

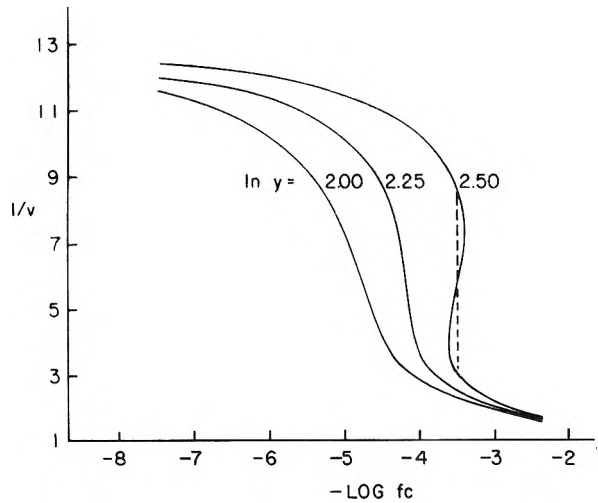

Fig. 1.—Expansion of protein as a function of pH.

including interaction with the solvent, $\theta = B_\alpha/B$, $y_{\alpha\alpha} = e^{-w\alpha\alpha/kT}$, etc., and $w_{\alpha\alpha}$, $w_{\alpha\beta}$ and $w_{\beta\beta}$ are nearest neighbor hydrogen bond and van der Waals energies.

The length of a chain is

$$l = B[l_\alpha\theta + l_\beta(1 - \theta)] \qquad (4)$$

where l_α and l_β are the lengths of α and β units. Thus, according to the assumption mentioned above, θ is related to V by

$$V = V^*[\theta + (l_\beta/l_\alpha)(1 - \theta)]^3 \qquad (5)$$

where V^* is the volume the protein molecule would occupy if $\theta = 1$ (all α units). $V^* \geqslant V_0$, where V_0 is the volume of "dry" protein in the absence of solvent.

Excluding electrostatic effects, the binding free energy[3] is

$$\Delta A_2 = -kT[B^0 \ln B^0 - N \ln N - (B^0 - N) \ln (B^0 - N) + N \ln j] \qquad (6)$$

where j is the partition function of a bound proton.

We now turn to the electrostatic problem. The spherical region occupied by the molecule contains protein penetrated somewhat by electrolyte solution. If the concentration of the i-th ionic species (with valence z_i) far from the sphere is c_i, then its average concentration inside where the potential is ψ is taken as

$$c_i\alpha e^{-z_i\epsilon\psi/kT}$$

where α is the volume fraction of solvent

$$\alpha = (V - V_0)/V \qquad (7)$$

Similarly, we use for the average dielectric constant inside the sphere

$$D_i = \alpha D + (1 - \alpha)D_i^0$$

where D is the dielectric constant of the solvent and D_i^0 is the dielectric constant of "dry" protein ($D_i^0 \cong 2$ or 3). In view of the approximate nature of our treatment and the range of values of α we are interested in ($\alpha \geqslant 0.15$), the term in D_i^0 can be dropped:

$$D_i = \alpha D \qquad (8)$$

Inside the sphere the Poisson-Boltzmann equation is then

$$\nabla^2\psi = -\frac{4\pi}{\alpha D}\left[\frac{n^*\epsilon}{V} + \sum_i z_i\epsilon c_i\alpha e^{-z_i\epsilon\psi/kT}\right] \cong -\frac{4\pi n^*\epsilon}{\alpha DV} + \kappa^2\psi \qquad r \leqslant a \qquad (9)$$

where

$$\kappa^2 = \frac{4\pi\epsilon^2}{DkT}\sum_i z_i^2 c_i \qquad (10)$$

$$a = (3V/4\pi)^{1/3} \qquad (11)$$

Outside the sphere

$$\nabla^2\psi = \kappa^2\psi \qquad r \geqslant a \qquad (12)$$

This is essentially the problem encountered by Hermans and Overbeeck.[7] The solution is

$$\psi_{in}(r) = \frac{4\pi n^*\epsilon}{\kappa^2\alpha DV} + C_1\left(\frac{e^{\kappa r} - e^{-\kappa r}}{r}\right) \qquad r \leqslant a \qquad (13)$$

$$\psi_{out}(r) = \frac{C_2 e^{-\kappa r}}{r} \qquad r \geqslant a \qquad (14)$$

From the boundary conditions

$$\psi_{in}(a) = \psi_{out}(a)$$

$$\alpha D\psi_{in}'(a) = D\psi_{out}'(a)$$

we find

$$C_1 = \frac{4\pi n^*\epsilon a(1+\kappa a)}{\kappa^2\alpha DV[e^{\kappa a}(\alpha - \alpha\kappa a - 1 - \kappa a) + e^{-\kappa a}(-\alpha - \alpha\kappa a + 1 + \kappa a)]} \qquad (15)$$

$$C_2 = \frac{4\pi n^*\epsilon a e^{\kappa a}}{\kappa^2\alpha DV} + C_1(e^{2\kappa a} - 1) \qquad (16)$$

This reduces to the Hermans-Overbeeck result when $\alpha = 1$. The electrostatic free energy ΔA_3 is then

$$\Delta A_3 = \int_0^1\int_0^a 4\pi r^2 dr \frac{n^*\epsilon}{V} d\lambda\, \psi_{in}(r, \lambda) \qquad (17)$$

where λ is the usual charging parameter. We find, putting $\kappa a = x$

$$\Delta A_3 = \frac{8\pi^2 n^{*2}\epsilon^2}{\kappa^5\alpha DV^2}\left\{\frac{x^3}{3} + \frac{x(1+x)[e^x(x-1) + e^{-x}(x+1)]}{e^x(\alpha - \alpha x - 1 - x) + e^{-x}(-\alpha - \alpha x + 1 + x)}\right\} \qquad (18)$$

where α and x are functions of V and n^* is a function of N. If we expand Eq. (18) in powers of x, we obtain

$$\Delta A_3 = \frac{8\pi^2 n^{*2}\epsilon^2 a^5}{45\alpha DV^2}\left[(1 + 5\alpha) - 5\alpha x + \left(-\frac{2}{21} + \frac{13}{3}\alpha - \frac{5}{3}\alpha^2\right)x^2 + \ldots\right] \qquad (19)$$

Returning now to Eq. (1), the extent of binding of hydrogen ions follows from

$$\mu = \frac{\partial A}{\partial N} = \mu^0 + kT \ln c \qquad (20)$$

where c is the hydrogen ion concentration (activity) in solution and μ^0 is a standard ($c = 1$) free energy per molecule. We find from Eqs. (1), (6), (19) and (20)

$$\ln fc = \ln\frac{N}{B^0 - N} + \left[\frac{3\epsilon^2}{10(3/4\pi)^{1/3}DkTV_0^{1/3}}\right](n+N)\left\{\frac{v^{1/3}\left(4 - \frac{10}{3}v\right)}{1-v} - \frac{10}{3}x_0 + \frac{\frac{2}{3}\left(\frac{18}{7} - v - \frac{5}{3}v^2\right)x_0^2}{(1-v)v^{1/3}} + \ldots\right] \qquad (21)$$

where

$$v = V_0/V \qquad (22)$$

$$x_0 = \kappa a_0 \qquad (23)$$

$$a_0 = (3V_0/4\pi)^{1/3} \qquad (24)$$

$$f = je^{\mu^0/kT} \qquad (25)$$

Similarly, the equilibrium volume V of a protein molecule is determined by

$$\frac{\partial A}{\partial V} = 0 \qquad (26)$$

From Eqs. (1), (3), (5), (19) and (26), we derive for this condition

$$\frac{v^{*1/3}v^{2/3}}{3(V_0/BC)\left(\frac{l_\beta}{l_\alpha} - 1\right)}\ln\frac{1-\theta}{\theta}y^{2\theta}J = \left[\frac{\epsilon^2}{30(3/4\pi)^{1/3}DkTV_0^{1/3}}\right](n+N)^2\frac{v^{4/3}}{(1-v)^2}\left[(6 - 8v + 5v^2) - \frac{2(27 - 87v + 98v^2 - 35v^3)x_0^2}{21v^{2/3}} + \ldots\right] \qquad (27)$$

where

$$v^* = V^*/V_0 \qquad (28)$$

$$y = y_{\alpha\alpha}y_{\beta\beta}y_{\alpha\beta}^{-2} \qquad (29)$$

$$J = \frac{J_\alpha}{J_\beta}\left(\frac{y_{\alpha\beta}}{y_{\beta\beta}}\right)^2 \qquad (30)$$

Calculations

Yang and Foster extrapolate their results to zero ionic strength ($x_0 = 0$ here). In this case, only the leading terms in Eqs. (21) and (27) are retained. A numerical example at zero ionic strength is shown in Figs. 1 and 2, with parameters chosen to fit bovine serum albumin as well as possible: $B^\circ = 106$, $n = -6$, $T = 298.2^\circ$ K., $D = 78.54$, $V_0 = 9.137 \times 10^{-20}$ cc./molecule, $v^* = 1$, $V_0/BC = 274.5$ cc./mole and $l_\beta/l_\alpha = 2.363$. We include 0.06 g. of (relatively tightly bound) water per gram of protein as part of the "dry" protein, and we assume that there is an additional 0.14 g. of water[8] per gram of protein present at zero charge ($n + N = 0$). This gives, at zero charge, $v = 0.850$ and $\theta = 0.959$ (Eq. (5)). We then make three choices of $\ln y$; each one determines a value of $\ln J$, necessary to give $v = 0.85$ in Eq. (27) when $n + N = 0$. These are $\ln y = 2.0$, 2.25 and 2.50 and $\ln J = -0.681$, -1.161 and -1.641, respectively. The value $\ln y = 2.25$ corresponds to

$$-(w_{\alpha\alpha} + w_{\beta\beta} - 2w_{\alpha\beta}) = 1333 \text{ cal./mole}$$

for the net interaction between pairs of nearest neighbor units (three amino acid residues per unit). This is a reasonable order of magnitude.

Fig. 1 shows $1/v = V/V_0$ plotted against $-\log fc$, where

$$-\log fc = p\text{H} - \log f \qquad (31)$$

For $\ln y = 2.25$, there is an expansion in volume predicted of the order of a factor[9] of ten, over a few pH units. This agrees qualitatively, which is all that can be expected, with the behavior of the intrinsic viscosity found by Yang and Foster (the intrinsic viscosity should depend on volume as V^m, where $2/3 \leqslant m \leqslant 1$). The loop in the $\ln y = 2.5$ curve corresponds to a first order (α-β) phase transition which is not observed experimentally at 24.9°, though it might be at lower temperatures.

(7) J. J. Hermans and J. Th. G. Overbeeck, *Rec. trav. chim.*, **67**, 761 1948).

(8) This gives a total hydration of 0.2 g. water/g. protein, which is supposed to be typical.

(9) It should be noted that the α-β transition alone allows a *maximum* volume expansion of only $(2.363)^3 = 13.2$. See footnote 4. Also, the present theory would predict a similar expansion at high pH owing to the high negative charge.

Incidentally, a phase transition introduces an "all-or-none" type of behavior[1] not otherwise present.

The titration curve for the $\ln y = 2.25$ case is given in Fig. 2. Although no experimental curve is available for bovine or human serum albumin at zero ionic strength, the theoretical curve in Fig. 2 is almost certainly not steep enough. It would become more steep (and eventually vertical) at higher values of $\ln y$.

We discuss only first order electrolyte effects here. Suppose, following Eq. (19), we write in general

$$\frac{\Delta A_3}{kT} = \frac{(N+n)^2}{2}[\varphi(v) + x_0\Phi(v) + \ldots] \quad (32)$$

Then Eq. (21) appears as

$$\ln fc = \ln \frac{N}{B^0 - N} + (N+n)[\varphi(v) + x_0\Phi(v) + \ldots] \quad (33)$$

and Eq. (27) as

$$F(v) = (N+n)^2\left[\left(-\frac{1}{2}\frac{\partial\varphi}{\partial V}\right) + x_0\left(-\frac{1}{2}\frac{\partial\Phi}{\partial V}\right) + \ldots\right] \quad (34)$$

We then find, on expanding in powers of x_0

$$\ln fc = \ln fc_0 + x_0\Theta(v) + \ldots \quad (35)$$

and

$$v = v_0 - \frac{x_0\Theta(v_c)}{(\partial \ln fc_0/\partial v)_{v=v_0}} + \ldots \quad (c = c_0 = \text{const.}) \quad (36)$$

where

$$\Theta(v) = (N_0 + n)\left[\Phi - \frac{\varphi}{2}\frac{\partial\Phi/\partial V}{\partial\varphi/\partial V} - \frac{B^0}{2N_0(B^0 - N_0)}\frac{\partial\Phi/\partial V}{\partial\varphi/\partial V}\right] \quad (37)$$

The subscript zero on c_0, v_0 and N_0 refers to the limit $x_0 = 0$. In general we expect, on the right hand side of Eq. (37), Φ to be negative and the other terms to be positive, with Θ also positive. Thus v would increase with x_0 at constant c in Eq. (36)—that is, the protein molecule would decrease in volume when electrolyte is first added (c constant). This behavior is found experimentally by Yang and Foster. Unfortunately, the particular combination of model and approximations used in the electrostatic calculation here happens, by cancellation, to give Φ independent of V (compare Eqs. (21) and (33)), and hence $\partial\Phi/\partial V = 0$ and $\Theta < 0$ in Eq. (37). This behavior is opposite to that just described (but it is reversed by the second order term at rather low electrolyte concentration—of the order of 10^{-3} M). Any refinements will undoubtedly make Φ dependent on V as expected in general.

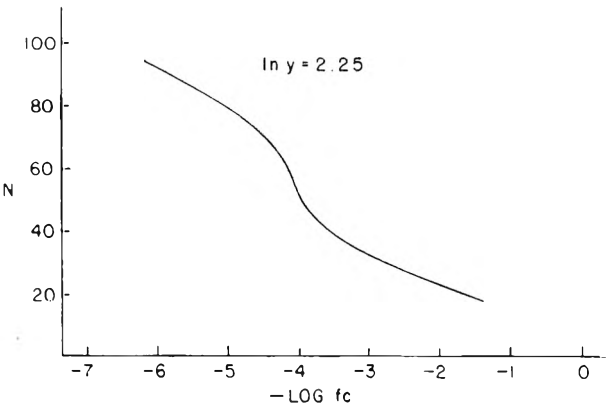

Fig. 2.—Titration curve of protein.

Conclusion

The preliminary calculations reported here indicate that the suggestion of Yang and Foster is a reasonable possibility from a theoretical point of view. Of course the calculations do not provide any *direct* evidence that this suggestion is actually correct. The discrepancy between theory and experiment on the direction of the salt effect is presumably due to the approximate nature of the electrostatic part of the theory.

Other expansion mechanisms might also prove to be "reasonable possibilities" in the above sense. We are, in fact, examining Tanford's[2] proposal (swelling caused by breakage of cross-links) in an analogous fashion. The direction of the salt effect will be the same in this case, incidentally, unless the electrostatic theory is modified.

THE PROPERTIES OF ASBESTOS. II. THE DENSITY AND STRUCTURE OF CHRYSOTILE[1]

BY FRED L. PUNDSACK

Contribution from the Johns-Manville Research Center, Manville, New Jersey

Received August 26, 1955

It is shown that the tubular structure hypothesized for chrysotile asbestos is not compatible with experimentally determined density values for sealed, solid blocks of asbestos fiber. The data indicate that the fundamental fibers are packed together efficiently with very little void space. The only void space observed appears to be associated with the volume occupied by sorbed water. Sorption and desorption of water probably causes reversible swelling of the fiber bundles. It is hypothesized that the fundamental fibers may exist as sheet- or ribbon-like structures possessing a certain degree of distortion due to limited curvature about the fiber axis.

The unusual nature of serpentine minerals ($3MgO{\cdot}2SiO_2{\cdot}2H_2O$) which occur in massive, pseudo-fibrous and fibrous (chrysotile) forms has led numerous investigators to attempt a structural analysis of the various species. Chrysotile was classified first as an amphibole structure with a repeating $Si_4O_{11}^{-6}$ unit,[2] but this was revised later to a layer- or sheet-type structure with a repeating

(1) Preceding paper in this series, F. L. Pundsack, THIS JOURNAL, **59**, 892 (1955).

(2) B. E. Warren and W. L. Bragg, *Z. Krist.*, **76**, 201 (1930).

$Si_4O_{10}^{-4}$ unit.[3] Although there appears to be general agreement that chrysotile has a sheet- or layer-type structure, many workers have pointed out that the fundamental sheet structure must be distorted in some way to account for the X-ray diffraction patterns which are observed.[4-6] In recent years interest in the structural characteristics of chrysotile has been stimulated by the almost simultaneous publication by Bates, Sand and Mink[7] in this country and Noll and Kircher[8] in Germany of electron photomicrographs of chrysotile which appear to show the fibers in the form of hollow tubes. Hillier and Turkevich[9] had previously noted this phenomenon in passing. Recently a number of attempts have been made to correlate X-ray diffraction data from chrysotile with the hypothesized tubular structure.[10-12]

It is apparent that a tubular structure of the type hypothesized for chrysotile will contain considerable void volume (*i.e.*, space not occupied by chrysotile) when the fibers are packed into solid bundles of the type found in nature. Thus, if the density of naturally occurring blocks of fiber is determined in a liquid which does not penetrate the fiber blocks, the magnitude of the void volume can be ascertained, and the existence of a tubular structure can be shown to be either possible or highly improbable.

Experimental

Materials.—The chrysotile fiber used for the density determinations in water was selected from a supply of No. 1 Danville Crude from Canada. The analysis of this material has been reported previously.[1] Portions of the selected solid fiber blocks were broken off into unopened bundles about 2.4 cm. long and 0.4-0.5 cm. in diameter. The samples were examined carefully for flaws and imperfections. Density determinations on these specimens are referred to as density values for "blocks of fiber." After the experimental runs had been completed on these blocks of fiber, they were opened carefully by hand and found to be free of any foreign inclusions which might otherwise invalidate the measurements.

The density determination in air was carried out with an essentially flawless, translucent specimen of chrysotile from Arizona. This sample was in the form of a slightly irregular block about 5 cm. × 3 cm. × 1.6 cm. with a mass of approximately 58 g.

Distilled water with a specific resistance $>5 \times 10^5$ ohms was used for density determinations in an aqueous medium.

Density Measurements.—Two 25-ml. capacity pycnometers fitted with thermometers and side-arm capillary tubes were calibrated to ±0.002 cc. with the liquid being used in the density measurements. Samples were weighed out into the pycnometer flasks, and then they were outgassed in accordance with a method described by Tschapek[13] and later used successfully by Culbertson and Weber.[14] The procedure consists of adding enough liquid to the flask to cover the sample and then evacuating the system in a vacuum desiccator to just below the vapor pressure of the liquid. This method effectively removes adsorbed air from the system. After the system had been outgassed a sufficient length of time (determined by repeated runs until a constant density was attained) the vacuum was broken and the flask filled with liquid and allowed to come to room temperature, 25 ± 1°. The pycnometer unit was assembled and the density determined. The actual temperature of the system was read to within 0.1° from the thermometer in the pycnometer flask. After the density values had been obtained for the unsealed specimens the samples were collected, dried and the density calculated on both an "as-is" (*i.e.*, original sample weight which includes sorbed water) and a dry basis.

For the "sealed block" density determinations unopened blocks of chrysotile were weighed and then dipped in molten paraffin at about 78°. This procedure formed a relatively smooth, even coating of solidified paraffin over the entire block of fiber. Subsequent gas adsorption measurements showed that the coating was impervious. The density of the "sealed blocks" was determined in water, and then the value was corrected for the density of the paraffin present. Sorbed water content of the blocks was determined by dehydration runs on untreated fiber blocks from the same source. The untreated blocks were weighed under the same conditions of relative humidity as the blocks used in the density determinations. The density of the paraffin, 0.901 g./cc., was determined independently by coating glass rods of known volume with the molten paraffin.

The density determination in air on the specimen of fiber from Arizona was carried out simply by mapping the contours and profile of the block on graph paper and calculating the volume on the basis of the mapped dimensions. The block was weighed and then the sorbed water content was determined on a small portion of the block by the procedure described below.

Water Determinations.—Experiments showed that reversibly sorbed water could be removed from chrysotile by drying the material at temperatures between 175 and 200°. At temperatures much above 200° a slight, non-reversible water loss occurs in chrysotile. Therefore, for purposes of calculating the density of the fiber samples on a dry sample basis the water loss up to 175° was considered sorbed water. As an approximation the sorbed water was assumed to occupy the same volume as an equal quantity of free water, and this correction was used to obtain the density of the solid fiber. Although the sorbed water may actually occupy a volume slightly less than that of free water, this assumption is not critical to the conclusions reached in this work.

Theoretical

When hollow cylindrical tubes with an outer radius r_1 and an inner radius r_2 are placed together in hexagonal close-packing the ratio of the gross volume of the bundle of tubes, V_G, to the volume of the solid, V_S, is

$$\frac{V_G}{V_S} = \frac{2\sqrt{3}}{\pi}\left(\frac{r_1^2}{r_1^2 - r_2^2}\right) \qquad (1)$$

Equation 1 may be rearranged and reciprocal density values D substituted for corresponding volumes to give

$$D_S = \frac{2\sqrt{3}}{\pi} D_G \left(\frac{r_1^2}{r_1^2 - r_2^2}\right) \qquad (2)$$

where

D_S = absolute density of the solid
D_G = observed gross density of the fiber bundle

Equation 2 reflects the relationship of the density of the solid to the observed bundle density when the liquid fails to penetrate the void volume. If the fibers are solid (*i.e.*, $r_2 = 0$), or the liquid penetrates the intrafibril pores but not the interfibril pores, equation 2 reduces to

$$D_S = \frac{2\sqrt{3}}{\pi} D_G \qquad (3)$$

When the liquid penetrates all pores

$$D_S = D_G \qquad (4)$$

(3) B. E. Warren and K. W. Hering, *Phys. Rev.*, **59**, 925 (1941).
(4) V. A. Fock and V. A. Kolpinsky, *J. Phys. U.S.S.R.*, **3**, 125 (1940).
(5) B. E. Warren, *Am. Mineralogist*, **27**, 235 (1942).
(6) E. Aruja, *Mineralog. Mag.*, **27**, 65 (1944).
(7) T. F. Bates, L. B. Sand and J. F. Mink, *Science*, **111**, 512 (1950).
(8) W. Noll and H. Kircher, *Naturw.*, **37**, 540 (1950).
(9) J. Hillier and J. Turkevich, *Anal. Chem.*, **21**, 475 (1949).
(10) E. J. W. Whittaker, *Acta Cryst.*, **7**, 827 (1954)
(11) E. J. W. Whittaker, *ibid.*, **8**, 261, 265 (1955).
(12) H. Jagodzinski and G. Kunze, *Neues Jahrb. Mineral. Monatsh.*, **95**, 113, 137 (1954).
(13) M. W. Tschapek, *Kolloid-Z.*, **63**, 343 (1933).
(14) J. L. Culbertson and M. K. Weber, *J. Am. Chem. Soc.*, **60**, 2695 (1938).

D_S, which is essential to the utilization of the preceding equations, can be calculated readily from X-ray diffraction unit cell data available in the literature. The data on the dimensions of a unit cell of the composition $Mg_6(OH)_8Si_4O_{10}$ are summarized in Table I. Using the average values $a = 5.33$ Å., $b = 9.24$ Å., and $c = 7.33$ Å. the absolute density of chrysotile is 2.56 g./cc. Since the samples used in this work contained about 2% FeO + Fe_2O_3 isomorphously substituted for magnesium,[1] the theoretical density of 2.56 can be corrected to 2.58 g./cc. to take this into account. This correction is incidental since it is within the range of experimental error.

TABLE I

UNIT CELL ($Mg_6(OH)_8Si_4O_{10}$) DATA FOR CHRYSOTILE

Axis	Warren and Bragg[2]	Warren and Hering[3]	Aruja[6]	Whittaker[15]	Padurow[16]
a	5.33	5.33	5.32	5.33	5.33
b	9.25	9.24	9.2	9.2	9.26
c	7.33	7.33	7.31	7.33	7.36

The magnitude of D_G to be expected for hollow tubes of the dimensions which have been suggested,[17] $r_1 = 175$ Å. and $r_2 = 75$ Å., can be calculated from equation 2 by using $D_S = 2.58$. In this case $D_G = 1.91$ g./cc. assuming a sealed block in which no penetration of liquid into the void volume occurs.

Results and Discussion

The data for a series of density measurements on both sealed and unsealed blocks of fiber are summarized in Table II. It is clearly evident from the data on the paraffin-sealed blocks that they do not contain the void space required by a hollow tube structure. In fact, the results strongly suggest that the only appreciable void space in the solid blocks of fiber is that occupied by sorbed water. Furthermore, the void space is not constant, but increases as the sorbed water content increases. That is, the blocks of fiber must swell as water is sorbed. The only exception among the sealed blocks is sample no. 6 which has a density slightly lower than one would expect. In view of the consistent behavior of the other values it seems likely that the value for no. 6 may have been low because of a slight imperfection in the otherwise solid block of fiber.

TABLE II

DENSITY OF SEALED AND UNSEALED SOLID BLOCKS OF FIBER

Sample	Sorbed H_2O, %	Gross sample,[a] g./cc.	Chrysotile,[b] g./cc.
Sealed 1	0	2.57	2.57
Sealed 2	0	2.55	2.55
Sealed 3	0	2.56	2.56
Sealed 4	0	2.56	2.56
Sealed 5	2.2	2.48	2.57
Sealed 6	1.3	2.48	2.53
Sealed 7	0.8	2.53	2.56
Unsealed 8	1.0	2.51	2.55
Unsealed 9	1.0	2.53	2.57
Unsealed 10	0.7	2.56	2.58
Arizona[c]	2.0	2.45	2.53

[a] Density of gross sample including sorbed water but excluding paraffin. [b] Calculated on the assumption that sorbed water occupies a volume of 1 cc./g. [c] The density of this sample was determined in air.

The fact that the sealed samples which contain essentially no sorbed water have density values closely approximating the theoretical absolute density of chrysotile indicates that the fibers in a desorbed condition are packed together with very little void space. This behavior is not compatible with a hollow tube structure. In order to account for the close-packing of the fibers it seems more plausible to view them as strip or ribbon-like structures which may be distorted by limited curvature about the fiber axis.[18] This type of structure awaits confirmation by X-ray diffraction studies.

The density values obtained for the unsealed blocks of fiber in water indicate the consistent nature of the measurements. In the unsealed blocks the only appreciable void space measured is also that occupied by sorbed water. Taken alone the values for the unsealed blocks could not conclusively establish the improbability of a tubular structure. However, the results on sealed blocks indicate that when unsealed blocks of fiber are placed in water, the blocks probably sorb water and swell although initially the only appreciable void space present is that occupied by water sorbed prior to immersion.

Measurement of the density of the block of Arizona chrysotile in air furnishes additional confirmation of the improbability of the existence of a tubular structure in chrysotile. Considering the crudeness of the method, the results are in good agreement with the premise that the only significant void space in bundles of fiber is that occupied by sorbed water. This void space is much less than would be required by a tubular structure.

A series of studies of the amount of water sorbed by chrysotile as a function of relative humidity indicates that the maximum amount of sorbed water retained by blocks of fiber at 100 per cent. relative humidity and 25° is approximately 2.5 per cent. If, as seems probable, sorbed water causes the fiber bundles to swell, the maximum degree of swelling can be calculated using the sorbed water value at 100 per cent. relative humidity. One gram of desorbed fiber occupies

$$\frac{1}{2.58} = 0.388 \text{ cc./g.}$$

When 1 g. of chrysotile sorbs the maximum amount of water the gross sample will weigh 1.026 g. and occupy a volume of

$$0.388 + 0.026 = 0.414 \text{ cc./g. chrysotile}$$

The apparent change in volume of the block of fiber is 0.026 cc./g. chrysotile. The percentage increase in volume over the range of complete desorption to complete sorption would be

$$\frac{0.026}{0.388} \times 100 = 6.7\%$$

Experimental work is now in progress to observe directly the swelling of fiber bundles and to establish

(15) E. J. W. Whittaker, *Acta Cryst.*, **5**, 143 (1952).
(16) N. N. Padurow, *ibid.*, **3**, 204 (1950).
(17) G. J. Young and F. H. Healey, THIS JOURNAL, **58**, 881 (1954).
(18) Such a limited curvature has been suggested for antigorite, a so-called massive variety of serpentine, by J. Zussman, *Mineralog. Mag.*, **30**, 498 (1954).

whether the swelling is of the predicted order of magnitude.

No satisfactory explanation of the hollow-tube appearance of chrysotile fibers when viewed in the electron microscope[7-9,19] can be offered other than to suggest the obvious: the sample viewed in the electron microscope no longer bears a one to one relationship with the native fiber. Whether this is the result of the treatment the fibers have received during the preparation or of the exposure to the electron beam in a high vacuum remains to be determined.

(19) R. K. Iler, "The Colloid Chemistry of Silica and Silicates," Cornell University Press, Ithaca, N. Y., 1955, p. 208.

Acknowledgment.—The successful execution of this work is due in large part to Mr. George Reimschussel who made many of the density measurements reported here. Mr. Marion Badollet and Mr. William Streib made available certain excellent specimens of chrysotile which were measured in the course of this investigation.

CHANGES IN PHYSICAL PROPERTIES OF GRAPHITIZED CARBON RODS UPON GASIFICATION WITH CARBON DIOXIDE[1,2]

BY P. L. WALKER, JR., AND EMILE RAATS

Department of Fuel Technology, The Pennsylvania State University, University Park, Pennsylvania

Received September 1, 1955

Changes in the physical properties of graphitized carbon rods after gasification to different burn-offs at 1000° and to 11% burn-off at temperatures between 970 and 1372° have been determined. The physical properties investigated were surface area, total and incremental pore volume, average pore radius, macropore surface area and specific reaction rate. The results can be explained if the carbon rods are considered to be composed of relatively homogeneous, non-porous particles of petroleum coke bound together by a thin shell of coal tar pitch coke, which essentially consists of a condensed "bubble type" structure.

Introduction

The widespread importance of the heterogeneous gasification reactions of carbons in present-day industry necessitates a complete understanding of the mechanism of these reactions. On the one hand, the primary interest in gasification is related to the conversion of carbonaceous materials to either gaseous fuels or synthesis gas. Here of primary concern is the attainment of high gasification rates. On the other hand, the primary interest is connected with the lack of gasification of carbons and graphites when used as electrodes, structural carbons or moderators in atomic reactors. In either case, a basic understanding of the relationship between reactivity of carbon to gases and the physical properties of the carbons is essential.

In the present work, the reactivity of a highly graphitized carbon with carbon dioxide, as a function of burn-off and temperature, has been compared with changes in the physical structure of the carbon. This work is an extension of the finding of Walker and Rusinko,[3] who investigated the reactivities of six different carbons.

Experimental

Carbon.—The samples used were National Carbon Company AGKSP special graphite spectroscopic electrodes containing an ash content less than 0.01%. They were 5 cm. long by 1.3 cm. in diameter. A more detailed description of the manufacture of graphitized carbon can be found elsewhere.[4]

Reaction Rate Apparatus.—The reactor was the same as that described in a recent gasification study.[5] Two methods were used to suspend the samples in the reactor. For reaction studies to 1 g. weight loss (11% burn-off) at different temperatures, a hole 1/8-inch in diameter and 1/8-inch deep was drilled into the top of the sample. Into this hole was cemented a 1/8-inch diameter ceramic rod which connected to the balance. In studies to carbon burn-offs greater than 1 g., it was found that reaction weakened the bond between the rod and sample sufficiently to result in the inability of the rod to support the sample during weighing. For this work, a 1/8-inch hole was drilled through the center of the samples. The ceramic support in this case consisted of a base plate 1/2-inch in diameter connected directly to the 1/8-inch rod. The carbon sample was placed over the 1/8-inch rod and sat on the base plate with no cement being used.

Mercury Porosimeter.—A description of the design and operation of the mercury porosimeter used has been given recently.[6]

Low Temperature Gas Adsorption Apparatus.—A standard gas adsorption apparatus was employed and has been described recently.[6] Surface areas and micropore volume distributions were determined from the adsorption and capillary condensation of nitrogen using the BET equation[7] and Pierce technique,[8] respectively.

Results

Effect of Gasification of Carbon Rods to Different Burn-Offs at 1000° on their Physical Properties.—In studying the effect of gasification of carbon rods to different burn-offs on their physical properties, it was desirable to work at a sufficiently low temperature so that the gasification process proceeded uniformly through the sample. It was found from the uniformity of the bulk density profile data, a technique previously described,[6] that a gasification temperature of 1000° fulfilled this requirement.

The reaction rate curves for four carbon rods

(1) Based on a Ph.D. thesis submitted by Emile Raats to the Graduate School of The Pennsylvania State University, June, 1955.

(2) This paper presents the results of one phase of research carried out under Contract No. AT(30-1)-1710, sponsored by the Atomic Energy Commission.

(3) P. L. Walker, Jr., and F. Rusinko, Jr., THIS JOURNAL, **59**, 241 (1955).

(4) H. W. Abbott, "Encyclopedia of Chemical Technology," Vol. 3, The Interscience Encyclopedia Inc., New York, N. Y., 1949, pp. 1-23.

(5) P. L. Walker, Jr., R. J. Foresti, Jr., and C. C. Wright, *Ind. Eng. Chem.*, **45**, 1703 (1953).

(6) P. L. Walker, Jr., F. Rusinko, Jr., and E. Raats, THIS JOURNAL, **59**, 245 (1955).

(7) P. H. Emmett, *A.S.T.M. Tech. Publ.*, **51**, 95 (1941).

(8) C. Pierce, THIS JOURNAL, **57**, 129 (1953).

gasified at 1000° with carbon dioxide to 11.5, 23.0, 34.5 and 46.0% burn-off are shown in Fig. 1. It is seen that the gasification rate increases gradually to a maximum at *ca.* 2-g. weight loss (23.0% burn-off) and then decreases upon further gasification. The extended period of constant reaction rate characteristic of some other carbons investigated[3,5] is not found in this case.

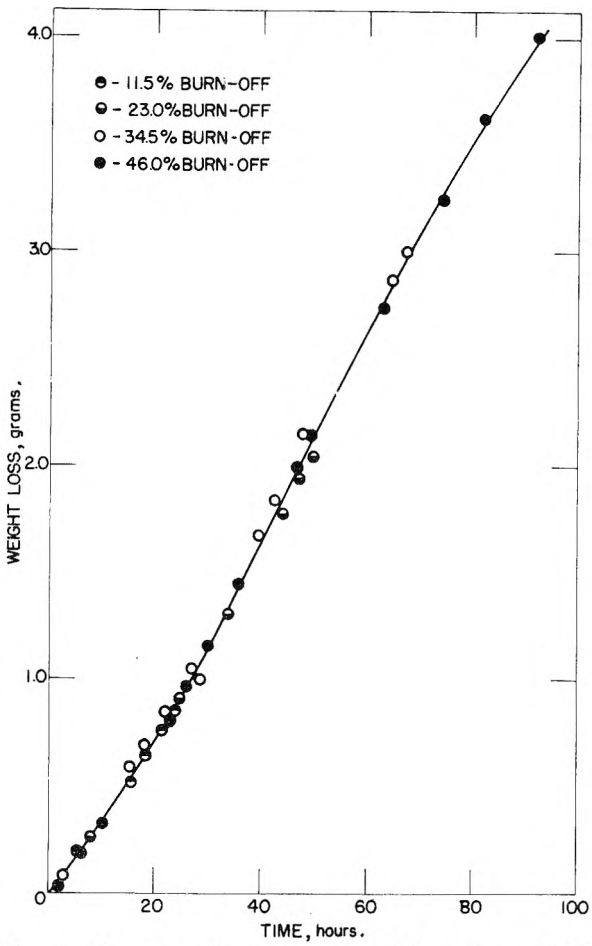

Fig. 1.—Reaction rate curves for graphite rods at 1000°.

Figure 2 shows the sorption isotherm of nitrogen on the unreacted sample from which its surface area and micropore volume distribution were determined. This type II isotherm is quite typical of those found for all the carbon samples gasified.

Table I summarizes the data on surface area, apparent density and average pore radius of the carbon rods before and after the different degrees of gasification. It is seen that there is a marked increase in both specific and total surface area of the carbon rods up to approximately 23.0% burn-off. Further gasification, at least up to 46.0% burn-off, produces a decrease in both surface areas.

The apparent densities, determined by a weighing technique using a specific gravity bottle and mercury as displacement fluid, naturally decrease with gasification. Pore volumes, calculated from the difference of the reciprocals of apparent and true density[9] increase with burn-off.

(9) The true density is 2.269 g./cc., as calculated from X-ray diffraction values of 3.357 Å. for the interlayer spacing and 1.416 Å. for the C–C bond distance in the layer plane.

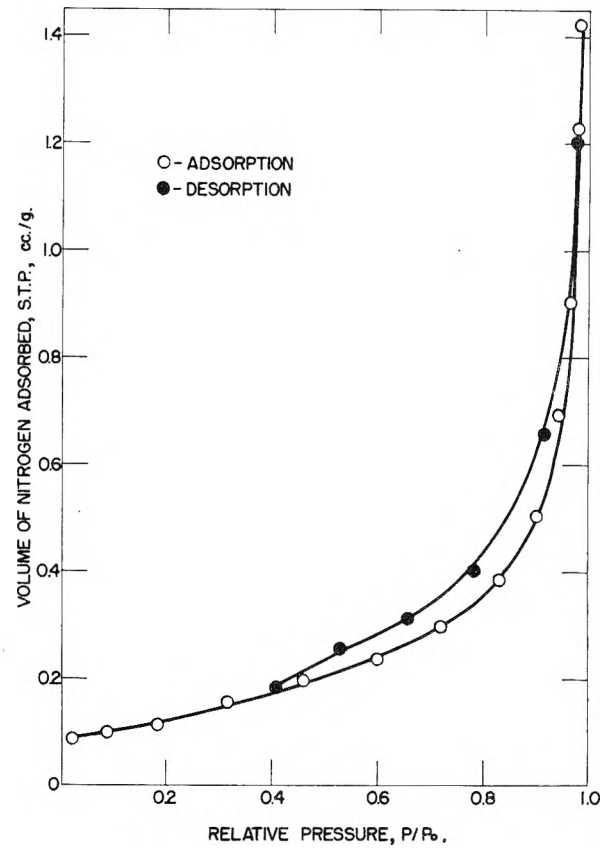

Fig. 2.—Adsorption isotherm for nitrogen at 77.2°K. on unreacted graphite rod.

Average pore radii are calculated using the relationship for cylindral pores,[10] $\bar{r} = 2V/A$, where V is the total pore volume and A the total surface area. It is seen that upon gasification to only 11.5% burn-off there is a marked decrease in average pore radius over the unreacted sample. This is followed by a further, minor decrease in radius up to 23.0% burn-off and then an increase in radius with further gasification.

TABLE I

SURFACE AREA, DENSITY AND POROSITY DATA FOR GRAPHITE RODS AFTER VARIOUS BURN-OFFS AT 1000°

Burn-off, %	Surface area, m.²/g.	Total surface area, m.²	Apparent density, g./cc.	Pore vol., cc./g.	Av. pore radius, Å.
Unreacted	0.41	3.54	1.562	0.199	10,140
11.5	1.61	12.15	1.378	.285	3,520
23.0	2.02	13.55	1.255	.355	3,480
34.5	2.03	11.31	1.154	.426	4,120
46.0	1.72	8.23	1.076	.488	5,530

It is of interest to examine the relationship between reaction rate, surface area and total pore volume as a function of burn-off. Table II presents these data. It is seen that the specific reaction rate expressed per unit of total surface area continually increases with burn-off—a particularly large increase being observed after 34.5% burn-off. On the other hand, the specific reaction rate expressed per unit of total pore volume reaches a maximum at approximately 23.0% burn-off and then decreases.

(10) P. H. Emmett and Thomas W. DeWitt, *J. Am. Chem. Soc.*, **65**, 1253 (1943).

TABLE II

CORRELATION OF AVERAGE INSTANTANEOUS REACTION RATE WITH SURFACE AREA AND PORE VOLUME AT VARIOUS BURN-OFFS

Burn-off, %	Av. reaction rate, g./hr.	Specific reaction rate, g./m.^{2} hr. $\times 10^3$	Specific reaction rate, g./cc. hr. $\times 10^2$
11.5	0.040	3.29	1.87
23.0	.052	3.84	2.20
34.5	.045	3.98	1.93
46.0	.040	4.86	1.76

Table III presents detailed data on the distribution of micropore volume in pore radius increments covering the range 14.7 to 400 Å. for the unreacted and gasified samples. It is seen that in all radius increments the total micropore volume reaches a maximum at 23.0 or 34.5% burn-off. For the specific micropore volume, there are two exceptions to the above maxima; the volume in pores from 14.6 to 20 Å. and 50 to 75 Å. continue to increase over the entire burn-off range.

Table IV presents detailed data on the distribution of macropore volume in pore radius increments covering the range 400 to 130,000 Å. In contrast to the behavior of the total micropore volumes all going through maxima with increasing burn-off, the total macropore volumes show maximum, increasing, and decreasing values with burn-off depending upon the radius increments. Particularly to be noted are the steady and marked decrease in total pore volume for pore radii from 20,000 to 30,000 Å. and the comparable increase in total pore volume for pore radii from 30,000 to 60,000 Å. The specific macropore volumes go through a maxima with increasing burn-off up to a pore radius of 20,000 Å., the volume in the 20,000 to 30,000 Å. range shows some over-all decrease, and the specific macropore volume in pores from 30,000 to 130,000 shows a continual increase with burn-off.

It is found that the sum of pore volumes calculated from micropore and macropore distributions is from 2.1 to 5.8% less than the total pore volume as calculated from the density data, with no trend apparent with increasing burn-off. In all probability this is due, in part, to the fact that the density calculated from X-ray data does not take inaccessible or "blind pores" into consideration. For example, it was shown by Dresel and Roberts,[11] by comparing helium with X-ray densities, that unreacted, synthetic graphite has roughly 6% closed pore volume, which is in qualitative agreement with this work.

The reason that the discrepancy in volumes does not decrease upon gasification in the present case probably can be explained as follows. The slope of the mercury porosimeter curve for the unreacted carbon rod is essentially zero at the upper limit (130,000 Å.), indicating little or no volume above this pore size. This is not the case for the gasified rods, the shape of the curve indicating the existence of a significant volume in pores greater than 130,000 Å. Since the pore volume determined by density measurements is thought to include all pores up to approximately 200,000 Å.,[12] the two methods will be in disagreement by the magnitude of the pore volume between 130,000 and 200,000 Å. Therefore, possibly the unaccounted-for volume in the gasified samples is predominantly due to volume above the upper limit of porosimeter measurements rather than to "blind pore" volume.

In a manner analogous to that discussed previously,[6] macropore areas are calculated from porosimeter data and shown in Table V. It is seen that the percentage contribution of the macropore area to the total area decreases markedly upon gasification. Using the total micropore volumes determined by gas adsorption and the total micropore areas determined by difference, an average micropore radius is calculated. It is seen that the unreacted sample has a calculated average pore radius significantly greater than 400 Å. On the other hand, the gasified samples all have average pore radii markedly less than 400 Å.

Effect of Gasification of Carbon Rods to 11% Burn-off at Various Temperatures on their Physical Properties.—Carbon rods were gasified to 1.0 g. (11%) weight loss at a series of temperatures between 970 and 1372°. Table VI presents data on the specific surface area, apparent density, specific pore volume and average pore radius of these samples after gasification. Since the gasified samples all have the same final weight, total surface areas and total pore volumes are not presented in this case. It is seen that the specific surface area increases with increasing gasification temperature up to 1224° and then decreases. This is in qualitative agreement with the findings of Petersen, Walker and Wright,[13] who in the same apparatus as used in the present work found a maximum area developed at *ca.* 1180° for a more reactive carbon, which also developed a considerably higher surface area upon gasification.

Developed apparent densities and pore volumes are also found to be affected by gasification temperatures but not in as uniform a manner as surface areas. As in the previous results to different burn-offs, the average pore radius decreases markedly upon gasification temperature up to 1224° and then increases with higher temperatures.

Table VII presents data on the total micropore volumes in pore radius increments. No obvious trend is seen to exist between the incremental pore volumes and gasification temperatures. However, samples gasified at 1200 to 1246° do have maximum incremental volumes for most of the radius ranges listed. This observation parallels the development of maximum surface area at *ca.* 1224°.

Table VIII presents data on total macropore volumes in pore radius increments. Here again no obvious trend between gasification temperature and incremental pore volume is observed. Figure 3 emphasizes the close similarity of macropore distributions for four of the samples gasified at different temperatures. These are also typical of samples gasified at other temperatures.

(11) E. M. Dresel and L. E. J. Roberts, *Nature*, **171**, 170 (1953).

(12) J. L. Ritter and L. C. Drake, *Ind. Eng. Chem., Anal. Ed.*, **17**, 782 (1945).

(13) E. E. Petersen, P. L. Walker, Jr., and C. C. Wright, *Ind. Eng. Chem.*, **47**, 1629 (1955).

TABLE III

MICROPORE VOLUMES IN PORE-RADII INCREMENTS AS CALCULATED FROM GAS ADSORPTION DATA

Pore radius range, Å.	Vol. in range indicated after different burn-offs, cc. × 10^5					Vol. in range indicated after different burn-offs, cc./g. × 10^4				
	Unreacted	11.5%	23.0%	34.5%	46.0%	Unreacted	11.5%	23.0%	34.5%	46.0%
14.7– 20	0.3	2.6	3.0	2.6	2.4	0.3	3.5	4.5	4.7	5.1
20– 36	1.3	3.3	3.6	3.5	2.1	1.5	4.4	5.4	6.3	4.4
36– 50	0.8	1.5	2.1	1.6	1.1	0.9	2.0	3.1	2.9	2.3
50– 75	1.4	2.5	2.8	2.6	2.3	1.6	3.3	4.2	4.7	4.9
75–100	1.3	2.8	2.7	2.8	2.1	1.5	3.7	4.0	5.0	4.4
100–150	2.3	4.7	5.9	4.3	3.4	2.6	6.3	8.8	7.7	7.2
150–200	1.5	4.8	5.8	3.8	2.9	1.7	6.4	8.7	6.8	6.1
200–300	2.7	7.8	9.8	9.7	5.8	3.1	10.4	14.6	17.4	12.2
300–400	3.1	6.9	16.6	8.3	3.7	3.6	9.2	24.8	14.9	7.8

TABLE IV

PORE VOLUMES IN PORE RADII INCREMENTS IN THE MACROPORE RANGE AS DETERMINED BY THE MERCURY POROSIMETER

Pore radius range, Å.	Vol. in range indicated after different burn-offs, cc.					Vol. in range indicated after different burn-offs, cc./g. × 10^2				
	Unreacted	11.5%	23.0%	34.5%	46.0%	Unreacted	11.5%	23.0%	34.5%	46.0%
400– 1,000	0.04	0.04	0.04	0.03	0.02	0.5	0.5	0.6	0.5	0.4
1,000– 2,000	.04	.06	.07	.03	.02	.5	.8	1.0	0.5	0.4
2,000– 3,000	.02	.05	.08	.04	.03	.2	.7	1.2	0.7	0.6
3,000– 6,000	.05	.05	.10	.12	.08	.6	.7	1.5	2.2	1.7
6,000– 10,000	.02	.12	.11	.14	.10	.2	1.6	1.6	2.5	2.1
10,000– 20,000	.29	.54	.47	.30	.25	3.3	7.2	7.0	5.4	5.3
20,000– 30,000	.97	.70	.72	.55	.37	11.2	9.3	10.8	9.9	7.8
30,000– 40,000	.13	.15	.23	.50	.59	1.5	2.0	3.4	9.0	12.4
40,000– 60,000	.08	.10	.12	.32	.48	0.9	1.3	1.8	5.7	10.1
60,000–130,000	.02	.20	.24	.22	.20	0.2	2.7	3.6	4.0	4.2

TABLE V

DISTRIBUTION OF SURFACE AREA BETWEEN MACROPORES AND MICROPORES AS DETERMINED BY MERCURY POROSIMETER

Burn-off, %	Total surface area, $m.^2$	Macropore area, $m.^2$	Micropore area, $m.^2$	Macropore area, %	Micropore vol., cc.	Av. micropore radius, Å.
Unreacted	3.54	3.47	0.07	98.0	0.015	(4,270)
11.5	12.15	4.33	7.82	35.6	.037	94
23.0	13.55	4.04	9.51	29.8	.052	110
34.5	11.31	3.62	7.69	32.0	.039	102
46.0	8.23	2.84	5.39	34.5	.026	96

TABLE VI

SURFACE AREAS, APPARENT DENSITIES, PORE VOLUMES AND AVERAGE PORE RADII OF GRAPHITE RODS REACTED TO 11% BURN-OFF AT VARIOUS TEMPERATURES

Temp., °C.	Surface area, $m.^2/g.$	Apparent density, g./cc.	Pore vol., cc./g.	Av. pore radius, Å.
Unreacted	0.41	1.562	0.199	10,140
970	1.67	1.402	.273	3,270
1090	2.10	1.448	.250	2,380
1130	2.23	1.437	.255	2,280
1158	2.37	1.422	.262	2,210
1200	2.48	1.419	.264	2,130
1224	2.66	1.415	.266	2,000
1246	2.62	1.372	.288	2,200
1342	2.21	1.459	.245	2,220
1372	2.21	1.426	.260	2,350

It is again found that the sum of pore volumes calculated from micropore and macropore volume distributions is less than that calculated from density data. There is a decrease in the unaccounted-for pore volume upon gasification. In the original sample, it is 5.8%; and in the gasified samples, it ranges from 0.4 to 3.7%. However, there is no systematic variation between the unaccounted-for pore volume and gasification temperature.

It is found that the percentage contribution of the macropore surface areas, as calculated from porosimeter data, to the total surface area (BET)

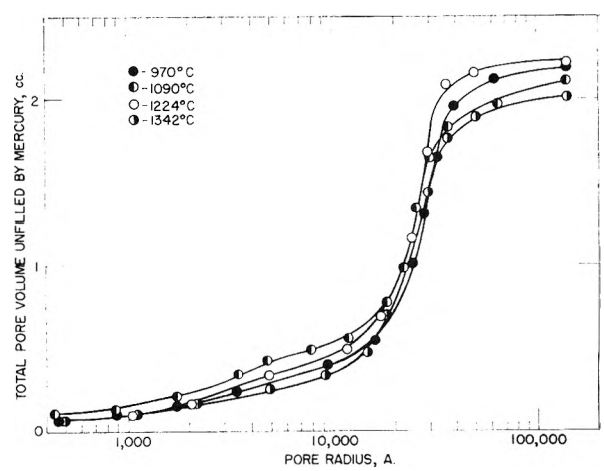

Fig. 3.—Change in macropore volume of graphite rods at various temperatures for 11.0% burn-off.

varies from 20.7 to 31.1%, it reaching the minimum value at 1224°. Furthermore, the average micropore radius, calculated as previously discussed,

TABLE VII

PORE VOLUMES IN PORE-RADII INCREMENTS IN THE MICROPORE RANGE FOR 11% BURN-OFF AT VARIOUS TEMPERATURES, AS CALCULATED FROM GAS ADSORPTION DATA

Pore radius range, Å.	Unreacted	Vol. in range indicated for 11% burn-off at various temp., cc. × 10^3								
		970°	1090°	1130°	1158°	1200°	1224°	1246°	1342°	1372°
14.7– 20	0.3	1.8	2.8	4.0	2.3	3.1	3.9	3.1	4.0	1.7
20– 36	1.3	3.8	5.2	4.2	4.7	5.1	5.5	5.3	4.2	5.5
36– 50	0.8	2.2	1.9	1.7	1.3	1.9	1.7	2.0	2.5	1.7
50– 75	1.4	2.7	2.8	3.4	2.8	2.7	2.7	3.8	3.4	3.0
75–100	1.3	3.5	3.0	4.0	2.7	5.1	3.0	3.4	3.2	3.4
100–150	2.3	4.9	5.6	5.9	4.5	8.5	6.0	5.8	5.3	6.3
150–200	1.5	3.8	6.1	4.2	4.6	6.0	5.0	6.7	3.3	5.2
200–300	2.7	12.1	12.6	10.2	7.3	8.4	9.3	12.8	7.4	7.4
300–400	3.1	8.0	11.1	10.2	7.3	6.5	7.5	12.9	7.9	6.5

TABLE VIII

PORE VOLUMES IN PORE-RADII INCREMENTS IN THE MACROPORE RANGE FOR 11% BURN-OFF AT VARIOUS TEMPERATURES, AS DETERMINED BY THE MERCURY POROSIMETER

Pore radius range, Å.	Unreacted	Vol. in range indicated for 11% burn-off at various temp., cc.								
		970°	1090°	1130°	1158°	1200°	1224°	1246°	1342°	1372°
400– 1,000	0.04	0.04	0.04	0.03	0.04	0.03	0.03	0.03	0.03	0.03
1,000– 2,000	.04	.08	.08	.06	.08	.06	.06	.10	.06	.06
2,000– 3,000	.02	.09	.08	.06	.10	.09	.07	.03	.05	.05
3,000– 6,000	.05	.15	.13	.12	.14	.22	.12	.10	.07	.09
6,000– 10,000	.02	.08	.08	.08	.09	.13	.09	.11	.09	.07
10,000– 20,000	.31	.35	.29	.32	.34	.30	.37	.65	.39	35
20,000– 30,000	1.04	.75	.87	.69	.84	.78	.95	.69	.73	.78
30,000– 40,000	0.14	.21	.19	.60	.20	.26	.31	.19	.33	.38
40,000– 60,000	.09	.11	.13	.17	.11	.14	.07	.18	.13	.14
60,000–130,000	.02	.14	.10	.10	.14	.08	.04	.16	.07	.10

ranges from 105 to 59 A. for the reacted samples, reaching a minimum also at 1224°.

Discussion

Before analyzing the results of this work, it is desirable to describe as clearly as possible the nature of the carbon rods. The original raw materials used for the production of these rods consisted of *ca.* 25% coal tar pitch and 75% calcined petroleum coke. According to Abbott,[14] for rods of the size used in this work all of the coke is less than 60 mesh (250 μ), with *ca.* 60% by weight passing 200 mesh (74 μ). Upon mixing and extruding of the green rods, the coke particles are coated with a layer of pitch to a thickness amounting to *ca.* 7% of the particle diameter.[15] Baking of the green rods to *ca.* 1000° is primarily a destructive distillation process whereby the lighter fractions of the pitch (approximately 40% by weight) are volatilized away leaving behind a binder coke structure resembling a collection of condensed bubbles. The loss in weight also results in some shrinkage of the binder and in the formation of cracks in part of the bubble structure. The rods are then graphitized to 3000°, resulting in a product in which each particle can be visualized as consisting of a highly graphitic, homogeneous inner core (filler carbon) surrounded by a "slightly less" graphitic outer shell (binder carbon).[16]

Results on the unreacted carbon rod lead to the following conclusions, if the above picture is kept in mind.

1. The original surface area of 0.4[1] m.^{2}/g. indicates that there is relatively little available internal particle porosity. That is, Petersen,[18] using the microscope sizing technique developed by Petersen, Walker and Wright[19] on a typical sample of petroleum coke, calculated an area of 0.11 m.^{2}/g. assuming no particle porosity.

2. A rod porosity of 31% suggests that the particles are packed in essentially a rhombohedral array, which has an ideal porosity of 25.95%.[20] The difference, *ca.* 5%, agrees well with the unaccounted-for pore volume, 5.8%, which is thought to be primarily located in completely closed bubbles of binder carbon.

3. A calculated micropore surface area (Pierce technique) of 0.54 m.^{2}/g., which is greater than the total surface area, suggests the presence of some micropore constrictions. These constrictions are possibly cracks leading into larger diameter bubbles of binder carbon.

4. Likewise, as previously reasoned, the calculated macropore surface area from porosimeter data is too high. This suggests again the presence of

(14) Private communication from H. W. Abbott, 1952.

(15) S. Mrozowski, "Physical Properties of Carbons and the Formulation of the Green Mix," paper presented before the 2nd Carbon Conference at Buffalo, N. Y., June 9, 1955.

(16) The degree of difference in the graphitic character of the filler and binder carbon is, of course, primarily determined by the nature of the starting raw materials. Abbott[14] suggests that the binder carbon is only slightly graphitic, whereas, X-ray diffraction results[17] on the residual carbon structure upon gasification of these rods indicates a similar interlayer spacing in the two carbons.

(17) P. L. Walker, Jr., and F. Rusinko, Jr., *Fuel*, **34**, S22 (1955).

(18) E. E. Petersen, Ph.D. Thesis, The Pennsylvania State University, 1953.

(19) E. E. Petersen, P. L. Walker, Jr., and C. C. Wright, *A.S.T.M. Bulletin*, **183**, 70 (July 1952).

(20) J. M. Dallavalle, "Micromeritics," Pitman Publ. Corp., New York, N. Y., 1948, p. 128.

pore constrictions in the form of cracks in the binder carbon.[6]

Results on the carbon rods reacted to different burn-offs at 1000° lead to the following conclusions.

1. The relatively large increase in specific surface area for 11.5% burn-off, followed by a much smaller increase for further, comparable weight losses, suggests that the majority of the early activation is obtained by opening up area which was originally closed. It is visualized that this consists of selectively breaking through relatively thin walls of binder carbon leaving the exposed area of the inner bubble walls. On the other hand, the homogeneous and rather non-porous graphitized petroleum coke particles develop little porosity upon gasification, in line with the findings of Schaeffer, Smith and Polley,[21] who oxidized graphitized carbon black particles. Gasification beyond 11.5% burn-off results in some surface area increase mainly because of the reacting through of thicker bubble walls of binder carbon surrounding the larger filler particles. Finally upon opening up of all available binder carbon area (between 23.0 and 34.5% burn-off), the specific area commences to decrease because of the higher efficiency of destroying area per unit weight of binder carbon reacted. The specific reaction rate (per unit surface area) markedly increases after 34.5% burn-off, however, since the specific rate of the filler carbon is higher than that of the binder carbon.

2. The increase in total micropore volume in all radius increments up to 23.0% burn-off should be due primarily to the opening of the bubble structure of the binder carbon. The particularly large increase in volume for pores from 14.7 to 36 Å. for 11.5% burn-off coincides with the initial, high increase in surface area.

3. The substantial decrease in macropore volume in the range 20,000 to 30,000 Å. upon 11.5% burn-off, accompanied by the large increase in volume for pores from 60,000 to 130,000 Å. suggests that the majority of macropore constrictions in the original sample was of the former size.

4. The large increase in pore volume in the range 10,000 to 20,000 Å. upon 11.5% burn-off indicates the opening up of previously closed-off pore volume in this range. Subsequent decrease in pore volume for pores between 10,000 and 30,000 Å. with gasification and increase in pore volume from 30,000 to 60,000 Å. suggests the complete destruction of some pore walls in the binder carbon, leaving larger bubbles.

(21) W. D. Schaeffer, W. R. Smith and M. H. Polley, "Surfaces of Heat Treated Carbon Blacks," paper presented before the 2nd Carbon Conference at Buffalo, N. Y., June 9, 1955.

5. For the reacted samples, the calculated micropore surface areas are all less than the total surface area. This indicates that the micropore constrictions were significantly opened up by gasification.

6. Likewise, the calculated macropore surface areas of the reacted samples give reasonable figures for the average micropore radii, indicating opening up of macropore constrictions. Furthermore, the relative constancy of average pore radius with increasing burn-off past 11.5% suggests that the removal of the pore constrictions was accomplished prior to this burn-off.

Results on the carbon rods reacted to 1 g. weight loss at a series of temperatures lead to the following conclusions.

1. The increase in surface area with gasification temperature up to 1224° can be explained by the higher efficiency of surface area development in the binder carbon as compared to the filler carbon. The lower the reaction temperature the more uniform will be the gasification of carbon through the rod[6] and, likewise, through individual particles composing the rod. This means that since the percentage of filler carbon reacted per unit weight loss is at a maximum at the lowest temperature, the over-all resulting surface area development will be at a minimum. As the gasification temperature is increased, non-uniformity of reaction will be the greater within particles (filler plus binder) than radially across the rod. This is because of the much larger pore size available for transport of gas between particles than within particles. This will result in decreasing the percentage of filler carbon reacted per unit weight loss and, hence, increasing the surface area development. However, as temperature is further increased, diffusion of the reactant gas between particles will not be sufficiently rapid to supply gas to the interior of the sample.[22] Finally, even though the fraction of the sample being reacted has a greater percentage of binder carbon activated and, hence, a greater surface area per unit weight, the resulting surface area for the entire sample will decrease because of the unreacted portion. In the limit, at sufficiently high temperatures, reaction will be found to occur solely on the surface of the rod with little area increase.

2. The reasoning for the other data follows in line with point 1 and the discussion under different degrees of burn-off at 1000°.

Acknowledgment.—The authors wish to thank Frank Rusinko for his interest and help in this work.

(22) P. L. Walker, Jr., and E. Raats, THIS JOURNAL, **60**, 370 (1956).

EFFECT OF GAS DIFFUSION IN GRAPHITIZED CARBON RODS ON THEIR GASIFICATION RATE WITH CARBON DIOXIDE[1,2]

BY P. L. WALKER, JR., AND EMILE RAATS

Department of Fuel Technology, The Pennsylvania State University, University Park, Pennsylvania

Received September 1, 1955

At high temperatures, the experimental gasification rates of graphitized carbon rods are found to deviate progressively more from their intrinsic gasification rates, as temperature is increased. This is shown to be caused by the increasing control of the reaction by the rate of transport of carbon dioxide through the internal pores of the carbon rod. The diffusional-resistance concepts used to correct the apparent activity of catalysts to their true values are found to apply equally as well for the correction of the reactivity of carbon rods with carbon dioxide.

Introduction

Workers[3-7] have shown that the physical structure of porous catalysts can be of importance in determining reaction rates. In general, the faster the reaction and the smaller the average pore size the smaller the fraction of the internal surface of the catalyst which participates in the catalytic reaction. This can result in the apparent activity of a catalyst deviating progressively more from the true activity as temperature is increased. Or, in essence, if a reaction rate constant based on the experimental activity of a catalyst is used, the Arrhenius plot can show activation energies below the true value.

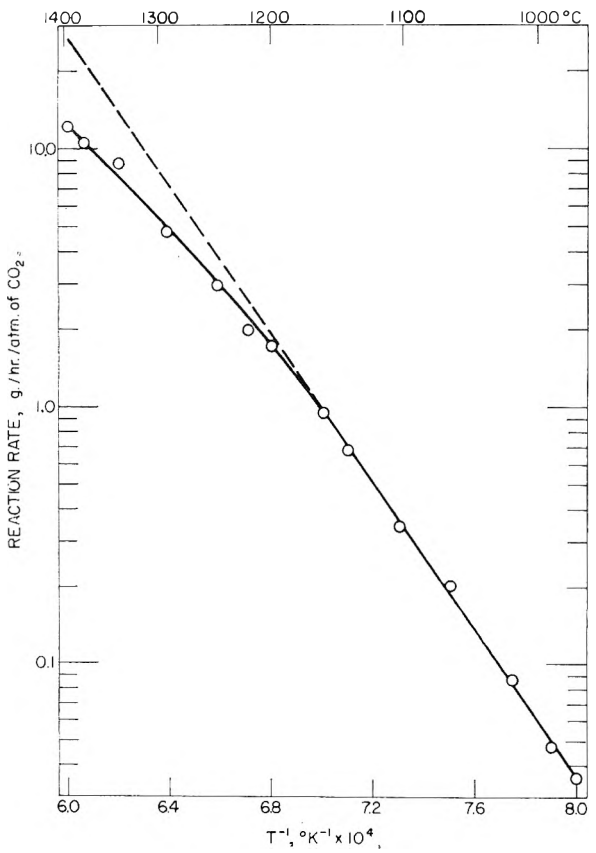

Fig. 1.—Arrhenius plot of instantaneous reaction rates at 11% burn-off.

The above workers have shown that the physical properties of a catalyst, along with internal gaseous diffusion rates, can be used to quantitatively correct the apparent activity to the true activity of the catalyst. A similar approach has been employed in the present work to correct the apparent reactivity of graphitized carbon rods with carbon dioxide to the true value as the gasification temperature is varied from 970° to 1392°.

Experimental

The samples and reaction rate apparatus used were described in an accompanying paper.[8] The apparatus and procedure used to experimentally determine the diffusion coefficient of hydrogen-nitrogen through the porous carbon rods, $D_{eff(H_2-N_2)}$, have been described previously.[9,10] $D_{eff(H_2-N_2)}$ for pellets cut parallel and perpendicular to the direction of rod extrusion were 0.088 ± 0.005 cm.²/sec. (6 samples) and 0.053 ± 0.007 cm.²/sec. (8 samples), respectively, at S.T.P. conditions.

Results and Discussion

Instantaneous reaction rates at 11% burn-off are presented on an Arrhenius plot in Fig. 1. As previously reasoned,[11] in the simplest case the reaction rate can be expressed as $R = k(CO_2)(C)$, where (CO_2) and (C) are the concentrations of carbon dioxide and carbon, respectively. In this particular case, the concentration of carbon is assumed proportional to weight of carbon, which is a constant at all temperatures for 11% burn-off. Furthermore, the concentration of carbon dioxide is taken as the average over the external sample length, it varying from 1.0 to 0.76 atm. for the temperature range investigated.

From Fig. 1, it is seen that the Arrhenius plot yields a straight line with an activation energy of 66 kcal./g. mole over the temperature range 970° to *ca.* 1130°. Above 1130°, the activation energy continually decreases, it having a value of 44 kcal./g. mole (a ratio of E_{true} to E_{exp} of 1.5) at 1392°.

A qualitative attempt at correcting for the increasing divergence of the experimental data from the straight-line Arrhenius plot can be made by dividing the above rates by the total surface area of the sample produced upon 11% burn-off. The

(1) Based on a Ph.D. thesis submitted by Emile Raats to the Graduate School of The Pennsylvania State University, June, 1955.

(2) This paper presents the results of one phase of research carried out under Contract No. AT(30-1)-1710, sponsored by the Atomic Energy Commission.

(3) E. W. Thiele, *Ind. Eng. Chem.*, **31**, 916 (1939).

(4) A. Wheeler, *Advances in Catalysis*, **3**, 249 (1951).

(5) P. B. Weisz and C. D. Prater, *ibid.*, **6**, 144 (1954).

(6) C. Bokhoven and W. Van Raayen, THIS JOURNAL, **58**, 471 (1954).

(7) J. Hoogschagen, *Ind. Eng. Chem.*, **47**, 906 (1955).

(8) P. L. Walker, Jr., and Emile Raats, THIS JOURNAL, **60**, 364 (1956).

(9) P. L. Walker, Jr., and F. Rusinko, Jr., *ibid.*, **59**, 241 (1955).

(10) Reference 5, p. 189.

(11) P. L. Walker, Jr., R. J. Foresti, Jr., and C. C. Wright, *Ind. Eng. Chem.*, **45**, 1703 (1953).

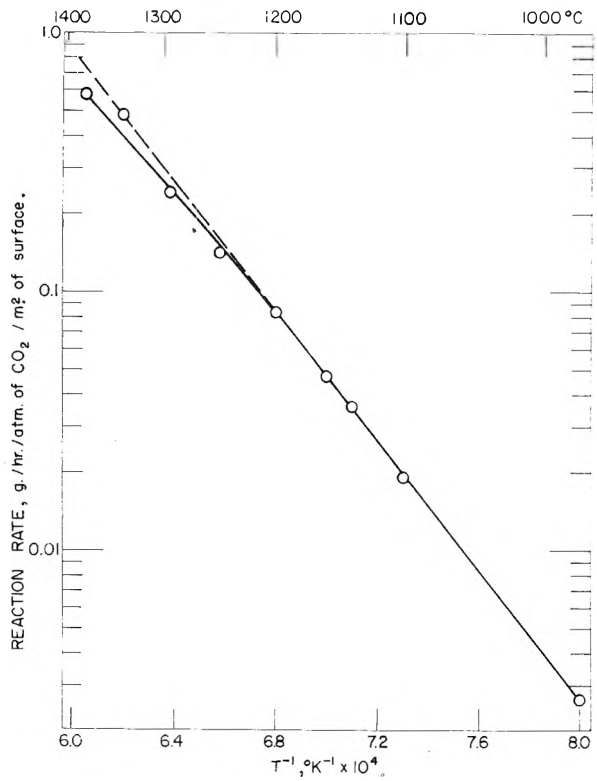

Fig. 2.—Arrhenius plot of instantaneous reaction rates per unit of total surface area at 11% burn-off.

concentration of carbon is now assumed proportional to its total surface area instead of its weight. Furthermore, as previously reasoned,[8] the continual decrease in surface area with increasing gasification temperatures above 1224° is attributed to an increasing concentration of the reaction zone closer to the sample periphery. Therefore, this decreasing area is qualitatively related to the increasing control of the reaction by diffusion; and dividing through by the area should, to some extent, compensate for the influence of diffusional resistance. Figure 2 shows the Arrhenius plot, which yields a straight line over the temperature range 970° to *ca.* 1200°, with an activation energy of 58 kcal./g. mole. Above 1200° there is some decrease in activation energy to 51 kcal./g. mole. at 1372°, giving a ratio of E_{true} to E_{exp} of 1.1. However, the use of surface area to qualitatively correct for diffusional resistance is clearly demonstrated in this case.

A quantitative approach at correcting the experimental data for diffusional resistance can now be considered in line with the authors' introductory comments. The approach of Weisz and Prater[5] is closely followed. Briefly, the experimental rate, dn/dt, divided by a diffusion factor, η, gives the corrected rate. For a spherical particle and a reaction with no volume change

$$\eta = \frac{3}{\varphi}\left(\frac{1}{\tanh \varphi} - \frac{1}{\varphi}\right) \text{ and } \varphi = R\sqrt{\frac{k_v}{D_{eff}}}$$

where R = particle radius, k_v = velocity constant per unit particle volume, and D_{eff} = the effective gas diffusion coefficient. Further, if a first-order reaction is assumed,[12] k_v can be eliminated giving a

(12) M. W. Thring and P. H. Price, *Iron and Coal Trades Rev.*, **169**, 347 (1954).

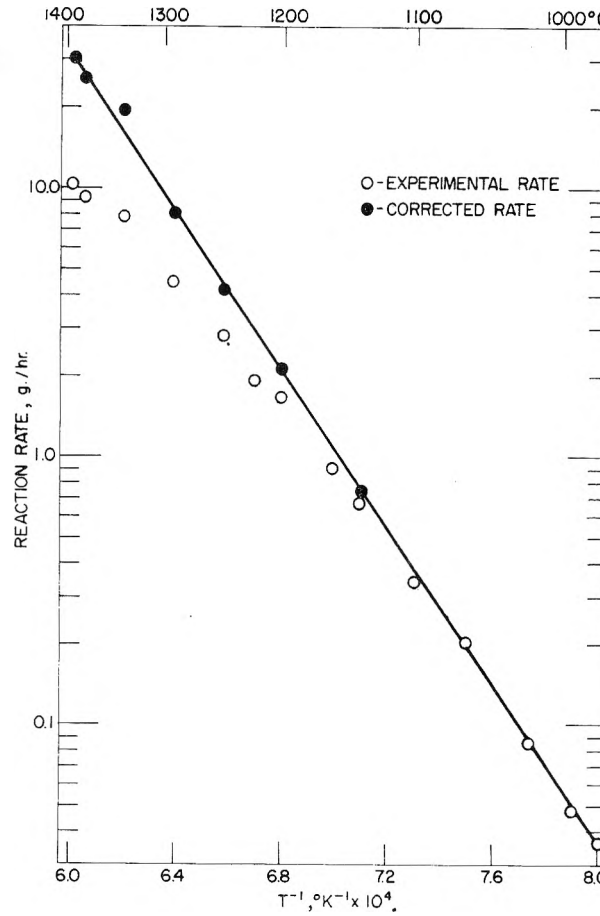

Fig. 3.—Arrhenius plot of instantaneous reaction rates at 11% burn-off with corrections for diffusional effects on first-order kinetics.

new modulus θ, which contains only observable variables.

$$\theta = \frac{R^2}{VD_{eff}} \frac{1}{(CO_2)} \frac{dn}{dt} = \varphi^2\eta$$

where V = the external volume of the carbon sample and (CO_2) is again the average concentration of CO_2 along the external length of the sample.

Values of η are determined from a plot of η *vs.* $\varphi^2\eta$ under the following conditions:

1. The same value of η is observed at 0.74 φ for a first-order reaction with doubling of volume ($C + CO_2 = 2CO$), as is observed at φ for no volume change.[13] This fact must be taken into account when the internal diffusion is occurring through pore diameters significantly greater than the mean free-path of the gas molecules. In the present case, internal diffusion through the carbon rods is visualized as primarily occurring between particle voids, which have their pore diameters concentrated above 10,000 Å.[8] Since the mean free-path of molecules at 1 atm. pressure is *ca.* 1000 Å., the above correction is necessary.

2. Even though the above functions were specifically derived for a spherical particle, they are rather insensitive to particle geometry; and R may be considered the radius of the cylindrical carbon sample.[14] This is a particularly good approxima-

(13) Ref. 5, p. 162.

(14) Private communication from P. B. Weisz, 1953.

tion in the present case, since reaction at the ends of the carbon sample is prevented by ceramic plates.

3. The effective diffusion coefficient, concerned with carbon dioxide diffusing through carbon monoxide, should be essentially identical to that for diffusion of carbon dioxide through nitrogen. The latter is calculated as a function of temperature for bulk diffusion (pore diameter > 10,000 Å. for atm. pressure reaction) from the experimental data by the relations $D \sim M^{-0.5}$ and $D \sim T^{1.5}$. The experimental value of $D_{\text{eff}(H_2-N_2)}$ perpendicular to rod extrusion is used as a basis, since transport in this direction is obviously of primary importance in determining diffusional control.

4. The pressure differential from the exterior to the interior of the carbon rod caused by an increase in gas volume upon reaction and its effect in setting up forced flow of molecules from the sample is considered negligible.

Figure 3 shows the Arrhenius plot of the corrected rate data, it yielding a good straight line over the entire temperature range 970 to 1392° with an activation energy of 66 kcal./g. mole.

The effects of other assumptions on the diffusion factor, η, were investigated. If Knudsen diffusion is assumed to be affecting the reaction rates instead of bulk diffusion, D is proportional to $T^{0.5}$ and condition 1 above can be ignored. However, this is seen to considerably over-correct the rate data; a rate of 37 g./hr. being calculated at 1292° as compared to a correct value of 8.0 g./hr., for example.

Golovina[15] studied rates of diffusion of carbon dioxide through electrode-carbon membranes, prepared in essentially the same manner as the present rods, and found D to be proportional to $T^{1.3}$ over the temperature range 20 to 600°. If this relationship is used, the corrected rates are somewhat too high. However, this agreement can be improved by selecting a higher value for $D_{\text{eff}(H_2-N_2)}$ used in the calculations. Considering the fact that upon uniform gasification of a carbon rod at 900° some increase in $D_{\text{eff}(H_2-N_2)}$ was observed,[16] an increase is perhaps not unreasonable. On the other hand, at high temperatures where diffusional effects become important, the D_{eff} for the interior portion of the rod, which is still unreacted, should primarily control the depth of reaction penetration.

Acknowledgment.—The authors wish to thank Dr. P. B. Weisz of the Socony-Mobil Laboratories for his interest in the work.

(15) E. S. Golovina, *Doklady Akad. Nauk S.S.S.R.*, **85**, 141 (1952).

(16) P. L. Walker, Jr., F. Rusinko, Jr., and E. Raats, THIS JOURNAL, **59**, 245 (1955).

THE HYDROGEN ION COULOMETER

BY H. W. HOYER

Department of Chemistry, Hunter College, New York, N. Y.

Received September 2, 1955

A new type of coulometer is described based upon the removal of hydrogen ion and chloride ion from a standard solution of hydrochloric acid in potassium chloride solution. As little as one and as many as 360 coulombs have been successfully determined. The method is particularly suited for systems in which a predetermined quantity of electricity is to be passed through a solution. The end-point can then be selected with an ordinary *p*H meter at a *p*H equal to that of the distilled water used in preparing the standard solution.

Introduction

A number of coulometers for measuring small quantities of electricity have been described in the literature. With the exception of Meites' electromechanical coulometer[1,2] and Wilson's mercury voltammeter[3,4] these microcoulometers are adaptations of conventional coulometers to micro methods.[5-7] The passage of 10 coulombs (approximately 1.04×10^{-4} equiv.) of electricity corresponds to the liberation of approximately 11.2 mg. of metallic silver in a silver coulometer or of 1.2 ml. of hydrogen in a gas coulometer. Determination of these small quantities by any customary method is susceptible to errors of at least several per cent. It is the purpose of this communication to describe a hitherto unreported system which can readily detect and measure the passage of as little as one coulomb of electricity to a precision of a few parts per thousand.

The electrochemical reaction in this new coulometer is the removal of hydrogen and chloride ions from a standard solution of hydrochloric acid and potassium chloride in CO_2 free distilled water. One electrode, the anode, is of the silver–silver chloride type while the other is a platinum cathode. The end-point may be selected in the vicinity of *p*H 7.0 with an ordinary *p*H meter or the acid remaining may be titrated with standard base. Greater precision is obtainable if it is possible to bring the final *p*H to that of the distilled and CO_2-free water used in preparing the standard solution. An error of even 0.1 *p*H unit in estimating the end-point in the vicinity of *p*H 7.0 becomes a percentage error of only 0.025% when as little as 10^{-4} equivalent of hydrogen ion is determined.

Experimental

The essential features of the coulometer used in this investigation include a beaker of approximately 200-ml. capacity, a platinum electrode with a surface area of 4 sq. cm. and a silver foil electrode having a total surface area of 175 sq. cm. The solutions were prepared by weighing out

(1) L. Meites, *Anal. Chem.*, **24**, 1057 (1952).

(2) S. Bogan, L. Meites, E. Peters and J. M. Sturtevant, *J. Am. Chem. Soc.*, **73**, 1584 (1951).

(3) C. T. R. Wilson, *Proc. Cambridge Phil. Soc.*, **19**, 345 (1920).

(4) W. O. Reevely and A. R. Gordon, *Trans. Electrochem. Soc.*, **63**, 167 (1933).

(5) I. Berkes, *Mikrochemie Mikrochem. Acta*, **40**, 160 (1952).

(6) H. von Wartenberg and H. Schutza, *Z. Electrochem.*, **36**, 254 (1930).

(7) K. Fischbech, *Z. anorg. allgem. Chem.*, **148**, 97 (1925).

constant boiling hydrochloric acid into specially distilled and CO_2-free water made approximately 0.1 *N* with respect to KCl. Changes in *p*H of the solution during the passage of the current were observed with a continuously indicating *p*H meter. Adequate mixing of the solution during each determination was provided by a magnetically driven stirrer. The customary glass and calomel *p*H electrodes which were used did not, of course, affect the *p*H of the solutions.

The validity of the procedure was checked by two different methods. For the larger quantities of electricity a silver coulometer was placed in series with the hydrogen ion coulometer. With the passage of lesser equivalents of electricity the error involved in measuring the quantity of silver deposited became significant. Further evaluation of the procedure was then continued by a graphical method. The potential drop across a Leeds and Northrup standard 10 ohm resistance was measured with a potentiometer at fixed intervals of time and the quantity of electricity passed determined from a plot of the current *versus* the time.

The results of these tests are tabulated in Table I. In all of these determinations current was passed through the system until the *p*H of the solution became identical with that of the distilled, CO_2-free water used in preparing the solutions. The column headed "Gravimetric" refers to the equivalents of constant boiling HCl weighed out while the column headed "Electrometric" gives the equivalents of hydrogen ion removed electrically and determined as described above. The graphical procedure was employed in experiments 2, 3, 8, 9 and 10. The ten determinations involved the passage of from 360 to as little as 1.18 coulombs of electricity and showed an average deviation of 3.3 parts per thousand.

TABLE I

EQUIVALENTS OF HYDROGEN ION COMPARISON OF GRAVIMETRIC AND ELECTROMETRIC DATA

Experiment	Gravimetric	Electrometric	Difference, %
1	3.731×10^{-3}	3.750×10^{-3}	0.5
2	2.565×10^{-3}	2.560×10^{-3}	0.2
3	2.356×10^{-3}	2.366×10^{-3}	0.4
4	2.276×10^{-3}	2.267×10^{-3}	0.4
5	2.157×10^{-3}	2.163×10^{-3}	0.3
6	4.563×10^{-4}	4.569×10^{-4}	0.1
7	1.936×10^{-4}	1.946×10^{-4}	0.5
8	1.028×10^{-4}	1.031×10^{-4}	0.3
9	5.705×10^{-5}	5.706×10^{-5}	0.0
10	1.223×10^{-5}	1.216×10^{-5}	0.6

Discussion

When a solution of hydrochloric acid and potassium chloride is electrolyzed with a platinum cathode and a silver anode the anode reaction will be

$$Ag + Cl^- \longrightarrow AgCl + e^- \quad (1)$$

while at the cathode

$$H^+ + e^- \longrightarrow {}^1/_2H_2 \quad (2)$$

The net effect is the removal of one equivalent of HCl for each equivalent of electricity passed.

Since the coulometer depends upon the removal of hydrogen ions from solution, every precaution must be observed to prevent the introduction of extraneous acid into the system. This implies the use of a carbon dioxide-free system. For our purposes the desired CO_2-free water was obtained by distilling distilled water through a tin condenser and then bubbling CO_2-free air through the water for one or two days. This gave samples of water with *p*H values of from 6.4 to 6.9.

Because the change in the *p*H of the solution depends upon the migration of ions it becomes important to examine all possible means by which current can pass through the solution. In the solutions used the only ions present are H^+, Cl^-, K^+ and enough OH^- to satisfy the ionization constant for water. In such a system and on a clean platinum cathode the only possible reaction, even at hydrogen ion concentrations of 10^{-7}, can be reaction (2) above.

The standard oxidation potential for reaction (1) is -0.222 volt. Since relatively minute amounts of chloride ions are removed by the electrochemical reaction, the concentration of this ion will remain approximately constant at 0.1 *M* throughout the experiment. Under the given conditions neither chlorine gas or oxygen will be liberated since the standard oxidation potential for the production of the former is -1.36 volts and for the latter is -1.23 volts.

In spite of the theoretical considerations which seem to limit the electrode reactions to reactions (1) and (2) the initial experiments indicated that current was being carried by a path or paths other than these reactions and that this secondary path was introducing an error of from 1 to 2% in the determination. This effect was traced to the presence of colloidal silver chloride which began to appear when the deposit of silver chloride upon the anode become too thick. Increasing the area of the silver anode to 175 sq. cm. was found to eliminate the effect when less than 4×10^{-3} equivalent of electricity, approximately 390 coulombs, were passed through the solution.

Another and for some purposes perhaps more convenient but less accurate method of utilizing the above described coulometer would be to titrate the HCl remaining after a given quantity of electricity has been passed through the solution. The accuracy of the determination then depends upon the accuracy of the titration. In the electrophoresis work in progress in the author's laboratory and undoubtedly in many other cases it is possible to electrolyze a given quantity of HCl and so utilize the fullest possible accuracy of this hydrogen ion coulometer.

NOTES

THE SOLUBILITY OF CHLORINE IN TITANIUM TETRACHLORIDE AND OF CARBON DIOXIDE AND OXYGEN IN CHLORINE[1]

By Walter F. Krieve and David M. Mason[2]

Jet Propulsion Laboratory, California Institute of Technology, Pasadena, Calif.

Received June 27, 1955

The solubility of chlorine in liquid titanium tetrachloride was determined at 20 and 30° for mixtures containing from 0 to 100 mole % chlorine. These data were required in a calorimetric determination of the heat of formation of titanium tetrachloride to correct for the heat of solution of chlorine in titanium tetrachloride.

The solubility of carbon dioxide in chlorine at 0 and 25° was measured up to about 6.6 mole % carbon dioxide and the solubility of oxygen in chlorine at 25° up to 1.7 mole % oxygen. The chief impurities in commercially-pure chlorine were found to be carbon dioxide and air, and it thus was of interest to determine the solubility of carbon dioxide and oxygen which would cause errors in the calorimetric determination of the heat of formation of titanium tetrachloride. Such solubility data aided in the purification of liquid chlorine.

For the solubility measurements commercial chlorine was purified by fractional distillation to remove air and CO_2. Titanium tetrachloride of 99.999% purity provided by the National Bureau of Standards and pure samples of carbon dioxide and oxygen manufactured by Matheson Co., Inc., were also used. Stainless steel PVT bombs of 175-cc. capacity and calibrated stainless steel Bourdon gages were employed in the solubility measurements. A known weight of gas was admitted by a system of valves from one PVT bomb to another bomb, which contained a known amount of liquid and which was submerged in a constant temperature bath maintained to within 0.1° of a given temperature. The weight of gas admitted to the second bomb was determined by measuring the change in pressure in the first bomb. After equilibrium was established, the pressure in the second bomb was measured and the solubility calculated from the pressure data. All pressure measurements were made to within 0.5%. Gas densities were obtained from existing volumetric data for chlorine,[3] carbon dioxide[4] and oxygen.[5] The partial pressure of liquid carbon tetrachloride[6] was negligible compared with the partial pressure of chlorine.[7] Corrections were made for the partial pressure of chlorine in the determination of the solubility of carbon dioxide and oxygen by assuming Raoult's law was followed by the chlorine.

In Table I are shown results of the measurements of solubility of chlorine in titanium tetrachloride. The data show a slight departure from Raoult's law. Also shown are solubility data for carbon dioxide and oxygen in liquid chlorine, respectively.

Table I

Experimental Values of the Solubility of Chlorine in Titanium Tetrachloride and of Carbon Dioxide and Oxygen in Chlorine

Chlorine (A) in titanium tetrachloride				Carbon dioxide (A) in chlorine				Oxygen (A) in chlorine	
20°		30°		0°		25°		25°	
Mole % A	Partial pressure A (atm.)	Mole % A	Partial pressure A (atm.)	Mole % A	Partial pressure A (atm.)	Mole % A	Partial pressure A (atm.)	Mole % A	Partial pressure A (atm.)
25.13	1.50	42.27	3.39	1.06	0.772	0.976	1.10	0.785	5.22
35.85	2.20	48.44	3.93	1.593	1.10	1.42	1.50	0.936	6.67
43.58	2.71	55.71	4.63	2.135	1.67	2.04	2.21	1.31	9.13
49.64	3.13	64.12	5.41	2.983	2.29	2.98	3.03	1.49	10.53
56.74	3.67	71.07	6.14	3.945	2.90	3.80	3.85	1.65	11.99
64.99	4.24			4.950	3.59	4.74	4.80		
72.29	4.76			5.640	4.10	5.46	5.55		
				6.582	4.78	6.43	6.54		

(1) This paper presents the results of one phase of research carried out at the Jet Propulsion Laboratory, California Institute of Technology, sponsored by the Department of Army, Ordnance Corps, and the Department of Navy, Office of Naval Research, under Contract No. DA-04-495-Ord 18.

(2) Department of Chemistry and Chemical Engineering, Stanford University, Stanford, California.

(3) R. E. Hulme and A. B. Tillman, *Chem. Eng.*, **56** (No. 1), 99 (1949).

(4) R. L. Sweigert, P. Weber and R. L. Allen, *Ind. Eng. Chem.*, **38**, 185 (1946).

(5) R. W. Millar and J. D. Sullivan, U. S. Bur. Mines Tech. Paper 424 (1928).

(6) H. Schafer and F. Zeppernich, *Z. anorg. allgem. chem.*, **272**, 274 (1953).

(7) M. Pellaton, *J. chim. phys.*, **13**, 426 (1915).

EXCHANGE BETWEEN ADSORBED AND DISSOLVED SULFATE IONS

By Cecil V. King and Boris Levy[1]

Chemistry Department, New York University, New York 3, New York

Received September 6, 1955

During the course of a study on the adsorption and exchange of silver salts on silver[2] it was found that if a silver coupon were immersed in a radioactive solution of $Na_2S^*O_4$, removed from the solution, and then washed with water, a measurable

(1) Chemical & Physical Laboratory, RCA, Lancaster, Penna.

(2) C. V. King and B. Levy, This Journal, **59**, 910 (1955).

TABLE I

ADSORPTION-EXCHANGE IN $S^{=}$–$S^{*}O_4^{=}$ SYSTEMS

Temperature, ambient (~25°); volume of solution, 50 cc.

System	Concn. of soln., M	Wt. of powder, g.	Time, hr.	Radio-activity, % change	Conductivity, % change
Ag_2S–$Na_2S^{*}O_4$	1.38×10^{-2}	25	88.5	− 5.7	0.0
		25	88.5	− 3.4	+ 0.3
Ag_2S–$Ag_2S^{*}O_4$	1.43×10^{-2}	25	2	−13.4	− 8.4
		25	2	−11.8	− 7.0
	1.16×10^{-2}	25	2.3	−12.8	− 6.0
		25	12	−10.8	− 6.6
		25	27	−13.3	− 6.0
		25	29.5	−20.4	− 7.8
Ag–$Na_2S^{*}O_4$	1.38×10^{-2}	25	2	− 2.0	+ 0.3
		25	2	− 4.9	+ 0.6
Ag–$Ag_2S^{*}O_4$	1.16×10^{-2}	25	9.5	− 8.3	− 3.3
		25	26	− 3.6	− 3.6
	1.14×10^{-2}	25	3.5	+ 1.5	− 0.9
		25	3.5	+ 0.5	− 1.2
MnS–$Na_2S^{*}O_4$	1.14×10^{-2}	15	24	−25.9	+219
		15	24	−24.4	+219

TABLE II

ADSORPTION-EXCHANGE IN ZnS–$Na_2S^{*}O_4$ SYSTEM

Concn. of $Na_2S^{*}O_4$ solution = 1.14×10^{-2} M; volume of solution = 60 cc.; temperature, ambient (~25°).

Wt. of ZnS, g.	Time of run, hr.	Final $SO_4^{=}$ concn., M	Final no. of moles $SO_4^{=}$ on ZnS	No. of moles $SO_4^{=}$ exchanged	Adsorption-exchange, %
7.0812	24	1.195×10^{-2}	1.380×10^{-3}	0.804×10^{-3}	58.3
9.7311	45.75	1.130×10^{-2}	1.921×10^{-3}	1.139×10^{-3}	59.0
22.7335	94.25	1.395×10^{-2}	4.595×10^{-3}	2.687×10^{-3}	58.5
19.0025	94	1.395×10^{-2}	3.837×10^{-3}	2.283×10^{-3}	59.5

amount of activity remained on the silver. This activity was easily removed by short periods of immersion in 0.1 M KCN. Similar experiments in the range of 10^{-2} to 10^{-4} M $Na_2S^{*}O_4$ yielded data that fit a Langmuir type isotherm.

Since the experiments were performed in air, there was a definite possibility of sulfide contamination of the silver, which in turn, may have contributed to the activity left on the silver after washing.

It has been reported by Wahl and Bonner[3] that there is exchange between $S^{=}$ and $S^{*}O_4^{=}$ in the MnS(s)–$MnSO_4$(l) system. This is an error on their part since the original paper by Daudel, Daudel and Martin[4] reports exchange of Mn and makes no reference to S. Exchange of sulfur between $S^{=}$ and $S^{*}O_4^{=}$ would account for the inability to wash off all of the $SO_4^{=}$ on a silver coupon having a sulfide deposit. The possibility of exchange was, therefore, checked. (It has been shown previously that there is no $S^{=}$–$SO_4^{=}$ exchange in homogeneous solution.[5])

The method used was to combine conductimetric and radioactive measurements before and after shaking solutions of $Na_2S^{*}O_4$ and $Ag_2S^{*}O_4$ with Ag_2S, ZnS, MnS and Ag powders. Decrease in radioactivity of the solution could be due to adsorption and exchange, while decrease in conductivity is due to adsorption alone. Conductivity *vs.* concentration curves were obtained for Ag_2SO_4, Na_2SO_4 and $ZnSO_4$ solutions for calibration purposes in the concentration range of from 10^{-5} to 10^{-1} M.

Ideally, for dilute solutions if there were adsorption but no exchange, the per cent. decrease in conductivity should be equal to the per cent. decrease in radioactivity of the solution. In every case the decrease in radioactivity somewhat exceeded the decrease in conductivity. Part of the reason for this may be attributed to an enhanced conductivity of the solution due to soluble adsorbed or occluded salts. In the case of MnS and ZnS powders, there was actually a marked increase in conductivity.

Six experiments were performed with the Ag_2S–$Ag_2S^{*}O_4$ system, the time of shaking with radioactive solution ranging from 2 to 30 hours. The change in radioactivity and conductivity is seen to remain fairly constant (Table I). If there were slow exchange between $S^{=}$ and $S^{*}O_4^{=}$, one would expect the percentage change in radioactivity to depend quite strongly on the time. The Ag_2S was prepared by bubbling H_2S into a dilute $AgNO_3$ solution. Under these conditions it is quite likely that some NO_3^{-} ion will be adsorbed on the Ag_2S. The discrepancy between the radioactive and conductimetric measurements might be due to exchange between adsorbed NO_3^{-} ions and $SO_4^{=}$ ions in the solution as well as to soluble adsorbed or occluded salts. As the NO_3^{-} content of the Ag_2S was unknown, no way of testing this was possible.

A ZnS sample containing 2.01% by weight of $SO_4^{=}$ which could exchange with Cl^{-} ion was made

(3) A. C. Wahl and N. A. Bonner, "Radioactivity Applied to Chemistry," John Wiley and Sons, Inc., New York, N. Y., 1951, p. 363.

(4) P. Daudel, R. Daudel and M. Martin, *Bull. soc. chim. France*, **D**, 68 (1949).

(5) H. H. Voge, *J. Am. Chem. Soc.*, **61**, 1032 (1939).

available by Sylvania Electric Products, Inc.[6] Experiments were performed using varying amounts of this ZnS in 60 cc. of 0.1125 *M* $Na_2S^*O_4$, shaken for periods of from 24 to 94 hours (Table II). It was found in each case that the conductivity of the solution increased while the radioactivity decreased. On the assumption that the $ZnSO_4$ was leaving the surface of the ZnS, and thus causing an increase in the conductivity, a new $SO_4^=$ concentration was calculated from the measured increase in conductivity. The number of moles of $SO_4^=$ remaining on the ZnS powder was also obtained. From this information it was possible to calculate the percentage of the final $SO_4^=$ on the ZnS that exchanged with the $SO_4^=$ in the solution. Exchange with adsorbed material is defined by the term adsorption-exchange to differentiate it from exchange between bulk phases. In the present study it is used to describe the exchange between $SO_4^=$ ions adsorbed on ZnS and $SO_4^=$ ions in solution. This adsorption-exchange was found to remain constant regardless of time of shaking or amount of ZnS used, and to be about 59%. Adsorption-exchange alone is, therefore, sufficient to account for the observed decrease in radioactivity without the necessity of postulating $S^=$–$S^*O_4^=$ exchange. The same situation is probably equally true of the Ag_2S–$SO_4^=$ system, but this has not been proved.

The conclusions that may be drawn from this work are: (1) There is no $S^=$–$SO_4^=$ exchange. (2) Adsorption-exchange is important in systems consisting of precipitated material and may be expected to vary with the ions involved. (3) In the Ag_2S–$Na_2S^*O_4$ system the decrease in conductivity is practically zero, indicating that there is little or no adsorption of Na_2SO_4 on Ag_2S. (4) In the Ag–$Na_2S^*O_4$ system there is no measurable adsorption by this method. (5) In the Ag–$Ag_2S^*O_4$ system there is measurable adsorption.

(6) D. T. Palumbo and A. K. Levine, *J. Electrochem. Soc.*, **102**, 181 (1955), gives data on exchange of adsorbed $SO_4^=$ with Cl^- and of adsorbed Cl^- with $SO_4^=$.

THE GROWTH OF ICE LAYERS ON THE SURFACES OF ANATASE AND SILVER IODIDE[1]

By F. E. Karasz,[2] W. M. Champion and G. D. Halsey, Jr.

Department of Chemistry, University of Washington, Seattle, Washington

Received September 26, 1955

Introduction.—The equilibrium growth of adsorbed layers of solid xenon on the surface of three crystals has been shown[3,4] to be limited by the incompatibility of the two crystal structures. This fact was established by a study of the change of the argon isotherm with the thickness of the pre-adsorbed layer of xenon. Here we extend the study to pre-adsorbed layers of water (ice). Of the three underlying surfaces previously studied, we have omitted graphite, because of its hydrophobic nature, and confined our attention to the anatase and silver iodide samples used in the earlier work.

Anatase.—The standard Harkins and Jura anatase has been thoroughly characterized by these authors.[5] The area of the sample was estimated from a B.E.T. plot of the nitrogen isotherm on the sample. By use of the ratio $V_m(H_2O)/V_m(N_2) = 1.095$, which had been obtained by Harkins and Jura, it was found that 5.97 cc. of water vapor at S.T.P. was required to complete one monolayer on the 1.693-g. sample used. An accurate quantity of water vapor was obtained by dehydrating the necessary amount of $BaCl_2 \cdot 2H_2O$. Preliminary experiments had shown that this method, using adequate precautions, yielded the theoretical amount of water to within about 3%. The dehydration was carried out by heating to 200° for about one hour. The water vapor was carried over into the adsorption bulb which was kept at liquid nitrogen temperature.

It was found that the deposition of the water layers to ensure maximum uniformity on the surface was critical. To obtain reproducibility the rate of cooling during deposition had to be such that the temperature of the adsorption bulb fell from 20 to −70° over a period of not less than 12 hours. This low rate was achieved by evacuating the outer jacket surrounding the bulb to a very low pressure.[3] This procedure yielded reproducible isotherms on pre-adsorbed layers of water. This was checked in a number of cases by allowing the anatase to warm up to room temperature, at which most of the water would desorb, and then repeating the cooling with the same water, and repeating the isotherms. The reproducibility of this procedure was also checked by outgassing the anatase at 300° overnight and introducing a fresh sample of water and repeating the isotherms.

Measurements were made of argon isotherms on the bare anatase and on one, two, three, four, eight and twelve layers of pre-adsorbed water, at −196°. Nitrogen isotherms were obtained at the same temperature, on one, two, four and eight layers of water.

The results, Fig. 1, show that up to about 3 layers of pre-adsorbed water can be distinguished. More than 3 pre-adsorbed layers yield essentially the same isotherms. It may be noted that the argon isotherms do not give a good "point B" except for the isotherm on the bare surface, while the nitrogen isotherms are somewhat less affected by the water layers and all give a reasonable "point B."

Silver Iodide.—The anatase was now replaced by a sample of the high surface area silver iodide which had been used previously for argon on pre-adsorbed xenon measurements.[2] The sample had been stored in the absence of light and a B.E.T. plot of the nitrogen isotherm showed that its area per unit weight remained the same. As already reported it could not be outgassed at a temperature higher than 25° because of loss of area.

(1) This research was supported by Contract AF19(604)-247 with the Air Force Cambridge Research Center.

(2) Presented in partial fulfillment of the requirements for the Ph.D. degree.

(3) J. H. Singleton and G. D. Halsey, Jr., This Journal, **58**, 330 (1954).

(4) J. H. Singleton and G. D. Halsey, Jr., *Can. J. Chem.*, **33**, 184 (1955).

(5) G. Jura and W. D. Harkins, *J. Am. Chem. Soc.*, **66**, 1356 (1944).

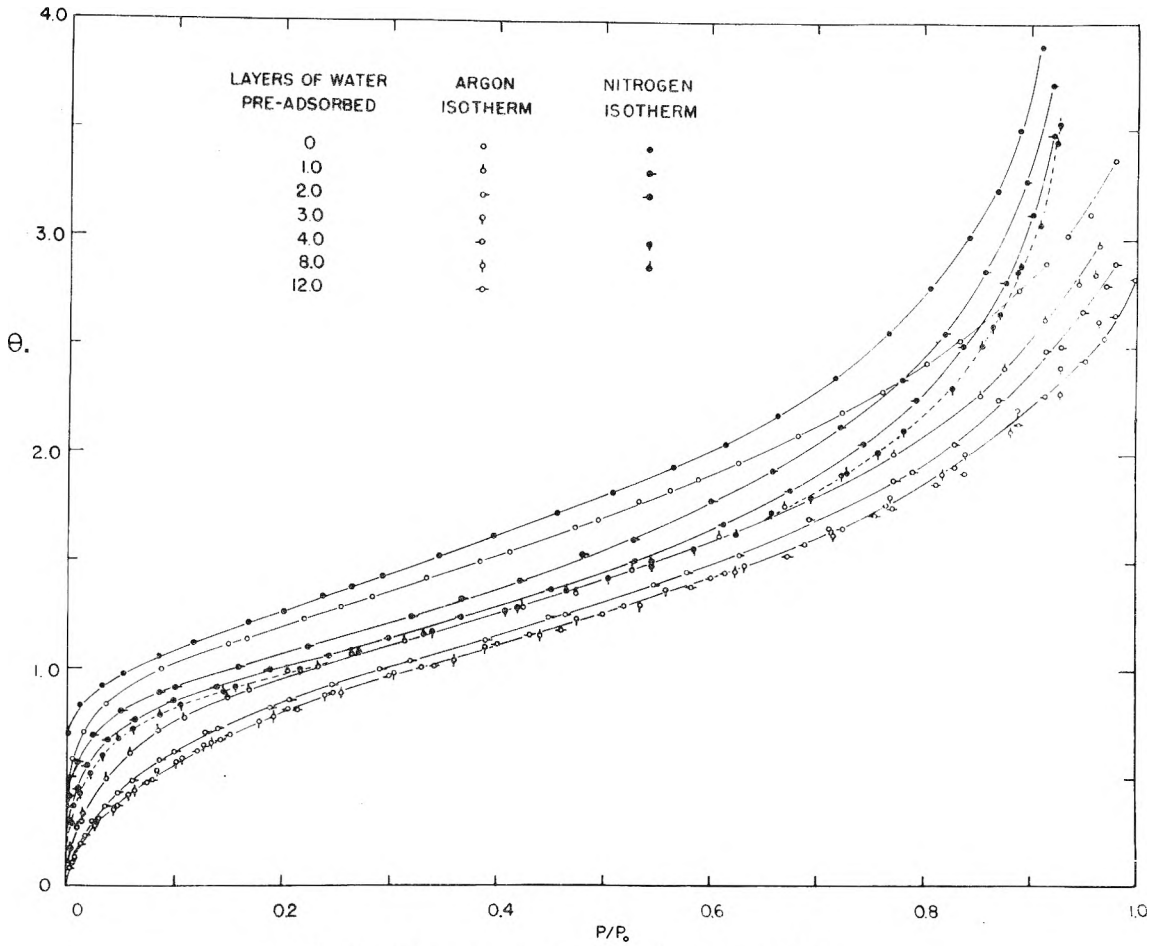

Fig. 1.—Adsorption of argon and nitrogen on anatase.

A small number of layers of water were pre-adsorbed on the silver iodide in the usual manner and argon isotherms measured for these systems. It was found that the isotherms, at 80°K., for the iodide with and without pre-adsorbed water were almost identical. It was possible to reproduce the bare surface isotherms by pumping off any water that had been introduced.

It was at first suspected that the water was not being adsorbed uniformly on the silver iodide. The rate of cooling was therefore still further reduced by increasing the heat capacity of the inner bulb and by using different cooling baths. With these measures it was possible to take up to 48 hours in cooling the sample from −40 to −75° which corresponds to the critical range for the mobility of the water, approximately 10^{-1} to 10^{-3} mm. An ammonia gas thermometer was used to measure the temperature.

In spite of this and other precautions it was again found that the argon isotherm with 5 layers of water in the sample bulb were almost the same as those measured on the bare surface (see Fig. 2).

The apparatus was then modified to enable water isotherms on the silver iodide to be measured. A pirani gage was constructed and calibrated *in situ* with water vapor. In one side of the gage the pressure was kept at 0.055 mm., corresponding to −45° at which temperature the isotherms were to be run and the pressure on the other side was varied by using a number of different freezing baths. The pirani gage was used at constant potential and a calibrated variable resistance was used to balance the bridge.

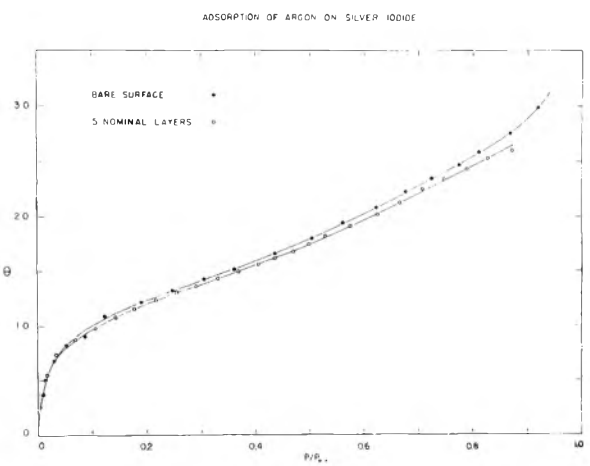

Fig. 2.—Adsorption of argon on silver iodide.

In running the isotherms the silver iodide was degassed at room temperature for 48 hours.

The water vapor was introduced into the adsorbent bulb using barium chloride hydrate. It was found that at −45.2° the adsorption was below the value at which isotherms could be obtained with the apparatus and techniques used. We conclude

that the growth of layers of ice on silver iodide does not take place under equilibrium conditions. The two surfaces are concluded to be energetically incompatible.

THE FAST CHLORIDE EXCHANGE BETWEEN HYDROCHLORIC ACID AND CHLOROAURIC ACID IN β,β′-DICHLORODIETHYL ETHER

By D. G. Tuck, Charles D. Coryell and John W. Irvine, Jr.

Department of Chemistry and Laboratory for Nuclear Science, Massachusetts Institute of Technology, Cambridge, Massachusetts

Received September 30, 1955

In recent years research has been carried out in this Laboratory on the extraction of acids of the general formula HMX_4 into various organic solvents, but the exact nature of the species which pass across the interfacial boundary and which exist in the organic phase is still the subject of some discussion.[1,2] The extraction coefficient of chloroauric acid $HAuCl_4$ into β,β′-dichlorodiethyl ether from varying strength hydrochloric acid solutions has been measured by Golden.[3] It was hoped that by studying the chloride exchange reaction between hydrochloric acid and the gold chloride species present in the organic phase some information might be obtained on the nature of these species. Furthermore, since the kinetics of this reaction in aqueous solutions has been reported by Rich and Taube,[4] the effect of medium on the ligand exchange rate could also be investigated. Using labeled hydrochloric acid, an extremely rapid rate of exchange has been observed. An ion-exchange method of separation has been employed which was shown not to induce much exchange; separations were complete in about 30 seconds.

Reagents

β,β′-Dichlorodiethyl Ether.—Carbide and Carbon Chemicals 100% β,β′-dichlorodiethyl ether[5] was distilled under reduced pressure from crystalline $FeSO_4 \cdot 5H_2O$. The fraction distilling at 74–76° at 16 mm. pressure of nitrogen was collected,[6] substantial head and tail fractions being rejected. The distillate was stored over anhydrous K_2CO_3 in the absence of light in order to prevent peroxide formation; suitable quantities were filtered immediately before use.

Acids.—A.R. grade HCl, HNO_3 and $HClO_4$ were used without further purification. Concentrations were determined by titration against standard aqueous NaOH solution.

Chloroauric Acid.—An aqueous stock solution containing approximately 100 mg./ml. Merck crystalline $HAuCl_4$ was diluted 25 times; $HClO_4$ was added to 2 *M* to increase the extraction coefficient which is low in the absence of acid. The mixture was shaken with an equal volume of fresh dichloroether and the phases separated by centrifuging. The extraction coefficient and hence the concentration of $HAuCl_4$ in the organic phase was determined by titration of the aqueous solution with 0.02 *f* $Na_2S_2O_3$ in the presence of excess potassium iodide before and after extraction.

Tagged Hydrochloric Acid.—Radioactive Cl^{38} was obtained by bombardment of A.R. KCl in the M.I.T. cyclotron for 15 minutes with 15 Mev. deuterons. The target material was then treated with concentrated H_2SO_4 and the evolved gases carried in a slow stream of air through a solution of HCl in dichloroether, prepared by solvent extraction of 6 *N* HCl. Titrations showed the HCl concentration normally to be of the order of 0.05 *f* in the ether.

Techniques

Ion-exchange Separation.—Columns of Dowex-1 (10% cross-linkage, 100–200 mesh) in the nitrate form were used, with a resin bed effectively 7 cm. long and 0.4 cm. diameter. The resin was converted to the nitrate form in bulk, dried at approximately 60° for 1 day, and soaked in dichloroether for some time prior to use.

The behavior of $HAuCl_4$ and HCl solutions in the dichloroether on such columns was tested separately. Using 2 ml. of $HAuCl_4$ solution (0.04 *f*) labeled with a mixture of radioactive gold isotopes (kindly supplied by Dr. P. Schonken of this Laboratory), it was found that the sorption of the gold species was quantitative and rapid. Elution with nitric acid in the ether (approx. 0.1 *f*) or with aqueous solution (approx. 4 *f*) did not remove the gold. The resin was then extruded from the column and counted in four fractions. The results showed that 90% of the gold was held in the upper half of the column. The total activity found by this procedure was 98% of that present in the original solution so that clearly the counting efficiency for resin samples is not significantly different from that involved in counting the ether solution. In view of this experimental agreement, it was felt that Cl^{38} present in $HAuCl_4$ after exchange could also be measured by this technique since it has even higher γ energy than the complex mixture of gold isotopes (prepared by deuteron bombardment of platinum).

For a 0.07 *f* solution of HCl in the dichloroether, take-up was 96% complete for a single passage down the column. The Cl^{38} could not be removed by washing with 0.1 *f* HNO_3 in the ether, but was eluted completely and rapidly with approximately 4.5 ml. of 4 *f* aqueous HNO_3. The addition of the aqueous acid causes the resin to swell noticeably so that elution becomes slower, even under suction, but this was not considered serious since the separation of the exchanging components of the solution was presumed to be complete when both were completely taken up on the column.

Exchange Conditions.—One ml. each of solutions of HCl* and $HAuCl_4$ in the dichloroether were mixed in a conical tube and the reaction mixture transferred to the widened mouth of the ion-exchange column. (This mixing technique was used to avoid possible pre-adsorption of one component on the resin.) Suction was applied and the mixture passed quickly down the column. The minimum time for this procedure was 30 seconds. The HCl* was then eluted with aqueous HNO_3 as described above and counted; the $HAuCl_4$* was measured by counting the resin phase after removal from the column. All experiments were carried out at room temperature.

Counting Procedure.—Solutions and resin samples were collected in glass vials and counted in a well-type scintillation counter.[7] Because of the decay of Cl^{38}, corrections were applied to normalize all counting rates to an arbitrary zero time. An experimentally determined half-life of 37.5 ± 0.5 minute (mean of three measurements) was used in these corrections.

Results

For all concentrations of HCl and $HAuCl_4$ investigated the exchange was found to be complete within the time required for the separation procedure. The lowest formal concentrations used were

Run	HCl	$HAuCl_4$	$HClO_4$[8]
1.3	0.004	0.010	0.052
1.4	.046	.006	.052
1.8	.016	.002	.032

(1) R. H. Herber, W. E. Bennett, D. R. Bentz, L. C. Bogar, R. J. Dietz, Jr., G. S. Golden and J. W. Irvine, Jr., 126th National Meeting of the American Chemical Society, Abstract 79, September 14, 1954.

(2) J. Saldick, ref. 1, Abstract 78.

(3) G. S. Golden, S.B. Thesis, Department of Chemistry, Massachusetts Institute of Technology, 1954.

(4) R. L. Rich and H. Taube, *J. Phys. Chem.*, **58**, 1 (1954).

(5) For convenience, this solvent will be referred to as dichloroether throughout the paper.

(6) D. R. Stull, *Ind. Eng. Chem.*, **39**, 517 (1947).

(7) J. W. Irvine, Jr., *Nucleonics*, **12**, No. 10, 62 (1954).

(8) The $HClO_4$ concentrations given here are those found for the extraction of $HClO_4$ from water into the dichloroether in the absence of $HAuCl_4$. Since $HAuCl_4$ is weakly ionized in the ether solutions, a small unknown correction should be applied to get the true concentration.

The specific activities in HCl and $HAuCl_4$ were identical within experimental error. By comparison with aliquots of the original HCl* solution, it was shown that a complete activity balance was being achieved.

Certain experiments were carried out to investigate the possibility of an exchange induced during the separation procedure. In these experiments, a solution of $HAuCl_4$ in dichloroether was run onto the column, which was then washed with the pure solvent. A 1-ml. aliquot of labeled HCl solution in the ether was then passed down the column and eluted in the usual manner. The percentage exchange occurring was calculated from the following equation

$$\% \text{ exchange} = \frac{\text{Cl activity on resin}}{\text{Cl activity eluted}} \times \frac{\text{HCl}}{4 \times \text{HAuCl}_4} \times 100$$

where the symbols represent the moles of each species concerned, and hence the ratio gives the equilibrium distribution of activity. The results of two experiments are given below.

Run	HCl (mmoles)	$HAuCl_4$ (mmoles)	% exchange
2.1	0.040	0.0051	3.1
2.3	0.071	0.0116	20.5

These values show that for low concentrations this effect is negligible. The increase in exchange with increasing concentration suggests that there is probably not so much an induced exchange but rather a fairly rapid isotopic exchange between HCl and the resin–$AuCl_4$ species in these experiments.

The exchange between HCl and the two chlorine atoms of the solvent was briefly investigated to ensure that this could not affect the results. A solution of labeled HCl in dichloroether was allowed to stand for 5 hours, after which 1 ml. was shaken with two 15-ml. portions of water and centrifuged. The non-extracted activity represented only 5% of that calculated for total exchange. For the much shorter time intervals between HCl absorption and the actual exchange experiments (normally about 30 minutes or less), this effect is negligible.

Discussion

Taking account of the results presented above, one can set an upper limit of approximately 10 seconds for the half-time of the HCl–$HAuCl_4$ exchange in the 0.01 *f* concentration region.

It has been emphasized elsewhere[9,10] that the rate of any reaction between two ions of the same charge should decrease as the dielectric constant D of the solvent decreases. For dichloroether, D = 21.2, whilst for water, D = 80. Comparison of the present results with those of Rich and Taube[4] shows a decrease by a factor of 20 or more in the half-time for the exchange for similar concentrations. It seems likely that this apparent contradiction with theory is due to reaction of uncharged species in the organic solution. For HCl in dichloroether conductance measurements show that this acid is only slightly ionized; the ionization constant[11] for ion-pair formation for millimolar solutions is of the order of 10^{-7}.

(9) G. Scatchard, *Chem. Revs.*, **10**, 229 (1932).
(10) D. Peschanski, *J. chim. phys.*, **50**, 634 (1953).
(11) A. M. Poskanzer, private communication.

The gold chloride probably also exists mainly in the dichloroether as $HAuCl_4$, or as has been suggested for indium bromide,[12] as the associated ion-pair $(H^+)(AuCl_4^-)$. The crystalline chloroaurates show a planar structure for the $AuCl_4^-$ ion[13] and if this exists in such an associated ion pair, the activated complex with HCl should be in a form favorable for ligand exchange.

The role of associated water in such molecules in organic solution is uncertain. The work of Gibson and Colles[14] indicates that for the bromoaurates water is essential for dissolution in dry diethyl ether, since they find that a mixture of $AuBr_3$, HBr and ether is immiscible in the absence of water, but addition of water causes $HAuBr_4$ to dissolve in the organic phase exothermically. This suggests that the species present in organic solutions has the formula $HAuX_4 \cdot nH_2O$ as has been shown to be the case for iron[15] in dichloroether.

Rich and Taube[4] have pointed out that for the Cl^-–$AuCl_4^-$ exchange in aqueous solution the presence of reductants in the solution can enhance the rate of exchange. It seems unlikely that in the highly purified dichloroether there would be an appreciable concentration of reducing entities and in fact, any impurities produced in this solvent would be expected to be oxidants.

Acknowledgment.—The senior author acknowledges a fellowship under the M.I.T. Foreign Students Summer Project. The experimental work was supported by the U. S. Atomic Energy Commission.

(12) L. A. Woodward and P. T. Bill, *J. Chem. Soc.* (*London*), 1699 (1955).
(13) A. F. Wells, "Structural Inorganic Chemistry," Oxford University Press, 1945, p. 290.
(14) C. S. Gibson and W. M. Colles, *J. Chem. Soc.* (*London*), 2407 (1931).
(15) J. Axelrod and E. H. Swift, *J. Am. Chem. Soc.*, **62**, 33 (1940).

THE KINETICS OF THE CS_2–NO REACTION AND THE MECHANISM OF LIGHT EMISSION IN THE EXPLOSIVE REACTION

BY WALTER ROTH AND THEODORE H. RAUTENBERG

General Electric Research Laboratory, Schenectady, New York

Received October 3, 1955

There has been a recent renewal of interest in flames supported by nitrogen oxides.[1-3] Van Liempt and de Vriend have studied the composition explosion limits and the light output of the reaction between CS_2 and NO.[4,5] They have reported luminous efficiencies as high as 83 lumens/watt. In addition, they have estimated an ignition temperature of 1900° from experiments with melting wires. In the course of determinations of P–T explosion limits for the CS_2–NO system, we have

(1) E. Bartholome and H. Sachse, *Z. Elektrochem.*, **53**, 326 (1949).
(2) H. Behrens and F. Rossler, *Naturwissenschaften*, **36**, 218 (1949).
(3) W. G. Parker and H. G. Wolfhard, Fourth Symposium on Combustion, 420–8 (1952); Fifth Symposium on Combustion 718–28 (1954).
(4) J. A. M. van Liempt and J. A. de Vriend, *Rec. trav. chim.*, **52**, 160 (1933).
(5) J. A. M. van Liempt and J. A. de Vriend, *ibid.*, **52**, 549 (1933).

been able to ignite mixtures in a 5-cm. diameter spherical silica vessel immersed in a furnace at temperatures as low as 775° and, in general, our ignition temperatures have been of the order of 1000° lower than those estimated by van Liempt and de Vriend. The explosion limits are of the thermal type and can be expressed approximately by log $(P/T) = A/T + B$[6] at pressures above about 20 cm. for mixture composition ratios, $(NO)/(CS_2)$, from 1 to 8. The slope, A, decreases sharply at the lower pressures, perhaps indicating an increasing importance of surface reactions at these pressures. In a separate series of experiments, a number of short pieces of silica tubing were put into the vessel such that the surface to volume ratio was doubled while the diameter of the vessel was not seriously altered. A comparison of the results is shown in Fig. 1. It can be seen that the effect of increased surface area is to increase the limit pressure at pressures below about 30 cm.

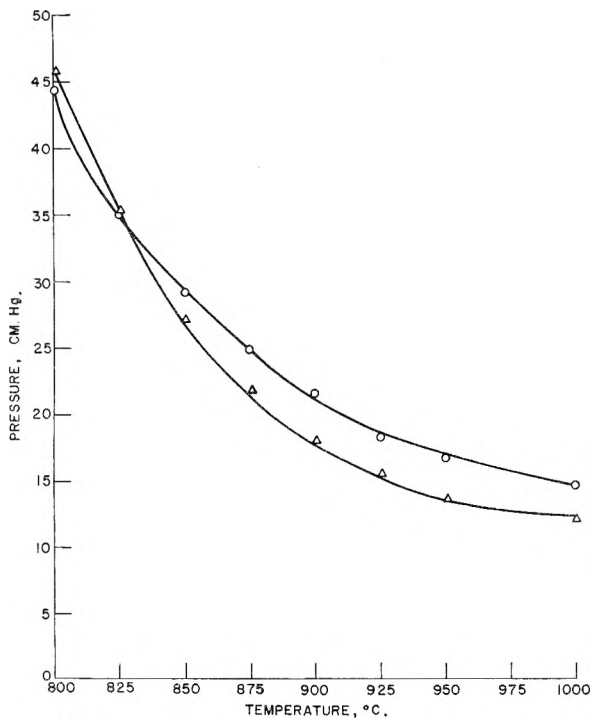

Fig. 1.—The effect of surface area on the $CS_2 + 3NO$ explosion limit: Δ, 5 cm. diameter vessel; O, same vessel with S/V doubled.

The thermal nature of the explosion limit has been confirmed by experiments with the addition of inert gases to the mixture $(NO)/(CS_2) = 3$. In these experiments, the results of which are given in Table I, it has been found that, for a given temperature, $P_m = p_d + (k_m/k_u)^{1/3}P_u$, where P_m is the explosion limit pressure for the diluted mixture, P_u for the undiluted mixture, p_d is the partial pressure of the diluent, and k's are thermal diffusivities at 273°K. The latter have been determined from thermal conductivities of the mixtures which were calculated by the method of Lindsay and Bromley.[7] Deviations of calculated from experimental results are well within the errors involved in the experiments and in the calculations of mixture thermal conductivities.

Table I

Effect of the Addition of Inert Gases on the Explosion Limit Pressure in cm. Hg of $CS_2 + 3NO$

Upper value is exptl. Lower value is calcd.

% A →	0	4.8	10.0	20.0	40.0
T, °C.					
825	35.2	36.1	37.8	...	...
		36.9	38.8		
850	27.2	...	...	...	...
875	21.7	23.2	24.0	24.6	...
		22.5	23.8	26.5	...
900	18.0	19.0	19.6	20.4	...
		18.7	19.8	20.0	...
925	15.3	15.5	16.7	17.2	22.6
		16.1	16.8	18.6	23.5
950	13.6	...	14.7	15.2	19.2
			15.0	16.6	20.8
1000	12.1	12.5	12.5	13.3	...
		12.7	13.4	14.8	

% He →	0	5.0	10.0
T, °C.			
850	27.2	...	31.1
			30.1
875	21.7	21.8	24.8
		23.8	25.3
900	18.0	19.7	20.2
		19.2	21.0
925	15.3	16.2	17.6
		16.5	17.8
950	13.6	14.1	15.4
		14.7	15.8
1000	12.1	12.8	13.5
		13.0	14.2

Explosions are characterized by a bright blue flash of light and a decrease in pressure. Deposition of sulfur is observed and this increases as the mixtures are made richer in CS_2. At temperatures slightly below the explosion limit a slow reaction has been observed. The rate of this reaction was measured at 750° for the mixture $(NO)/(CS_2) = 3.00$ and, despite the expectation that non-isothermal conditions would obtain, was found to fit a third-order rate law, second order with respect to NO and first order with respect to CS_2, with remarkable precision. The measured rate constant was $7.7 \pm 0.2 \times 10^{-9}$ mm.$^{-2}$ sec.$^{-1}$. Thermal decomposition of NO[8] could not have resulted in an error greater than 3% in the rate measurement. There is evidence which indicates that the reaction is non-chain, and of the third order, even in the explosive region. Since the reaction is thermally propagated, the rate of heat production must be equal to the rate of heat loss at the explosion limit. An equivalent statement is that a critical rate of heat production must be attained for explosion to become self-propagating. Then, if the reaction is second order with respect to NO and first order with respect to CS_2, it can be shown

(6) N. Semenoff, "Chemical Kinetics and Chain Reactions," Oxford Univ. Press, 1935, pp. 79–83; D. A. Frank-Kamenetzky, *Acta Physicochim.*, **10**, 365 (1939).

(7) A. L. Lindsay and L. A. Bromley, *Ind. Eng. Chem.*, **42**, 1508 (1950).

(8) H. Wise and M. F. Frech, *J. Chem. Phys.*, **20**, 22 (1952).

that the composition-pressure explosion limit should have a minimum in pressure at a mole fraction of NO of 2/3. This is actually the position of the minimum indicated by the work of van Liempt and de Vriend[4] and confirmed in our experiments. In addition, the 1/3 power dependence of pressure on thermal diffusivity indicates an overall third-order reaction. The explosion limit for a reaction exhibiting third-order kinetics is more accurately represented by $\log(P^3/T^2) = A/T + B$ where the slope $A = (E/2.303R)$. From the average slope, we have calculated an activation energy of 70 ± 5 kcal. This is in agreement with the heat of dissociation of an S-atom from CS_2. The latter value is about 70–80 kcal.; a specific value connot be determined because of uncertainties in the heats of dissociation of CS and sublimation of carbon.

If the reaction involved free radical chains, it would be expected that O-atoms would participate. In this event, evidence for the reaction NO + O → NO_2* should be detected. We have photographed spectra of CS_2–NO and CS_2–O_2 flashes in the visible region, using a Hilger Medium Quartz Spectrograph with a slit width of 25 μ and Eastman 103-F plates. Ignition was accomplished with exploding 1 mil tungsten wires. These spectra exhibit identical features. Two continua are evident, one from 4900 Å. to the short wave length limit of the explosion vessel (3100 Å.) and the other from 5500 Å. to the long wave length limit of the plate (7000 Å.). Superimposed on the continua are weak SO bands and stronger S_2 bands. As the pressure is increased the bands are observed to decrease in intensity while the continua increase in intensity. At a sufficiently high pressure, the bands disappear entirely. Most important is the fact that neither of the continua can be ascribed to the reaction NO + O → NO_2* since this could not occur in the CS_2–O_2 flashes. Furthermore, the region 4900–5500 Å. is one of very low intensity, whereas the continuum of NO_2* → NO_2 + $h\nu$ is strong in this region. In addition, mass spectrometric analyses indicated that no NO_2 was present among the products even when NO was initially present in excess. These facts rule out the reactions SO + O → SO_2*, CS + O → COS*, and CO + O → CO_2*, as emitters of the continua in CS_2–NO flashes. Nevertheless, the continuum from 4900 Å. to the violet was observed to go through an intensity maximum with variation in initial mixture composition at the same composition at which mass spectrometric analyses of products indicate a maximum in SO_2 production for both CS_2–NO and CS_2–O_2 flashes. This would indicate that an excited SO_2 is the emitter of the short wave length continuum. Furthermore, this continuum appears to be the same one observed by Gaydon[9] in the SO_2 after-glow. If the reaction SO + O → SO_2* occurs during CS_2–O_2 flashes, the energy of the reaction is enough to take the continuum down to about 1900 Å. Formation of SO_3 could not be responsible for light emission since this compound is never observed among the products.

(9) A. G. Gaydon, *Proc. Roy. Soc.* (*London*), **A146**, 901 (1934).

Third-order gas phase reactions involving NO are thought by some to proceed *via* the formation of a collision dimer of NO. If this dimer were to lose one O-atom in reaction with CS_2 or CS, there is the possibility that an N_2O residue would remain. N_2O is indeed observed among the products, but appears only when NO is initially in excess as might be expected since N_2O can react further with CS_2. The presence of N_2O as an intermediate suggests a possible reaction for the formation of excited SO_2. This may be formed by

$$SO(^3\Sigma) + N_2O(^1\Sigma) \longrightarrow SO_2(^3\Sigma) + N_2(^1\Sigma)$$

where, if the N_2 is produced in its ground electronic state, the Wigner–Witmer correlation rules[10] indicate that the electronic state of the SO_2 must be $^3\Sigma$. Magnetic susceptibility measurements[11] on gaseous SO_2, indicate that it is diamagnetic. This establishes its ground state as a singlet state. Radiation of the continuum would, in this case, involve a forbidden triplet–singlet transition. However, the selection rules may be weakened somewhat by a non-linearity of the SO_2 analogous to the situation encountered in the CO_2 continuum observed in CO–O_2 explosions.[12] In addition, the heavy S-atom would be expected to contribute to this weakening. From the heat of the SO–N_2O reaction, we can set an upper limit for the position of the excited state of SO_2 above the ground state of 110 kcal. if SO is in its ground state, and 220 kcal. if SO is in the excited state which results in radiation of the SO band system. In both cases, the upper limit results when it is assumed that all of the reaction energy is carried away by the SO_2 and none by the N_2.

The long wave length continuum goes through an intensity maximum at a mixture composition which is different from the optimum for the SO_2 continuum. It is felt that $COS(^3\Pi)$ is responsible for this radiation by analogy with $CO_2(^3\Pi)$. The reaction CS + O → COS involving an O-atom has been ruled out. Furthermore, this would have enough energy to take the continuum to 1900 Å. The reaction CO + S → COS* can, on energetic grounds, result in a continuum to 4750 Å. On the basis of arguments already discussed, the COS would have to be formed in a triplet excited state. COS has been found among the products of the reaction when CS_2 is initially in excess.

(10) E. Wigner and E. E. Witmer, *Z. Physik*, **51**, 859 (1928).
(11) P. Pascal, *Compt. rend.*, **148**, 413 (1909).
(12) R. S. Mulliken, *J. Chem. Phys.*, **3**, 720 (1935).

EFFECT OF IODINE ON THE RADIOLYSIS OF BENZENE[1]

BY ROBERT H. SCHULER

Contribution from the Chemistry Department, Brookhaven National Laboratory, Upton, L. I., N. Y.

Received October 4, 1955

Burton and Patrick[2] have shown that the hydrogen yield from the radiolysis of benzene is little affected by the presence in solution of sub-

(1) Research performed under the auspices of the U. S. Atomic Energy Commission.
(2) M. Burton and W. N. Patrick, *J. Chem. Phys.*, **22**, 1150 (1954).

stances such as *p*-terphenyl and anthracene which greatly increase the fluorescence of the irradiated solutions. A concentrated solution of *m*-terphenyl in benzene was shown to have a somewhat lower yield of hydrogen than pure benzene. The present work shows that a similar small decrease in the hydrogen yield is observed for concentrated iodine solutions in benzene.

Experimental

Ten-cc. samples of Phillips Research Grade (99.93%) benzene were degassed on a high vacuum line, sealed and irradiated for from one to four days inside a cylindrical Co^{60} source[3] having an intensity of 276,000 R./hr. The sample was then reattached to the vacuum line and the fractions volatile at liquid nitrogen temperature and at $-120°$ were pumped to a McLeod gage for measurement and subsequently to a Saunders-Taylor apparatus for analysis.[4] Based on the rate of oxidation of ferrous ion in the Fricke dosimeter [$G(Fe^{+++}) = 15.45$] energy was absorbed in the benzene at the rate of 2.38×10^{17} e.v. cc.$^{-1}$ min.$^{-1}$. It is assumed here that the absorption of energy is proportional to the electron density of material irradiated.

Results and Discussion

The yields of hydrogen and C_2 gas observed for pure benzene and for three concentrated iodine solutions are given in Table I. The gas volatile at liquid nitrogen temperature was found to be 98 to 99% hydrogen, little or no methane being formed. The radiation yield for hydrogen production from pure benzene observed in the present work using γ-radiation is slightly higher than that found by Manion and Burton[5] for electron bombardments at much higher intensities. The C_2 gas yield is somewhat lower than the values of 0.022[5] and 0.020[6] observed in the electron bombardment studies.

TABLE I

EFFECT OF IODINE ON THE RADIOLYSIS OF BENZENE

Iodine concn., *M*	Irradiation period, min.[c]	H_2[a] produced, moles $\times 10^6$	$G(H_2)$[b]	$G(C_2)$[b]
0	1390	2.07	0.0377[d]	...
0	4560	6.81	.0378[d]	0.0185[d]
.020	1690	2.40	.0360	.0169
.037	1580	2.21	.0354	...
.206	1355	1.80	.0306	.0151

[a] From a 10-cc. sample. [b] Molecules per 100 e.v. [c] Energy is absorbed in the benzene at the rate of 2.38×10^{17} e.v. cc.$^{-1}$ min.$^{-1}$. [d] Manion and Burton[5] gave a yield of 0.0357 for H_2 and 0.022 for C_2 for 2.0 Mev. electrons.

It is seen that the dissolved iodine has little effect on the hydrogen yield except at very high concentrations. A drop in yield of 23% is observed for a solution 0.2 *M* in I_2 which may be compared with a 25% drop found by Burton and Patrick[2] for a 0.25 *M* *m*-terphenyl solution. The effect of iodine appears to be the same in lowering the H_2 and C_2 yields.

It has previously been shown in the case of cyclohexane that for dilute solutions ($<10^{-3}$ *M*) of iodine the yield of hydrogen remains unaltered[7] while for more concentrated solutions (10^{-3} to 5 $\times 10^{-2}$ *M*) a drop in the hydrogen yield occurs.[8] The radiolysis of benzene is affected to a much smaller extent by the presence of a given concentration of iodine than is the radiolysis of aliphatic hydrocarbons.

Since iodine is expected to be a good scavenger for hydrogen atoms, the fact that the hydrogen yield is not suppressed by the presence of iodine indicates that its production occurs almost entirely by processes which form molecular hydrogen in a single step, *i.e.*, that hydrogen atoms do not play an important intermediary role in this radiolysis. Hentz[9] has commented that available data on the radiolysis of cyclohexane–deuterobenzene mixtures also indicates the importance of ultimate molecule modes of decomposition of the benzene. Gordon and Burton[6] have shown that the hydrogen produced from benzene–deuterobenzene mixtures contains appreciable HD. The formation of HD without the intervention of hydrogen atoms requires the production of a hydrogen molecule from two different benzene molecules in a one-step process. This is conceivably closely related to the formation of cross-links in the radiolysis of hydrocarbons.

The presence of iodine potentially introduces electron traps into solution so that the charge neutralization steps might be expected to be altered and result in a change in the chemistry of the system. That little change in yield is observed appears to indicate either that the electrons from the ionization processes return to neutralize their original partners as proposed by Burton, Magee and Samuel[10] or that the benzene itself serves as a powerful electron attaching agent. The small effect of iodine at high concentrations is presumably due to energy transfer processes which follow the initial absorption of energy. A similar transfer of energy has been demonstrated by Williams and Hamill[11] for solutions of methyl iodide in benzene.

(3) B. Manowitz, *Nucleonics*, **11**, [3] 18 (1953).

(4) *Cf.* R. H. Schuler and C. T. Chmiel, *J. Am. Chem. Soc.*, **75**, 3792 (1953), for gas analysis procedure.

(5) J. P. Manion and M. Burton, THIS JOURNAL, **56**, 560 (1952).

(6) S. Gordon and M. Burton, *Disc. Faraday Soc.*, **12**, 88 (1952).

(7) C. C. Schubert and R. H. Schuler, *J. Chem. Phys.*, **20**, 518 (1952).

(8) R. H. Schuler, to be published.

(9) R. Hentz, THIS JOURNAL, **59**, 380 (1955).

(10) M. Burton, J. N. Magee and A. H. Samuel, *J. Chem. Phys.*, **20**, 760 (1950); A. H. Samuels and J. N. Magee, *ibid.*, **21**, 1080 (1953).

(11) R. R. Williams, Jr., and W. H. Hamill, *Radiation Research*, **1**, 158 (1954).

DIELECTRIC DISPERSION BEHAVIOR OF AMYLOPECTIN ACETATE–TRICRESYL PHOSPHATE SYSTEMS[1]

BY CHARLES F. FERRARO AND JOHN J. MAURER

Department of Chemistry, Fordham University, New York 58, New York

Received October 18, 1955

The effects of internal and external plasticization on the electrical properties of the naturally occurring polymers amylose, amylopectin and cellulose are under investigation in This Laboratory. This article reports the observed variations of the dielectric constants, ϵ', and the dielectric loss factors, ϵ'', of disks of amylopectin acetate plasticized with *o*-, *m*- and *p*-tricresyl phosphate and tri-*o*-cresyl thiophos-

(1) The reported data are from the results of a Ph.D. investigation, in progress, carried out by John J. Maurer in the Department of Chemistry, Fordham University.

TABLE I

DIELECTRIC DISPERSION OF AMYLOPECTIN ACETATE–TRICRESYL PHOSPHATE SYSTEMS AT 45°

Frequency, kc.	System: o-TCP ε′	o-TCP ε″	m-TCP ε′	m-TCP ε″	p-TCP ε′	p-TCP ε″	T-o-CthioP ε′	T-o-CthioP ε″
0.10	5.01	0.331	5.34	0.299	5.69	0.381	4.83	0.580
0.20	4.76	.405	5.21	.391	5.56	.433	4.50	.585
0.50	4.48	.426	4.96	.481	5.37	.452	4.22	.338
1.00	4.23	.309	4.67	.448	5.20	.515	4.10	.205
2.00	4.10	.238	4.41	.397	5.03	.523	4.07	.122
5.00	4.01	.152	4.20	.269	4.76	.666	4.03	.081
10.00	3.94	.110	4.08	.175	4.41	.612	4.01	.040
20.00	3.91	.094	4.03	.133	4.21	.442	3.99	.040
50.00	3.87	.093	4.00	.108	4.07	.285	3.96	.079
100.00	3.83	.092	3.95	.099	3.99	.199	3.94	.079

phate measured at 45.0° over the frequency range of 10^2 to 10^5 c.p.s. In all cases, the plasticizer concentration was 25.0% by weight. The measurements suggest that the observed frequency range of dispersion is related to the polarity of the plasticizer molecule.

Experimental

A. Apparatus.—Measurements of ϵ' to ±0.5% and ϵ'' to 2.0% were carried out with the following General Radio Co. equipment: Type 716-C Capacitance Bridge, Type 1302-A Oscillator, Type 1474 Amplifier and Null Detector equipped with Filter Type 1603-A, and Type 1690 Dielectric Film Holder. The temperature of the disks and the Film Holder was regulated to ±0.1° by use of an air thermostat. The DC conductivities of the disks were measured with a General Radio Co. Megohmmeter Type 1862-B and corrections were applied to the ϵ'' values as pointed out by Fuoss.[2]

B. Materials. 1. Corn Amylopectin Acetate (CBUA).—Corn starch supplied through the courtesy of Corn Products Refining Co. was defatted and fractionated by the method of Schoch.[3] The amylopectin content of the ethanol-precipitated fraction was measured as 88.3% by the method of French, Rundle and Bates.[4] This was acetylated, and the product analyzed, by the procedure of Mullen and Pascu.[5] (Calcd. acetyl, 44.7%; found 39.4%.)

2. Tricresyl Phosphate Derivatives (TCP).—*o*-, *m*-, *p*-TCP and tri-*o*-cresyl thiophosphate were obtained commercially. The reported boiling points were 263–265° (20 mm.) for the *o*-TCP and 273–275° (17 mm.) for *m*-TCP and the melting points were 76–78° and 43.5–45.0° for T-*o*-CthioP and *p*-TCP, respectively.

3. Polymer-Plasticizer Disks.—These were prepared by dissolving the two components in chloroform, evaporating the solvent, and pressing the resulting sheet (after cutting) in a Carver Laboratory Press. With regard to all the disks, the pressure employed was 10,000 p.s.i., the temperature varied from 108 to 110°, and the time varied from 2 to 12 hours. The diameters were 2.00 inches and the thicknesses varied from 0.0626 to 0.0938 inches. All disks were formed in a stainless steel mold. They were coated with aluminum foil by means of Vaseline prior to the measurements of the electrical properties.

Results and Discussion

The calculated values of ϵ' and ϵ'' for the four systems are recorded in Table I, and the inflection points of the ϵ' values and the maxima of the ϵ'' values as a function of log frequency are shown in Fig. 1. To determine whether the observed differences in the frequencies at which ϵ''_{max} values occur were possibly related to the polarity of the plasticizer molecule, the relative polarities of the latter were determined by measuring the difference, ΔC, in total capacitance between solution and solvent for benzene solutions of concentrations 8.000 g. per 100.00 ml. A dielectric cell containing 19.00 ml. was employed in conjunction with the General Radio Co. Capacitance Bridge Type 716-C. The frequency employed was 10^6 c.p.s., and the measurements were performed at room temperature. From the values of ΔC, listed in Table II, it is seen that the polarity of the plasticizer molecules are in the order T-*o*-CthioP < *o*-TCP < *m*-TCP < *p*-TCP.

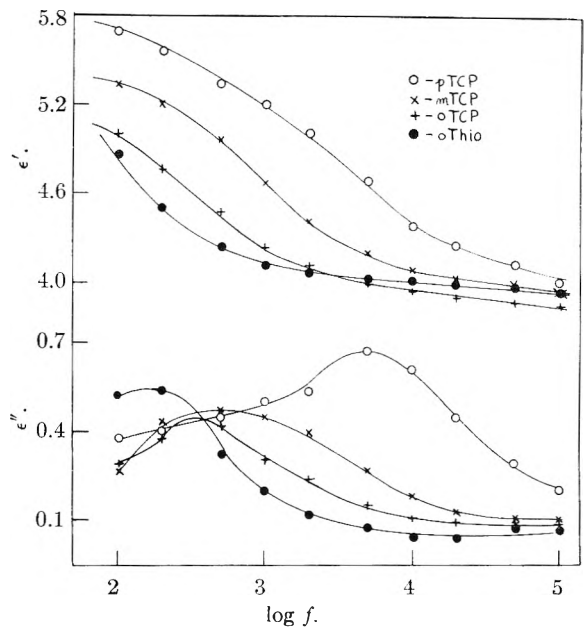

Fig. 1.—ϵ' and ϵ'' values for CBUA–TCP disks 25% plasticizer, 45°.

TABLE II

Plasticizer	ΔC ($\mu\mu$f.)
T-*o*-CthioP	13.0 ± 0.2
o-TCP	20.1
m-TCP	20.6
p-TCP	22.8

This also represents the order of the frequencies at which the values of ϵ''_{max} appear for the four systems.

A possible explanation of this observed relationship lies in the assumption that the rotating dipolar units are combinations of plasticizer and polymer molecules, a mechanism previously suggested by Fitzgerald and Miller[6] for the system polyvinyl

(2) R. M. Fuoss, *J. Am. Chem. Soc.*, **63**, 369 (1941).
(3) T. J. Schoch, *ibid.*, **64**, 2957 (1942).
(4) D. French, R. E. Rundle and F. L. Bates, *ibid.*, **65**, 142 (1943).
(5) J. W. Mullen and E. Pascu, *Ind. Eng. Chem.*, **34**, 1209 (1942).
(6) E. R. Fitzgerald and R. F. Miller, *J. Coll. Sci.*, **8**, 148 (1953).

chloride–dimethylthianthrene. The amylopectin acetate molecule has an average molecular weight of 10^7 with approximately 1300 branches,[7] and it is therefore expected that chain entanglement is present. Chain segments are possibly unraveled by dipole–dipole interaction with plasticizer molecules, the extent increasing with the increasing polarity of the plasticizer molecules.

Acknowledgment.—This research was conducted under Contract AF 33(616)-322 with the United States Air Force, the sponsoring agent being the Aeronautical Research Laboratory of the Wright Air Development Command.

(7) A. L. Potter and W. Z. Hassid, *J. Am. Chem. Soc.*, **70**, 3774 (1949).

MOLARITY QUOTIENTS FOR THE FORMATION OF COMPLEXES BETWEEN CADMIUM IONS AND AMINES CONTAINING SULFUR[1]

By Charles R. Bertsch, W. Conard Fernelius and B. P. Block

College of Chemistry and Physics, The Pennsylvania State University, State College, Pa.

Received November 2, 1955

A recent publication[2] reports values for the dissociation constants of $CH_3SCH_2CH_2NH_2$, $S(CH_2CH_2NH_2)_2$ and $(—CH_2SCH_2CH_2NH_2)_2$ and for the molarity quotients of complexes of these amines with Cu^{++}, Ni^{++}, Co^{++} and Zn^{++}. These measurements have now been extended to include Cd^{++}.

Experimental

The preparation and purification of the amines as well as the methods of measurement and calculation are described elsewhere.[2,3]

Data and Results

The measurements of *p*H and calculation of $\bar{n}$ and [A] permit the evaluation of the molarity quotients recorded in Table I. It is not possible to determine the values for these amines with Mg^{++} because precipitates form before appreciable coördination takes place.

Discussion

A comparison of the values for the formation molarity quotients of Cd^{++} with each of the pairs: $CH_3SCH_2CH_2NH_2$ and $H_2NCH_2CH_2NH_2$, $S(CH_2CH_2NH_2)_2$ and $HN(CH_2CH_2NH_2)_2$, and $(-CH_2SCH_2CH_2NH_2)_2$ and $(-CH_2NHCH_2CH_2NH_2)_2$ shows clearly that coördination through sulfur is not as strong as through nitrogen in agreement with previous findings[2] for Cu^{++}, Ni^{++} and Co^{++}. In fact, log Q_1 for $S(CH_2CH_2NH_2)_2$ is only slightly greater than $^2/_3$ log Q_1 for $HN(CH_2CH_2NH_2)_2$ and the log Q_1 values for $(-CH_2SCH_2CH_2NH_2)_2$ and $CH_3SCH_2CH_2NH_2$ are only slightly greater than $^1/_2$ the log Q_1 values for $(-CH_2NHCH_2CH_2NH_2)_2$ and $H_2NCH_2CH_2NH_2$, respectively. If it is assumed that each nitrogen atom in the amines contributes equally to the value of Q_1, then the results clearly indicate the very slight contribution of coördination through sulfur. However, the sulfur atom does take part in the coördination to some extent because, for each of the pairs of amines mentioned above, the maximum value of $\bar{n}$ for the sulfur-containing amines never exceeds that for the corresponding amine without sulfur.

A comparison of the values of the molarity quotients of Cd^{++} for $S(CH_2CH_2NH_2)_2$ with those of Zn^{++} (log Q_1 = 5.31; log Q_2 = 3.57) shows that the first formation[7] constant for Cd^{++} is somewhat higher than that for Zn^{++} while the second is somewhat lower. Precipitates formed with Zn^{++} and $CH_3SCH_2CH_2NH_2$ and $(-CH_2SCH_2CH_2NH_2)_2$ but not with Cd^{++}. This behavior also indicates the greater stability of the Cd^{++} complexes. For polyamines containing no heterocoördinating atom the Zn^{++} complexes are somewhat more stable than those of Cd^{++}.[4-10] This behavior seems to be in line with the marked tendency of Hg^{++}, Pt, etc., to form stable sulfur complexes.

Table I

Molarity Quotients of Amines with Cd^{++} at 30° in 1 *M* KNO_3

	log Q_1	log Q_2	log Q_3	
$CH_3SCH_2CH_2NH_2$	3.22	2.3		
$S(CH_2CH_2NH_2)_2$	5.47	3.52		
$(—CH_2SCH_2CH_2NH_2)_2$	5.61	2.44		
$H_2NCH_2CH_2NH_2$	5.63	4.59	2.07	(25°, 1.0 *M* KNO_3)[4]
$HN(CH_2CH_2NH_2)_2$	8.45	5.4		(20°, 0.1 *M* KCl)[5]
$(—CH_2NHCH_2CH_2NH_2)_2$	10.92	3.19		(30°, 1.0 *M* KNO_3)[6]

(1) This investigation was carried out under contract N6-onr 26913 between The Pennsylvania State University and the Office of Naval Research.

(2) E. Gonick, W. C. Fernelius and B. E. Douglas, *J. Am. Chem. Soc.*, **76**, 4671 (1954).

(3) B. P. Block and G. H. McIntyre, Jr., *ibid.*, **75**, 5667 (1953).

(4) J. Bjerrum and P. Anderson, *Kgl. Danske Videnskab Selskab, Math.-fys. Medd.*, **22**, No. 7, 3 (1945).

(5) J. E. Prue and G. Schwarzenbach, *Helv. Chim. Acta*, **33**, 985 (1950).

(6) H. B. Jonassen, G. G. Hurst, R. B. LeBlanc and A. W. Meibohm, This Journal, **56**, 16 (1952).

(7) E. Gonick, Ph.D. Thesis, The Pennsylvania State University, 1951.

(8) J. Bjerrum and P. Anderson, *Kgl. Danske Videnskab Selskab, Math.-fys. Medd.*, **11**, No. 5, 82 (1931).

(9) G. A. Carlson, J. P. McReynolds and F. H. Verhoek, This Journal, **67**, 1335 (1945).

(10) (a) G. Schwarzenbach, *Helv. Chim. Acta*, **33**, 974 (1950); (b) J. E. Prue and G. Schwarzenbach, *ibid.*, **33**, 963, 995 (1950).

Follow
the
newest
field... **NON-METALLICS**

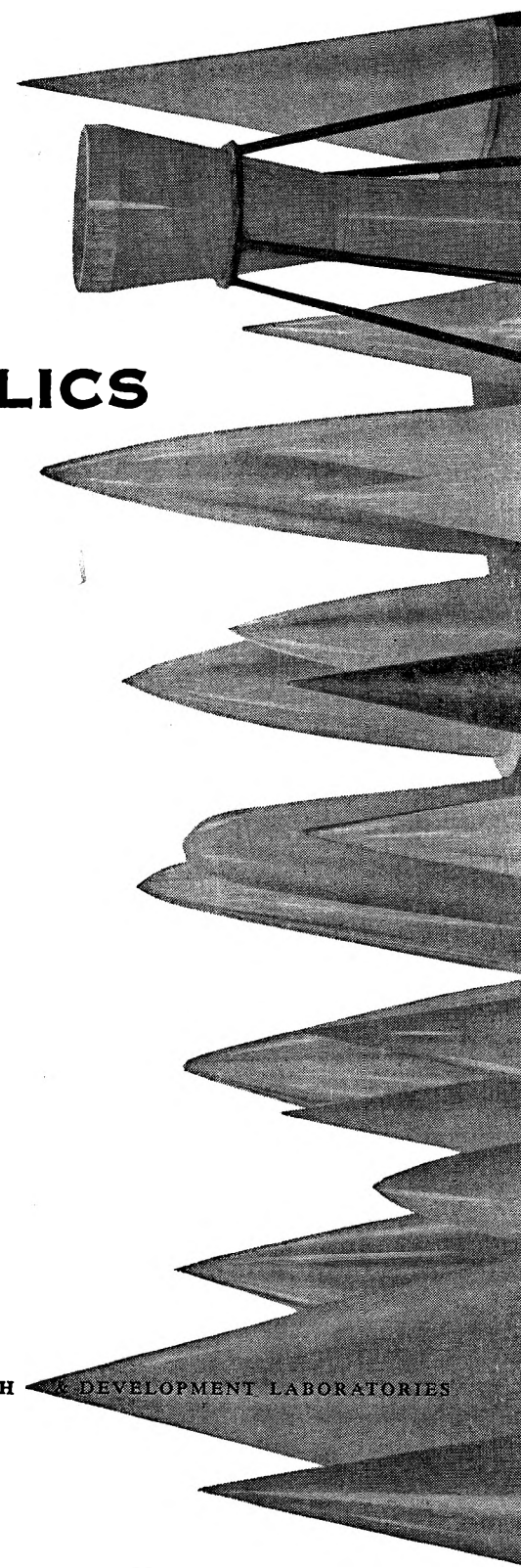

HUGHES RESEARCH AND DEVELOPMENT LABORATORIES HAVE SEVERAL OPENINGS FOR CHEMICAL AND OTHER ENGINEERS IN DEVELOPMENT LEADING TO PRODUCTION OF NEW APPLICATIONS FOR NON-METALLIC MATERIALS.

ENGINEERS AND PHYSICISTS

Hughes Laboratories are engaged in a highly advanced research, development and production program involving wide use of non-metallic materials in missile and radar components. The need is for men with experience in these materials to investigate the electrical, physical, and heat-resistant properties of plastics and other non-metallics.

ENGINEERS OR APPLIED PHYSICISTS

These men are required to plan, coordinate, and conduct special laboratory and field test programs on missile components. Experience is required in materials development, laboratory instrumentation, and design of test fixtures.

RESEARCH CHEMIST

The Plastics Department has need for an individual with a Ph.D. Degree, or equivalent experience in organic or physical chemistry, to investigate the basic properties of plastics. Work involves research into the properties of flow, mechanisms of cure, vapor transmission, and electrical and physical characteristics of plastics.

Scientific Staff Relations

HUGHES RESEARCH & DEVELOPMENT LABORATORIES

Culver City,
Los Angeles County, California